Design and Development of Compact Chipless RFID Tags with High Data Encoding Capacity

A thesis submitted by

NIJAS C.M

in Partial fulfilment of the requirements for the degree of

DOCTOR OF PHILOSOPHY

Under the guidance of

Prof. P. MOHANAN

COCHIN UNIVERSITY OF
SCIENCE AND TECHNOLOGY

DEPARTMENT OF ELECTRONICS

FACULTY OF TECHNOLOGY

COCHIN UNIVERSITY OF SCIENCE AND TECHNOLOGY

KOCHI- 682 022

KERALA

March 2015

"Design and Development of Compact Chipless RFID Tags with High Data Encoding Capacity"

Ph.D. Thesis under the Faculty of Technology

Author

Nijas C.M.
Research Scholar
Department of Electronics
Cochin University of Science and Technology
Kochi - 682022
Email: nijasmhmmd@gmail.com

Supervising Guide

Dr. P. Mohanan
Professor
Department of Electronics
Cochin University of Science and Technology
Kochi - 682022
Email: drmohan@gmail.com

Department of Electronics
Cochin University of Science and Technology
Kochi - 682022

March 2015

*D*edicated to the Almighty, Parents, Teachers

and Dear Ones.......

DEPARTMENT OF ELECTRONICS
COCHIN UNIVERSITY OF SCIENCE AND TECHNOLOGY,
KOCHI, INDIA.

Dr. P. Mohanan
(Supervising guide)
Professor
Department of Electronics
Cochin University of Science and Technology

Certificate

This is to certify that the thesis entitled *"Design and Development of Compact Chipless RFID Tags with High Data Encoding Capacity"* is an authentic record of the research work carried out by Mr. Nijas C. M. under my supervision and guidance in the Department of Electronics, Cochin University of Science and Technology in partial fulfilment of the requirements for the Ph.D degree under the Faculty of Technology and no part of this work has been submitted before for the award of any other degree, diploma or associateship in any other University.

I further certify that the corrections and modifications suggested by the audience during the pre-synopsis seminar and recommended by the Doctoral Committee of Mr. Nijas C. M. are incorporated in the thesis.

Kochi-22
March 2015   **Prof. P. Mohanan**

Declaration

I hereby declare that the thesis entitled **"Design and Development of Compact Chipless RFID Tags with High Data Encoding Capacity"** is an authentic record of the research carried out by me under the supervision of Prof. P. Mohanan, Professor, Department of Electronics, Cochin University of Science and Technology in partial fulfilment of the requirements for the Ph.D degree under the Faculty of Technology and that no part of this work has been submitted before for the award of any other degree, diploma or associateship in any other University.

Kochi-22
March 2015   Nijas C. M.

Acknowledgement

In the name of Allah, the Most Gracious and the Most Merciful,

I remember with gratitude…

My supervising guide, Dr. P. Mohanan, Professor, Department of Electronics, Cochin University of Science and Technology, for his valuable guidance, advices and timely care extended to me throughout the research period.

Prof. K. Vasudevan, Department of Electronics, Cochin University of Science and Technology for his constant encouragement and concern. His dedication for research is always a leading source of energy.

Dr. C.K. Aanandan, Professor and Head Department of Electronics, Cochin University of Science and Technology for the advice, discussions and care rented during these years.

Prof. P.R.S. Pillai, Prof. Tessamma Thomas, Dr. James Kurian and Dr. M. H. Supria, Department of Electronics, Cochin University of Science and Technology for their support.

My sincere thanks to Dr. K. G. Nair, former Head and founder of Electromagnetics and Antennas Research (CREMA) Laboratory in Department of Electronics, Cochin University of Science and Technology, for establishing full-fledged laboratory that enabled me to do my research work in a well reputed laboratory in the country.

My seniors at CREMA, especially Dr. Sujith Raman, Dr. Suma M N, Dr. Deepu V, Dr. Sariv V P, Dr. Nishamol M S, Dr. Laila D, Dr. Shameena V A and Dr. Rohit K Raj for their guidance, support and care. Their views and way of analysis had a strong impact on me.

My friends at CREMA, especially Deepak U, Dinesh R, Tony Sir, Abdul Rasheed, Roshna T K, Sajitha V R, Vineesh P V, Sreenath S, Ashkar Ali, Prakash Sir, Sumitha Miss, Anitha V R, Anila P V, Indhu K K, Titu K Samson, Jayakrishanan,

Kochi- 22   Nijas C M

<u>ABSTRACT</u>

The main objective of this thesis is to develop a compact chipless RFID tag with high data encoding capacity. The design and development of chipless RFID tag based on multiresonator and multiscatterer methods are presented first. An RFID tag using using SIR capable of 79bits is proposed. The thesis also deals with some of the properties of SIR like harmonic separation, independent control on resonant modes and the capability to change the electrical length. A chipless RFID reader working in a frequency band of 2.36GHz to 2.54GHz has been designed to show the feasibility of the RFID system. For a practical system, a new approach based on UWB Impulse Radar (UWB IR) technology is employed and the decoding methods from noisy backscattered signal are successfully demonstrated. The thesis also proposes a simple calibration procedure, which is able to decode the backscattered signal up to a distance of 80cm with 1mW output power.

Contents

LIST OF PUBLICATIONS

RESUME

INDEX

<div align="right">

Chapter | **1**

</div>

INTRODUCTION TO RFID TECHNOLOGY

1. Introduction

2. RFID System

3. Applications of RFID

4. RFID Vs Barcode

5. Chipless RFID

6. Chipless RFID tag for sensor application

7. Data Encoding Techniques in Chipless RFID

8. Thesis Outline

9. Reference

Abstract

This chapter highlights a brief description of evolution and working of an RFID system. Basic block diagram of an RFID system such as RFID reader, RFID tag and Middleware software are presented. Comparison of RFID technology with barcode is analysed and discussed various merits and demerits of RFID system. New Chipless RFID technology and its working principle based on time and frequency domain are explained. The chapter also covers literature survey of various types of chipless RFID tags and different encoding techniques. Organisation of the thesis is outlined at the end of the chapter.

1. Introduction

Radio-Frequency Identification (RFID) is recently being used in a wide range of applications such as Supply Chain Management (SCM), health care, traffic monitoring, retail, access control, etc. [1]-[7]. The idea behind the RFID tag is to store a unique identification number, same as that of a bar code or a magnetic strip on the back of a credit card or ATM card. To retrieve information stored in the bar code or magnetic strip, the device must be

scanned in a close proximity with its scanning device. But in RFID, the data transfer between RFID tag and RFID Reader is done wirelessly and hence enables remote identification.

RFID technology was introduced during the 2nd World War for the Identification Friend or Foe (IFF) aircrafts. In this method friend aircraft is identified from enemy aircraft by assigning a unique identifier code to aircraft transponders. In 1945, the first RFID tag was developed by Leon Theremin known as "the Thing". This was an espionage tool for the Soviet Union, built into the Great Seal and offered to the U.S. ambassador in Moscow [8]. The gift hung in the U.S. Embassy for many years and used by Russia for spying. Its principle of operation is based on the backscattering technique. Spying the conversation is done by parking a vehicle near to US embassy and sending an interrogation signal towards the espionage device. Fig.1.1 shows the front view and exploded view of the Great Seal of United State. Block diagram of "the Thing" is given in the Fig.1.2. When an antenna in "the Thing" is illuminated by an incident EM wave, electric currents are generated on its conducting parts. Same antenna is coupled to an EM resonating cavity.

Figure 1.1 Great seal of United States and an exploded view of the device. Courtesy: Wikipedia.

The membrane of the cavity vibrates in accordance with the sound/ conversation in the room. This will alter the impedance of the cavity and hence changes the antenna impedance. Therefore incident currents on the antenna is modulated with sound waves. The backscattered signal from the espionage tool is demodulated at the receiver.
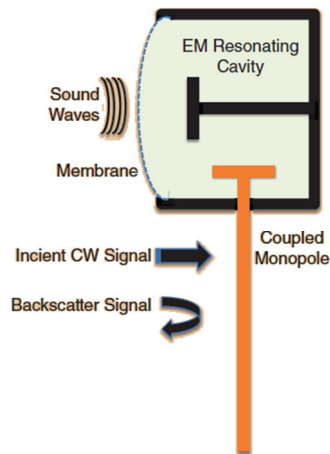
Figure 1.2 The eavesdropping device developed by L. Theremin ("the Thing"). Courtesy: Smail Tedjini et. al. [8].

The operating principle of a conventional RFID is the backscatter modulation, which was explained by Harry Stockman in 1947 [1]. Fig.1.3, describes a block diagram of an RFID tag. Incident wave from the reader will wake up the control circuit in the RFID tag. Depending on the tag type, unique code stored in the Silicon chip will transmit back to the reader via backscattered signal. Unique code is encoded in the interrogation signal by altering the impedance of the antenna using an impedance modulator circuit. The backscattered signal is modulated depending on the unique code and it is decoded by the reader.
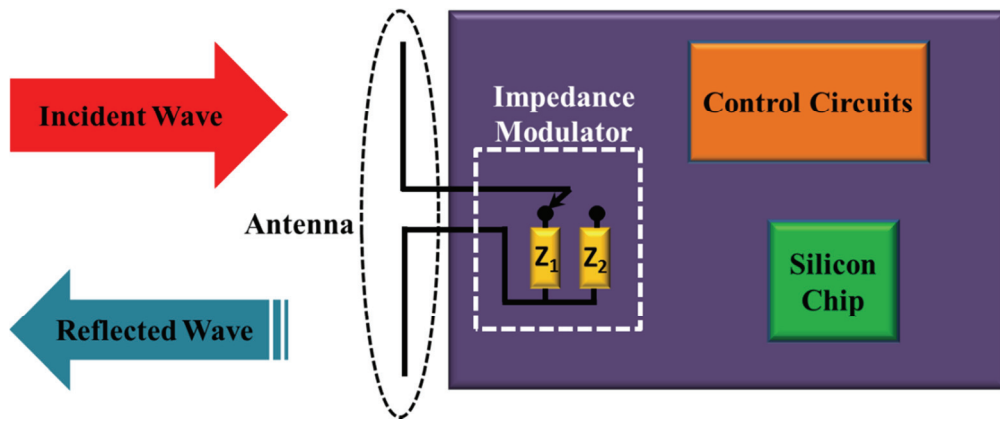
Figure 1.3 Block diagram of a commercial RFID tag

2. RFID System

RFID system consists of mainly three components as shown in Fig.1.4.

2.1. RFID Reader

2.2. RFID Tag

2.3. Middleware software

Figure 1.4 RFID System with three basic components, 1. RFID reader, 2. RFID tag and 3. Middleware software.

2.1. RFID Reader

An RFID reader, also known as an interrogator, is a device that provides the connection between the tag data and the system software. The

reader communicates with tags that are within its range of operation, performing tasks including sending an interrogation signal, filtering (searching for tags that meet certain criteria), decoding data from the tag, writing (or encoding by rewriting the IC) to selected tags, etc.

The reader uses an antenna to capture data from tags. It then passes the data to a computer for processing. Readers can be placed in a stationary position in a store or factory, or integrated into a mobile device such as a portable handheld scanner.

2.2. RFID Tag

RFID tag contains the identification code which is stored in the Silicon chip. The tags memory can be read-only, read-write, or write-once and read-many. RFID tag also comprises of an antenna, control circuits and a substrate that holds it all together. Each tag carries information such as serial number, model number, location of assembly, and other data as in the case of Electronic Product Code (EPC) which is designed as a universal identifier that provides a unique identity for every physical object anywhere in the world.

RIFD tags are available at different frequency bands like low frequency (LF), high frequency (HF) to the microwave bands, as shown in Fig.1.5. LF (typically in 125 kHz) and HF (with 13.56 MHz) RFID systems can communicate up to 1m read range with the use of inductive coupling. Due to the large operating wavelength compared with tag size, RFID tags operating in these bands are less prone to the effect of metal/liquid environments, thus offering robust readability in practice. UHF RFID tags, typically operating in 866-868MHz (European (EU) countries) and 902-928MHz (North American Continent) have a longer read range up to 10m or more, with a faster data rate. On the other hand, the reading performance of

UHF tags depends on the working environment. They are incapable of penetrating materials such as metals, liquids, dusts and fog. Commonly used frequencies at microwave band for RFID technologies are 2.45GHz and 5.8 GHz.
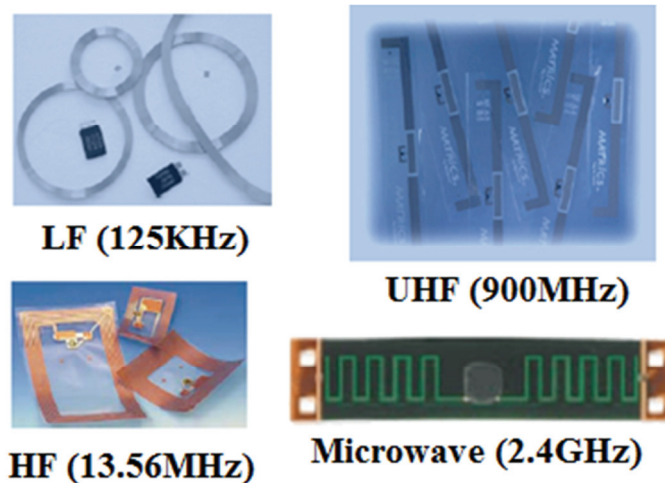
Figure 1.5 Different Chipped RFID tags

Depending on the power handling method in the tag, RFID can be classified as Passive, Semi Passive and Active Tags.

2.2.1 Passive Tags

Passive tags do not contain their own power source, such as battery and cannot initiate communication with the reader. Power transmitted from the reader is used for powering the IC and establishing communication between reader and tag. Due to the lack of own power sources, the read range of the tag is usually up to 2 ft for inductively coupled and up to 20 ft for backscattered tags. These tags have more life time compared with other types. Passive tags are the least expensive tags and are normally used in places where the tags are not reusable, ie., consumable items. Passive tags normally have limited data storage capability. Block diagram of the passive

RFID tag is shown in Fig.1.6. As shown in the figure, the tag consists of electronic circuits like rectifier, supply regulator, clock generators, etc.
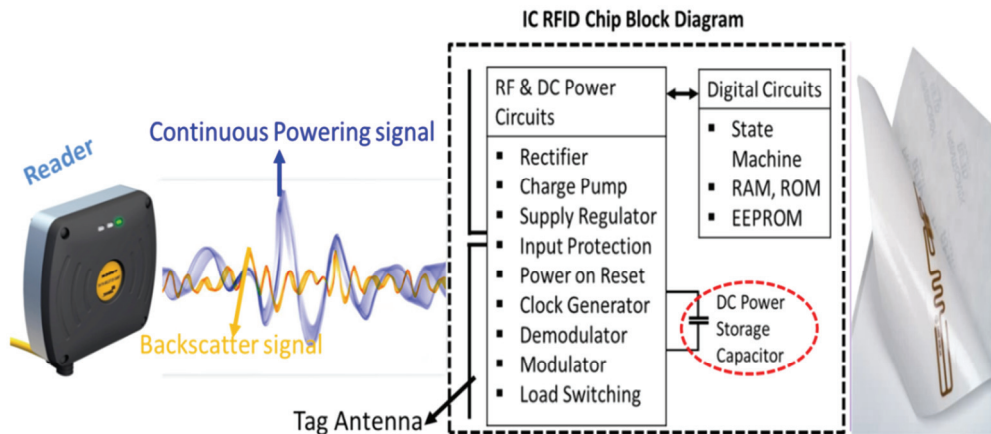
Figure 1.6 Block diagram of a Passive RFID tag.

2.2.2. Semi passive Tags

These are also called Battery Assisted Tags (BATs). Such tags have on-board power supply to provide power to the IC to keep it alive. The communication between the tag and reader is similar to passive tags. Longer read ranges up to 100 ft are possible compared to the passive tags. Because of the on-board battery, tag can be used for sensor application like temperature, pressure, humidity, etc. Due to the absence of any active transmitter, these tags do not contribute to any radio noise. These tags have more memory capacity than the passive tags. Depending on the size of the battery, Semi passive tags are more expensive, bigger in size, and heavier. The life of these types of tag is determined by the life of the battery.

2.2.3. Active Tags

These tags have an on-board battery and a transmitter. The battery supplies power to both the IC and the transmitter. Due to the presence of

transmitter, it doesn't have to rely on an interrogator to transmit its data by backscatter coupling. Tags with range up to several kilometres are available, depending on the battery and transmitter. On-board environmental sensors and memory with higher data rate are also available with these tags. These types of tags can be used in Real-Time Location Systems (RLTS). Active tags can have a sleep mode and consumes the least power in the idle stage. Thus the battery life and the tag's life can be elongated. These tags use two different frequencies for transmission and reception of data (downlink and uplink). The active tags are the most expensive tags and are limited in their usage by cost factor. Due to the presence of an on-board transmitter, these tags contribute largely to radio noise.

2.3. Middleware Software

Middleware software maintains the interface and the software protocol to encode and decode the identification data from the reader into a mainframe or personal computer. This is the intermediate between the interrogator and the enterprise layer. Middleware sends and collects data directly from the interrogator, performs a business-related process regarding the data, read data, stores the data as per the requirement and sends data to the enterprise applications. Middleware also comprises the software used to monitor, configure, and manage the hardware of the interrogator. Data gathered from middleware are sent to the enterprise application stored in the computer. After the process application software can update the data in the server through the internet.

3. Applications of RFID

Only dreams can limit the application of RFID. Nowadays, RFID tags are applied in almost every business process and are projected to be applied everywhere that exists in the real world. Because of the use of radio waves in RFID, it does not require line-of-sight to operate. That means, the tag can be hidden inside the item or box that is to be identified and still be read. Another feature of RFID is the ability to read many tags at the same time. Again, there is a huge savings potential in not having to manually present the reader to each item to be identified. Applications fall into two main categories: short range applications in which the reader and the tag must be in close proximity (such as access control), and medium to long range applications in which the distance may be greater (such as reading across a distribution centre dock door) [2]-[3].

4. RFID Vs Barcode

The most widely adopted method for product identification is barcodes. The barcode is a vertically stripped identification tag printed on products, allowing retailers to identify billions of products. There are two types of barcodes that are widely used; one-dimensional (1D), which represent data in the widths (lines) and the spacing of parallel lines, and two dimensional (2D), which come in patterns of squares, dots, hexagons and other geometric patterns within images [4]. The former one is common in most household products, while 2D barcode is common in industrial products where more information is needed to be stored in the label. 2D barcodes have a maximum capacity of 128 bits and hence can be comparable with Electronic Product Code (EPC). Barcodes data capacity comes from diffraction of light rays from strip edges. They are increasingly being used and also appear more on consumer goods. In the case of 1D barcodes, the

maximum capacity is 41 bits (eg: EAN 13 barcodes). Barcodes are much smaller, less expensive and work with the same accuracy on various materials in which they are placed. Barcodes can directly print into plastic or paper materials and therefore the only cost involved is the ink. Although appropriate in many instances, there are cases where barcodes cannot meet the need. Even though RFID and barcodes are two techniques of auto-identifications, they are different in many ways. Table 1 shows a comparison of RFID with barcode [2], [5].

Table 1: Comparison between RFID and Barcode

	RFID	Barcodes
Read Range	Up to 100's of feet or more (Active Tag)	Several inches up to 2 feets
Read Rate	1000's of tag simultaneously	Only one at a time
Read/Write	Many RFID tags are Read/Write	Read only
Technology	RF (Radio Frequency)	Optical (Laser)
Line of Sight	Not required	Required
Human Capital	Once up and running system is completely automated	Labourers must scan each item
Durability	High, can read through the obstacles like paper, fabric, wood, etc. through which EM wave can propagate	Low. Easily damaged or removed; cannot be read if dirty or greasy.
Security	High. Difficult to replicate. Data can be encrypted.	Low. Much easier to reproduce or counterfeit.

Therefore the retailers were looking for a solution to overcome the limitations of barcodes. Fortunately, RFID could become a promising solution for this. RFID could eventually replace barcodes in some applications where bulk counting is routinely performed. However, the cost of the RFID tags still makes it inappropriate for low-cost applications. Thus, almost 70% of the articles are still tagged using barcodes. Approximately 15000 billion units are fabricated each year for this purpose. The main inconveniences of RFID technology is its cost. Chip tags are not normally available below $0.3 for orders

less than one million tags [9]. The marginal cost of a barcode is approximately less than one tenth of a cent. Privacy is another major anxiety with RFID technology. Remote access and data sharing implies abuse usage of private information. Tags could be read without a person's knowledge because humans cannot sense radio signals.

5. Chipless RFID

Application Specific Integrated Circuits (ASIC) design on Silicon wafer and testing along with the tag antenna result in a costly manufacturing process. Chipped tags are fabricated on a Silicon wafer and there is a fixed cost per wafer (around US $1,000). The cost of the RFID chip can be assessed by knowing the required silicon area of the RFID chip. Alternative solution to this problem is the design of a new RFID tag without having any silicon chip and other costly circuits. RFID tag without Silicon chip is called Chipless RFID. In these types of tags unique number is stored in time or frequency domain. Most chipless RFID systems are based on using the electromagnetic properties of materials and/or designing various conductor layouts to achieve particular electromagnetic properties.

5.1. Review of Chipless RFID Tags

The main challenge for researchers when designing chipless RFID tags is how to encode data without the presence of a chip. There are two methods reported in the literature. They are,

5.1.1. Time Domain Reflectometry (TDR)-based chipless tags

5.1.2. Spectral signature-based chipless tags.

5.1.1. Time Domain Reflectometry (TDR)-Based Chipless Tags

TDR-based chipless RFID tags are interrogated by sending a signal from the reader in the form of a pulse and listening to the echoes of the pulse sent by

the tag. A train of pulses are thereby created by tag, which can be used to encode data. Popular RFID tag operating on the principle of TDR is explained here

5.1.1.1. SAW (Surface Acoustic Wave) Tag

An example of a nonprintable TDR-based chipless RFID tag is the SAW tag developed by RFSAW Inc. [10]. SAW tags are excited by a chirped Gaussian pulse sent by the reader centred around 2.45 GHz ISM Band [11]–[15]. A schematic diagram showing the working of SAW tag is depicted in Fig.1.7. The RF interrogation pulse is initially picked up by the tag antenna and converted to SAW using an InterDigital Transducer (IDT). The SAW propagates across the piezoelectric crystal (with a velocity of 3158m/s for ST-X Quartz substrate and 3488m/s for Y-Z Lithium Niobate substrate) and is reflected by a number of reflectors, which create a train of pulses with phase shifts [16]–[23]. The train of pulses is converted back to an EM wave using the IDT and detected at the reader end where the tag's ID is decoded [24]-[33].
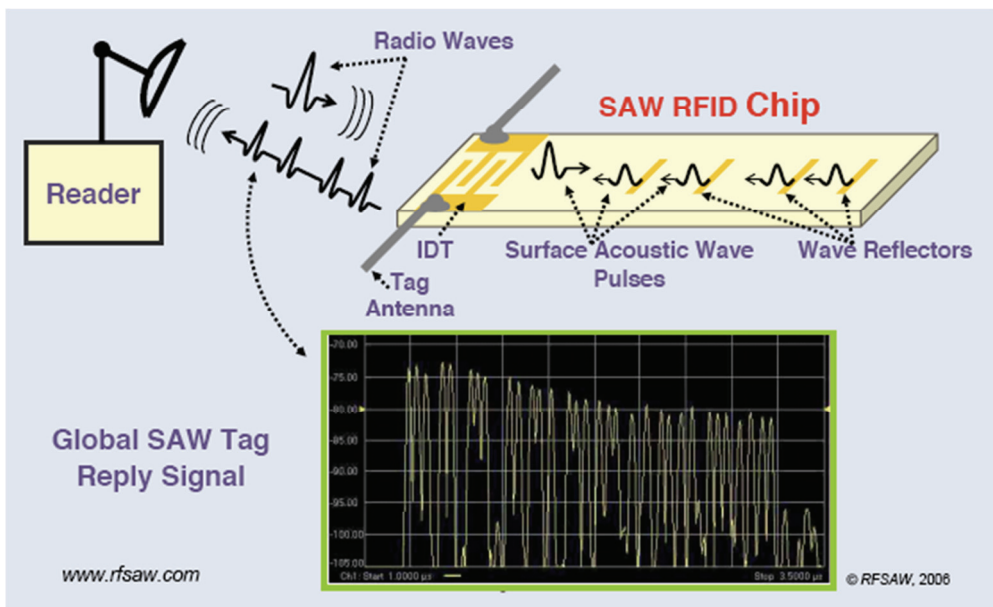
Figure 1.7 System architecture of SAW tag. Courtesy: S. Harma et. al. [10].

Even though RFSAW Inc. has fabricated RFID tags with a data encoding capacity of 96 bits, the cost of the tag is almost same as that of commercial RFID. This is due to the fabrication tolerance of the order of μm and also required piezoelectric substrate with Interdigital Transducers.

5.1.1.2. Delay Line based Tag

Delay-line-based chipless tags consist of antenna with a transmission line of specific length. The tag is operated by using a microstrip discontinuity after a section of delay- line, as reported in [34]–[36]. A delay-line-based chipless tag is shown in Fig.1.8. The tag is excited by a short (1ns) EM pulse. The tag consists of two microstrip transmission line branches, one, a relatively short straight branch and the other, a longer meandered branch. The ends of the microstrip branches are either terminated with a resistor equal to characteristic impedance Z_0 to avoid reflections. The signals in each of the branches get delayed by different amount. Using isolators, the signal in the meandered branch is tapped on it. The tapped signals with different time delays are superimposed on to the straight branch to produce an output signal as shown in Fig.1.9. Only eight bits were successfully tested with delay line method, which shows the limited potential of this technology.
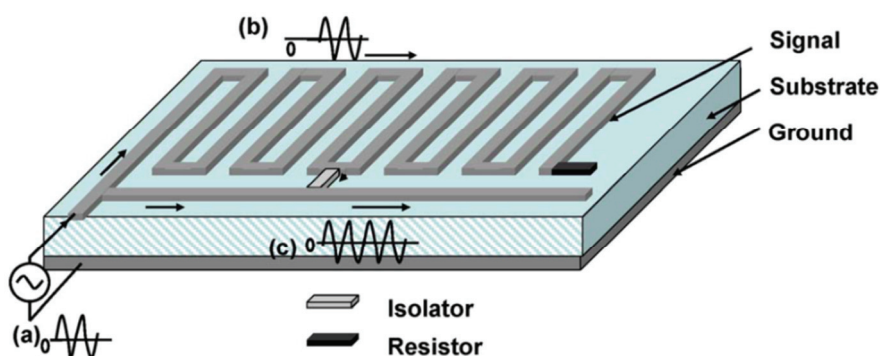
Figure1.8 Schematic diagram of transmission delay line based ID generation circuit. Courtesy: A. Chamarti et. al. [34].
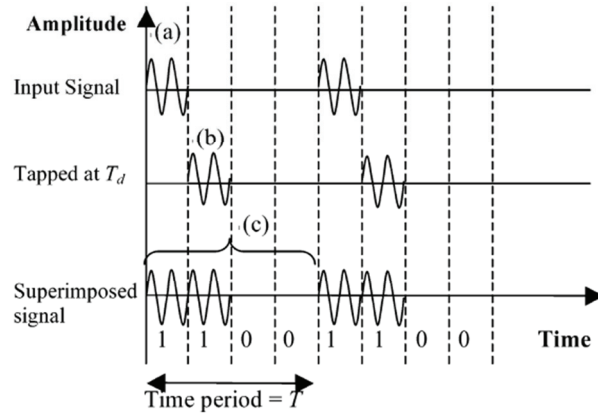
Figure 1.9 Binary code generation by the superimposition of delayed signals. Courtesy: A. Chamarti et. al. [34].

Another Delay line based tag is reported by Raji. S. N et. Al. [37]. In this tag group delay of the backscattered signal is used for encoding data. Transmission lines with different length are selected for creating different group delay as shown in Fig.1.10. While increasing the length of the C section, group delay at the port 2 can be varied. Large length of C section creates amplitude distortion in the group delay; hence it results in low bit encoding capacity. Delay line based time domain tags are detailed in Chapter 3.
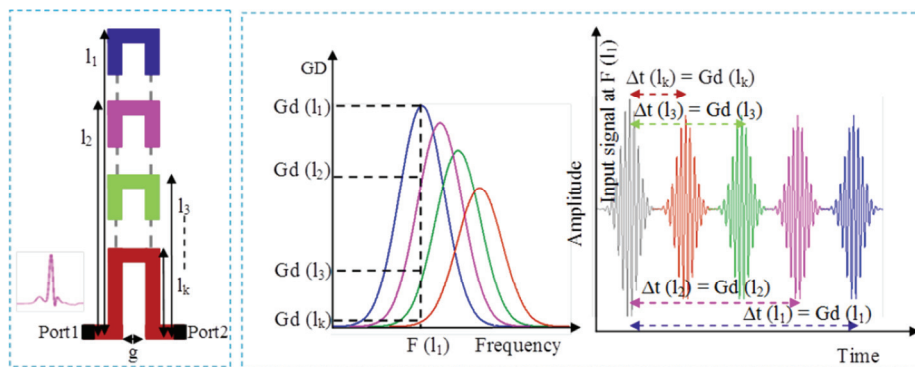
Figure 1.10 Principle of encoding for cascaded commensurate C-sections. a) Prototype (for simplicity, only one C-sections is represented). b) Group delay Vs frequency response. c) Corresponding time domain response to the spectral component. Courtesy: Raji Nair et. al. [37].

5.1.2. Spectral Signature Based Chipless Tags

Spectral signature-based chipless tags use a specific frequency band to encode data using resonant structures or metallic patterns. Each data bit is usually associated with the presence or absence of a resonant peak or dip at a predetermined frequency in the spectrum. The advantages of these tags are, they are fully printable, robust, greater data storage capability and low cost. But, these tags require large frequency spectrum for data encoding, and orientation alignment with reader antenna. A wideband Voltage Controlled Oscillator (VCO) with RF components are also needed at the reader end. Spectral signature based tag showing better data encoding capacity than time domain based tags except SAW tag. Hence there are many RFID tags working in the frequency domains are reported in the literature [37]-[55].

Planar circuit chipless RFID tags are designed using standard planar microstrip/coplanar waveguide/stripline resonant structures, such as antennas, filters, and fractals. They are printed on dielectric substrates. Reported frequency domain based tags can be grouped into two categories,

5.1.2.1. Multiresonator based tags

5.1.2.2. Multiscatterer based tags

The multiresonating chipless tag comprises three main components: the transmitting (Tx) and receiving (Rx) antennas and multiresonating circuit. Multiresonating circuit in most of the reported tag consists [38]-[45] of narrow band high Q filters using different microwave resonators like spiral, split ring, C like structures, etc. These resonators are either connected or coupled to microwave transmission line and both ends of the transmission line are connected to two UWB antennas.

The Multiscatterer based tags consist of resonators with different dimensions and each resonator will act as receiving antenna, filter and retransmitting antenna. Hence size requirement for the UWB antennas and transmission line can be eliminated and these tags show good bit encoding capacity than multiresonator based tag.

5.1.2.1. Multiresonator Based Tags

A block diagram of a multiresonator based tag with basic components is shown in Fig.1.11 [38]. The chipless RFID tag consists of a vertically polarized UWB disc-loaded monopole receiving tag antenna, a multiresonating circuit, and a horizontally polarized UWB disc-loaded monopole retransmitting tag antenna [38]. The tag is interrogated by the reader by sending a frequency swept continuous wave signal with constant amplitude and phase. When the interrogation signal reaches the tag, it is received using the receive monopole antenna and propagates towards the multiresonating circuit. The multiresonating circuit encodes data bits using cascaded spiral resonators, which introduce amplitude attenuations and phase jumps at particular frequencies of the spectrum. After passing through the multiresonating circuit, the signal contains the unique spectral signature of the tag, and is transmitted back to the reader using the transmit monopole tag antenna. The receiving and retransmitting tag antennas are cross-polarized in order to minimize interference between the interrogation signal and the retransmitted encoded signal containing the spectral signature. Fig.1.12 shows a 35-bit tag [39], designed on Taconic TLX-0 (ε_r = 2.45, h = 0.787 mm, tan δ = 0.0019) substrate. All the 35 amplitude variations in the frequency due to 35 resonators in the tag are depicted in Fig.1.13. Same variations can be observed in phase of the backscattered signal [39].
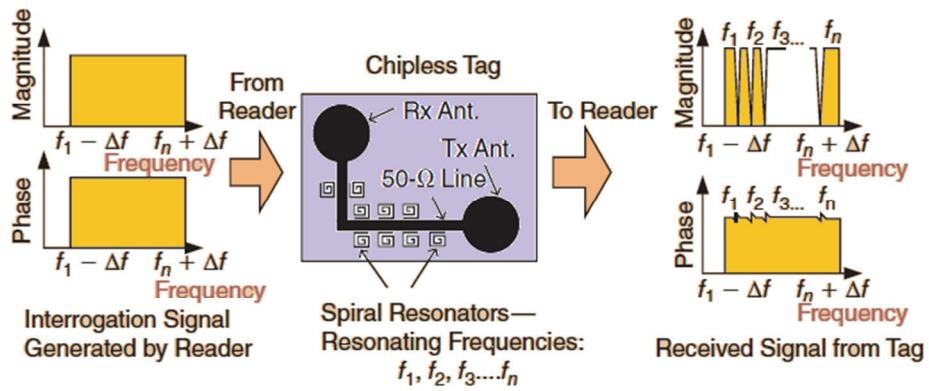
Figure 1.11 Structure and operation of a multiresonator-based chipless RFID tag. Courtesy: S. Preradovic et. al. [38].
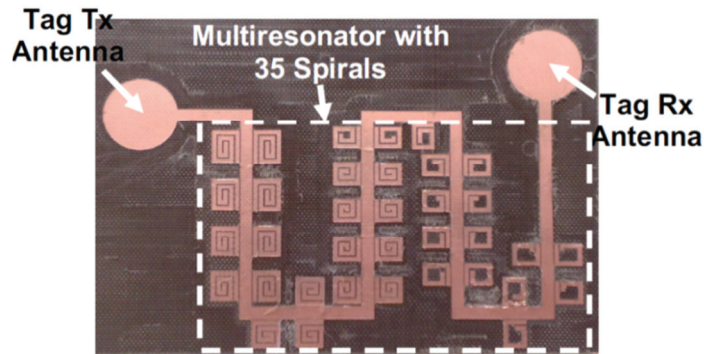
Figure 1.12 Photograph of 35-bit chipless RFID tag (length=88mm, width=65mm). Courtesy: S. Preradovic et. al. [38].
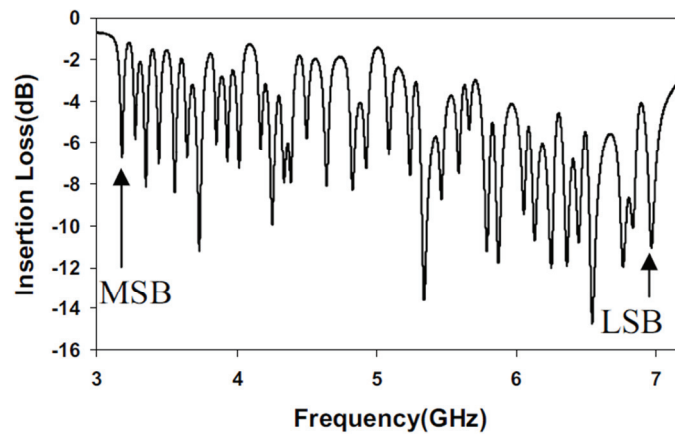
Figure 1.13 Measured insertion loss of the multiresonating tag with 35 bits of data. Courtesy: S. Preradovic et. al. [38].

Chipless RFID tag using different types of multiresonating circuits are reported in the literature [39]-[45]. The multiresonator circuit using Modified Complementary Split Ring Resonators (MCSRR) is proposed in [42]. Fig.1.14 shows the layout of conventional CSRR and MCSRR on CPW transmission line. Instead of representing one bit with one resonator, here two bits are proposed by modifying (shorting or opening) inner and outer rings of MCSRR. Fig.1.15 shows the all four combinations of 2 bit data obtained by modifying the single MCSRR structure. Even though the tag has double data capacity than others, the resonator is placed on the CPW feed line. As the number of resonator increases, the amplitude distortion through the transmission line also increases. Hence bit encoding capacity is limited.
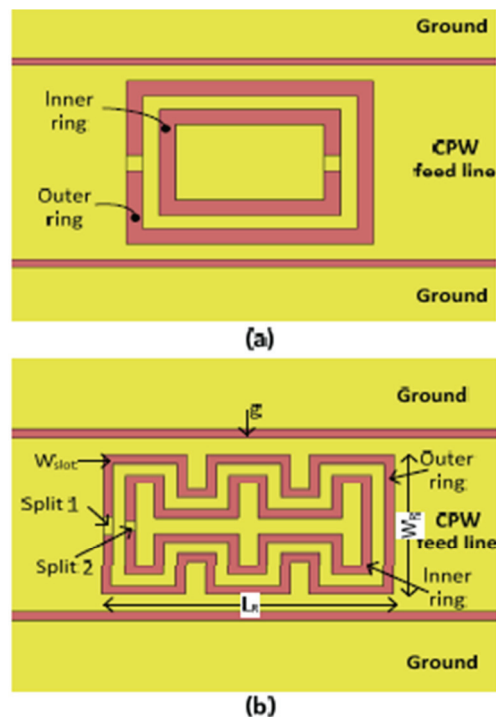
Figure 1.14 (a) Layout of a conventional Complementary Split Rectangular Ring Resonator (CSRRR) (b) layout of the proposed modified complementary split ring resonator (MCSRR). Courtesy: Md. Shakil Bhuiyan et. al. [42].
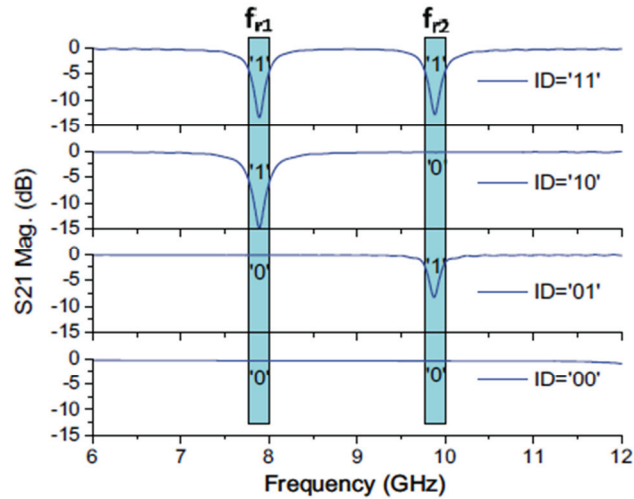
Figure 1.15 Insertion loss (S_{21}) responses of MCSRR configured to generate all four bit combinations. Courtesy: Md. Shakil Bhuiyan et. al. [42].

5.1.2.2. Multiscatterer Based Tag

Multiscatterer based tag consists only of scatterers with different dimensions. The space requirement for two UWB antennas and transmission line reported in the multiresonator based tags can be removed. The similar electromagnetic response of the mutiresonator based tag can be achieved with a structure using multiple signal processing scatterers [46]-[54]. Each scatterer serves as a receiving antenna, a filter and a transmitting antenna. Normally, each scatterer (see Fig.1.16) will receive an interrogation signal from the reader and reflects back to the reader as quasi-optical way. At resonance, it will generate a different EM signature. The chipless tag proposed in [46] is the first design reported based on this principle. Although it has a limited coding capacity of the order of 5 bits compared to 35 bits [39], but the size requirement for this tag is less compared to 35bit tag. This demonstrates the miniaturization potential of this approach.

RF barcodes are constructed with arrays of microstrip dipoles on a dielectric substrate with the metallic ground plane. Detection is based on reflection characteristics. The interrogator emits electromagnetic energy, and the frequency content of the reflected energy from the RF barcodes is analysed to determine which codes on the tagged item in the detection zone. Multiscatterer based tags using metallic strip working in the ISM bands (2.4GHZ, 5.2GHz and 5.8GHz) are shown in Fig.1.16 [46]. The backscattered signal from tag is shown in Fig.1.17.
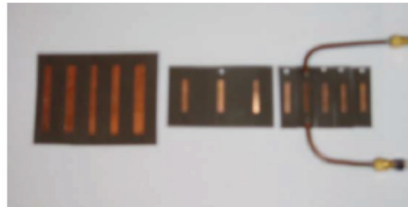
Figure 1.16 Full range of RF barcode elements at 2.4, 5.25 and 5.8 GHz bands with near field measurement probes. Courtesy: I. Jalaly et. al. [46].
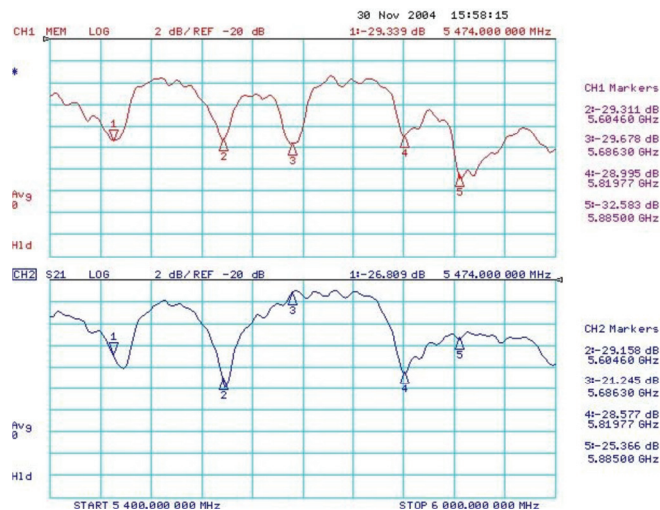
Figure 1.17 Bistatic S_{21} measurement results at 1.5m read range for 5-bit RF barcode representing 11111 (top) and 11010 (bottom), where a '1' is indicated by a 'null' or RF energy absorption at the corresponding frequency. Courtesy: I. Jalaly et. al. [46].

A depolarising based chipless RFID tag is reported in [52]. In this tag resonators are designed in such a way that it will interrogate the tag with one polarisation and decoded with orthogonal polarisation. Commonly used metallic shapes (cylinders and rectangle) scatter the incident wave in the same polarisation of transmitted signal. Hence the orthogonally polarised backscattered signal mostly comprises of the signal from the depolarised resonators. Two types of resonators are proposed in [52], dual L shaped resonator and 45^0 shorted dipole. Fig.1.18 shows the resonators with current pattern at resonance and RCS of each resonator. There are some drawbacks due to the presence of higher harmonics in the integral multiples of the fundamental mode with these resonators. Amount of surface current generated at the resonant frequency determines its backscattered signal strength. But in dual L shaped resonators, the total current is distributed in two orthogonal directions, thus reduce the reading distance. In case of 45^0 shorted dipole, multiple numbers of resonators with same dimensions are required to generate enough backscattered power. If the item embedded with the tag is rotated about 45^0, tag became polarisation dependent and the scatterer cannot produce depolarised backscattered signal.

Majid Manteghi et. al. successfully represented the resonant frequency of the RFID tag in complex domains (Real and Imaginary) and its extraction method using different methods like singularity expansion method, Short-Time Matrix Pencil Method etc. [53] -[57]. The relations between the persistence of the complex resonant modes along time Vs frequency are successfully demonstrated using numerical and experimental methods.
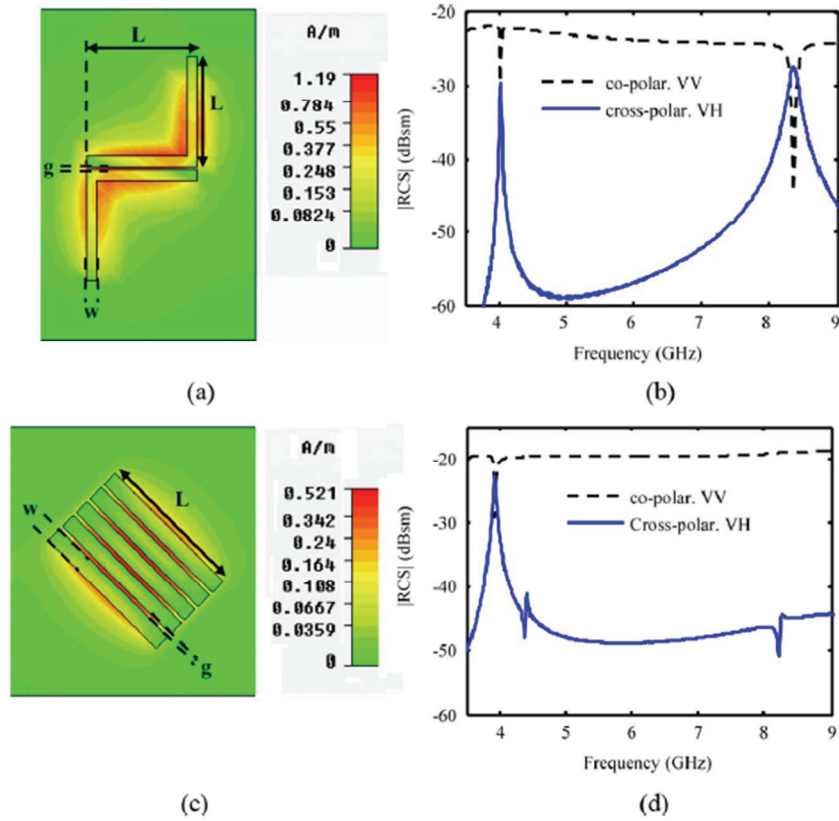
Figure 1.18 (a) and (b) Tag based on dual-L resonators. (a) Surface current density at resonance. (b) Simulated RCS response for co-polarization (VV) and cross-polarization (VH). The tag dimensions are L = 11.4mm and g = 0.5 mm. (c) and (d) 45^0 rotated shorted dipoles tag. (c) Surface current density at resonance. (d) Simulated RCS response for co-polarization (VV) and cross-polarization (VH). The tag dimensions are L = 19mm, g = 0.5mm and w = 2mm. Courtesy: Arnaud Vena et. al. [52].

UWB IR (Impulse Radar) technique is used for the analysis of RFID tags. Fig.1.19 shows the photograph of the notched elliptical dipole tag used for the measurements [57]. Pole signature of the three bit RFID tag using simulation analysis is plotted in Fig.1.20. Resonant frequencies due to the notch in the dipole resonators are found to be at 5.65, 7.08, and 8.45 GHz with pole at 3GHz due to the dipole structure.
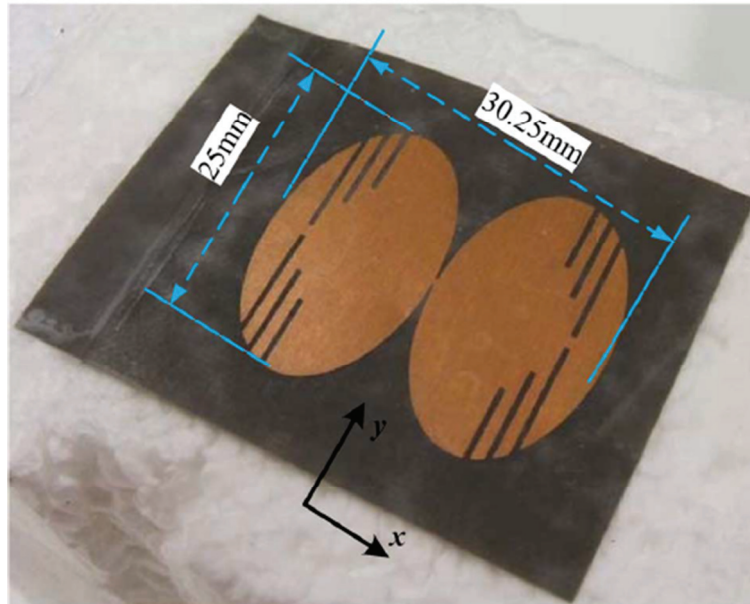
Figure 1.19 Photograph of the notched elliptical dipole tag. Courtesy: A. T. Blischak et. al. [57].
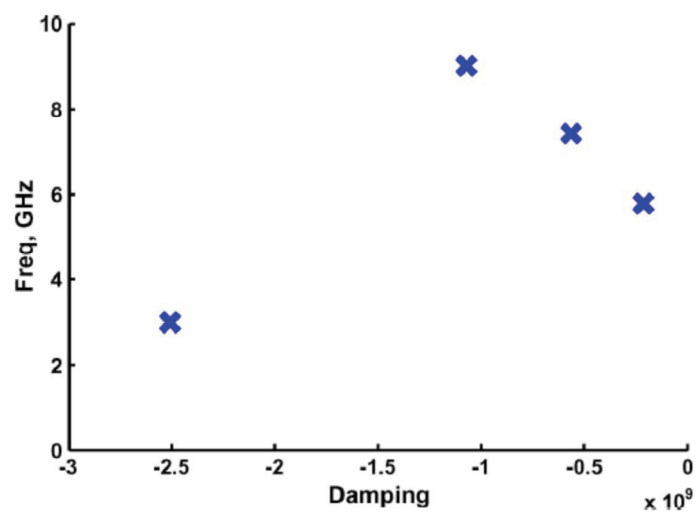
Figure 1.20 Pole signature for notched elliptical dipole tag extracted from simulated time-domain scattered fields resulting with impulsive plane wave excitation. Courtesy: A. T. Blischak et. al. [57].

RFID tags for secure applications are also presented in the literature [45], [58]. Instead of using scattering in the free space, this type of tags uses

secure reader zone like slotted wave guides. RFID technology for on-touch data transfer applications is proposed in [38]. A Single bit is used for identification. The proposed measurement system comprises of a rectangular waveguide and an RFID tag consists of a substrate with rectangular metal resonator. The resonant frequency of the tag (size of the rectangular patch) is above the waveguide cutoff frequency. Fig.1.21 shows the geometry of the tag and measurement setup inside the S band waveguide. Fig.1.22 shows the simulated frequency response through the waveguide with different conditions. Different IDs are generated by dividing S band frequency (2.5GHz to 5GHz) into small section (1MHz) and the reader will check for the position of resonance in the band.
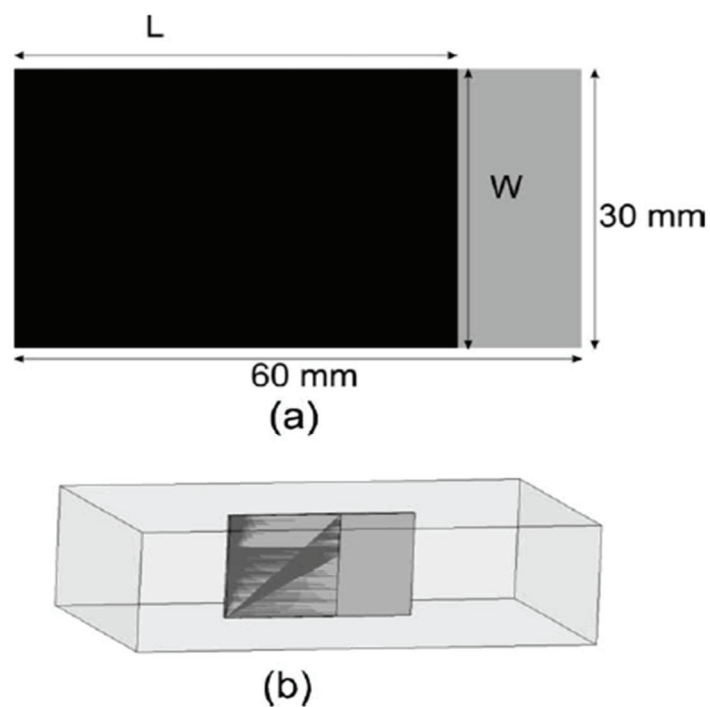
Figure 1.21 (a) Geometry of the chipless RFID tag. (b) Waveguide measurement setup..
Courtesy: Sreejith M Nair et. al. [38].
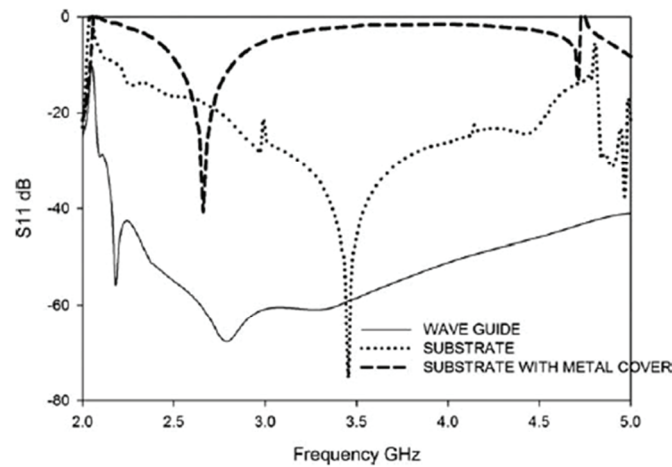
Figure 1.22 Simulated reflection coefficients of matched waveguide, matched waveguide loaded with substrate, and matched waveguide loaded with metalized substrate. Courtesy: Sreejith M Nair et. al. [38].

6. Chipless RFID Tag for Sensor Application

The main attracting applications of chipless RFID tag is to encode data along with sensor, which is used for detecting various conditions like humidity, pressure, temperature, presence of gases, etc. [47], [59] -[72]. In conventional RFID, physical parameters are detected by using chip IC or a passive lumped component. The analog voltage variations due to these sensors are generally converted to a digital signal with an ADC (Analog to Digital Converter) embedded in the tag IC and then stored in the memory. In chipless RFID tag sensors are working based on the variation of the amplitude, phase or resonant frequency of the backscattered signal with changes in the physical parameters.

Amplitude detection based chipless RFID tag sensor is reported in [63]. Depending on the level of water content behind the RFID tag, the backscattered signal strength changes so that this variation can be detected by the reading system. C like scatterer is used as the sensing element and the backscattered power from the tag with different water level are depicted in Fig.1.23.
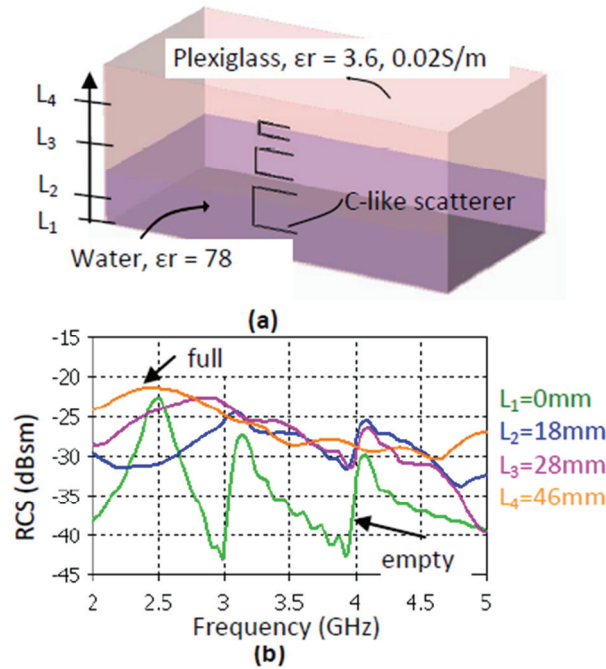
Figure 1.23 (a) "C" shape resonators embeded in a water tank. (b) │RCS│ results obtained with CST Microwave Studio. Courtesy: A. Guillet et. al. [63].

Chipless RFID tag for temperature sensing is reported in [65]. Tag performs real time temperature sensing using the dielectric property of temperature dependent high K polyamides. Introducing high K dielectric material changes the equivalent capacitance of the LC resonator which varies with environmental temperature. A dedicated resonator can perform the sensing whereas the other cascaded resonators used for encoding the ID of the tag. Fig.1.24 shows the top and side view of the spiral resonator modified with Stanyl Polyamide for temperature sensing. Stanyl polyamide has a linear variation of dielectric constant with temperature, ie., dielectric constant of the material increases with increasing temperature. Measured resonant frequency variation with dielectric constant is shown in Fig.1.25; here other two resonant frequencies are used to encode the ID.
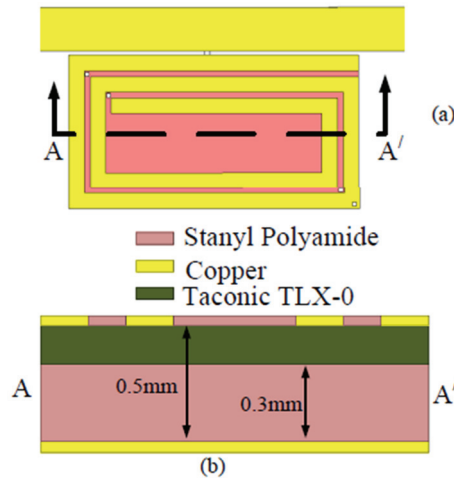
Figure 1.24 Layout of modified spiral resonator as a temperature sensor (a) Top view. (b) Cross sectional view. Courtesy: E. Amin et. al. [65].
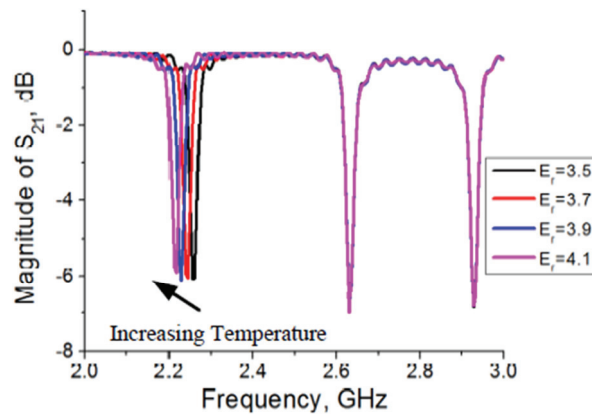
Figure 1.25 Measured magnitude of Insertion Loss (S$_{21}$) of the RFID tag with modified spiral resonator. Courtesy: E. Amin et. al. [65].

The CNL (Carbon Nanotube Loaded) in chipless RFID tag comprises a UHF RFID antenna and a single-walled carbon nanotube (SWCNT) designed for toxic gas detection is reported in [47]. The CNL chipless RFID tag is shown in Fig.1.26. The antenna and SWCNT were printed using inkjet printing technology. The chipless tag antenna is a bowtie meander-line dipole antenna. The SWCNT is placed between the input ports of the antenna in order to enable data encoding.

The SWCNT is highly sensitive to the presence of ammonia (NH_3), and its impedance characteristics when placed in air and NH_3 are shown in Fig.1.27. From Fig.1.27 it is clear that the CNL chipless RFID tag operates by varying the amplitude of the backscattered signal, depending on the concentration of NH3. Amplitude variation of the backscattered signal is due to the RCS variation influenced by the change of the impedance of SWCNT. The amplitude variation of the backscattered power of the tag can be detected at the reader end and decoded to estimate the level of NH3.
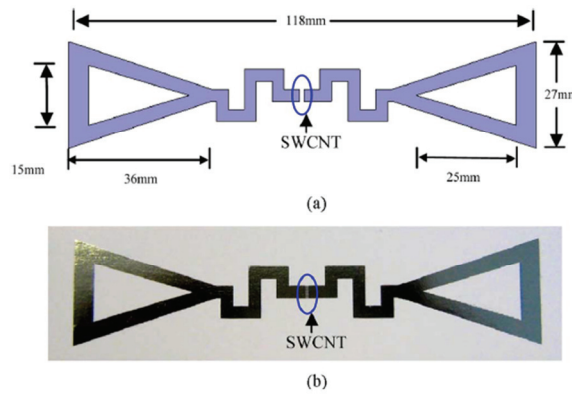
Figure 1.26 The RFID tag module on flexible substrate: (a) configuration; (b) photograph of the tag with inkjet-printed SWCNT film as a load. Courtesy: L. Yang et. al. [47].
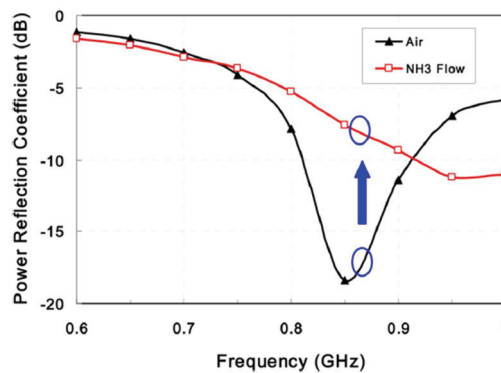
Figure 1.27 The calculated power reflection coefficient of the RFID tag with a SWCNT film before and after the gas flow. Courtesy: L. Yang et. al. [47].

7. Data Encoding Techniques in Chipless RFID

Different bit encoding techniques are reported in the literature for time and frequency domain based tags. Encoding technique will enhance data storage capacity of the tag while keeping the tag size small. Different data encoding techniques are

7.1. Pulse Position Modulation (PPM)

PPM method is effectively utilised in the time domain based RFID tags. The incident pulse from the reader is received by the tag antenna and guided through the substrate (for SAW tag) [16] or transmission line [34]-[36], [49]. Several reflectors along the substrate or transmission line with different lengths are used to create reflected pulses at specific times. Depending on the reflected pulse position, the reader can extract the ID using PPM (Pulse Position Modulation) scheme. Fig.1.28 shows the PPM technique used in the SAW tag and Fig.1.29 shows the PPM technique implanted on a transmission delay line based tag [49].
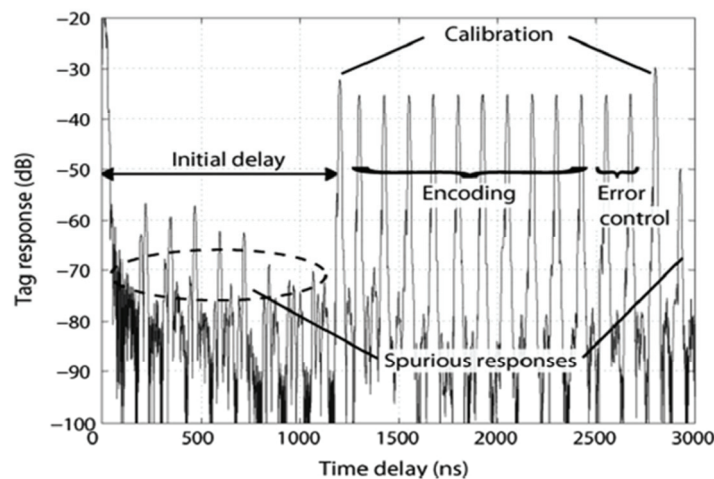
Figure 1.28 Simulated SAW tag Response. Courtesy: T. Han et. al. [16].
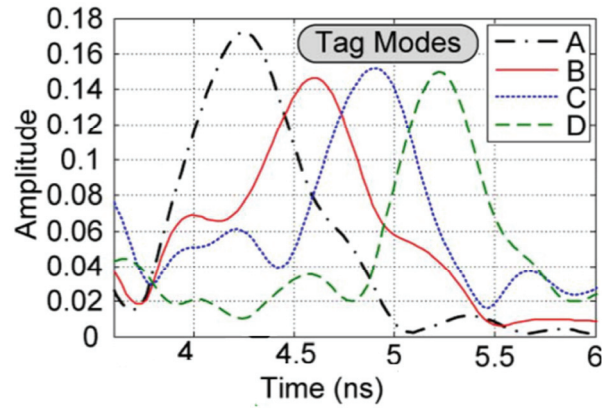
Figure 1.29 Measured time responses of four tags with different delays [49].

7.2. Presence or Absence Coding Technique

This technique is used in frequency domain based tag [39]-[42], in which each resonator is assigned with predetermined frequency. Presence or absence of resonance at that frequency determines the data (0 or 1). Hence, one resonator can store one bit information. As data encoding increases, the size of the tag also increases. Fig.1.30 shows the method of encoding data; here half wavelength dipole is used as a microwave resonator. Schematic diagram (as seen in Fig.1.30) of a backscattered signal with and without second resonator can encode two different spectral ID (1111 and 1011).
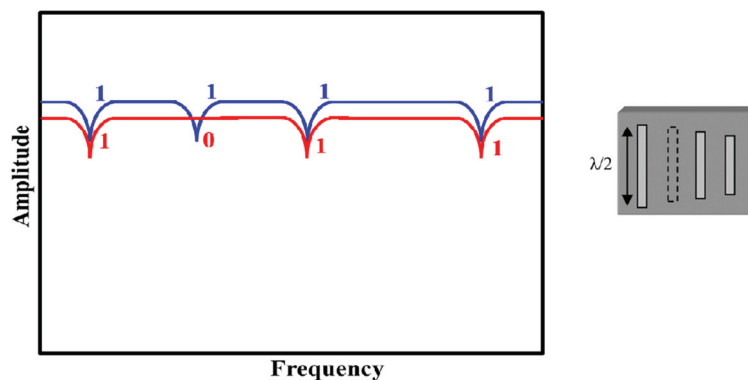
Figure 1.30 Presence or Absence coding technique, scattered signal with and without second resonator.

7.3 . Phase Coding Technique.

The phase can also be used to encode data by adding complex load in the resonator or antenna. Phase encoding method in the backscattered signal with structural variation of the resonator is presented [73] and Fig.1.3 shows the backscattered phase changes with different structural variation. Balbin et. al. [12] use multiple patch antennas connected to a stub of variable length and encode data by varying the phase of each antenna independently.
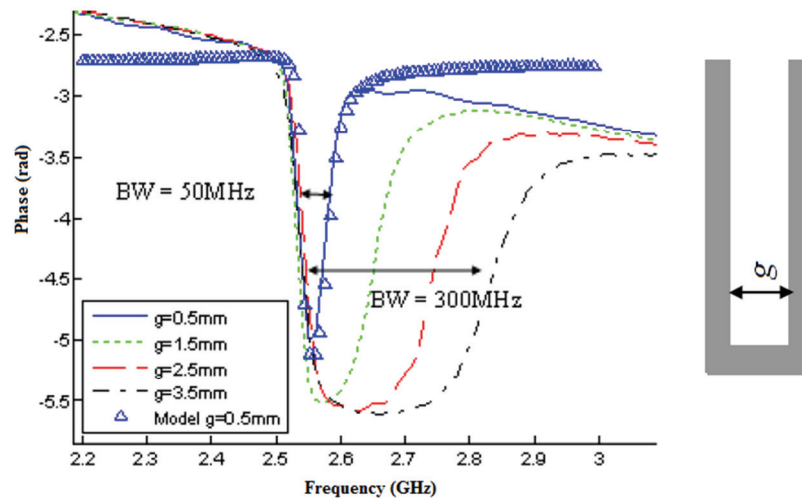
Figure 1.31 Phase encoding technique. Courtesy: A. Vena et. al. [73].

7.4. Frequency Shift Coding (FSC) Technique

Apart from using the presence or absence of resonance, in FSC, resonators are assigned with different frequency band [51]-[52]. Fig.1.32 shows the method of encoding data for N resonator using FSC technique. Here resonators are assigned with a frequency span (Δf) and each frequency span is divided into different resolution bandwidth (δf). The δf represents the bandwidth required for the resonator to represent its resonant dip or peak. Therefore, one resonator can represent more number of states. This method is

more appropriate to encode large data while RFID tag having lesser number of resonators.
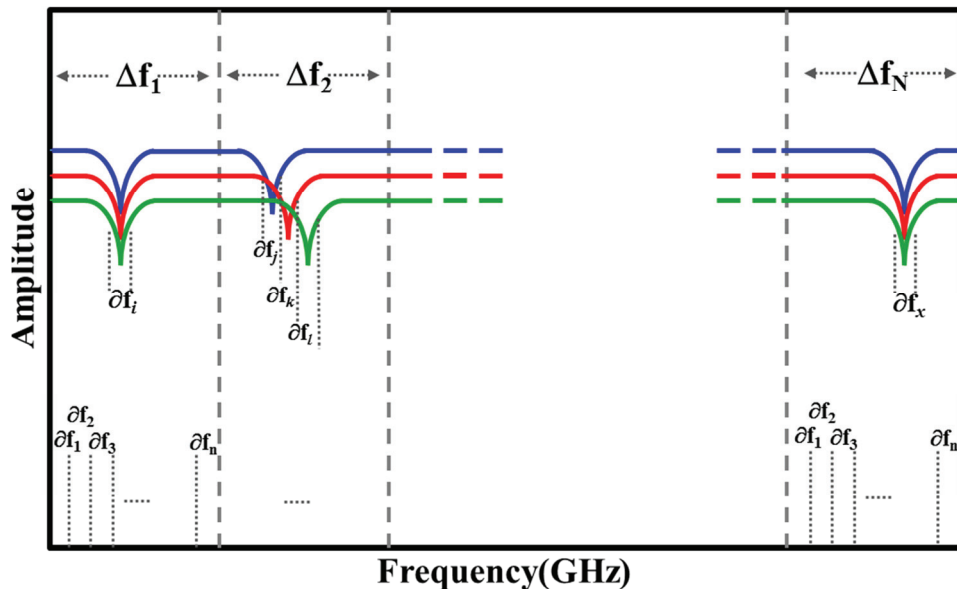
Figure 1.32 Frequency Shift Coding Technique. Courtesy: A. Vena et. al. [52].

7.5. Hybrid Coding Technique

This coding method is proposed by Arnaud Vena et.al. [51]. The technique is a combination of Frequency Shit Coding and Phase Coding Technique. Author proposes a tag consist of 'C' like resonator (as seen in Fig.1.33), in which resonant frequency and phase can be controlled independently. The resonant frequency is controlled by the length of the resonator (L) ($\lambda/2$ resonator) and phase variation is done by varying the gap (g). The technique delivers good encoding capacity, but it requires frequency spectrum of around 500MHz to accommodate change in the phase variation. Resonators with independent control over resonant frequency and phase are difficult to achieve.
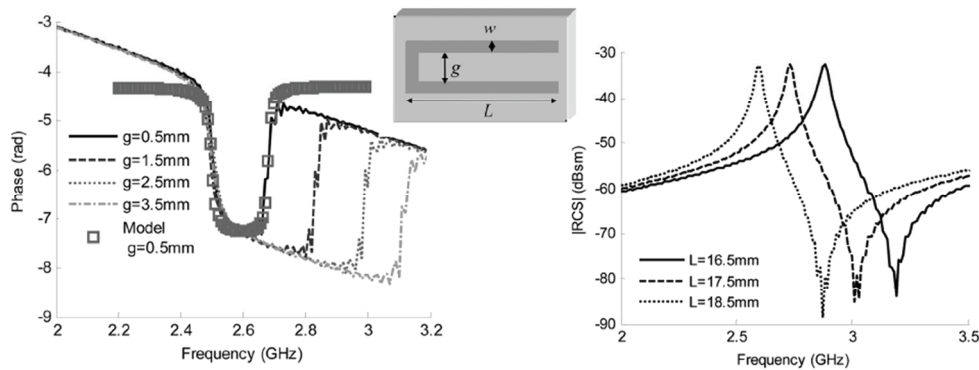
Figure 1.33 Hybrid Coding Technique, Phase is varied by changing the gap (g) and the resonant frequency is varied by length L. Courtesy: A. Vena et. al. [51].

8. Thesis Outline

The thesis investigates both frequency spectra based chipless RFID tags (Multiresonating and Multiscatterer). The first type of tag is a multiresonator based one and it demonstrated using microstrip open stub resonators with a data encoding capacity of 8 bits. Another tag based on multiscatterer is designed using Stepped Impedance Resonator with a data encoding capacity of 79 bits. Time domain analysis of the backscattered signal is also investigated with a practical measurement scenario.

The objectives of the work presented in the thesis are:

❖ To identify the suitable resonators for encoding information in the frequency domain.

❖ Design of compact tags using above resonators.

❖ Find methods for encoding more number of bits using new techniques.

❖ Selection of suitable calibration technique.

❖ Extraction of the spectral content of RFID tag from the backscattered signal with different practical scenario like noisy signal, moving target, paper pack, metal container, etc.

❖ Development of an algorithm for the spectral extraction from backscattered signal.

❖ Development of an RFID reader prototype.

Organisation of the thesis

This section provides a brief description of the chapters presented in this thesis.

Chapter 1: Introduction to RFID Technology

This chapter describes the available RFID tags in the literature and its working principle. The evolution of chipless RFID technology and theory behind its working is also discussed. This chapter presents a comprehensive review of available chipless RFID tags on the market and reported in peer-reviewed journals and conferences. Chipless RFID tags based on different encoding techniques are reviewed with illustrations.

Chapter 2: Multiresonator Based Chipless RFID Tag using Microstrip Open Stub Resonator

A compact chipless RFID tag using microstrip open stub resonator is discussed in this chapter. Equivalent circuit of single open stub resonator is designed and validated with Agilent ADS and Ansys HFSS software. The chapter also deals with a parametric study for the optimisation of frequency bandwidth to incorporate more number of resonances in a limited frequency span. An 8 bit RFID tag consists of two UWB antenna and multiresonating

circuit using open stub resonator is presented and its working is validated experimentally.

Chapter 3: Multiscatterer Based Chipless RFID Tags using Stepped Impedance Resonator (SIR)

The design of a UWB (3.1-10.6GHz) chipless RFID tag utilising SIR as multiscatterer is described in this chapter. Advantages of SIR, such as independent control over harmonic modes and control over the electrical lengths are also utilised for tag design. Three types of RFID tags with different bit encoding techniques and coding density of 79bits with five SIRs are discussed. Different bit encoding techniques is also incorporated for the enhancement of bit encoding capacity. A simple amplitude detection method for identifying resonant dips in the backscattered signal is also proposed.

Chapter 4: RFID Reader for Multiscatterer Based Chipless RFID Tags

A simple working setup of chipless RFID reader with single antenna as transmitter and receiver is explained in this chapter. MIT Coffee Can RADAR is modified as an RFID reader working in the ISM band centred at 2.4GHz. Proposed reader can be used for signal extraction from multiscatterer based tag and successfully decoded the data up to a distance of 5cm. RFID tag with single bit and two bits are measured using proposed tag and its results are validated with Network Analyser.

Chapter 5: Time Domain Analysis of Frequency Spectra Based Chipless RFID Tags

Benefits of time domain analysis using UWB Impulse Radar techniques on the frequency spectra based tag is discussed in this chapter. By combining time domain analysis on frequency spectra based tag, enables the

spectral extraction and identification of data from noisy signals, moving items, metallic containers, etc. Simple algorithm is also developed for removing or minimising unwanted reflection from the backscattered signal.

Chapter 6: Conclusion and Future Perspective

All the relevant points about the work are concluded in the thesis with an insight to future work

The thesis also includes the bibliography and a list of publications by the author in the related field.

Appendix: 2.4GHz ISM Band Doppler Radar

Appendix explains the working principle of RADAR capable of sensing range and relative speed. Architecture of Doppler RADAR is presented with six RF components from mini-circuit and it is designed to operate at 2.4GHz ISM band. Measurements were taken inside the university campus road and relative speed of vehicles is calculated from the doppler frequency shift.

9. Reference

[1] H. Stockman, "Communication by means of reflected power," Proc. IRE, pp. 1196–1204, Oct. 1948.

[2] Y. Xiao, S. Yu, K. Wu, Q. Ni, C. Janecek and J. Nordstad, "Radio Frequency Identification: Technologies, Applications, and Research Issues", WIRELESS COMMUNICATIONS AND MOBILE COMPUTING Wirel. Commun. Mob. Comput. 2007.

[3] E. Perret, S. Tedjini and R.S. Nair, "Design of Antennas for UHF RFID Tags", Proceeding of the IEEE, Vol.100, Issue 7, pp.2330-2340.

[4] M.R. H. Khandokar, G. Tangim, M. K. Islam, M. N. I. Maruf, "Simultaneously Multiple 3D Barcodes Identification Using Radio Frequency", 2nd International Conference on Signal Processing Systems (ICSPS), 2010, pp.633-636.

[5] G. R.T. White, G. Gardiner, G. Prabhakar, and A. A. Razak, "A Comparison of Barcoding and RFID Technologies in Practice," Journal of Information, Information Technology, and Organizations, Volume 2, 2007, pp.119-132.

[6] IDTechEx. An Introduction to RFID and Tagging Technologies, 2002.

[7] Arkansas Radio Compliance Retail Suppliers: Available online http://rfid.uark.edu/2060.asp.

[8] Smail Tedjini, Nemai Karmakar, Etienne Perret, Arnaud Vena, Randika Koswatta, and Rubayet E-Azim , "Hold the Chip" IEEE microwave magazine, August 2013.

[9] V. Subramanian, J. M. J. Fréchet, P. C. Chang, D. C. Huang, J.B. Lee, S. E. Molesa, A. R. Murphy, D. R. Redinger, And S. K. Volkman, "Progress Toward Development of All-Printed RFID Tags: Materials, Processes, and Devices", Invited Paper, Proceedings of the IEEE, Vol. 93, No. 7, July 2005, pp. 1330-1338.

[10] S. Harma, V. P. Plessky, C. S. Hartmann, and W. Steichen, "SAW RFID tag with reduced size," in Proc. IEEE Ultrasonics Symp. 2006, Vancouver, Canada, Oct. 2006, pp. 2389–2392.

[11] Y. Y. Chen, T. T. Wu, and K. T. Chang, "A COM analysis of SAW tags operating at harmonic frequencies," in Proc. IEEE Ultrasonics Symp. 2007, New York, Oct. 2007, pp. 2347–2350.

[12] S. Harma, V. P. Plessky, L. Xianyi, and P. Hartogh, "Feasibil- ity of ultra-wideband SAW RFID tags meeting FCC rules," IEEE Trans. Ultrason., Ferroelect., Freq. Contr., vol. 56, no. 4, pp. 812–820, Apr. 2009.

[13] S. Harma, V. P. Plessky, and X. Li, "Feasibility of ultra-wideband SAW tags," in Proc. IEEE Ultrasonics Symp. 2008, Beijing, China, Nov. 2008, pp. 1944–1947.

[14] P. Brown, P. Hartmann, A. Schellhase, A. Powers, T. Brown, C. Hartmann, and D. Gaines, "Asset tracking on the international space station using global SAW tag RFID technology," in Proc. IEEE Ultrasonics Symp. 2007, New York, Oct. 2007, pp. 72–75.

[15] V. P. Plessky, S. N. Kondratiev, R. Stierlin, and F. Nyffeler, "Saw tags: New ideas," in Proc. IEEE Ultrasonics Symp. 1995, Cannes, France, Nov. 1995, vol. 1, pp. 117–120.

[16] T. Han, W. Wang, H. Wu, and Y. Shui, "Reflection and scatter- ing characteristics of reflectors in SAW tags," IEEE Trans. Ultrason., Ferroelect., Freq. Contr., vol. 55, no. 6, pp. 1387–1390, June 2008.

[17] T. Han, W. Wang, J. M. Lin, H. Wu, H. Wang, and Y. Shui, "Phases of carrier wave in a SAW identification tags," in Proc. IEEE Ultra- sonics Symp. 2007, New York, Oct. 2007, pp. 1669–1672.

[18] N. Saldanha and D. C. Malocha, "Design parameters for SAW multi-tone frequency coded reflectors," in Proc. IEEE Ultrasonics Symp. 2007, New York, Oct. 2007, pp. 2087–2090.

[19] S. Harma, C. Kim, S. M. Balashov, and V. P. Plessky, "Properties of narrow metal reflectors used in reflective array compressors and

surface acoustic wave tags," in IEEE MTT-S Int. Microwave Symp. Dig. 2007, Honolulu, HI, June 2007, pp. 2051–2054.

[20] D. Puccio, D. Malocha, and N. Saldanha, "Implementation of orthogonal frequency coded SAW devices using apodized reflectors," in Proc. IEEE Int. Frequency Control Symp. Exposition 2005, Vancouver, Canada, Aug. 2005, pp. 892–896.

[21] S. Harma, W. G. Arthur, C. S. Hartmann, R. G. Maev, and V. P. Plessky, "Inline SAW RFID tag using time position and phase encoding," IEEE Trans. Ultrason., Ferroelect. Freq. Contr., vol. 55, no. 8, pp. 1840–1846, Aug. 2008.

[22] S. Harma, V. P. Plessky, C. S. Hartmann, and W. Steichen, "Z-path SAW RFID tag," IEEE Trans. Ultrason., Ferroelect., Freq. Contr., vol. 55, no. 1, pp. 208–213, Jan. 2008.

[23] S. Harma, W. G. Arthur, R. G. Maev, C. S. Hartmann, and V. P. Plessky, "Inline SAW RFID tag using time position and phase encoding," in Proc. IEEE Ultrasonics Symp. 2007, New York, Oct. 2007, pp. 1239–1242.

[24] J. Liu and J. Yao, "Wireless RF identification system based on SAW," IEEE Trans. Ind. Electron., vol. 55, no. 2, pp. 958–961, Feb. 2008.

[25] N. Saldanha and D. C. Malocha, "Low loss SAW RF ID tags for space applications," in Proc. IEEE Ultrasonics Symp. 2008, Beijing, China, Nov. 2008, pp. 292–295.

[26] L. Wei, H. Tao, and S. Yongan, "Surface acoustic wave based radio frequency identification tags," in Proc. IEEE Int. Conf. e-Business Engineering 2008, Xi'An, China, Oct. 2008, pp. 563–567.

[27] J. Yao, J. Liu, and B. Gao, "The realization of a passive identification tag transmitter based on SAW," in Proc. 4th Int. WirelessCommunications, Networking and Mobile Computing 2008, Dalian, China, Oct. 2008, pp. 1–4.

[28] J. Liu and J. Yao, "A new wireless RF identification system," in Proc. 6th World Congr. Intelligent Control and Automation 2006, Dalian, China, June 2006, pp. 5191–5195.

[29] S. Schuster, S. Scheiblhofer, A. Stelzer, and A. Springer, "Model based wireless SAW tag temperature measurement," in Proc. Asia-Pacific Microwave Conf. (APMC) 2005, Suzhou, China, Dec. 2005, pp. 4–7.

[30] E. L. Tan and Y. W. M. Chia, "Green's function and network analysis of quasi-2D SAW ID-tags," in Proc. IEEE Ultrasonics Symp. 2000, San Juan, PR, Oct. 2000, pp. 55–58.

[31] D. Enguang and F. Guanping, "Passive and remote sensing based upon surface acoustic wave in special environments," in Proc. Microwave and Optoelectronics Conf. 1997, Natal, Brazil, Aug. 1997, vol. 1, pp. 133–139.

[32] D. Puccio, D. C. Malocha, N. Saldanha, D. R. Gallagher, and J. H. Hines, "Orthogonal frequency coding for SAW tagging and sensors," IEEE Trans. Ultrason., Ferroelect., Freq. Contr., vol. 53, no. 2, pp. 377–384, Feb. 2006.

[33] G. Buckner and R. Fachberger, "SAW ID tag for industrial application with large data capacity and anticollision capability," in Proc. IEEE Ultrasonics Symp. 2008, Beijing, China, Nov. 2008, pp. 300–303.

[34] A. Chamarti and K. Varahramayan, "Transmission delay line- based ID generation circuit for RFID applications," IEEE Micro- wave Wireless Compon. Lett., vol. 16, no. 11, pp. 588–590, Nov. 2006.

[35] J. Vemagiri, A. Chamarti, M. Agarwal, and K. Varahramyan, "Transmission line delay-based radio frequency identification (RFID) tag," Microwave Opt. Technol. Lett., vol. 49, no. 8, pp. 1900– 1904, 2007.

[36] S. Shretha, J. Vemagiri, M. Agarwal, and K. Varahramyan, "Transmission line reflection and delay-based ID generation scheme for RFID and other applications," Int. J. Radio Freq. Identification Tech- nol. Appl., vol. 1, no. 4, pp. 401–416, 2007.

[37] Raji Nair, Etienne Perret, and Smail Tedjini, "Novel Encoding in Chipless RFID Using Group Delay Characteristics" 2011 SBMO/IEEE MTT-S International Microwave & Optoelectronics Conference (IMOC), Oct. 29-Nov. 1, 2011.

[38] S. Preradovic, I. Balbin, and N. Karmakar, "The development and design of a novel chipless RFID system for low-cost item tracking," in Proc. Asia Pacific Microwave Conf. (APMC) 2008, Hong Kong, Dec. 2008, pp. 1–4.

[39] S. Preradovic and N. Karmakar, "Design of fully printable planar chipless RFID transponder with 35-bit data capacity," in Proc. 39th European Microwave Week, Rome, Italy, Sept. 2009, pp. 13–16.

[40] S. Preradovic, S. Roy, and N. Karmakar, "Fully printable multibit chipless RFID transponder on flexible laminate," in Proc. Asia Pacific Microwave Conf. (APMC'09), Singapore, Dec. 2009, pp. 2371– 2374.

[41] S. Preradovic, I. Balbin, N. Karmakar, and G. Swiegers, "A novel chipless RFID system based on planar multiresonators for bar code replacement," in Proc. IEEE Int. Conf. RFID 2008, Las Vegas, NV, Apr. 2008, pp. 289–296.

[42] Md. Shakil Bhuiyan, AKM Azad and Nemai Karmakar, "Dual-band Modified Complementary Split Ring Resonator (MCSRR) Based Multi-resonator Circuit for Chipless RFID Tag" 2013 IEEE Eighth International Conference on Intelligent Sensors, Sensor Networks and Information Processing, Melbourne, VIC, 2-5 April 2013, pp- 277 – 281.

[43] Pimsiripom Narkcharoen and Suneat Pranonsatit, "The Applications of Fill until Full (FuF) for Multiresonator-based Chipless RFID System", The 8th Electrical Engineeringl Electronics, Computer, Telecommunications and Information Technology (ECTI) Association of Thailand - Conference 2011, pp -176-179.

[44] Giovanni Andrea Casula, Giorgio Montisci, Paolo Maxia and Giuseppe Mazzarella, "A narrowband chipless multiresonator tag for UHF RFID", Journal of Electromagnetic Waves and Applications, Vol. 28, No. 2, 214–227, January 2014.

[45] M. Nair Sreejith, V. A. Shameena, M. Nijas, and P. Mohanan, "Novel chipless rf identification technology for on-touch data transfer applications", Microwave and Optical Technology Letters, Vol. 54, No. 10, October 2012.

[46] I. Jalaly and D. Robertson, "RF barcodes using multiple frequency bands," in IEEE MTT-S Microwave Symp. Dig., Long Beach, CA, Jun. 2005, pp. 139–141.

[47] L. Yang, R. Zhang, D. Staiculescu, C. P. Wong, and M. M. Tentzeris, "A novel conformal RFID-enabled module utilizing inkjet-printed antennas and carbon nanotubes for gas-detection applications," IEEE Antennas Wireless Propagat. Lett., vol. 8, pp. 653–656, 2009.

[48] David Girbau, Ángel Ramos, Antonio Lázaro, Sergi Rima, and Ramón Villarino, "Passive Wireless Temperature Sensor Based on Time-Coded UWB Chipless RFID Tags", IEEE Transactions on Microwave Theory and Techniques, Vol. 60, No. 11, November 2012.

[49] S. Mukherjee, "Chipless radio frequency identification by remote measurement of complex impedance," in Proc. 37th Euro. Microwave Week, Munich, Germany, Oct. 2007, pp. 1007–1010.

[50] I. Balbin and N. C. Karmakar, "Phase-encoded chipless RFID transponder for large-scale low-cost applications," IEEE Microw. Wireless Compon. Lett., vol. 19, no. 8, pp. 509–511, Aug. 2009.

[51] Arnaud Vena, Etienne Perret and Smail Tedjini, "Chipless RFID Tag Using Hybrid Coding Technique", IEEE Transactions on Microwave Theory and Techniques, Vol. 59, No. 12, December 2011.

[52] Arnaud Vena, Etienne Perret and Smail Tedjini, "A Depolarizing Chipless RFID Tag for Robust Detection and Its FCC Compliant UWB Reading System", IEEE Transactions on Microwave Theory and Techniques, VOL. 61, NO. 8, August 2013.

[53] M.Manteghi, "A space-time-frequency target identification technique for chipless RFID applications," in Proc. IEEE Antennas Propag. Soc. Int. Symp. (APSURSI), 2011, pp. 1–4.

[54] M. Manteghi and Y. Rahmat-Samii, "Frequency notched UWB ellip- tical dipole tagwith multi-bit data scattering properties," in Proc.IEEE Antennas Propag. Soc. Int. Symp., San Diego, CA, USA, 2007, pp. 789–792.

[55] A. Blischak and M. Manteghi, "Pole residue techniques for chipless RFID detection," in Proc. IEEE Antennas Propag. Soc. Int. Symp., 2009, pp. 1–4.

[56] A. Blischak and M. Manteghi, "Pole-residue analysis of a notched UWB elliptical dipole tag," presented at the URSI-USNC National Radio Science Meeting, Boulder, CO, USA, 2009.

[57] A. T. Blischak and M.Manteghi, "Embedded singularity chiplessRFID tags," IEEE Trans. Antennas Propag., vol. 59, no. 11, pp. 3961–3968, Nov. 2011.

[58] Md. Aminul Islam and Nemai Chandra Karmakar "A Novel Compact Printable Dual-Polarized Chipless RFID System", IEEE Transactions on Microwave Theory and Techniques, Vol. 60, No. 7, July 2012.

[59] Sangkil Kim, Manos M. Tentzeris, Anya Traille, Hervé Aubert, "A Dual-Band Retro directive Reflector Array on Paper Utilizing Substrate Integrated Waveguide (SIW) and Inkjet Printing Technologies for Chipless RFID Tag and Sensor Applications", 2013 IEEE MTT-S International Microwave Symposium Digest (IMS), Seattle, WA, PP No. 1 – 4, 2-7 June 2013.

[60] Stevan Preradovic, Nemai Kamakar, Emran Md. Amin, "Chipless RFID Tag with Integrated Resistive and Capacitive Sensors", Proceedings of the Asia-Pacific Microwave Conference 2011, pp. 1354 – 1357, 2011.

[61] E. Amin, S. Bhuiyan, and Nemai C. Karmakar, "Development of a Low Cost Printable Chipless RFID Humidity Sensor,", IEEE Sensors Journal, Vol. 14, No. 1, January 2014.

[62] S. Shrestha, M. Balachandran, Mangilal Agarwal, Vir V. Phoha and Kody Varahramyan, "A Chipless RFID Sensor System for Cyber Centric Monitoring Applications," IEEE Transactions on Microwave Theory and Techniques, Vol. 57, No. 5, May 2009.

[63] A. Guillet, A. Vena, E. Perret, and S. Tedjini, "Design of a chipless RFID sensor for water level detection," 2012 15 Int. Symp. Antenna Technol. Appl. Electromagn., pp. 1–4, Jun. 2012.

[64] S. Kim, J. Cooper, M. M. Tentzeris, R. Herre, S. Gu, and T. Lasri, "A novel inkjet-printed chipless RFID-based passive fluid sensor platform," 2013 IEEE Sensors, pp. 1–4, Nov. 2013.

[65] E. Amin and Nemai Karmakar, "Development of a Chipless RFID Temperature Sensor Using Cascaded Spiral Resonators," IEEE Sensors, pp. 554- 557, 2011.

[66] S. Kim, M. M. Tentzeris, L. Cnrs, Anya Traille and Hervé Aubert "A Dual-Band Retrodirective Reflector Array on Paper Utilizing Substrate Integrated Waveguide (SIW) and Inkjet Printing Technologies for Chipless RFID Tag and Sensor Applications," pp. 2301–2302, 2013.

[67] A. Vena, E. Moradi, K. Koski, A. Babar, L. Sydänheimo, Manos M. Tentzeris and L. Ukkonen, "Design and Realization of Stretchable Sewn Chipless RFID Tags and Sensors for Wearable Applications," 2013 IEEE International Conference on RFID Design, Orlando. FL, USA, pp. 176–183, 2013.

[68] E. Amin, N. Karmakar, A. C. Rfid, and P. D. Sensor, "Partial Discharge Monitoring of High Voltage Equipment Using Chipless RFID Sensor," Proceedings of the Asia-Pacific Microwave Conference 2011, pp. 1522–1525, 2011.

[69] M. Hasani, S. Member, A. Vena, L. Sydänheimo, L. Ukkonen, and M. M. Tentzeris, "Implementation of a Dual-Interrogation-Mode Embroidered RFID-Enabled Strain Sensor," IEEE Antennas and Wireless Propagation Letters, Vol. 12, pp. 1272–1275, 2013.

[70] A. Lazaro, A. Ramos, R. Villarino, and D. Girbau, "Active UWB Reflector for RFID and Wireless Sensor Networks," IEEE Transactions on Antennas and Propagation, Vol. 61, No. 9, Pp. 4767–4774, September 2013.

[71] E. M. Amin and N. C. Karmakar, "Development of A Low Cost Printable Humidity Sensor for Chipless," IEEE 2012 International Conference on RFID -Technologies and Applications (RFID - TA), pp. 165–170, 2012.

[72] W. T. Chen, K. M. E. Stewart, J. Carroll, R. Mansour, and A. Penlidis, "Novel Gaseous Phase Ethanol Sensor Implemented With Under loaded RF Resonator For Sensor-Embedded Passive Chipless RFIDs, The 17th International Conference on Solid-State Sensors, Actuators and Microsystems (TRANSDUCERS & EUROSENSORS XXVII), Barcelona, pp. 2059–2062, June 2013.

[73] A. Vena, E. Perret, and S. Tedjini, "RFID chipless tag based on multiple phase shifters," in 2011 IEEE MTT-S International Microwave Symposium, 2011, pp. 1–4.

.... ೞ೩ ....

Chapter **2**

MULTIRESONATOR BASED CHIPLESS RFID TAG USING MICROSTRIP OPEN STUB RESONATOR

Abstract

Compact multiresonator based chipless RFID tag employing open stubs in a microstrip transmission line is proposed. The prototype of the tag is fabricated on a substrate of dielectric constant 4.4 and loss tangent 0.0018. The multiresonator tag consists of microstrip open stub resonators and cross polarised transmitting and receiving disc monopole antennas. Equivalent circuit of the single bit tag is studied and validated with simulation results. A prototype of 8 bit data encoded tag is demonstrated in this chapter. Method for enhancing the performance of the RFID tag is also proposed. Magnitude or group delay response of the backscattered signal is used to decode the tag information. The readable range of the tag is found to be 40cm inside the anechoic chamber, using a PNA E8362B network analyser with source power of 0dBm.

2.1. Introduction

As explained in the earlier chapter, the frequency spectra based chipless RFID tags can be divided into two categories, multiresonator and multiscatterer based tags. This chapter highlights the design and development of multiresonator based tag. It consist of a receiving antenna for the reception of the interrogation signal from the RFID reader, a multi resonating structure consist of a number of resonators and a retransmitting antenna. Multiresonator circuit is basically a narrow band rejection filter comprises of different resonators and it will alter the amplitude and phase of the interrogating signal. The output of the filter is connected to a transmitting antenna which will retransmit the encoded signal back to the reader. Block diagram of the multiresonator based chipless RFID system is depicted in Fig.2.1. The system is not based on radar cross section (RCS) backscattering, but on retransmission of the interrogation signal with the encoded unique spectral ID. RFID reader for the multiresonator based system consists of two linearly polarised wide band antennas orthogonally polarised to each other. This arrangement helps the reader to minimise direct coupling between the reader antennas and also reduces the mutual coupling between the interrogation and backscattered signals. RFID reader comprises of a wide band microwave source and other RF device like Low Noise Amplifier (LNA), directional coupler, power splitters, frequency mixer, etc. Reader has to generate an interrogation signal with constant phase and amplitude as shown in Fig.2.1. Backscattered or retransmitted signal from the chipless tag will have different amplitude and phase, which depends on the characteristics of the multiresonating circuit. A control section is also needed in the reader system to manage all the activities and communication with middleware software.
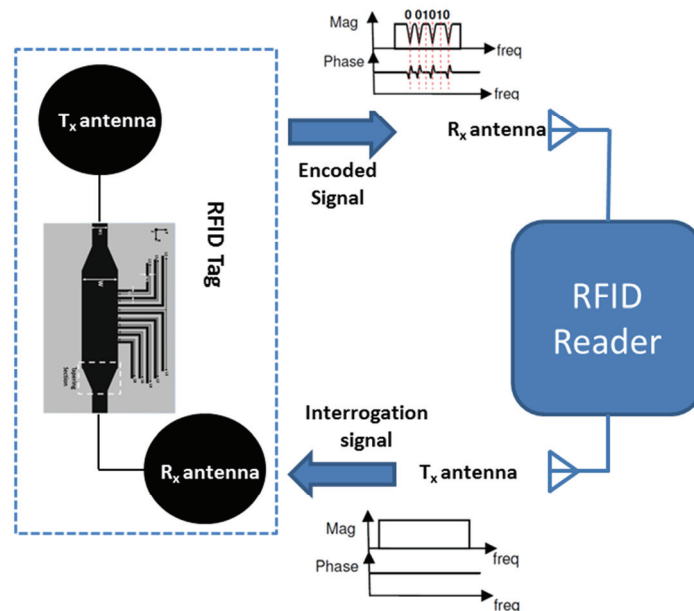
Figure 2.1 Block diagram of the multiresonator based RFID system

Components of a multiresonator based tag are

2.1.1. Multiresonating circuits

2.1.2. Receiving and retransmitting UWB antenna

2.1.1. Multiresonating Circuits

Numerous chipless RFID tags are reported based on the method proposed by Stevan Preradovic et.al. [1]-[9]. Multiresonating circuit is designed to attenuate particular frequency in the desired band. Basic resonators used in the design of multiresonating circuits are spiral, hair pin, 'C' like structures, split ring resonator (SRR), Complementary SRR (CSRR), Stepped Impedance Resonator (SIR), etc. Most of the tags are designed on microstrip based resonators [1]-[7] and some of them are based on CPW [8]-[9]. In CPW based multiresonating circuits, resonators are etched in the feed lines. In the case of microstrip based circuits, resonators are either connected

or coupled to the transmission line. Because of the resonators in the feed line, CPW based multiresonating circuits create more insertion loss with number of resonators and also requires large space in the feed line to accommodate lower frequency resonators. Fig.2.2 shows some of the resonators reported in the literature for the design of multiresonating circuits. Fig.2.2 (a) to (d) shows the multiresonating circuits based on microstrip line and Fig.2.2 (e) & (f) are based on CPW. In all cases, the size of the multiresonating circuit depends on the number of parameters like operating frequency band, dielectric properties of the substrate, the separation between the resonators, common coupling area between the transmission line and resonator, etc.
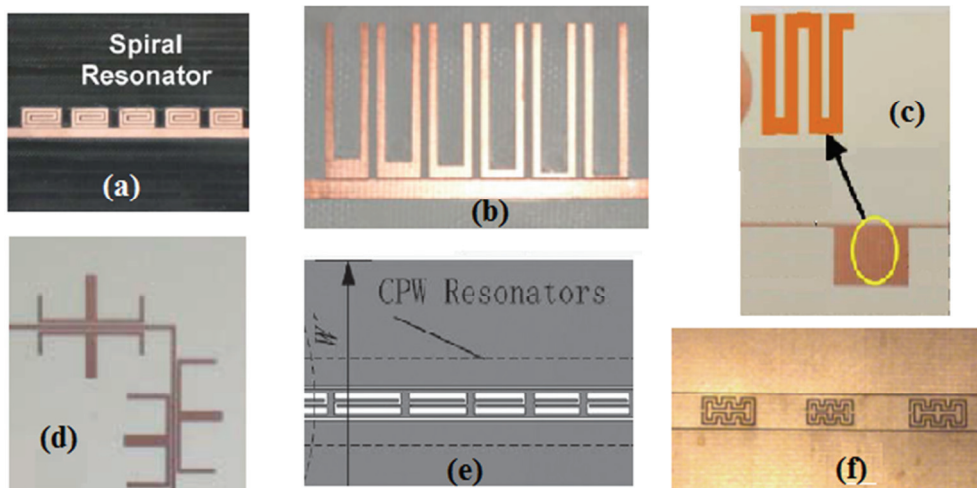
Figure 2.2 Reported resonators used for the design of multiresonator based tag. (a) to (d) : microstrip based resonators and (e) to (f): CPW based resonators.

2.1.2. Receiving and Retransmitting UWB Antenna

The complete design of RFID tag based on multiresonator requires two UWB antennas, one for receiving the interrogation signal from reader and another for retransmitting the encoded signal from the multiresonating circuits to the reader. This antenna should provide a good impedance match

and radiation characteristics at the desired frequency band. Fig.2.3 shows the reported antennas used in the design of the chipless tag. All the antennas are UWB with CPW or microstrip feed. The overall size of the antenna depends on substrate permittivity, geometry and lowest operating frequency of the tag. Compact tag antennas are preferred to accommodate more number of bits in a limited tag size (size of the credit card or bank note).
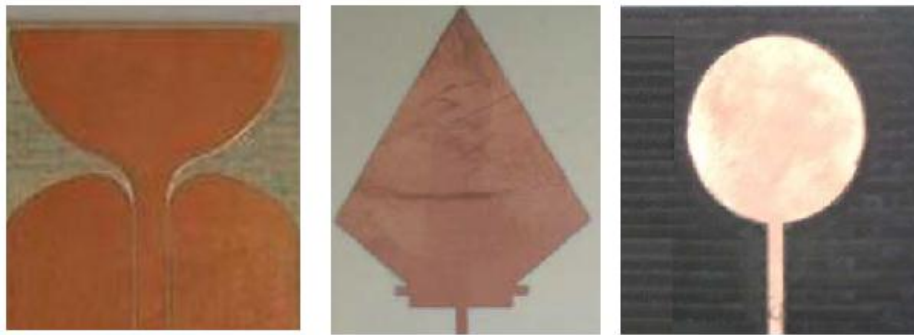
Figure 2.3 Reported antennas used for the design of multiresonator based chipless RFID tag [9],[7] and [1].

2.2. Expression for Free Space Losses in the Multiresonator Based Chipless RFID System

The expected power levels of the received signals from the chipless tags in an anechoic chamber (lossless environment) can be calculated using the Friis free-space transmission formula [10]. The power density of the signal that reaches the chipless RFID tag in free space is given by

$$S = \frac{P_t G_r}{4\pi r^2} \qquad (2.1)$$

where P_t is the transmitted power, G_r is the gain of the reader transmitting antenna and r is the distance between the tag and reader antenna. The power collected by the transponder antenna is defined as

$$P_a = SA_e = \frac{S\lambda^2 G_t}{4\pi} \tag{2.2}$$

where A_e is the effective area of the tag antenna, G_t is the gain of the tag antenna and λ is the wavelength. In this calculation, both antennas used by the RFID reader for transmission and reception of interrogation signal are identical. Similarly, antenna in the RFID tag for receiving and retransmitting is also considered as identical. Hence, the signal received by the reader after interrogating the tag is

$$P_{rx} = \frac{P_t \, G_t^2 G_r^2 \lambda^4 L(f)}{(4\pi r)^2} \tag{2.3}$$

where L(f) is the insertion loss of the tag's multiresonating circuit as a function of frequency f. Received signal strength P_{rx} should be above the noise floor, for the successful identification of backscattered signal. In the RFID system, the noise floor of the backscattered signal depends on the polarisation isolation between the reader antennas and environmental conditions (interference from different wireless systems, scattering from stationary objects, etc.)

2.3. Multiresonator Circuit Design Using Open Stub Resonator

This chapter proposes a multiresonator based chipless RFID tag using open stub resonators. The proposed tags are resonating at quarter wavelength ($\lambda/4$) whereas most of reported tag resonators are half wavelength ($\lambda/2$). Therefore, the sizes of the proposed resonators are small compared with other tags working on the same frequency. Another advantage is that open stub resonator is directly connected to the transmission line, but in normal tags a coupling is required. As shown in Fig.2.2, all the resonators have to be placed close to a transmission line with common coupling area between the two.

The evolution of an RFID tag from a simple microstrip transmission line using λg/4 open stub is demonstrated in Fig.2.4, where λg is the guided wavelength at the operating frequency. Ansys HFSS software is used for the simulation analysis. The width of the microstrip transmission line is found to be 3mm for 50Ω impedance and it is simulated on a substrate of dielectric constant 4.4, loss tangent 0.0018 and substrate height 1.6mm. To make compact tag, 'L' shape open stub resonator is placed on the transmission line as shown in Fig.2.4. Width (W_2) and length (L) of the open stub resonator is selected as 0.5mm and 21mm, respectively. The two 50Ω excitation ports are connected at the end of the microstrip transmission line with characteristic impedance of 50Ω (W_1 = 3mm). The simulated frequency response of the open stub resonator is depicted in Fig.2.5. Narrow band notch filter response at 2.12GHz is clearly shown in the figure. The resonant frequency (f_0) of a λg/4 resonator can be accurately found analytically by taking care of appropriate corrections due to open end [11] and microstrip bend [12] effects of the microstrip line. The length ΔL (seen in Fig.2.4) is the extended length due to open end fringing field on the microstrip line. Field distribution (surface current and E field) on the resonator at the resonant frequency (2.12GHz) is shown in Fig.2.6 and confirms the quarter wavelength operation at the resonant frequency.
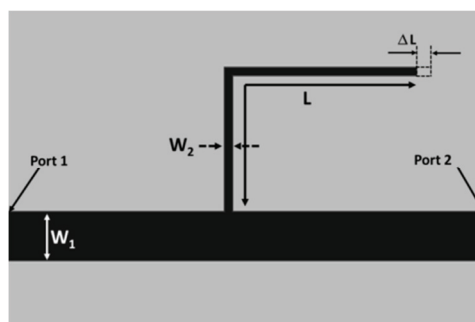
Figure 2.4 Microstrip Transmission line with open stub resonator, W_1 = 3mm, W_2 = 0.5mm, L = 21mm and ΔL = 0.629mm.
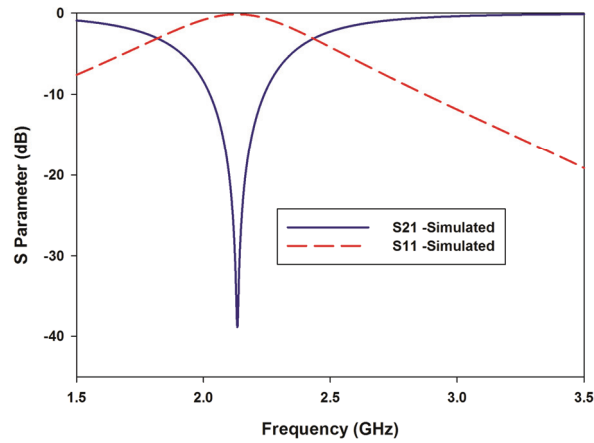
Figure 2.5 Simulated frequency response of the open stub resonator
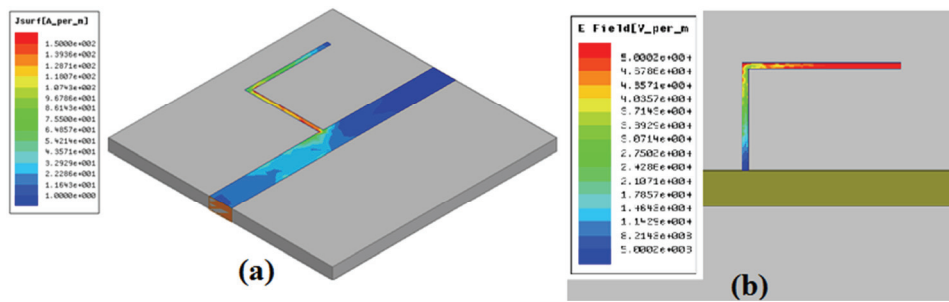
Figure 2.6 Field distribution on the open stub at resonant frequency (2.12GHz), (a) surface current distribution and (b) Electric field distribution

2.3.1. Equivalent Circuit Design of Open Stub Microstrip Resonator

Equivalent circuit of an open stub resonator can be derived by finding the capacitance and inductance of each section in the microstrip line. Open end fringing field and microstrip bend effects are also to be incorporated into the analysis for the accurate calculation of resonant frequency. Transmission line and open stub resonator are assumed to be lossless ie., distributed resistance is zero. Equivalent circuit of the open end microstrip line is shown in Fig.2.7. L_S and C_P are the equivalent series inductance and shunt capacitance per unit length of microstrip line, L_B and C_B are the equivalent series inductance and shunt capacitance due to microstrip bend. ΔC_P is the

shunt capacitance due to open end fringing field. Closed form expressions for finding the unknown quantities are given in the following steps [11]-[15].
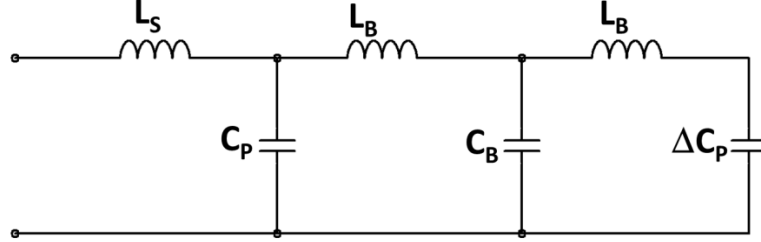
Figure 2.7 Equivalent circuit of a single open stub resonator

Series inductance (L_S) and shunt capacitance (C_P) of a microstrip line can be calculated by solving closed form equation [11].

$$Z_0 = \frac{87}{\sqrt{\varepsilon_r + 1.41}} ln \left[\frac{5.98h}{0.8W + T} \right] \ \Omega \tag{2.4}$$

$$C_P = \frac{2.64.10^{-11}(\varepsilon_r + 1.41)}{ln[5.98h/(0.8W+T)]} \ F/m \tag{2.5}$$

$$L_S = c_0 Z_0^2 \ \text{H/m} \tag{2.6}$$

where ε_r, h, W, and T are the permittivity, height of substrate, width of microstrip line and thickness of the metal, respectively. c_0 is the speed of light in the free space. Parallel capacitance C_B and series inductance L_B per unit length due to microstrip bend can be computed by [12].

$$\frac{C_B}{W}\left(\frac{pF}{m}\right) = \begin{cases} \frac{(14\varepsilon_r + 12.5)W/h - (1.83\varepsilon_r - 2.25)}{\sqrt{W/h}} + \frac{.02\varepsilon_r}{(W/h)} & \text{for } \frac{W}{h} < 1 \\ \frac{(9.5\varepsilon_r + 1.25)W}{h} + 5.2\varepsilon_r + 7 & \text{for } \frac{W}{h} \geq 1 \end{cases} \tag{2.7}$$

$$\frac{L_B}{h}\left(\frac{nH}{m}\right) = 100 \left\{ 4\sqrt{\frac{W}{h}} - 4.21 \right\} \tag{2.8}$$

Capacitance due to open end effect (ΔC_P) can be found by [13].

$$\Delta C_P = \frac{\Delta L \sqrt{\varepsilon_{re}}}{C_0 Z_C} \tag{2.9}$$

where ΔL is the extended length due to fringing field are given by

$$\frac{\Delta L}{h} = \frac{\xi_1\, \xi_3\, \xi_5}{\xi_4} \tag{2.10}$$

$$\xi_1 = 0.434907 \frac{\varepsilon_{re}^{0.81} + 0.26(W/h)^{0.8544} + 0.236}{\varepsilon_{re}^{0.81} + 0.189(W/h)^{0.8544} + 0.87}$$

$$\xi_2 = 1 + \frac{(W/h)^{0.371}}{2.35\varepsilon_r + 1}$$

$$\xi_3 = 1 + \frac{0.5274\tan^{-1}[0.084(W/h)^{1.9413/\xi_2}]}{\varepsilon_{re}^{0.9236}}$$

$$\xi_4 = 1 + 0.037\tan^{-1}[0.067(W/h)1.456].\,\{6 - 5\exp[0.036(1 - \varepsilon_r)]\}$$

$$\xi_5 = 1 - 0.218\, exp\left(\frac{-7.5W}{h}\right)$$

where ε_{re} is the effective dielectric constant of the microstrip line. As per the above equations, extracted values of inductance and capacitance of the open stub resonator and microstrip line are detailed in Table 1. The parameter L_TL_S and C_TL_P are the series inductance and shunt capacitance of the 50Ω microstrip transmission line shown in Fig.2.4.

Table 1: Extracted parameters

Parameter	Values
L_S	0.157nH/mm
C_P	0.048pF/mm
L_B	0.098nH
C_B	0.0156pF
ΔC_P	0.032pF
L TL_S	0.27nH/mm
C TL_P	0.11pF/mm

The equivalent circuit of the open stub resonator with 50Ω transmission line is modelled in Agilent ADS software with values given in Table 1 and its frequency response with HFSS simulation is validated. Fig.2.8 shows the equivalent circuit designed in Agilent ADS software with two ports connected across the 50Ω transmission line. Fig.2.9 shows the frequency response comparison between equivalent circuit and the 3D numerical result. Equivalent circuit results show good agreement with numerical results.
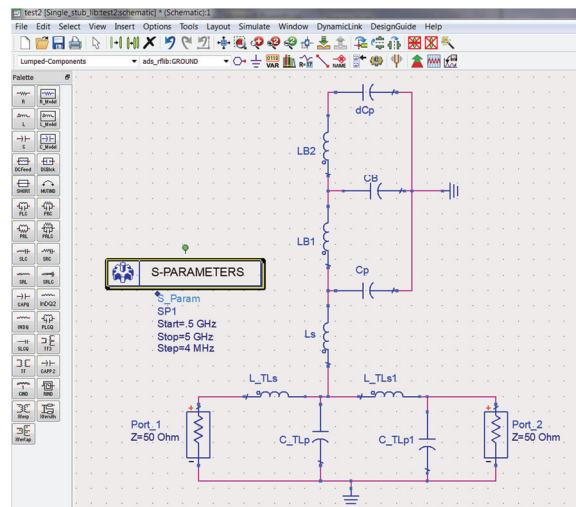
Figure 2.8 Equivalent circuit of an open stub resonator (Fig.2.4) connected with 50Ω transmission line using Agilent ADS.
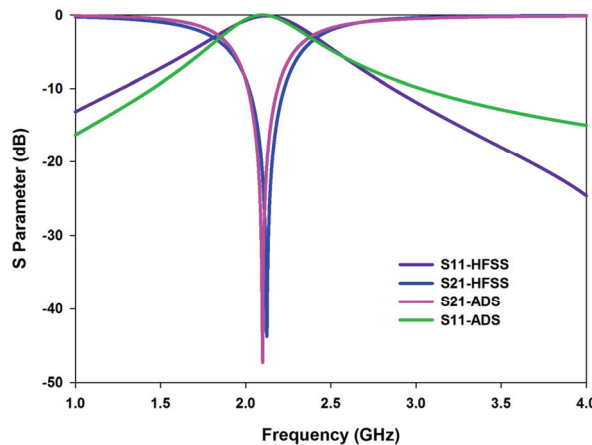
Figure 2.9 Frequency response of the above open stub resonator extracted using HFSS and Agilent ADS

2.4. Substrates for Chipless RFID Tag

Multiresonating circuit using open stub resonator is analysed with different substrate are discussed in this section. Different substrates used for the analysis are FR4 (ε_r = 4.3, tanδ = 0.02, h = 1.6mm), C-MET LK 4.3 (ε_r = 4.3, tanδ = 0.0018, h = 1.6mm), RT Duroid (ε_r = 2.2, tanδ = 0.0009, h = 1mm) and glossy paper (ε_r = 3, tanδ = 0.09, h = 0.22mm). The dimension of the open stub resonator given in the Fig.2.4 is analysed on different transmission lines designed on the above substrates with characteristic impedance (Z_0) of 50Ω. From the figure it is clear that, the resonator printed on a lossy glossy paper can also encode the data in the frequency spectrum, but it requires large bandwidth to represent resonance due to low Q. The better Quality factor can be achieved with low loss substrate (<<tanδ). The resonant frequency variation with respect to the dielectric constant of the structure is also shown in the figure. C-MET LK 4.3 substrate is used for the design and analysis of multiresonator based chipless tag, which is indigenously developed by C-MET (Centre for Materials for Electronics Technology, India). Substrate properties given by the manufacturer are given in Table 2.
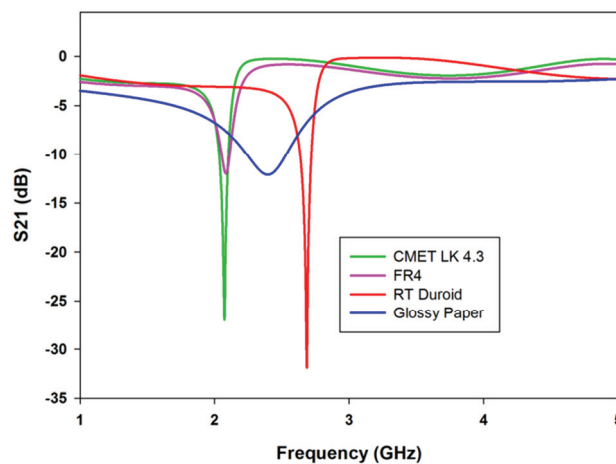
Figure 2.10. Simulated frequency response of the open stub resonator on different substrate.

Table 2. Material Properties of C-MET LK-4.3 Substrate

C-MET LK-4.3	Values
Dielectric constant	4.3 ±0.03 at 10 GHz
Loss tangent	0.0018 at 10 GHz
Temperature coefficient of dielectric constant	-27 ppm/°C
Linear coefficient of thermal expansion	19 ppm/°C
Copper peel strength	1.2 N/mm
Water absorption	0.05%
Thermal conductivity	> 1 W/mK

2.5. Optimisation of Open Stub Resonator

Frequency spectrum available for the design of chipless tag is limited due to allocation of bands to different applications. Hence, to encode more bits in the limited spectrum, the bandwidth of the resonators to represent the bit/resonator should be small as possible. It is noted that there is a band notch centred at 2.35GHz when an open circuited stub of length 18mm and width 0.5mm is connected to the 50Ω microstrip transmission line. Simulation analysis on different parameters of the single open stub resonator with microstrip line is carried out in this section. Fig.2.11 shows the variation of resonant frequency with respect to the width of the transmission line (W_1). As the width of transmission line increases, Fractional Band Width (FBW) decreases, ie. FBW changes from 39.42% to 12.57% when W_1 varies from 2mm to 7mm. The FBW is estimated using, FBW=$\Delta f/f_0$*100%, where Δf is the 3dB S_{21} band width and f_0 is the notch frequency. Similar parametric study on open stub resonator width (W_2) is also carried out and its frequency response is shown in Fig.2.12. FBW is decreased with the width of the resonator as demonstrated in Fig.2.12.
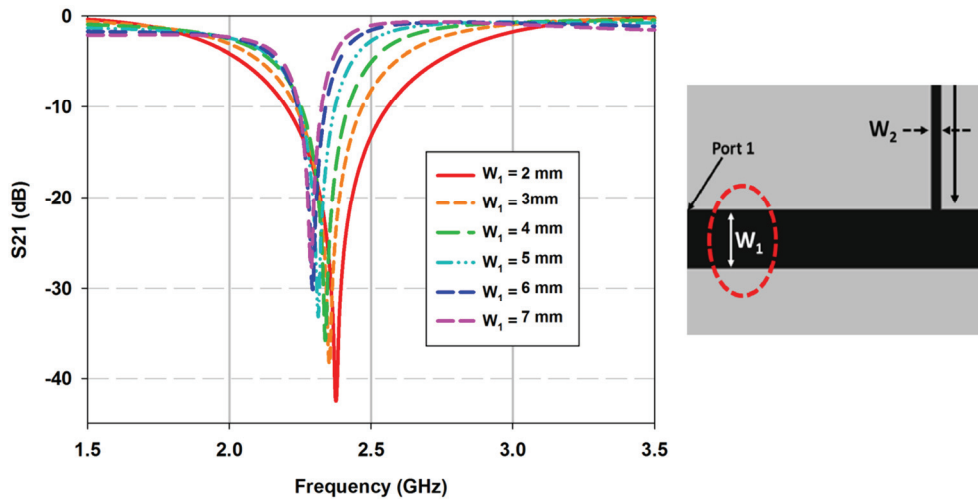
Figure 2.11 Frequency response of the structure with different transmission line width (W_1), ε_r = 4.3, tanδ = 0.0018, h = 1.6mm and W_2 = 0.5mm
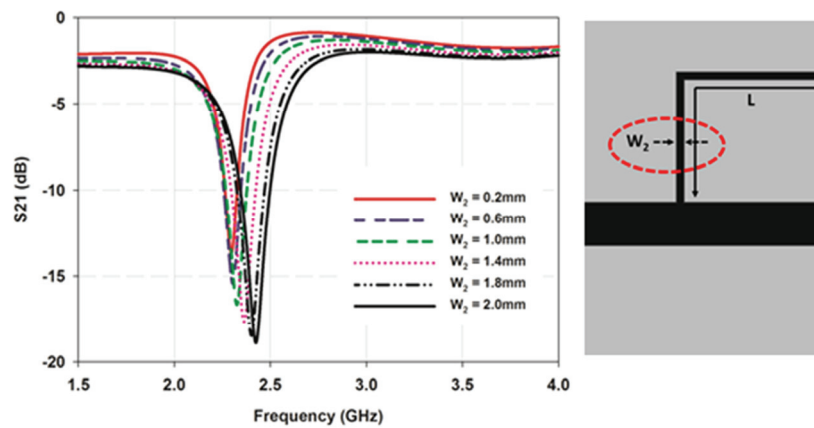
Figure 2.12 Frequency response of the structure with different open stub resonator width (W_2), ε_r = 4.3, tanδ = 0.0018, h = 1.6mm and W_1 = 3mm

The results of the parametric analysis shown in Fig.2.11 and 2.12 are detailed in Table 3. It is found that when the transmission line impedance is 50Ω (W=3mm), the system offers a Fractional Band Width (FBW) of 30.05%. As seen in the Table 3.a increasing the width of the transmission line will reduce the FBW. However, when the transmission line impedance is about 28Ω (W= 7mm), optimum FBW (12.57%) is achieved. It is noted that

further decrease in the impedance of the transmission line distorts the S_{21} characteristics. So this impedance is selected for further analysis. From Table.3.b it is again found that when the width of the λg/4 stub (W_2) is decreasing, FBW of the resonator is also decreasing. Due to the fabrication limitation, the width W_2 is taken as 0.5mm in the present study. It is also observed that there is a small frequency shift with the width of the stub. This may be due to the increased inductance of the stub for small width [17]. Similarly, the small shift in the resonance with the width of the transmission line may be due to the change in effective capacitance of the line with width.

Table 3: Parametric Study on Open Stub Resonator and Microstrip Transmission Line

Table 3.a L = 18 mm, W_2 = 0.5mm			Table 3.b L = 18 mm, W_1 = 3mm		
W_1 (mm)	F_0 (GHz)	FBW (%)	W_2 (mm)	F_0 (GHz)	FBW (%)
2	2.37	39.42	0.3	2.33	27.27
3	2.35	30.05	0.5	2.35	30.05
4	2.32	23.50	0.7	2.36	33.69
5	2.31	17.90	0.9	2.38	37.21
6	2.30	15.11	1.1	2.41	39.48
7	2.29	12.57	1.3	2.44	40.08
8	2.27	9.21	1.5	2.47	44.45

To reduce the impedance mismatch between antenna terminal (50Ω) and microstrip transmission line (28Ω), an impedance transformer section (tapering section) is also included [18]. The length of this tapering section (L_T) is equal to $0.25\lambda_d$, where λ_d is the wavelength in the substrate corresponding to the lowest frequency of operation. Final model of the single bit open stub resonator based mutiresonator circuit is depicted in Fig.2.13. A parametric study on the multiresonating circuit with different resonator length (L) is depicted in Fig.2.14 and all other parameters of the structures are same as that shown in Fig.2.13. It is clear from the figure that, the resonant

frequency of the multiresonating structure can be easily controlled by the resonator length.
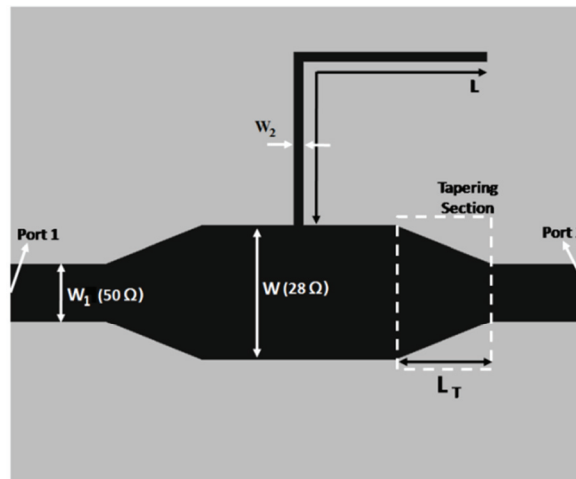
Figure 2.13 Final model of a single bit open stub resonator based mutiresonator circuit, where W_1 = 3mm, W_2 = 0.5mm, W= 7mm L_T = 12 mm, L = 18mm, ε_r = 4.3, $\tan\delta$ = 0.0018 and substrate height = 1.6mm.
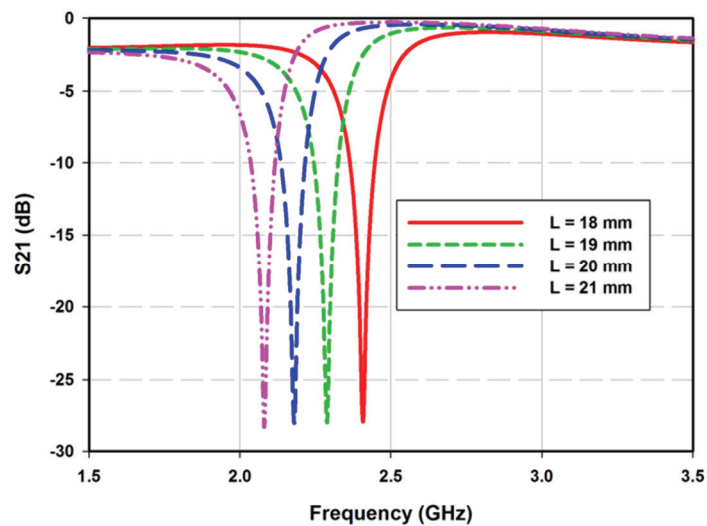
Figure 2.14 Simulated resonant frequency variation of open stub resonator with respect to its length (L).

2.6. Tag Design

From the above knowledge, a multiresonator circuit with 8 open stub resonator is designed and fabricated on a C-MET LK 4.3 substrate. Fig.2.15 shows the structure of the proposed 8 bit multiresonator circuit with an overall dimension of $30 \times 25 \times 1.6 \text{mm}^3$. Each resonator is independently resonating at its quarter wavelength frequency ($\lambda g/4$). To minimise the mutual coupling between the two resonators they are kept 1mm apart. Experiments of the multiresonating circuit are conducted using the PNA E8362B network analyser. Fig.2.16 shows the measured and simulated frequency response of the 8 bit RFID tag. The simulated results are in good agreement with the measured one. The resonant frequencies of the circuit are found to be at 2.08GHz, 2.23GHz, 2.36GHz, 2.56GHz, 2.81GHz, 3.21GHz, 3.61GHz and 4.03GHz.
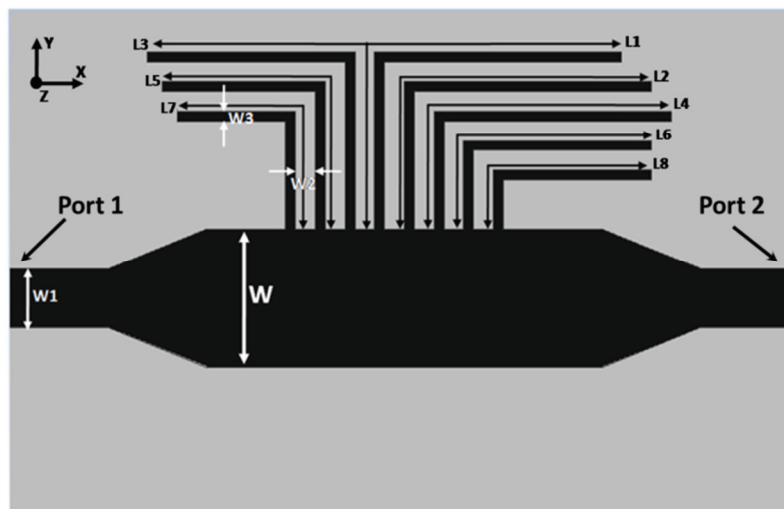
Figure 2.15 Proposed 8 bit open stub RFID tag, where ε_r = 4.3, tanδ = 0.0018, h =1.6mm, W = 7mm, W1 = 3mm, W2 = 1mm, W3 = 0.5mm, L1 = 21mm, L2 = 19.5mm, L3 = 19 mm, L4 = 17.5mm, L5 = 15.25mm, L6 = 13.5mm, L7 = 11.5mm and L8 = 10.5mm
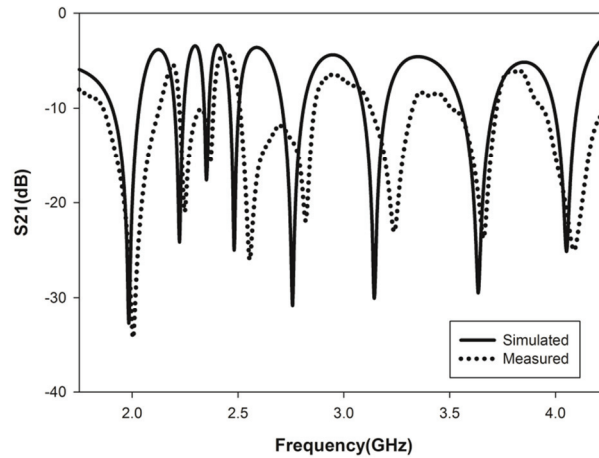
Figure 2.16 Simulated and measured frequency response of the proposed 8 bit tag [1111 1111] shown in Fig.2.15.

Absence or Presence Coding technique is used in the design of present tag, hence one resonator can represent 1 bit of information. The presence of the resonance at a predefined frequency indicate bit 1 and absence will indicate bit 0. Fig.2.17 shows the method of generating different bit combination from the mutiresonator circuit. Instead of removing entire resonator from the tag, the connection between transmission line and resonator is removed to minimise the frequency shift in the multiresonating circuit. Measured transfer function (S_{21}) of the tag with different bit combinations are depicted in Fig.2.18.
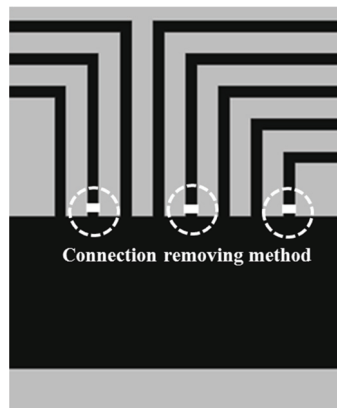
Figure 2.17 Structure of the multiresonating circuit with disconnected open stub resonators
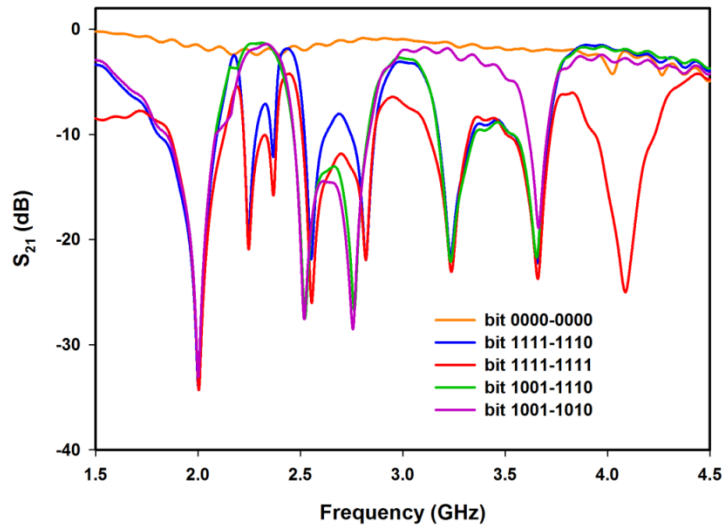
Figure 2.18 Measured frequency response of the multiresonator circuit with different bit combination

Bit information of the multiresonating tag also can be encoded in the group delay of the transfer function as shown in Fig.2.19. Group delay is defined as the negative derivative of the signal phase with respect to frequency. When a signal passes through a device or medium, it experiences both amplitude and phase distortion. The amount of distortion depends on the characteristics of the device/medium. A wave incident at the input of a device may have several frequency components. The group delay gives a measure of average time delay of input signal at each frequency or it gives a measure of the dispersive nature of the device. Mathematically, the group delay can be expressed as,

$$\tau_g = \frac{-d\theta(\omega)}{d\omega} \tag{2.11}$$

where θ and ω are the phase and the angular frequency of the signal.

If the phase of the backscattered signal varies, the group delay will vary with frequency ie., backscattered signal will have different delays at

different frequencies. From [19] it is clear that the group delay signal may have positive or negative symmetry depending on the phase change direction (+ve to –ve or –ve to +ve). The group delay plot is very efficient to analyse any nonlinearity that is present in the phase. From Fig.2.19, all the resonances can be easily identified from the backscattered group delay signal. Small shifts in the resonant frequency due to the removal of connection between the open stub and transmission lines are also shown in the figure.
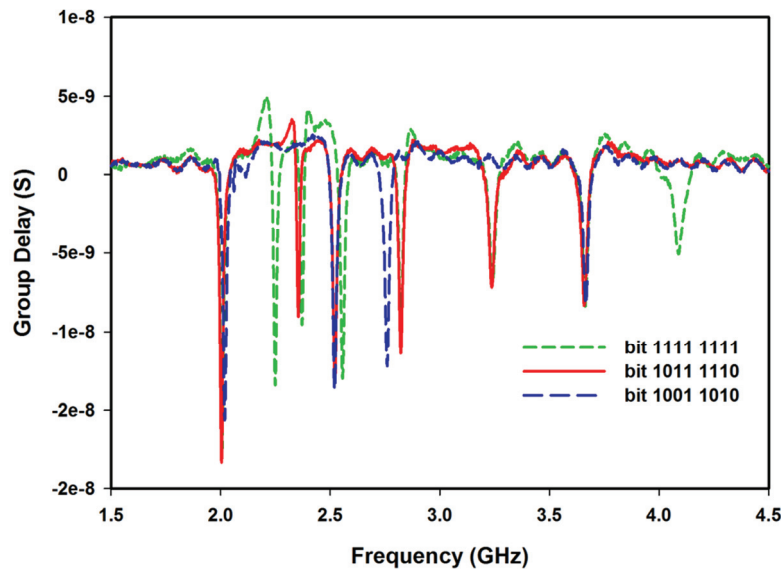
Figure 2.19 Group Delay of the multiresonator circuit with different bit combinations

2.7. Receiving and Retransmitting UWB Antennas: Disc Monopole Antenna

A complete chipless RFID tag requires two UWB antennas at the two ends of multiresonating circuit. Selection of UWB antenna in the multiresonator based tag depends on impedance match, polarisation, radiation pattern and overall size. The antenna should possess very good impedance match over the operating frequency band of the RFID tag and also need better

linear polarisation characteristics. For successful reception and retransmission of interrogation signal, the radiation pattern of the antenna also needs to be uniform. In this tag, microstrip disc monopole antenna is opted due to its simple structure and wide band operation [4]. Fig.2.20 shows the geometry of the monopole antenna, along with the design parameters. Measured return loss characteristic of the antenna from 1.5GHz to 11GHz is shown in Fig.2.21. The antenna shows very good impedance match over operating range of multiresonator circuits (1.9GHz to 4.5GHz).
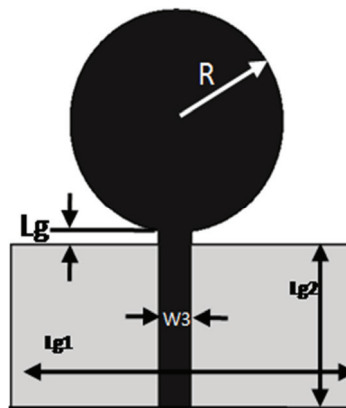
Figure 2.20 Disc monopole antenna ε_r = 4.3, tanδ = 0.0018, h = 1.6mm, R = 15mm, W3 = 3mm, Lg = 0.6mm, Lg1 = 40mm and Lg2 = 20mm
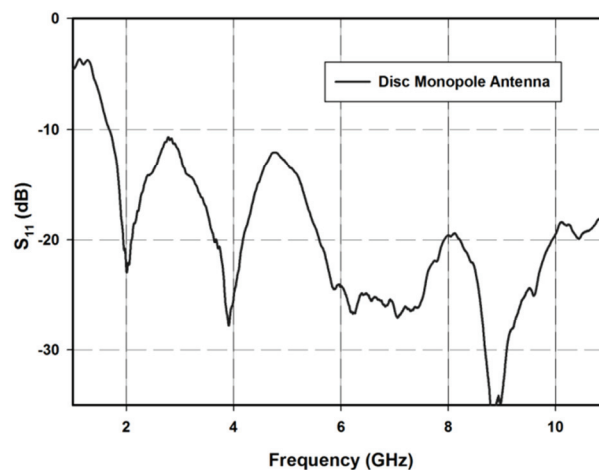
Figure 2.21 Measured reflection characteristics of Disc Monopole Antenna

The measured radiation patterns of the antenna both in H and E plane at 3GHz, 7GHz and 10GHz are shown in Fig.2.22. Over the frequency range of RFID tag, UWB antenna confirms omnidirectional radiation pattern. This antenna is not suitable for a wide range of application due to the degradation in the polarisation and radiation pattern. Above 7GHz radiation pattern of the antenna is changing drastically due to the excitation of higher order modes. For most of the angular directions (in E and H plane), the antenna is showing polarisation better than 20dB (below 7GHz), hence it will improve the isolation between received and retransmitted interrogation signal.
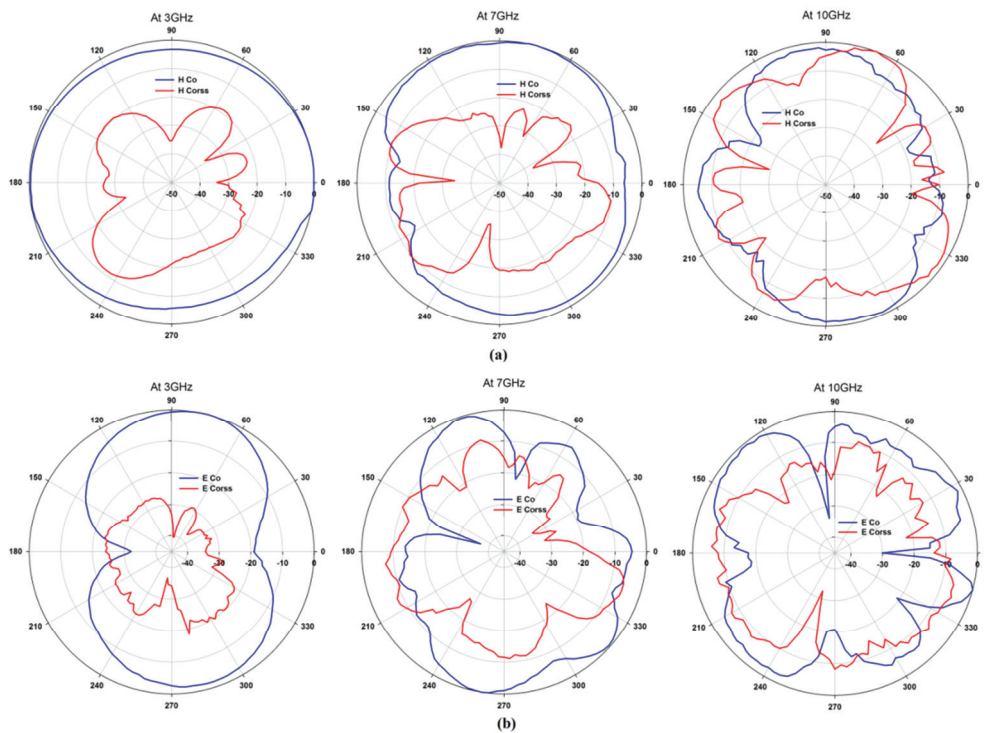
Figure 2.22 Radiation pattern of the Disc monopole antenna at three different frequencies (3GHz, 7GHz and 10GHz). (a) H Plane and (b) E Plane.

2.8. 8 bits Open Stub Resonator Based Multiresonating Chipless RFID Tag

Complete microstrip open stub resonator based multiresonating chipless RFID tag is shown in Fig.2.23. The receiving and retransmitting disc monopole antennas are connected in such a way that they are orthogonally polarised. The backscattered signal from the retransmitting antenna has been used for the encoding purposes. If all resonators operating at different frequencies (2.08GHz, 2.23GHz, 2.36GHz, 2.56GHz, 2.81GHz, 3.21GHz, 3.61GHz and 4.03GHz) are present, then the bit pattern is 1111 1111. The overall dimension of the RFID tag is 80x60x1.6 mm^3.
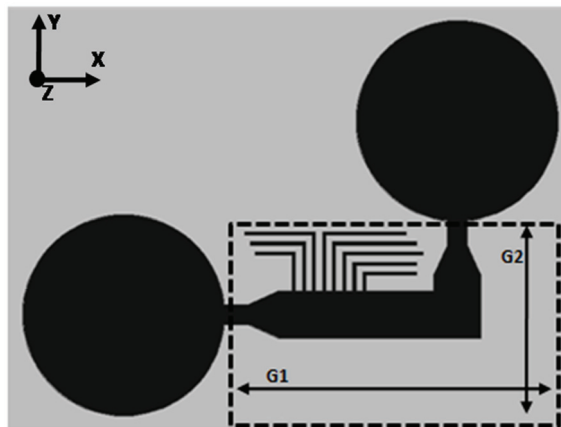
Figure 2.23. 8 bit RFID Tag with Disc Monopole antenna, G1 = 50mm, G2=30mm, dotted line showing the ground at the backside of the substrate (ε_r=4.4, tanδ=0.0018 and height=1.6mm)

2.9. Measurement System

Reader system proposed by S. Preradovic et. al [1]-[3] is opted for the measurement. Agilent PNA E8362B network analyser with transmitted power of 0dBm is used as the RFID reader and two medium gain horn antennas are

used at the reader end for transmitting and receiving signals from the RFID tag. Schematic diagram of the reader system with two cross polarised antennas and proposed chipless tag is shown in Fig.2.24. Proposed system requires proper arrangement with the reader and tag antenna for successful detection of the encoded signal. Fig.2.25 shows the gain of a linearly polarised reader antenna (horn) and tag antenna (disc monopole). In the desired frequency band the reader antenna has a gain of about 8-10dB and for the tag antenna it is about 1.5-4.5dB. Calibrations are not required to get the backscattered signal from the retransmitting antenna for a distance of 40cm due to the orthogonal polarisation arrangement of the RFID system. From the Friis transmission equation, the readable range of the tag can be further improved by setting high gain antennas at the reader and tag ends. Increasing the power from the microwave source can also be used to increase the range.
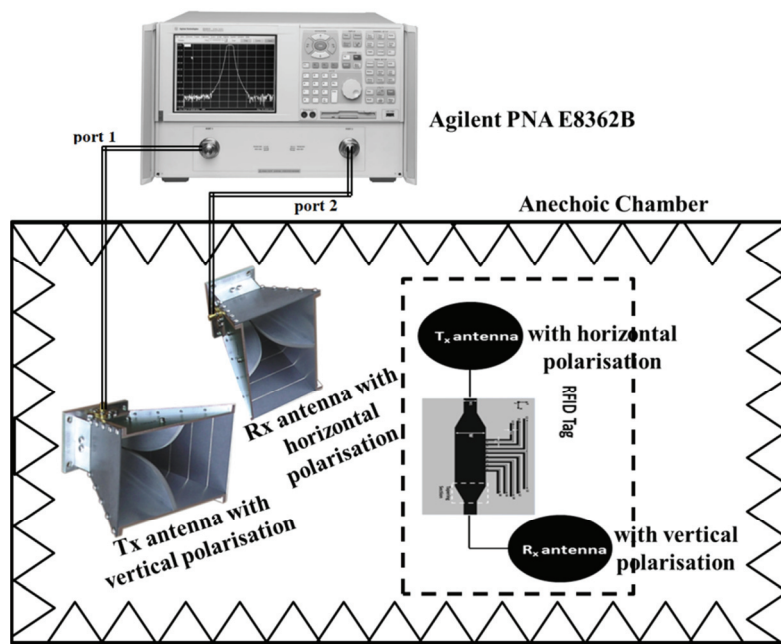
Figure 2.24 Schematic diagram of the measurement system using Agilent PNA E8362B.
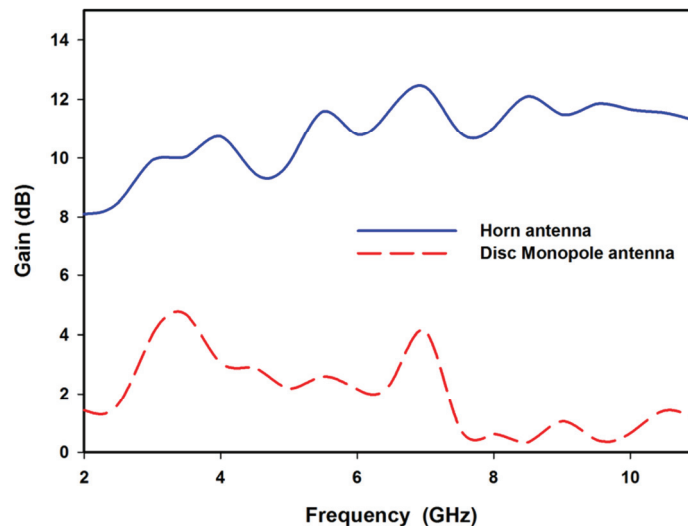
Figure 2.25 Gain of the reader antenna (horn) and tag antenna (disc monopole).

The RFID tag decoded up to a distance of 1-2 meters are reported in the literature, but it requires complex calibration procedure [20] - [21] including reference measurements with metal sheets and time domain gating, etc. These calibration techniques will create complex measurements which is not suitable for practical applications.

2.10. Result and Discussion

All the measurements are carried out inside the anechoic chamber and the measurement setup is shown in Fig.2.26. As shown in the figure, the RFID tag is placed at a distance of 40cm away from horn antennas. Identification of each bit is very clear from magnitude and group delay measurements. The typical response of the RFID tag for 1111 1111, 1001 1110, 1001 1010 and 1001 0010 bits are shown in Fig.2.27 to 2.30, respectively. All the bits can be identified from the backscattered magnitude and group delay signal. RFID without antenna in Fig.2.27 to 2.30, means the direct measurement of multiresonator circuit as shown in Fig.2.18. The band

notches are well defined and in the worst case the magnitude of the dip is better than 5dB. From the figure, it is well understood that the magnitude and group delay can be conveniently used for reading the tag.
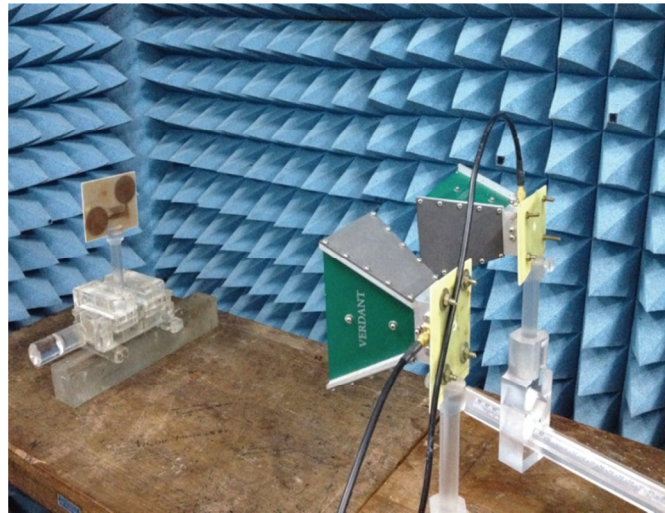
Figure 2.26 Measurement setup inside the anechoic chamber
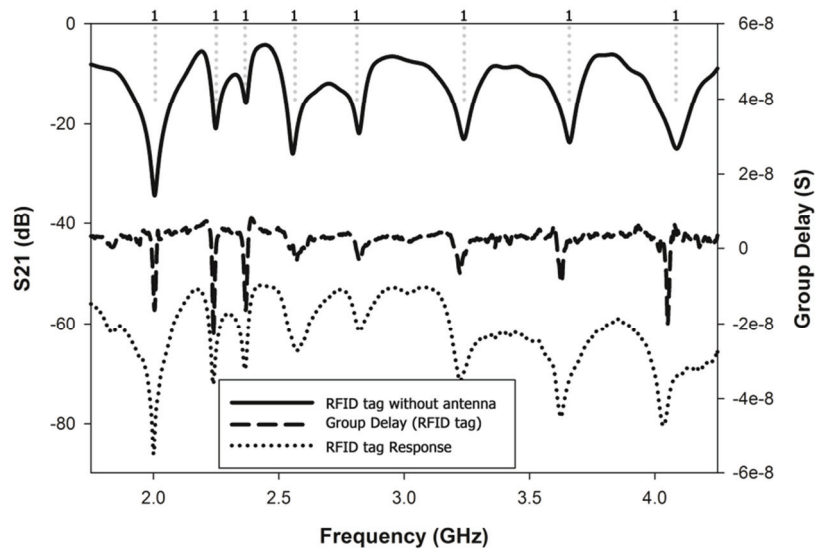
Figure 2.27 Measured backscattered response (Magnitude and Group delay) of RFID tag (11111111)
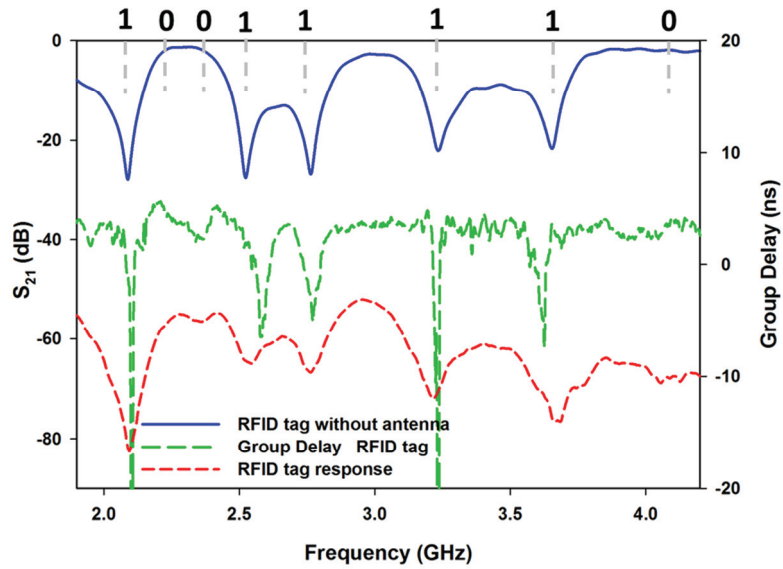
Figure 2.28 Measured backscattered response (Magnitude and Group delay) of RFID tag (10011110)
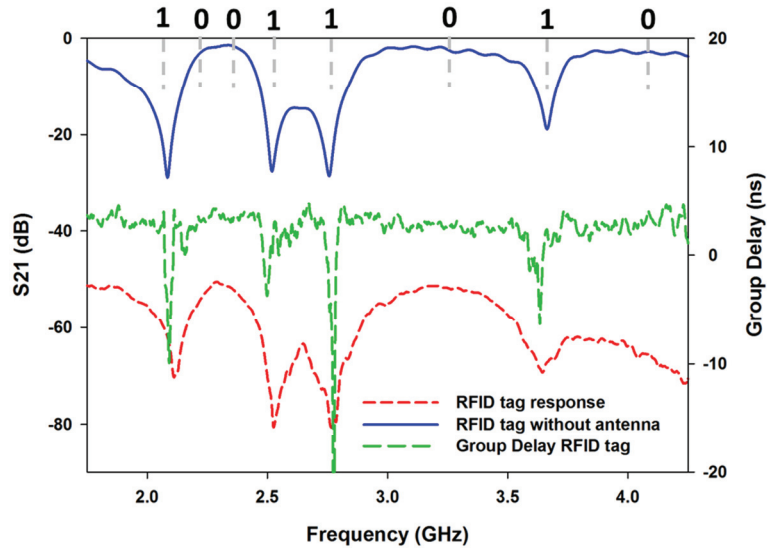
Figure 2.29 Measured backscattered response (Magnitude and Group delay) of RFID tag (10011010)
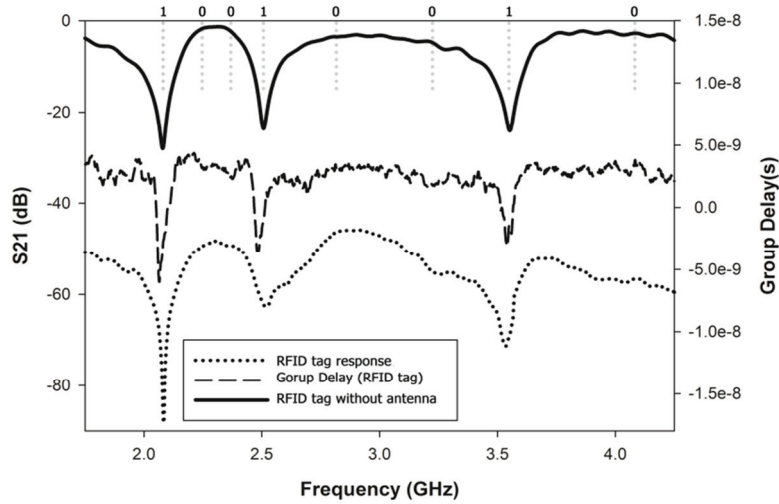
Figure 2.30 Measured backscattered response (Magnitude and Group delay) of RFID tag (10010010)

Proposed system successfully measured backscattered amplitude and phase (group delay) variation of different multiresonator based tag up to a distance of 40cm. Hence the system can be adopted for applications like automatic identification of items in the conveyor belt. The barcode technology can be replaced with the proposed system, providing proper arrangement with the reader.

2.11. Conclusion

A novel RFID tag with multiple open stub resonators is proposed in this chapter. The quarter wavelength resonance of the open stub resonator makes proposed tag more compact than other existing tags. Equivalent circuit model with different parametric studies are conducted on the open stub resonator. The tag enables to encode data in magnitude as well as in group delay. Without having any additional calibration technique, the proposed system is able to decode the tag information up to a distance of 40cm. The method introduced in this chapter can be effectively implemented using low cost substrate materials which in turn reduce the overall cost.

2.12. Reference

[1] S. Preradovic, I. Balbin, and N. Karmakar, "The development and design of a novel chipless RFID system for low-cost item tracking," in Proc. Asia Pacific Microwave Conf. (APMC) 2008, Hong Kong, Dec. 2008, pp. 1–4.

[2] S. Preradovic and N. Karmakar, "Design of fully printable planar chipless RFID transponder with 35-bit data capacity," in Proc. 39th European Microwave Week, Rome, Italy, Sept. 2009, pp. 13–16.

[3] S. Preradovic, S. Roy, and N. Karmakar, "Fully printable multibit chipless RFID transponder on flexible laminate," in Proc. Asia Pacific Microwave Conf. (APMC'09), Singapore, Dec. 2009, pp. 2371– 2374.

[4] S. Preradovic, I. Balbin, N. Karmakar, and G. Swiegers, "A novel chipless RFID system based on planar multiresonators for bar code replacement," in Proc. IEEE Int. Conf. RFID 2008, Las Vegas, NV, Apr. 2008, pp. 289–296.

[5] Pimsiripom Narkcharoen and Suneat Pranonsatit, "The Applications of Fill until Full (FuF) for Multiresonator based Chipless RFID System", The 8th Electrical Engineering Electronics, Computer, Telecommunications and Information Technology (ECTI) Association of Thailand - Conference 2011, pp -176-179.

[6] Giovanni Andrea Casula, Giorgio Montisci, Paolo Maxia and Giuseppe Mazzarella, "A narrowband chipless multiresonator tag for UHF RFID", Journal of Electromagnetic Waves and Applications, Vol. 28, No. 2, 214–227, January 2014.

[7] David Girbau, Javier Lorenzo, Antonio Lázaro, Carles Ferrater and Ramón Villarino, "Frequency-Coded Chipless RFID Tag Based on Dual-Band Resonators", IEEE Antennas and Wireless Propagation Letters, Vol. 11, 2012.

[8] Md. Shakil Bhuiyan, AKM Azad and Nemai Karmakar, "Dual-band Modified Complementary Split Ring Resonator (MCSRR) Based Multi-resonator Circuit for Chipless RFID Tag" 2013 IEEE Eighth International Conference on Intelligent Sensors, Sensor Networks and Information Processing, Melbourne, VIC, 2-5 April 2013, pp-277 – 281.

[9] Y. F. Weng, S. W. Cheung, T. I. Yuk, and L. Liu, "Design of Chipless UWB RFID System Using A CPW Multi-Resonator", IEEE Antennas and Propagation Magazine, Vol. 55, No. 1, February 2013.

[10] C. A. Balanis, Antenna Theory: Analysis and Design, 2nd ed. New York: Wiley, 1982.

[11] M. Kirsching, R. H. Jansen, and N. H. L. Koster, "Accurate model for open end effect of microstrip lines" Electronics Letters, 17, Feb. 1981,123-125.

[12] K. C. Gupta, R Garg, I Bhal and P. Bhartis, Microstrip Lines and slotlines" Second edition, Artech House, Boston, 1996.

[13] Antonije R. DjordjeviC and Tapan K. Sarkar, "Closed-Form Formulas for Frequency-Dependent Resistance and Inductance per Unit Length of Microstrip and Strip Transmission Lines", IEEE Transactions on Microwave Theory and Techniques, Vol. 42, No. 2, February 1994.

[14] K. C. Gupta, R. Gag, and R. Chadha, Computer-Aided Design of Microwave Circuiis. Boston: Artech, 1981.

[15] F. E. Gardiol, Introduction to Microwaves. Boston: Artech. 1984.

[16] A. R. Djordjevif, T. K. Sarkar, and S. M. Rao, "Analysis of finite conductivity cylindrical conductors excited by axially-independent TM electromagnetic field," IEEE Trans. Micmwave Theory Tech., vol. 33, pp. 96&966, Oct. 1985.

[17] Jia-Sheng Hong and M J Lancaster "Microstrip Filters for RF/Microwave Applications" A Wiley-Interscience publication, pp. 112-120, 2001.

[18] Peter A. Rizzi "Microwave Engineering Passive Circuits",Pearson publications, pp.152-54, 2007.

[19] Applied Radio Labs "Group Delay Explanations and Applications" ww.radiolab.com.au

[20] Arnaud Vena, Etienne Perret and Smail Tedjini "RFID Chipless Tag Based on Multiple Phase shifters" Microwave Symposium Digest (MTT), 2011 IEEE MTT-S International, pp.1-4, 5-10 June 2011.

[21] A. T. Blischak andM.Manteghi, "Embedded singularity chipless RFID tags," IEEE Trans. Antennas Propag., vol. 59, no. 11, pp. 3961–3968, Nov. 2011.

.............ೞೞ.............

MULTISCATTERER BASED CHIPLESS RFID TAGS USING STEPPED IMPEDANCE RESONATOR (SIR)

Abstract

This chapter discusses about the design and development of multiscatterer based Chipless RFID tag. The chapter also gives an introduction on various types of multiscatterer based tags reported in the literature. Backscattering mechanism, calibration method and characteristics of multiscatterer based chipless RFID tags are also discussed. Evolution of Stepped Impedance Resonator (SIR) from a transmission line resonator and various attractive properties of SIR, like control on electrical length, harmonic separation and independent control over resonant modes are explained. Three kinds of UWB multiscatterer based Chipless RFID tags using SIR are also proposed in this chapter. Finally, a chipless tag having data encoding capacity of 79 bits and Surface Coding Capacity greater than $7bits/cm^2$ with an overall dimension of $40x25mm^2$ is demonstrated. All the designs are validated with measured data and the spectral data is successfully decoded up to a distance of 50cm.

3.1. Challenges with Multiresonator Based Chipless Tag

In the frequency domain, the number of bits that can be represented by an RFID tag is directly proportional to the usable bandwidth and quality factor of each resonator. Chipless RFID technology is still in the research stage, however, designing a tag in the license free band ranging from 3.1-10.6GHz can demonstrate the advantages of the system compared with existing technologies. Due to the large bandwidth, more number of bits can be easily encoded. This chapter concentrates on the design and development of frequency domain based chipless RFID tag working in the UWB region.

Multiresonator based chipless RFID tag is the combination of different microwave components like UWB antennas, transmission line and microwave resonators [1]-[4]. The design of UWB chipless RFID tags based on multiresonator circuit are facing challenges due to following issues.

❖ RFID tag antenna radiation characteristics are not identical in the entire operating band as shown in the chapter 2. Thus, some resonant frequencies are difficult to detect usually at the higher bands.

❖ RFID tag utilising UWB antennas [2] occupies more than 50% of the tag space, and hence the large size tag.

❖ Proper orientation between reader and tag is required for successful detection of backscattered signal.

❖ The position of the resonator can be selected only with a limited degree of freedom because it has to be connected or coupled with the transmission line.

❖ Mutual coupling between the resonators.

Similar electromagnetic response of the multiresonating tag can be achieved with a structure using multiple scatterers [5]. Each scatterer/resonator serves as a receiving antenna, a narrow band filter and a transmitting antenna. Normally, each

scatterer receives the electromagnetic wave and reflects it back to the reader as a quasi-optical way. At resonance, it will generate a different electromagnetic pattern. Therefore chipless tag consisting of multiple scatterers can encode data by selecting its resonance at predefined frequencies. The Q factor of the scatterer determines the coding capacity of the tag and is a function of total tag losses namely, conduction, dielectric, surface wave and radiation losses. Surface wave and dielectric losses are negligible in thin substrates with low loss tangent. A metal thickness of the order of micro meters can be used to minimise the skin effect losses at these frequencies. The chipless tag proposed in [5], is the first design reported based on this method. Although it has a limited coding capacity of the order of 5 bits compared to 35 bits [1], the size of the tag required to represent bits is small. The design [1] requires a surface area of 1.66cm^2 to represent single bit, but [5] requires only 1.25 cm^2 for the same encoding. This demonstrates the miniaturization possibility of this approach.

3.2. Introduction to Multiscatterer Based Chipless RFID Tag

The first reported work related to RFID tag using multiscatterer is from Jalaly et. al. [5] based on RF barcodes which are constructed with arrays of metallic microstrip dipoles on a dielectric substrate with ground plane. Detection is based on reflection characteristics and the reader consists of two co-polarised antennas. The interrogator emits electromagnetic energy and the frequency content in the backscattered signal from the RF barcodes is analysed to decode the data. The obtained Q factor of the resonator is about 100 and it can support approximately 4 or 5 bits within the ISM (Industrial, Scientific and Medical) bands. This is insufficient for different applications. It is proposed by the author that, by straddling ISM bands, a practical RFID tag can be realised. Fig.3.1 shows RFID tag working in the three ISM bands (2.4, 5.25 and 5.8 GHz). Fig.3.2 shows the backscattered response of the tag at 5.8GHz ISM band.
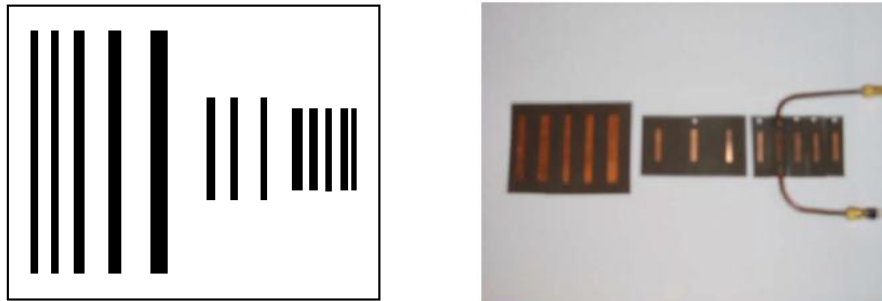
Figure 3.1 RF barcode elements at 2.4, 5.25 and 5.8 GHz bands with near field measurement probes. Courtesy: I. Jalaly et. al. [5].
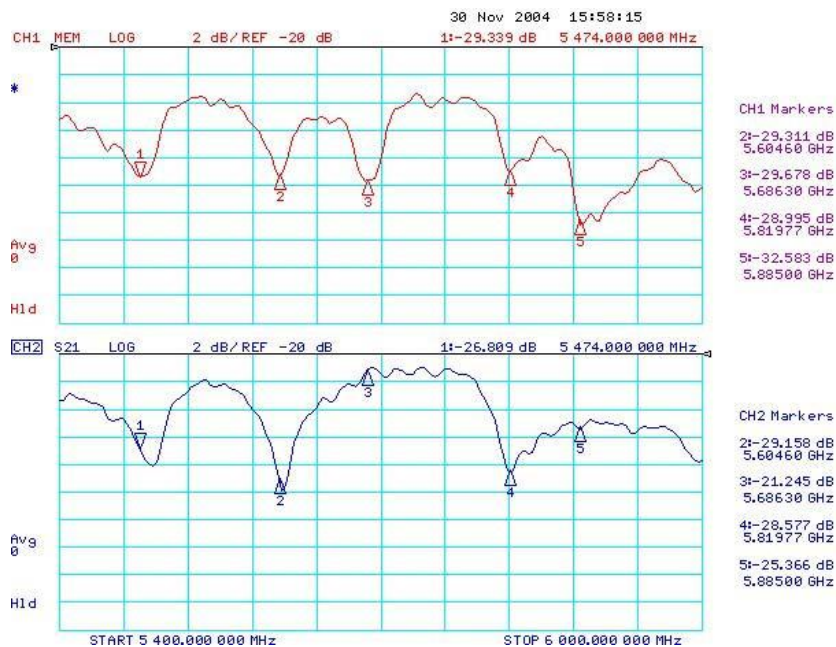
Figure 3.2 Bistatic S_{21} measurement results at 1.5m read range for 5-bit RF barcode representing 11111 (top) and 11010 (bottom), where a '1' is indicated by a 'null' or RF energy absorption at the corresponding frequency. Courtesy: I. Jalaly et. al. [5].

A compact 20 bit RFID tag operating in the frequency span of 2 GHz to 4 GHz with a size of 70x25mm^2 is presented in [12]. Fabrication process of the proposed tag is very cheap because it needs only one conductive layer (without ground plane), so that it can be fully printed directly on the product.

The main problem with single conductive layer based tag is, its inherent detuning effect, ie., variation in the resonance frequency due to surrounding objects and mutual coupling. The proposed 20 bit tags with different bit combinations are shown in the Fig.3.3. Fig.3.4 shows the simulated RCS of the tag with different bit combinations.
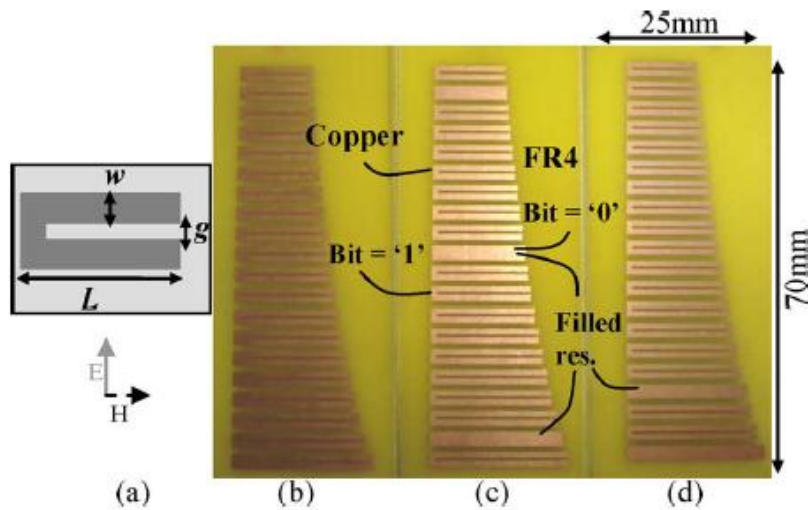
Figure 3.3 (a) Single scatterer. Realized 20-bit chipless tags (a) reference tag 1 having the maximal code (all '1'); (b) tag 2 with resonators 2, 11, and 19 filled to get '0'; (c) tag 3 with resonators 1 and 4 filled. Courtesy: A. Vena et. al. [12].
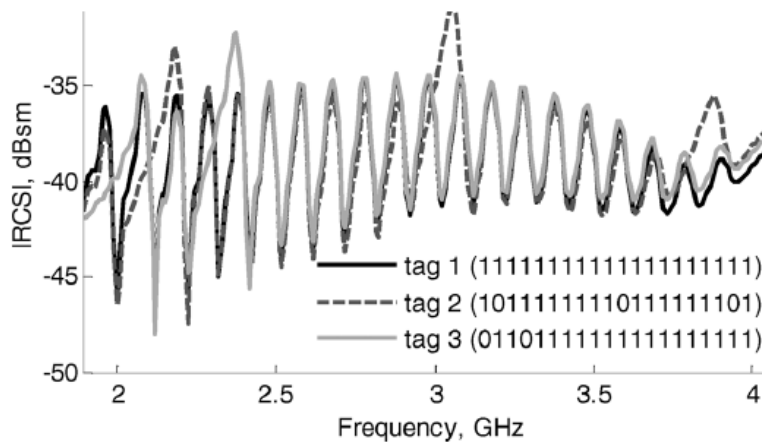
Figure 3.4 Simulated |RCS| response using CST Microwave Studio for different bit combinations. Courtesy: A. Vena et. al. [12].

The RFID system can also be realized by designing polarisation independent property. This can be achieved by either designing RFID tag resonators with polarisation independent capabilities [14]-[15] or by setting proper arrangement in the reader side [17]. Spectral information can be easily decoded from any of the linearly polarised reader signals. Polarisation of the backscattered signals may be the same or different from the transmitted signal and it mainly depends on the geometry of the scattering object. Arnaud Vena et al. [14] presented a polarisation independent tag using circular ring resonators. Similar type of RFID tags are reported in [15]. It is found that polarisation independent tags are designed by selecting resonator with symmetrical shape, hence resonant information can be decoded in both the horizontal and vertical polarised signals. Fig.3.5 shows the full wavelength (λ) field pattern at resonance on a circular ring resonator.
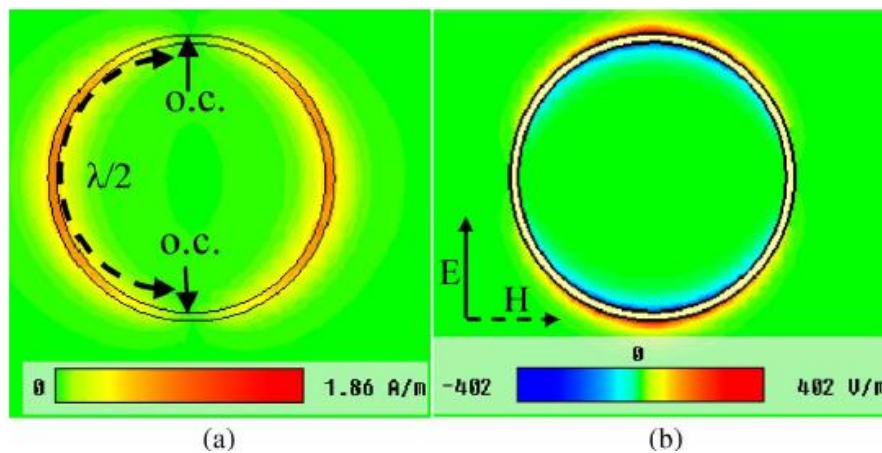
Figure 3.5 Field variation in a circular ring resonator a) surface current intensity along the ring b) Electrical field intensity. The plane wave incidence is normal to the tag surface, the radius R is set to 8 mm and the width w is 0.5 mm. Courtesy: A. Vena et. al. [14].

Aminul Islam et al. [17] have explained a printable Dual-Polarized Chipless RFID system with polarisation dependent scatterers, ie. resonators which excite only with single polarised signal (either horizontal or vertical),

where bit information is stored both in horizontally and vertically polarised resonators. RFID reader system consist of four antennas, two for transmitting and two for receiving the interrogation signal which are cross polarized (Fig.3.6 (a)). RFID tag consists of resonators, arranged in horizontal and vertical polarisations. Because of the polarisation dependent characteristics, the tag can hold same resonators arranged in both polarisations. Fig.3.6 (b) shows the backscattered signal from the tag using horizontally and vertically polarized signals. Hence, the capacity of the tag can be doubled and the proposed tags have Surface Coding Density more than 7bits/cm^2. But there are some drawbacks with the proposed system. Tag information can be read only a distance of 5cm and information decoding fails when the tag is rotated through 45^0, because resonators excite with both polarisations. A reader with two antennas arranged in orthogonal polarisation can be adopted to make polarisation independent reader system because the tag will definitely excite with any of the exciting polarisations.
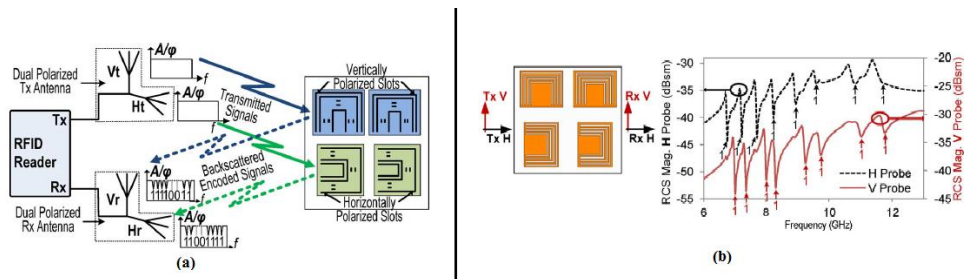
Figure 3.6 (a) Working principle of the proposed slot-loaded chipless RFID tag. (b) 16-b dual-polarized tag with all 1's and its frequency response. Courtesy: Md. Aminul Islam et. al. [17].

3.3. Backscattering from Multiscatterer Based Tag

The conductive geometries will reflect the electromagnetic waves in a particular way. The principle here is to create resonant peaks or dips in the

frequency spectrum of the backscattered signal which are distinguishable from each other. The phase change around the resonances can also be used for identification. From the electromagnetic response of a resonator, it is possible to create a link between the geometry of the resonator and its resonant frequency. In a practical RFID tag, generating resonator geometry for different bit patterns without the need of huge computational efforts is desirable.

The basic theory behind the scattering of resonant metallic objects is given by Vena et. al. [19]. Excitation of scatterer can be done by an interrogation signal in the form of an ultra-short pulse, or a broadband CW frequency sweep, by the RFID reader. When a wave is incident on a conductive surface of the tag, it will create some surface currents on the metal according to the intensity and polarisation of the incident wave. The current also depends on the shape and boundary conditions of the resonators. Scattering process from chipless RFID tag can be explained in time domain (Fig.3.7(a)). First, the main part of the energy is directly reflected by the structure in a quasi-optical way. This scattering mechanism is called structural mode, which depends only on the geometry of the tag. The remaining part of the received energy is stored in the resonator and re-emitted throughout the space with a process that occurs over time. The retransmission time depends on the quality factor of the resonators. This phenomenon is called antenna mode, which contains all the information about the resonant frequency of the tag. In this case, the signature is spread over the time and is made of a summation of damped sinusoids. The structural mode provides a large response but short in time duration while the antenna mode shows a resonant response spread in time, similar to the response of a high-quality factor tank circuit. The total electromagnetic response of the tag is the

superposition of the structural mode with an antenna mode. On analysing signals in the frequency domain by taking IFFT (Fig.3.7(b)), the structural mode is having a constant magnitude level with frequency, while antenna mode is having a selective response as peak or dip with a rapid 180° phase deviation. Depending on the phase of each mode, they can interfere constructively or destructively. As a result, it may appear as a peak or a dip respectively, in the spectrum, as seen in Fig.3.7.

Chapter 5 gives more discussion about structural mode and antenna mode from the multiscatterer based RFID tag.
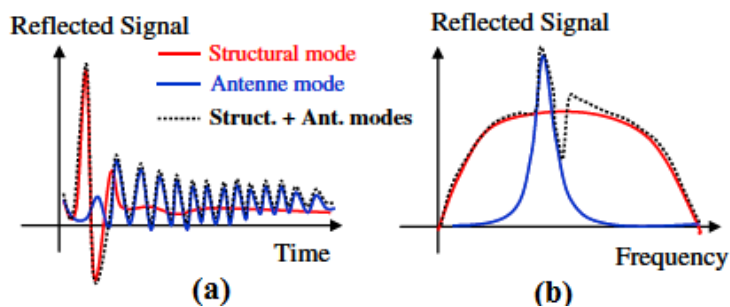
Figure 3.7 (a) Typical impulse response of a scatterer made by the addition of the structural and the antenna modes. (b) Frequency response of the scatterer. The addition of the two modes creates a destructive interference when they are 180° out of phase. Courtesy: A. Vena et. al. [19].

3.4. Criteria for Selecting Basic Scatterer

In literature, there are two types of multiscatterer based tags reported, resonator without ground plane and with ground plane. Single layer scatterers (without ground) are low cost, and their Q factors are not degraded drastically with substrate loss [12]. Hence these resonators are suitable for fabrication with FR4 substrate. Another advantage of single layer scatterer is the possibility of detection from both sides of the tag, which is not possible in the case of the tag containing resonator with ground plane. However it has some drawbacks also,

on comparison with the grounded resonator the Q factor of this resonator is low. To accommodate more number of bits in a given frequency band, Q factor should be as high as possible. The resonant frequency of the single plane resonator will vary considerably with nearby objects ie., detuning effects occur [12]. Spectral information of the tag will be incorrect due to a considerable shift in resonant frequency, while attaching it with metallic objects or high dielectric material. Compared with grounded resonator, mutual coupling between resonators are very high for the single layer tag. In most of the RFID applications, interrogation is possible from one side. Therefore present research work concentrates on the resonant structure with ground plane due to its high Q factor, low mutual coupling between nearby resonators and object on which it is tagged.

3.5. Characteristics of Chipless RFID Tag

There are some characteristics defined in the literature for the selection of frequency spectra based chipless RFID tag. They are explained below.

3.5.1. Bit Encoding Capacity (BCC)

The first key criterion of the tag is its Bit Encoding Capacity. It can be stated as the number of possible bit representations per unit frequency bandwidth (bits/GHz) of the tag. To ensure a dense coding in a given bandwidth, the tag should be able to generate resonances with very narrow bandwidths. Obviously, the selectivity is related to the Quality factor of the resonator and hence that has to be as large as possible.

3.5.2. Surface Coding Density (SCD)

Surface coding density, is the number of possible bit representations per unit area (bits/cm^2). SCD of the tag depends on the size and compactness of the resonator and on the dielectric property of the substrate.

Both Bit Coding Capacity and Surface Coding Density can be further enhanced by applying different encoding techniques like phase coding, Frequency Shift Coding (FSC), Hybrid coding, etc.

3.5.3. Readable Range

The strength of the backscattered signal from the tag determines the readable range of the system. It depends on parameters like radiated power from the reader, gain of the reader antenna, calibration and post processing of backscattered signal. RCS of the resonator depends on the area of the tag. It should be large for a good scatterer and should be small for a good Surface Coding Density. So there should be a compromise between these two parameters and selection can be made depending on the application.

3.5.4. Re-radiation Pattern and Polarisation

The re-radiation pattern at resonance is a factor to be taken into account so as to ensure the maximum energy is reflected towards the direction of the transmitted signal. Depending on the shape of the scatterer, polarisation of the backscattered signal may vary from the transmitted one. Indeed, in most cases, the detection system will consist of a single antenna for transmission and reception of interrogation signal. Therefore, depending on the polarisation property of the scatterer, proper antenna arrangement is required at the reader side.

3.5.5. Higher Harmonic Frequency

In most of the resonators harmonic frequencies are not independent, which determines the upper limit of the total usable bandwidth of the tag. To optimize the authorized bandwidth (3.1-10.6GHz), it is expected that, this upper limit should be beyond 10.6 GHz. Usually frequency of the first higher-order mode is equal to twice the frequency of the fundamental mode. For example, if the fundamental resonant mode is at 3.2GHz, then its harmonic modes can be generated at 6.4GHz, hence the frequency bands above this harmonic mode cannot be used for data encoding purposes. According to the authors' knowledge, there is no reported tag in the literature having full utilization of UWB spectrum.

3.6. Half Wavelength Transmission Line Resonator (Uniform Impedance Resonator)

Commonly used microwave transmission line resonator is the half wavelength resonator with two open-circuited ends. It is also called shorted dipole resonator. Fig.3.8 shows the geometry of the transmission line resonator. A strip conductor of uniform width and overall length equivalent to half wavelength is formed on a dielectric substrate. This structure can be expressed as a transmission line possessing uniform characteristic impedance with an electrical length of π radian. Such transmission line resonator will be referred to as Uniform Impedance Resonator (UIR). Transmission line resonators are widely used because of their simple design features. In the practical design, however, such resonators have a number of disadvantages, such as limited design parameters due to their simple structure and harmonic response at integer multiples of the fundamental resonance frequency.

A UIR is designed on an RT Duroid substrate with dielectric constant 2.2, loss tangent 0.0009 and substrate height 1mm. The Resonator is simulated in Ansys HFSS software with and without bottom ground plane. Plane wave excitation with X polarisation is used and it is placed on the broad side direction of the resonator. Length of the resonator is selected as 33mm for both cases. Fig.3.8 shows the basic structure of microstrip UIR and Fig.3.9 shows the backscattered electric field from the resonator with different configurations. From the figure it is clear that, the resonator with ground plane possesses high Q factor. Resonators with and without ground plane are resonating at different frequencies. Microstrip line based resonator is resonating at 3.1GHz while the resonator without ground plane is resonating at 3.68 GHz. This is due to more confinement of fields inside the microstrip substrate. Hence, more compact and high Q resonators can be designed using microstrip based structures. Resonators are also simulated with different angular rotation by rotating the tag along Y axis about 22.5^0. It is found that first harmonic frequencies are detected only when there is an angular shift of about 10^0. The first harmonic frequency of the resonator with and without ground plane is found to be 6.15GHz and 7.3GHz, respectively. To design an RFID tag working in the UWB frequency ranging from 3.1 to 10.6GHz, a resonator which does not generate any harmonic frequency in this band is required.
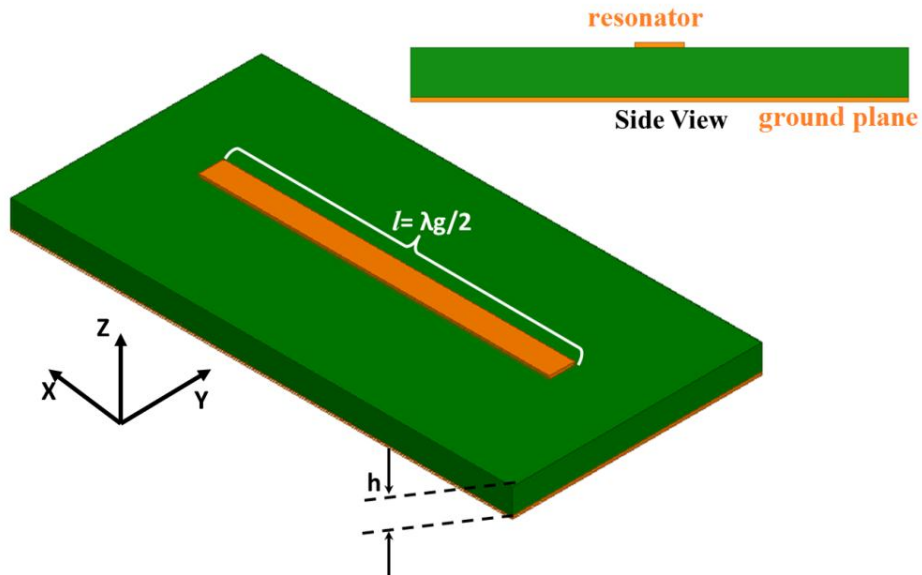
Figure 3.8 Microstrip line half-wavelength resonator, l = 33mm ε_r = 2.2 and h = 1mm
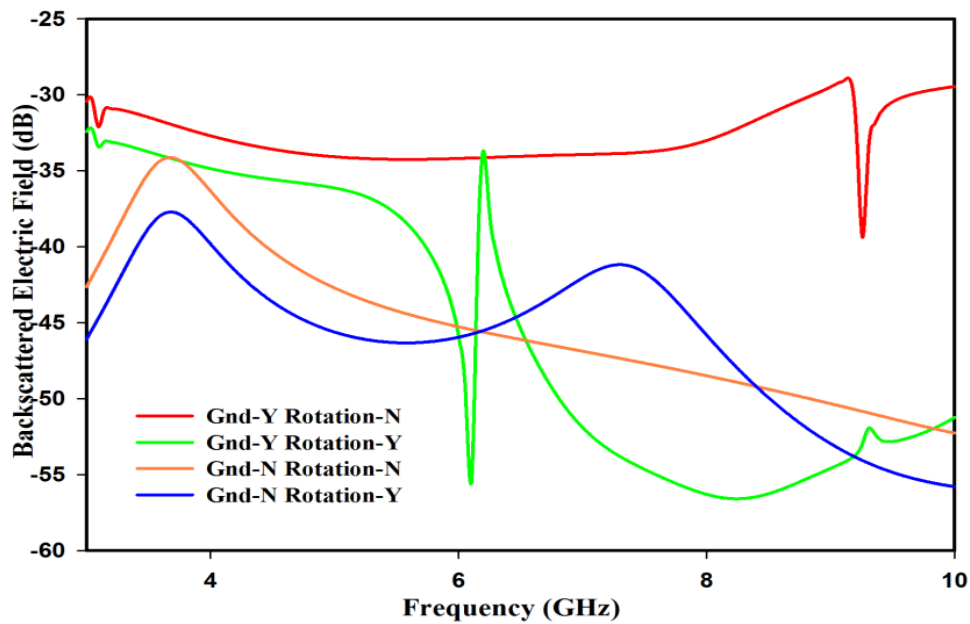
Figure 3.9 Backscattered electric field in X polarisation from UIR with different configurations.

To overcome the problems due to harmonic modes, it is a common method in the VHF band to load capacitors at both the open ends of the resonator. Then, the resonator length is shortened and spurious resonance frequencies are consequently shifted from the integer multiples of its fundamental frequency.

Fig.3.10 shows the structural variation of a half wavelength type resonator. The capacitor loaded UIR shown in figure (Fig.3.10 (b)) has a characteristic impedance of Z_1 and an electrical length of $2\theta_1$. When the angular resonance frequency ω_0 of this resonator corresponds to that of a half wavelength UIR shown in (a), the loading capacitance C is expressed as follows [20]:

$$c = \frac{Y_1 \tan\theta_2}{\omega_0} \tag{3.1}$$

where $Y_1 = 1/Z_1$, $\theta_2 = \pi/4 - \theta_1$

Looking from another point of view, by replacing both the θ_2 length transmission line components in (a) with an equivalent lumped element capacitor 'C' as in (b), the two circuits are found to be equivalent. The capacitor loaded UIR have the advantages of a small size and the capability of spurious response suppression. However, it is difficult to apply the capacitor loading above 1GHz, because the circuit loss of lumped elements capacitors C increases dramatically with frequency.
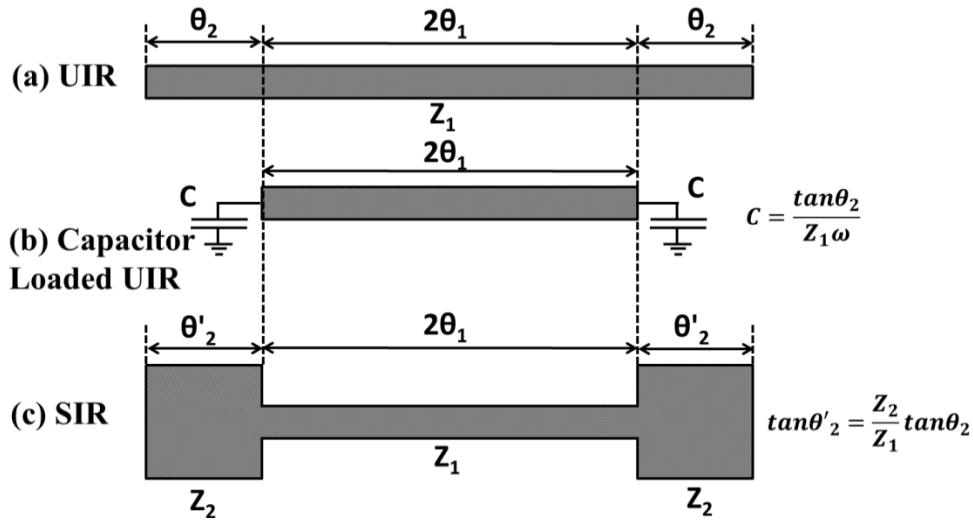
Figure 3.10 Structural variations of a half wavelength type resonator. (a) Uniform Impedance Resonator, (b) Capacitor Loaded UIR, (c) Stepped Impedance Resonator.

The loaded capacitance 'C' can be replaced by an open circuited transmission line with different characteristic impedance and it is shown in Fig.3.10(c). When $Y_2\tan\theta'_2 = Y_1\theta_2$, all three resonators will resonate at the same frequency. Thus a UIR can be transformed to Stepped Impedance Resonator (SIR) by properly cascading low and high impedance as shown in Fig.3.10(c). The problem with losses at high frequency can be reduced in this configuration.

3.7. Basic Structure of SIR

Transmission line resonators are most frequently used in frequency regions above the VHF band. The SIR is a TEM or Quasi-TEM mode resonators composed of more than two transmission lines with different characteristic impedances and is capable of shortening resonator length without degradation of unloaded Q. Fig.3.11 shows a typical example of the

SIR geometry. Figs.3.11 (a), (b), and (c) respectively show the examples of λg/4, λg/2 and λg type SIRs.

Characteristic impedances and corresponding electrical length of the SIR are denoted by Z_1 and Z_2, θ_1 and θ_2, respectively.
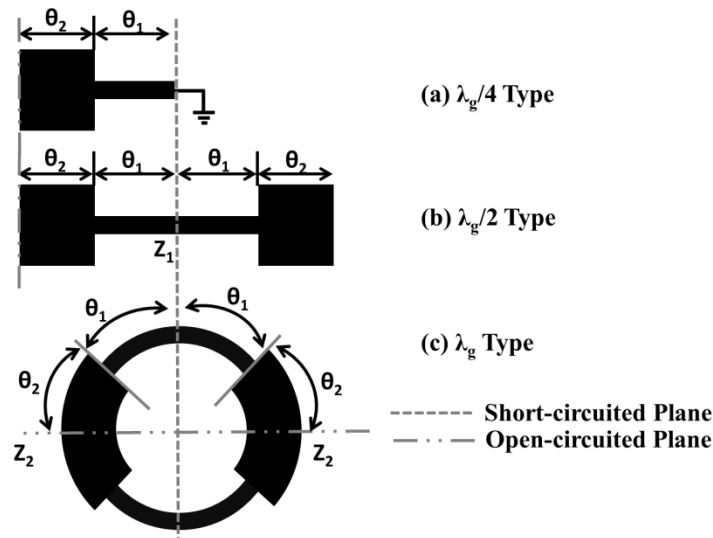
Figure 3.11 Basic structures of SIR. (a) Quarter wavelength, (b) Half wavelength and (c) Full wavelength.

The fundamental structural element common to all three types of SIR is a composite transmission line possessing both open and short circuited ends and a step junction in between. By defining this fundamental element, λg/4, λg/2, and λg-type SIR can, respectively, be looked upon as a combination of one, two, and four fundamental elements. An electrical parameter which characterizes the SIR is the ratio of the two transmission line impedances Z_1 and Z_2, and this can be defined by the following equation.

$$K = \frac{Z_2}{Z_1} \quad \text{(Impedance Ratio)} \tag{3.2}$$

3.7.1. Resonant Condition of SIR

This section discusses the conditions of fundamental and spurious resonance of the SIR. The mathematical method for finding fundamental and harmonic modes of the SIR is mentioned in [20]-[23]. The resonator structure to be considered here is shown in Fig.3.12. The SIR is symmetrical and has two different characteristic impedance lines, Z_1 and Z_2, of admittance Y_1 and Y_2. The admittance of the resonator from the open end, Y_i is given as [20].
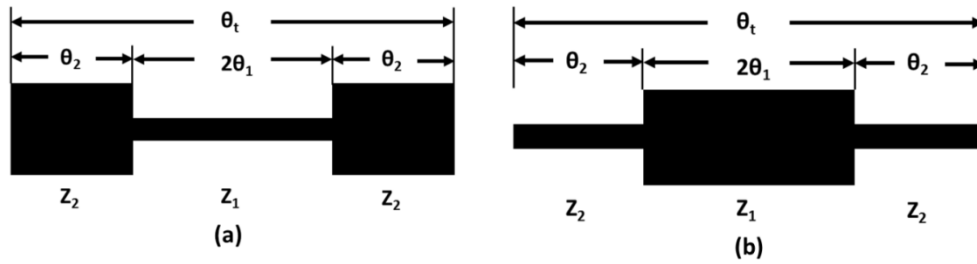
Figure 3.12 Basic Structure of SIR. (a) K < 1 and (b) K > 1.

$$Y_i = jY_2 . \frac{2(K\tan\theta_1 + \tan\theta_2).2(K - \tan\theta_1.\tan\theta_2).}{K(1 - \tan^2\theta_1).(1 - \tan^2\theta_2) - 2(1 + K^2).\tan\theta_1.\tan\theta_2} \qquad (3.3)$$

At resonance,

$$Y_i = 0) \qquad (3.4)$$

From (3.3) and (3.4) the resonance condition for odd modes (f_0, fs_2,..) can be expressed as

$$K.\cot\theta_2 = \tan\theta_1 \qquad (3.5)$$

where f_0, fs_2 are the fundamental and second harmonic modes of the SIR, respectively of the SIR. Resonant condition for even mode [21] (fs_1, fs_3,..) can be expressed as

$$K.\cot\theta_2 = -\cot\theta_1 \qquad (3.6)$$

where fs_1, fs_3 are the first and third harmonic modes of the SIR, respectively. To express the equation in simpler form, let us introduce a new term called Length Ratio (α), and it can be expressed as

$$\alpha = \frac{\theta_2}{\theta_1 + \theta_2} = \frac{2\theta_2}{\theta_t} \tag{3.7}$$

where $\theta_t = 2(\theta_1 + \theta_2)$ is the total electrical length of the resonator. Equations (3.5) and (3.6) can be modified as.

$$K.\cot\left(\frac{1}{2}\alpha.\theta_t\right) = \tan\left[\frac{1}{2}(1-\alpha).\theta_t\right] \tag{3.8}$$

$$K.\cot\left(\frac{1}{2}\alpha.\theta_t\right) = -\cot\left[\frac{1}{2}(1-\alpha).\theta_t\right] \tag{3.9}$$

It is noted that the fundamental frequency (f_0) and other higher order modes (f_{S1}, f_{S2},..) can be accurately determined by choosing a suitable combination of K and α. Value of θ_t for odd and even modes can be calculated separately by solving transcendental equations (3.8) and (3.9). The relation $\frac{f_0}{\theta_t} = \frac{fs_1}{\theta_t}$ ... can be used for finding resonant modes of SIR, where θ_t corresponds to total electrical length of the respective resonant mode. In the present analysis the effect of step junction at the high impedance and low impedance junction is neglected.
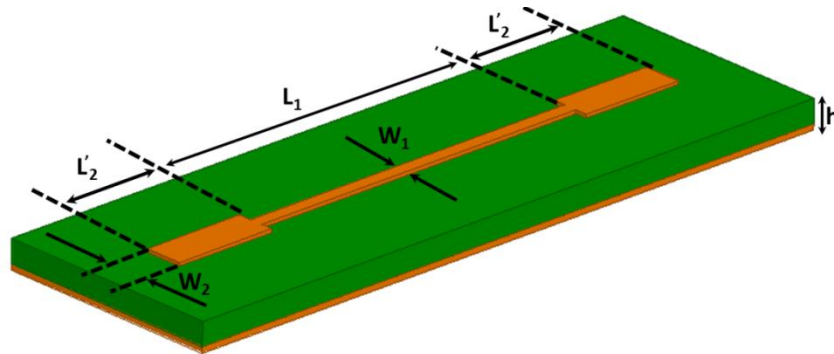
Figure 3.13 Microstrip version of SIR, K < 1, where K = 0.75, α = 0.6, L_1 = 11.8mm, L_2' = 8.21mm, W_1 = 0.5mm, W_2 = 1mm, ε_r = 2.2, tanδ = 0.0009 and h = 1mm.

In a UIR (K = 1), the fundamental and harmonic frequencies solely depend on the length of the resonator and first harmonic frequency will be equal to twice the fundamental frequency. Fig.3.12(a) and (b) show the typical structure of half wave length SIR for K<1 and K>1 respectively. Fig.3.13 shows the microstrip version of the SIR, with impedance and electrical length as SIR parameters. The effective length L'$_2$ can be expressed as $L'_2 = L_2 - \Delta L_2$, where L_2 is microstrip line length corresponding to the electrical length θ_2 and ΔL_2 is the extension of microstrip line due to fringing field [23]. Fundamental (f_0), first harmonic (fs_1) and second harmonic mode (fs_2) of SIR shown in Fig.3.14 are found to be 3.4GHz, 7.65GHz and 11.22GHz, respectively.

3.7.2. Fundamental Resonant Properties of SIR

The fundamental resonant condition can be expressed by odd mode equation (3.8). For odd-mode resonance, there is a voltage (E field) null along the symmetrical plane A-A' and it is shown in Fig.3.14. A half wavelength ($\lambda/2$) electric field distribution in the fundamental resonant frequency of 3.4GHz is clear from the field distribution. Detailed parameters of the SIR are given in the Fig.3.13.
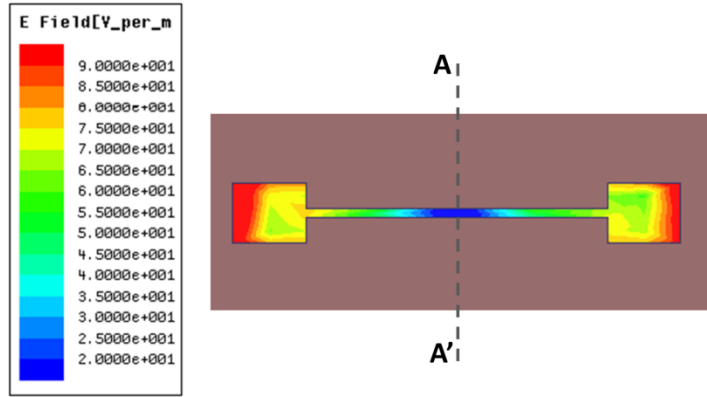
Figure 3.14 Electric field distribution in SIR at fundamental mode (3.4GHz).

One of the important property of SIR is the capability to change its total Electrical Length (θ_t) for the same resonant frequency by varying either or both Impedance Ratio (K) and Length Ratio (α). Fig.3.15 depicts the relation between Electrical Length (θ_t) and Length Ratio (α) with different Impedance Ratio (K) which is extracted by solving equation (3.8). From the figure it is clear that, for K<1 type of SIR, total Electrical Length (θ_t) will be smaller than that of UIR (π). Similarly, for K>1, total Electrical Length (θ_t) will be larger than UIR. In general, total Electrical Length (θ_t) of the SIR for fundamental mode can vary between $0 \leq \theta_t \geq 2\pi$. At fundamental mode, total electrical length (θ_t) of the SIR is found to be 0.91π for K and α value of 0.75 and 0.6, respectively. The physical length of the SIR will be smaller than that of the length calculated from total electrical length due to two open end sections in the SIR (open ended fringing field). It is also found that SIR with smaller and larger electrical length (θ_t) can be obtained by choosing length ratio (α) of 0.5, ie., $\theta_1 = \theta_2 = \theta$. Proper selection of K and α will lead the design of compact chipless RFID tags.
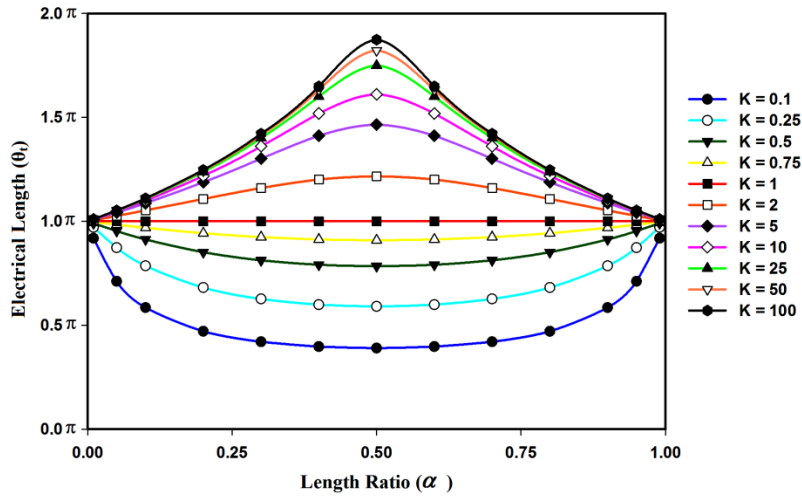
Figure 3.15 Universal curve for fundamental mode of the SIR.

3.7.3. First Harmonic Mode Properties of SIR

Resonant condition for first harmonic mode can be expressed by solving even mode equation (3.9). At even mode resonance, there is no current flow through the symmetrical plane A-A' and as it is depicted in Fig.3.16. A full wavelength current distribution is also shown at resonant frequency of 7.65GHz.
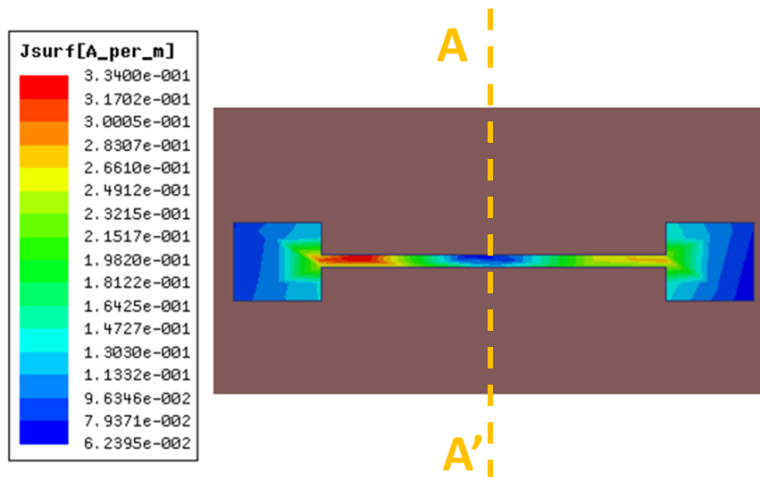
Figure 3.16 Surface current distribution in SIR at first harmonic mode

The plot between Electrical Length (θ_t) and Length Ratio (α) for different Impedance Ratio (K) is shown in Fig.3.17. From the figure it is found that, for an SIR with $\alpha < 0.5$ and K<1, then θ_t will be smaller than that of UIR ($<2\pi$) and for SIR with the same condition, except for K>1, θ_t will be larger than UIR ($>2\pi$). For $\alpha > 0.5$, conditions will be reversed, ie., for K>1, (θ_t) will be smaller than that of the UIR and for K<1, (θ_t) will be larger. When α is at 0, 0.5 and 1, θ_t will be same as that of UIR irrespective of the K values. By choosing different values of K & α, total Electrical Length (θ_t) of the SIR for first harmonic mode can be varied between $\pi \leq \theta_t \geq 3\pi$. Total Electrical Length of the SIR at the first harmonic mode is found to be 2.05π, for K of 0.75 and α of 0.6.
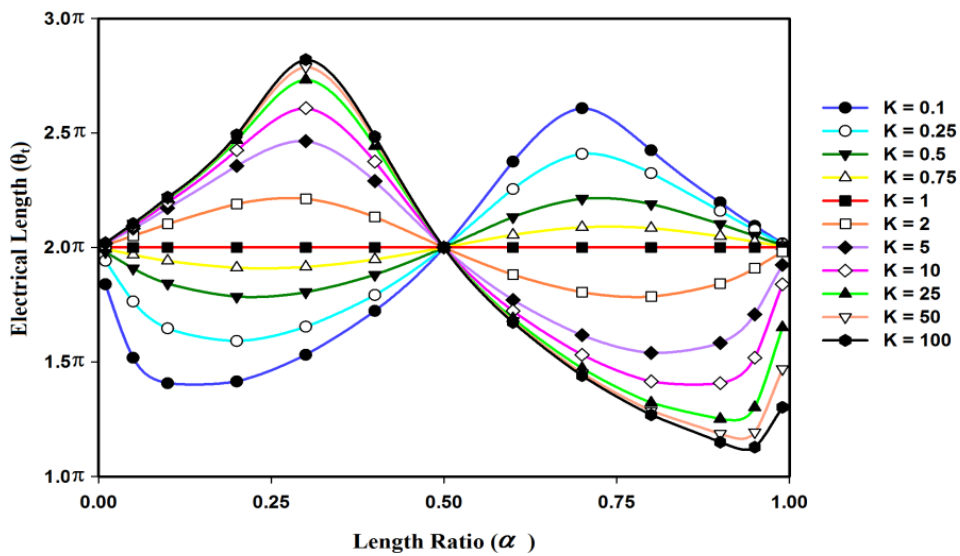
Figure 3.17 Universal curve for first harmonic mode of the SIR

3.7.4. Second Harmonic Mode Properties of SIR

The second harmonic mode condition can be expressed by solving odd mode equation (3.8). As explained in the case of the fundamental mode, there

is an E field null along the symmetrical plane A-A' and is shown in Fig.3.18.
A $3\lambda/2$ distribution of electric field in the resonator at second harmonic frequency of 11.22GHz is also depicted in Fig.3.18.
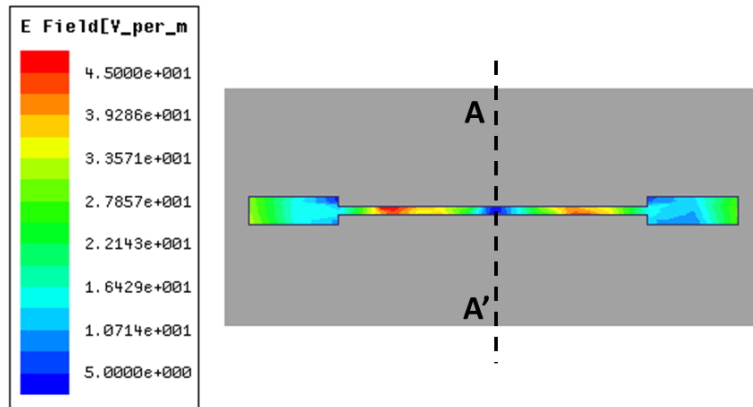
Figure 3.18 Electric field distribution in SIR at second harmonic mode
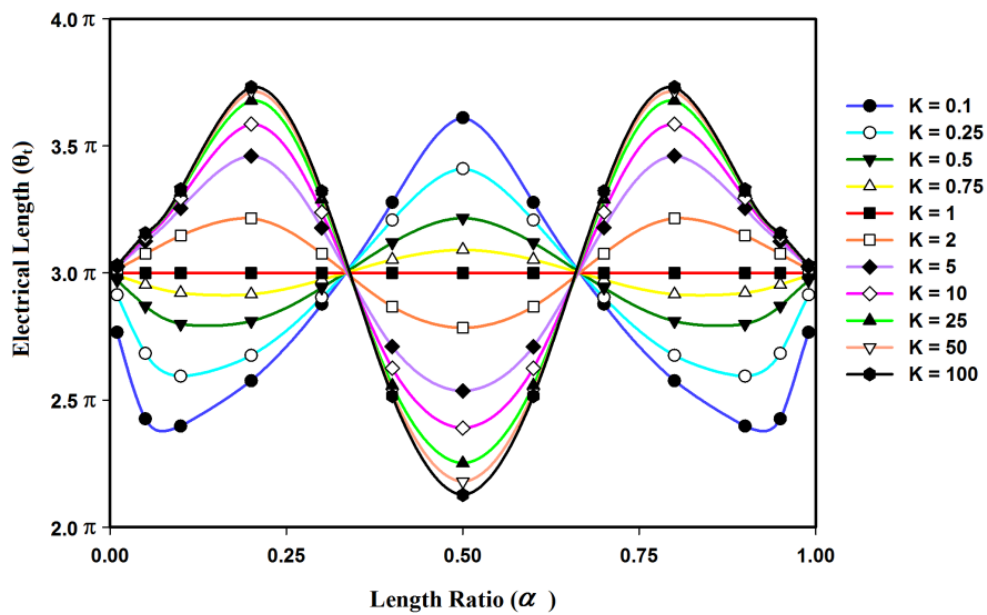
Figure 3.19 Universal curve for second harmonic mode of the SIR

The Relation between Electrical Length (θ_t) and Length Ratio (α) for different Impedance Ratio (K) is depicted in Fig.3.19. In Second harmonic mode, total electrical length (θ_t) will be equal to the electrical length of UIR for length ratio (α), equivalent to 0, 0.33, 0.66, and 1. With different value of K & α, total Electrical Length (θ_t) of the SIR for second harmonic mode is within the range of $2\pi \leq \theta_t \geq 4\pi$. For SIR with K<1 and α ranging from 0-0.33 & 0.66-1, θ_t will be larger than that of UIR (3π) and vice versa for K<1 type of SIR. In the case of K<1 & α ranging from 0.33-0.66, θ_t will be smaller than that of the UIR and vice versa for K>1 type SIR. Total Electrical Length of the SIR at the second harmonic mode is found to be 3.05π, for K = 0.75 and $\alpha = 0.6$.

3.7.5. Relationship between Fundamental and First Harmonic Mode.

The relationship between length ratio (α) and the ratio of first harmonic and fundamental mode (f_{S1}/f_0) of SIR with different values of impedance ratio (K) is depicted in Fig.3.20. It shows the possible separation between two modes (f_{S1} & f_0) with different SIR parameters. For example, in the case of UIR (K = 1), the first harmonic frequency will be always twice the fundamental mode, ie., $\frac{f_{S1}}{f_0} = 2$, for all values of K and α. An interesting fact in Fig.3.20 is that, larger the impedance ratio (K > 1), closer is the spacing between the fundamental mode and first harmonic mode ($f_{S1}/f_0 < 2$) and similarly, smaller the impedance ratio (K <1), larger is the spacing between the fundamental and first harmonic mode ($f_{S1}/f_0 > 2$). Hence the f_{S1} can be placed in the frequency range from $1.16f_0$ to $3.75f_0$ by changing the value of K from 0.25 to 7. Maximum or minimum shift in f_{S1} mode can be achieved by selecting α between 0.6 and 0.7.
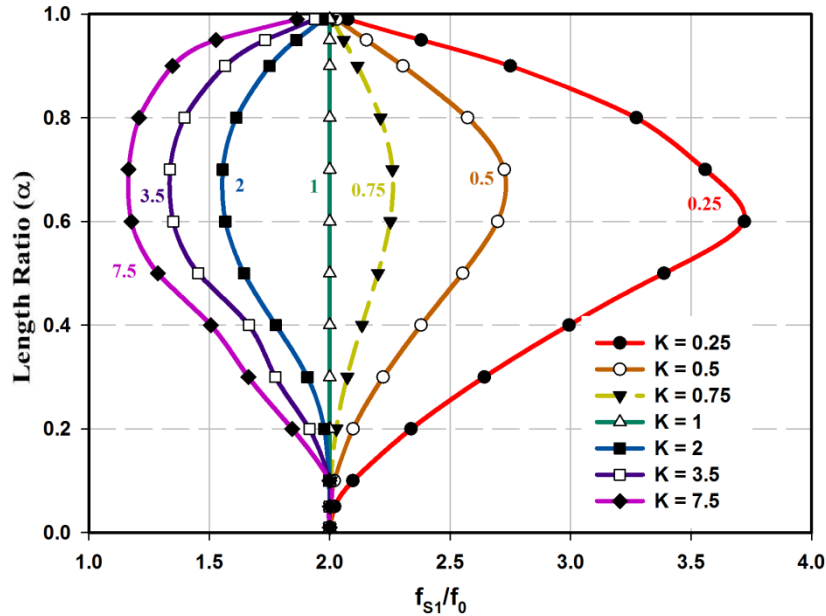
Figure 3.20 Relationship between Length Ratio (α) and f_{S1}/f_0 for different Impedance Ratio (K).

3.7.6. Relationship between Fundamental and Second Harmonic Mode.

The relationship between length ratio (α) and ratio of second harmonic and fundamental mode (f_{S2}/f_0) of the SIR with different values of impedance ratio (K) is depicted in Fig.3.21. As explained earlier, larger the impedance ratio (K > 1), closer is the spacing between the fundamental mode and second harmonic mode ($f_{S2}/f_0 < 3$). Similarly, smaller the impedance ratio (K <1), larger is the spacing between the fundamental and second harmonic mode ($f_{S2}/f_0 > 3$). The f_{S2} can be placed in the frequency range from $1.25f_0$ to $5.75f_0$ by changing the value of K from 0.25 to 25. Maximum or minimum shift in f_{S2} mode can be achieved by selecting α as 0.5. In the case of UIR, second harmonic mode will always be the third multiple of fundamental mode for all values of K and α, ie. $\frac{f_{S2}}{f_0} = 3$.
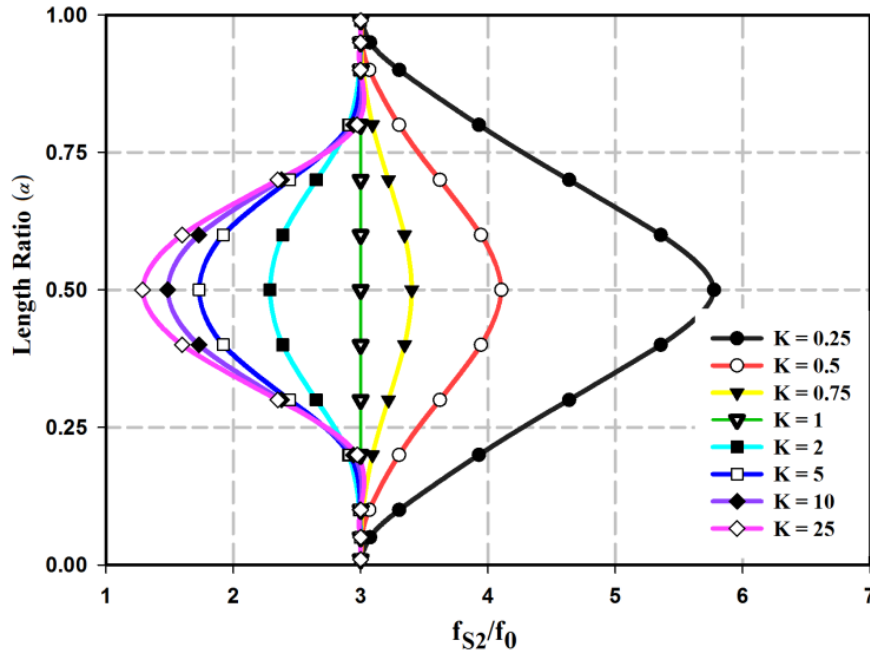
Figure 3.21 The relationship between Length Ratio (α) and f_{S2}/f_0 for different Impedance Ratio (K).

3.7.7. Relationship between First Harmonic and Second Harmonic Mode.

SIR provides ample freedom to place its frequency modes anywhere in the spectrum. Fig.3.22 shows the relation between length ratio (α) and ratio of second and first harmonic modes (f_{S2}/f_{S1}) of the SIR for different Impedance Ratio (K). The relationship between two modes (f_{S2} and f_{S1}) are quite different from the above two relations. Depending on the value of K and α, the separation between first harmonic mode and second harmonics can be designed on either lower or higher side of the UIR. Second harmonic of the SIR can be placed very close to the first harmonic mode and may also be placed much away from the position of the second harmonic mode of the UIR, by simply changing the value of Length Ratio (α). By selecting K>1

and α between 0.2 to 0.6 or selecting K <1 and α between 0.6 and 1, second harmonic mode can be placed very close to the first harmonic mode (closer up to $1.15f_{S1}$). Similarly, second harmonic mode can be placed very far away from the first harmonic mode (away up to $2.75f_{S1}$), by selecting K<1 and α between 0.1 and 0.6 or by selecting K>1 and α between 0.6 and 1.
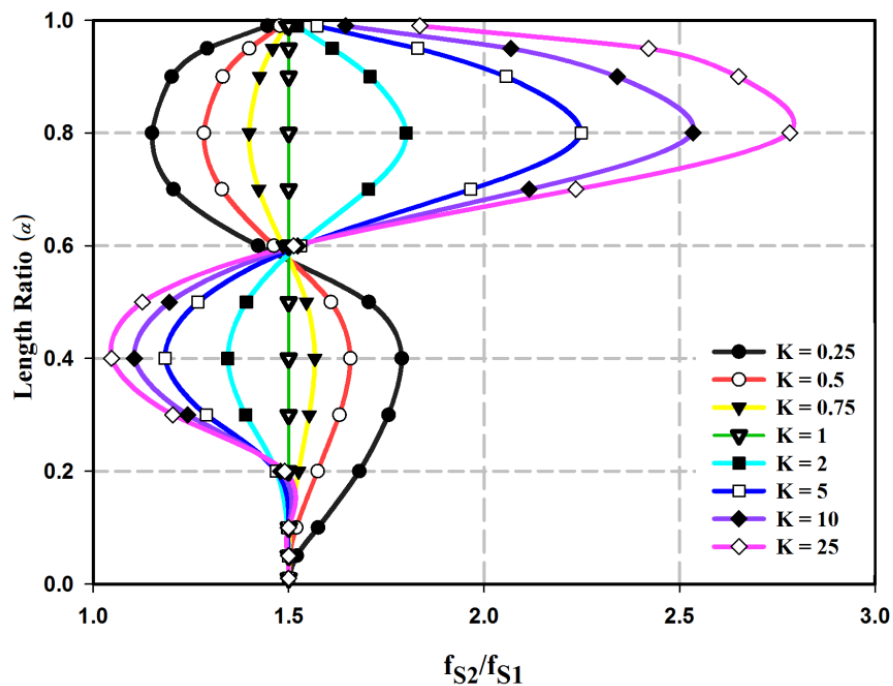
Figure 3.22 Relationship between Length Ratio (α) and f_{S2}/f_{S1} for different Impedance Ratio (K).

3.8. Simulation and Measurement for SIR Based Multiscatterer Chipless RFID Tag.

The proposed RFID system consisting of an RFID reader with single reader antenna and an RFID tag is shown in Fig.3.23. RFID reader with single reader antenna system provides a great degree of measurement freedom compared to two antenna system, in which reader antennas are placed at small

angular separation. Total dimension of the chipless RFID tag is smaller than the total radiating area of the high gain reader antenna. Therefore, placement of RFID tag in a common radiation zone of the reader antenna becomes difficult for practical applications.

The RFID tag is design and fabricated on both RT Duroid (ε_r = 2.2 and tanδ = 0.0009) and CMET LK-4.3 (ε_r =4.3 and tanδ = 0.0018) substrates. Finite Element Method based Ansys HFSS software with plane wave or linear antenna wave (used for the simulation of far field of a linear antenna) excitation is used for the simulation studies of the proposed system, in which source is placed at a distance of 10cm above the tag. The Fig.3.24 shows the basic simulation setup with a chipless RFID tag consisting of a single SIR. The E_x and K in Fig.3.24 is the polarisation of the incident field and its direction of propagation (pointing vector), respectively. Here polarisation of electric field in X direction and propagation in –ve Z direction. To limit the simulation area and avoid multiple reflection, RFID tag and plane wave source are covered with a radiation boundary as shown in the figure. For measurements, Agilent PNA E8362B Network Analyser with 1mW output power is used as the source. A Linearly polarized medium gain (10dB) horn antenna is used for transmission and reception of the interrogation signal.
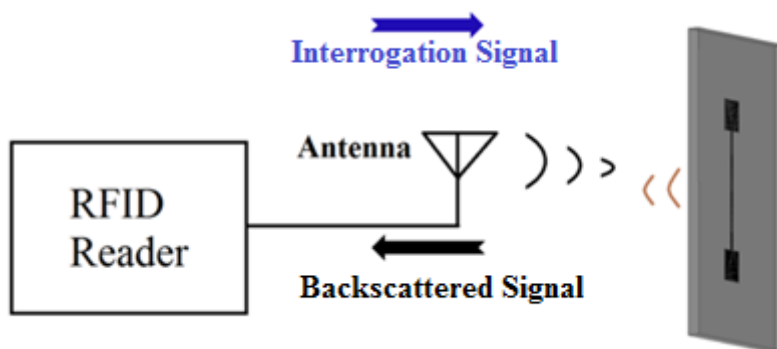
Figure 3.23 Proposed RFID System
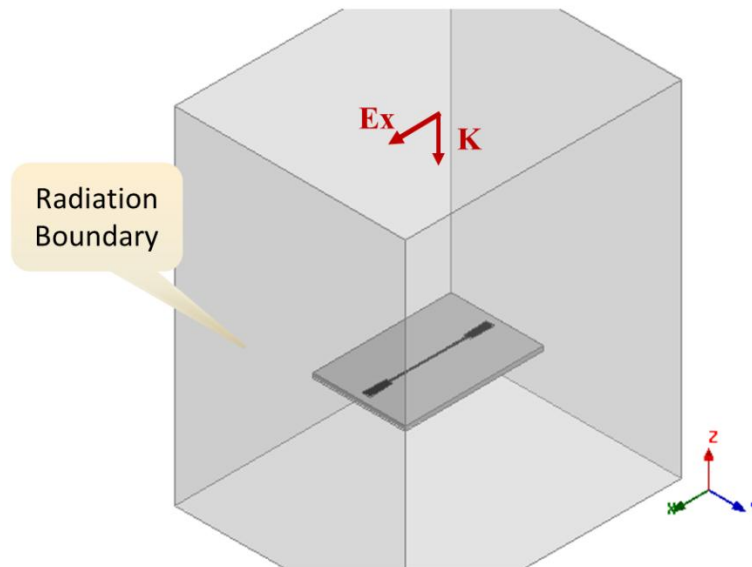
Figure 3.24 Simulation setup used in the HFSS software

3.9. Calibration Technique

In the proposed chipless RFID system, binary '1' can be identified from the presence of a resonant peak or dip in the backscattered signal. This depends on many factors like polarisation of the incident and scattered wave, shape of the resonator, etc. The backscattered signal in the reader system comprises of reflected signal from different objects and the main part of reflected signals are from the reader antenna (due to impedance mismatch), RFID tag, stationary objects, interference from nearby wireless gadgets, noise, etc. Therefore, suitable calibration is required for the successful extraction of encoded data. Calibration adopted here can be easily explained by analysing the signal in time domain [24]. Here a Gaussian pulse $x(t)$ having frequency range from 3.1GHz to 10.6GHz is used as the interrogation pulse. The backscattered signal $y(t)$ consists of three major components, the reflected signal $y_r(t)$ from the antenna terminal due to the impedance mismatch, the structural mode $y_s(t)$ due to the size and metallic structure of

the tag, and the antenna mode signal $y_a(t)$. The shape of the structural mode signal will be same as that of the input signal and it does not contain any information. The frequency information of the tag is contained in the antenna mode. Calibration procedure for the proposed system in frequency domain can be done by subtracting S_{11} without tag from S_{11} with tag. The ambiguities and clutter due to static objects in the background can be removed. The resultant signal contains only the structural and antenna mode of the RFID tag along with noise from the surrounding. Signal analysis can be explained by the following expression outlined in [24]. The signal $y_e(t)$ corresponding to S_{11} without tag, contains reflected signal $y_r(t)$ and noise $y_n(t)$. The noise in the measurement is due to reflection from stationary objects and white noise which will vary with time.

$$y_e(t) = y_r(t) + y_n(t) \qquad (3.10)$$

The signal $y(t)$ corresponding to S_{11} with tag contains reflected signal from the antenna, reflected signals from the RFID tag, and noise $(y_n'(t))$. It can be represented as,

$$y(t) = y_r(t) + y_s(t) + y_a(t) + y_n'(t) \qquad (3.11)$$

Taking the difference between (3.10) and (3.11) will remove the effect of reader antenna and also the clutter noise from the surroundings. Calibrated signal $y_c(t)$ thus contains only the backscattered signal from the RFID tag and white noise $\left(y_n''(t) = y_n'(t) - y_n(t)\right)$. The signal $y_c(t)$ can be expressed as

$$y_c(t) = y_s(t) + y_a(t) + y_n''(t) \qquad (3.12)$$

Measurements are carried out inside and outside the anechoic chamber with sufficient averaging to minimize the white noise level. In the present work, measurements are done with an averaging factor 16.

3.10. SIR with Independent Control Over Resonant Mode

As seen in the previous sections, all the resonant properties of SIR can be controlled by suitably selecting the value of K and α. Here SIR is designed on RT Duroid substrate with different K and α values for demonstrating the independent control of the fundamental and first harmonic frequencies. Fig.3.13 shows the basic structural dimensions of the SIR with K<1. Fig.3.25 & 3.26 shows the variation of resonant frequencies of the SIRs with different K values. Fig.3.25 depicts the fs_1 variation with different K values, while keeping f_0 at 3.4GHz and α at 0.4. The control on of f_{S1} from 5.36GHz to 9.5GHz (4.14GHz bandwidth) is achieved by varying K from 0.3 to 5. Similarly, Fig.3.26 depicts the variation of fundamental mode (f_0) with different K values, while keeping fs_1 and α at 8.5GHz and 0.4, respectively. Here control on f_0 from 3.03GHz to 5.24GHz (2.21GHz bandwidth) is achieved for different values of K. Detailed structural dimension of the different SIRs used in Fig.3.25 & 3.26 are given in Table 1. Measured and simulated results show good agreement with theoretical calculation using equation (3.8) & (3.9).
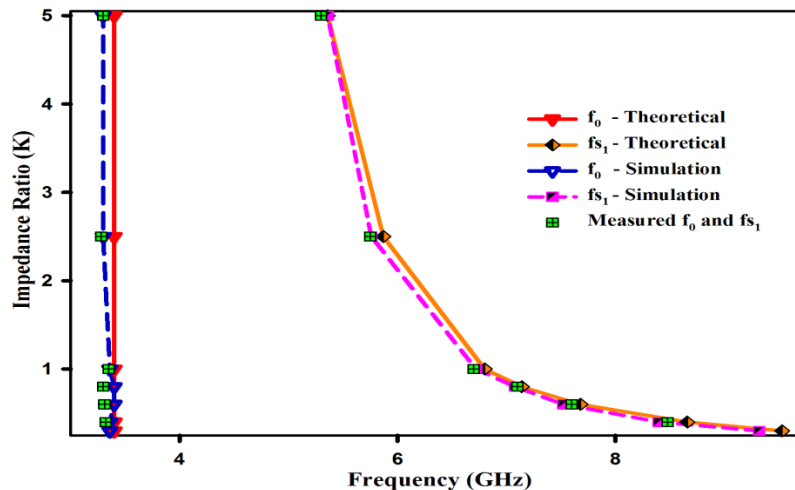
Figure 3.25 Variations in the first harmonic frequency with different values of K, while f_0 = 3.4GHz and α = 0.4, (r,θ,ϕ) = (20cm,22.5^0,0^0).
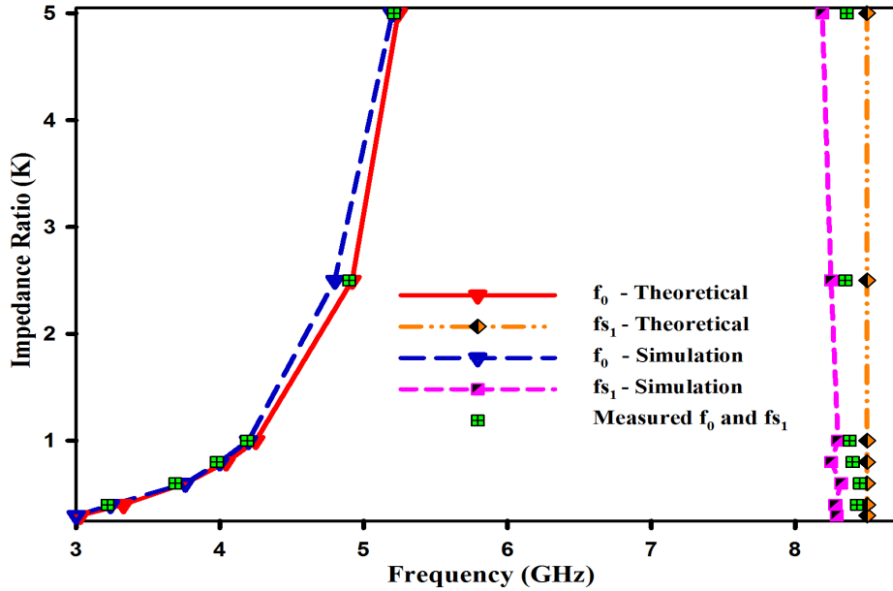
Figure 3.26 Variations in the first harmonic frequency with different values of K, while fs_1 = 8.5GHz and α = 0.4, (r,θ,ϕ) = (20cm,22.5^0,0^0).

Table 1: Structural Dimensions of SIR for Different K values α = 0.4, h = 1mm

K	W_1 (mm)	W_2 (mm)	f_0 = 3.4GHz Fig.3.25		fs_1 = 8.5GHz Fig.3.26	
			$2L_1$ (mm)	L'_2 (mm)	$2L_1$ (mm)	L'_2 (mm)
0.3	0.5	4.70	12.97	3.04	14.55	3.53
0.4	0.5	3.10	14.56	3.86	14.84	3.95
0.6	0.5	1.55	16.95	4.95	15.33	4.42
0.8	0.5	0.87	18.70	5.70	15.72	4.72
1.0	0.5	0.50	20.11	6.29	16.08	4.95
2.5	3.0	0.50	24.18	8.02	16.70	5.42
5.0	7.5	0.50	26.31	9.05	17.07	5.72

Variations of f_0 & fs_1 with respect to α are depicted in Fig.3.27 & 3.28. Fig.3.27 shows the variation in fs_1 by changing α is from 0.1 to 0.9 while keeping K at 0.6 and f_0 at 3.4GHz. A frequency band of 6.72GHz to 8.36GHz (bandwidth of 1.64GHz) in fs_1 is achieved by changing α from 0.1 to 0.7. Similarly, Fig.3.28 shows the variation of f_0, while fs_1 and K are kept

constant at 8.5GHz and 0.6, respectively. Tuneable bandwidth of 800MHz (3.4GHz-4.2GHz) for f_0 is obtained by changing α values. The structural dimensions of different SIRs for Fig.3.27 & 3.28 are detailed in Table 2.
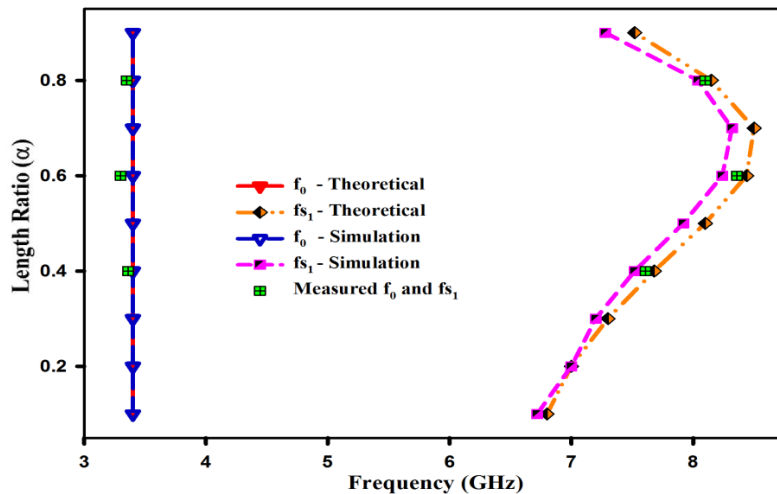
Figure 3.27 Variations in the first harmonic frequency with different Length Ratio, while f_0 = 3.4GHz and K = 0.6, (r,θ,ϕ) = (20cm,22.5^0,0^0).
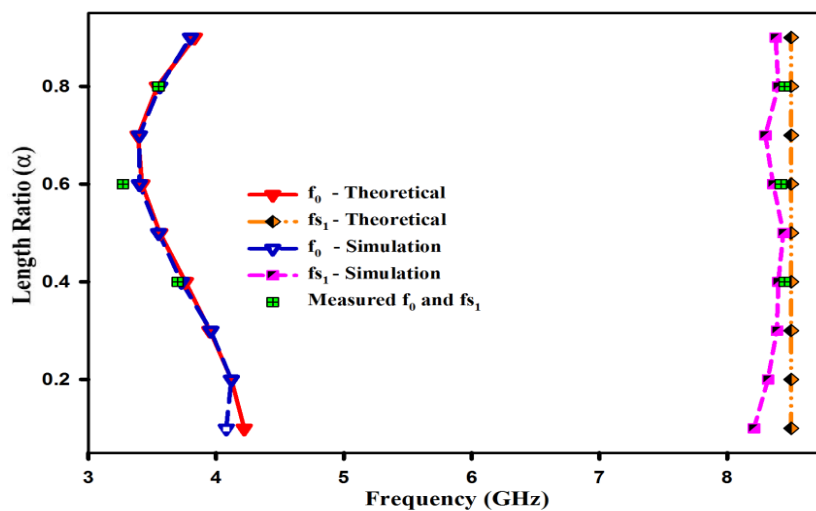
Figure 3.28 Variations in fundamental mode with different Length Ratio while fs_1 = 8.5GHz, where K = 0.6, (r,θ,ϕ) = (20cm,22.5^0,0^0).

Table 2: Structural Dimensions of SIR for Different α values. K = 0.6, W_1 = 0.5mm, W_2 = 1.55mm and h = 1mm

α	f_0 = 3.4GHz (Fig.3.27)		fs_1 = 8.5GHz (Fig.3.28)	
	$2L_1$ (mm)	L'_2 (mm)	$2L_1$ (mm)	L'_2 (mm)
0.1	28.28	0.97	22.74	1.23
0.2	23.91	2.36	19.71	2.39
0.3	20.19	3.66	17.35	3.62
0.4	16.95	4.95	15.33	4.97
0.5	14.03	6.28	13.38	6.51
0.6	11.30	7.70	11.22	8.19
0.7	8.65	9.28	8.65	9.83
0.8	5.97	11.09	5.73	11.17
0.9	3.14	13.21	2.78	12.19

3.11. Amplitude Detection Method

Backscattered signal power from the scatterer can change with resonant characteristics of the tag and also with other environmental parameters. Hence finding exact resonant frequencies of the tag is usually difficult when there is a variation in backscattered power in the desired frequency band (as seen in Fig.3.9). Even though at resonance amplitude variation are drastic compared to noises. Exact resonant frequency can be identified by simple post processing of backscattered signal. Equation (3.13) shows the difference operation technique on measured backscattered signal to find the exact resonant frequency.

$$y'(i) = |y(i+1) - y(i)| \qquad\qquad (3.13)$$

where y(i) is the backscattered magnitude at i^{th} frequency point and $y'(i)$ is the new value. Fig.3.29 shows the scattered signal from the SIR based tag and its post processed signal calculated using the above equation. A peak variation at resonance is clearly visible from the post processed signal. This

amplitude detection method is carried out and validated for all the measured backscattered signals.
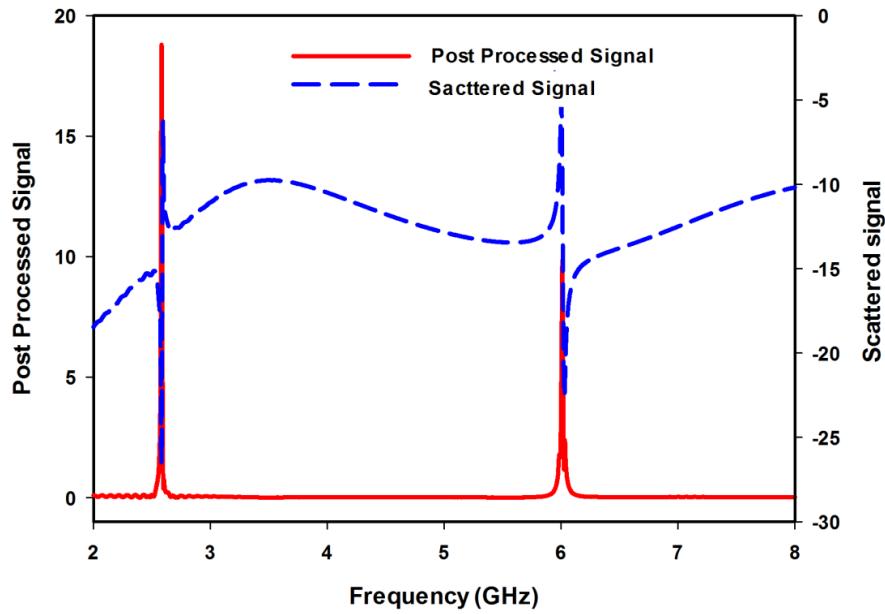
Figure 3.29 Simulated scattered signal from the resonator and its post processed signal.

3.12. Scattering Property of SIR

The proposed RFID reader system (seen in Fig.3.30) consists of only a single antenna, to interrogate and detect the backscattered signal from the tag. Hence for detection, polarisation of the received signal should be same as that of the transmitted signal. An SIR is designed on CMET LK-4.3 substrate with the fundamental mode at 3.4GHz and first harmonic mode at 7.68GHz for analysing the backscattered signal with different angular position. The K and α values for the SIR is selected as 0.6 and 0.4, respectively. The structural dimension of the SIR is given in Fig.3.30. The backscattered signals are measured for different θ and ϕ angles by rotating either tag or reader antenna. X and Y polarized signals are applied to RFID tag as shown

in the Fig.3.30. Fig.3.31 shows the backscattered signal with different values of ϕ and polarization, while keeping 'r' at 20cm and 'θ' at 22.5^0. The resonators respond well up to 60^0 with X polarization and are insensitive to Y polarization. Beyond 60^0 resonant dip in the f_0 mode is degraded and difficult to identify from the backscattered signal. All the resonances are successfully detected using amplitude detection method and it is depicted in Fig.3.32. Signal above the threshold value of 0.5 can be considered as the resonance.
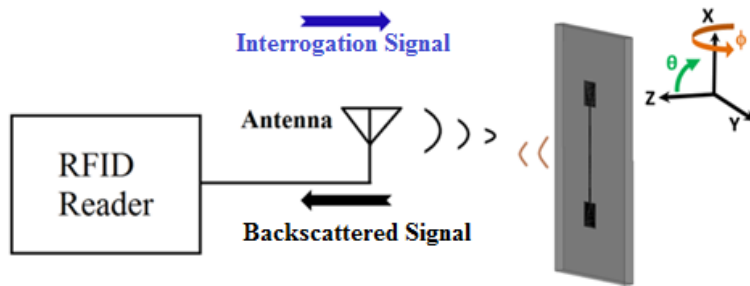
Figure 3.30 Proposed RFID system. Structural dimension of SIR (as shown in Fig.3.13) is W_1 = 0.5mm, W_2 = 1.8mm, $2L_1$ = 12.85mm, L'_2 = 3.37mm, ε_r = 4.3, tanδ = 0.0018 and h = 1.6mm.
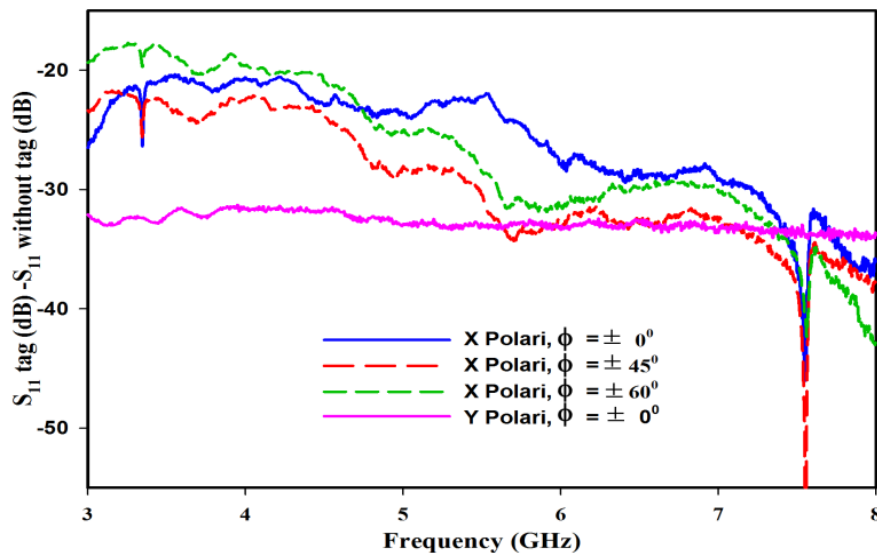
Figure 3.31 Measured backscattered signal with different ϕ values. (r,θ) = (20cm, 22.5^0) (anechoic chamber)
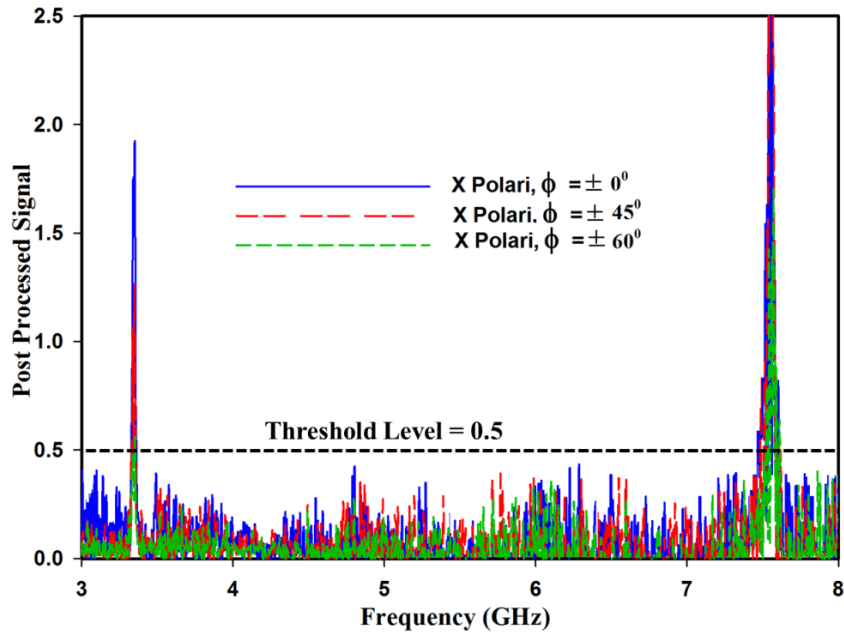
Figure 3.32 Post processed amplitude detected signal of Fig.3.

The frequency responses of the tag with different θ values are shown in Fig.3.33. Along broadside direction ($\theta = 0^0$, $\phi = 0^0$) only the fundamental mode (f_0) appears in the backscattered signal without any first harmonic (fs_1). However, fs_1 can be detected from other θ values up to 75^0. It is found that, the backscattered signals will cancel each other along the broad side direction due to opposite current at full wavelength pattern as shown in Fig.3.35. The post processed amplitude detection signal plotted in Fig.3.34 validated and it is shown in Fig.3.35. The resonators will respond to incident polarized signal (vertical and horizontal) when tag or reader antenna rotates 45^0 along the XY plane [7]. In the case of first harmonic mode, a current maximum occurs at the microstrip step junction. The step junction effect is neglected in the calculations and hence a small change in the theoretical and measured/simulated values of f_{S1} is observed.
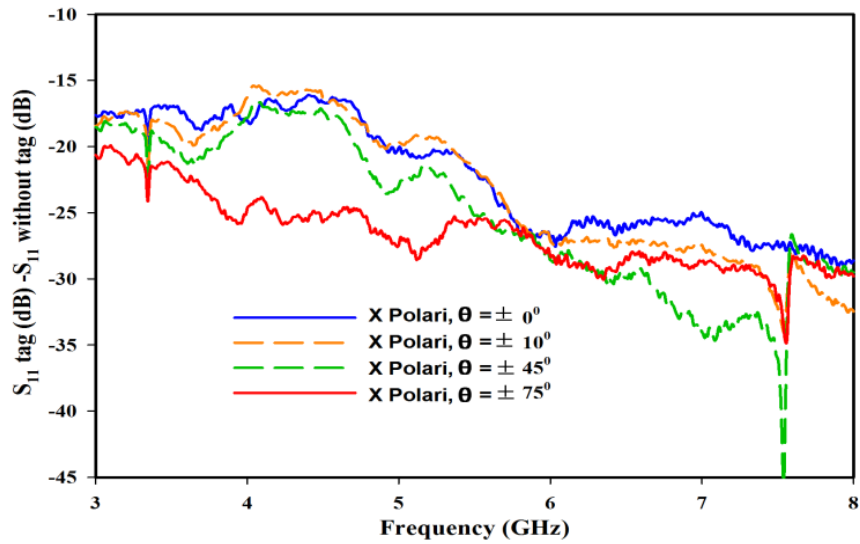
Figure 3.33 Measured backscattered signal with different θ values. (r, φ)= (20cm,0⁰) (anechoic chamber).
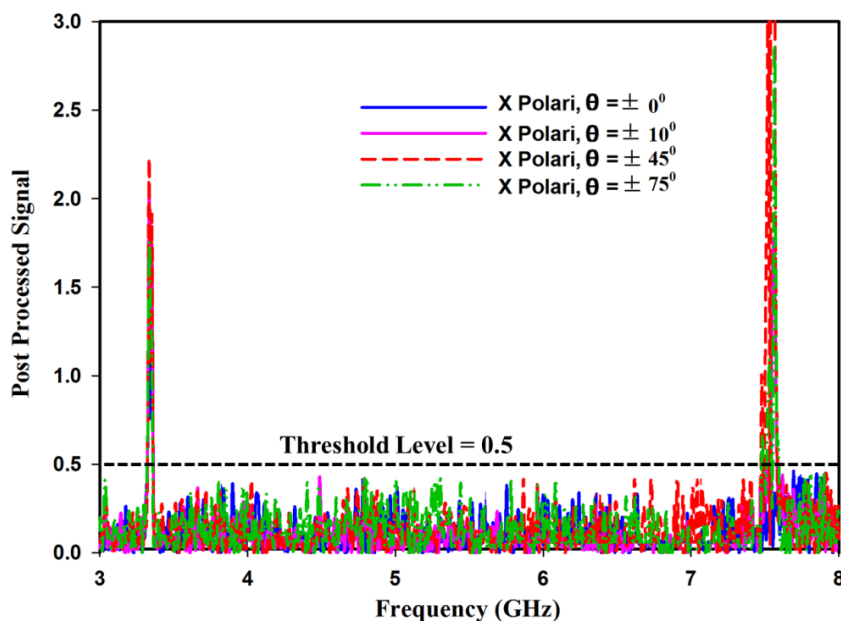
Figure 3.34 Post processed amplitude detected signal of Fig.3.33
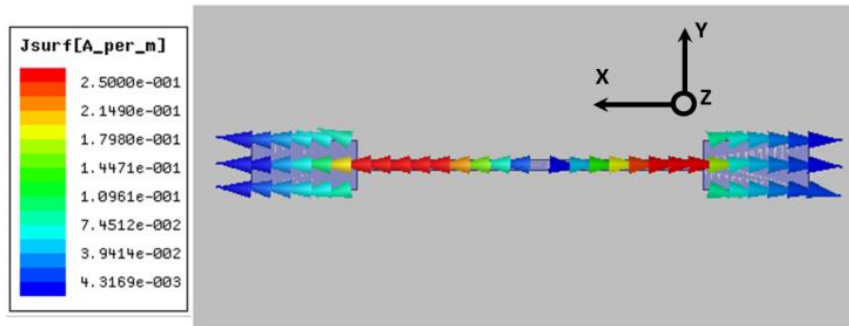
Figure 3.35 Surface current distribution in SIR at fs₁ (7.62GHz)

3.13. Substrate for Multiscatterer Based Chipless RFID Tag.

Selection of substrate material is important for the design of RFID tags. There are mainly three types of losses in the substrate, conduction loss, dielectric loss and radiation loss. Radiation losses are advantageous because it will enhance the backscattered power. Using copper as conducting material conduction losses can be minimised. Loss inside the material is playing significant role in the selection of suitable substrate. To analyse backscattered responses from different substrate material, an SIR is simulated the following materials.

1. **FR4 substrate** with dielectric constant of 4.4, loss tangent of 0.02 and substrate height of 1.6mm,

2. **Glossy Paper** with dielectric constant of 3, loss tangent of 0.09, substrate height of 0.22mm,

3. **CMET LK-4.3** with dielectric constant of 4.3, loss tangent of 0.0018, substrate height of 1.6mm,

4. **RT Duroid 5880** with dielectric constant of 2.2, loss tangent of 0.0009, substrate height of 1mm.

Simulated backscattered responses of the tag with different substrate are shown in Fig.3.36. It is found that, CMET LK-4.3 and RT Duroid possess sharp

resonance. Resonances are found to be at different frequency due to the variations in the dielectric permittivity. The amplitude at the resonant modes is changing with Q factor of the structure. Resonances are distinct using FR4 substrate, but the Q factor of the SIR is quite low. Bit encoding capacity of the tag will deteriorate with low Q structures due to the requirement of large bandwidth for representing resonance. The resonant frequencies are unable to detect with Glossy Paper and it may is due to the high dielectric losses inside the material. Therefore, low loss substrate materials are needed for the design of multiscatterer based chipless RFID tag. Hence, CMET LK-4.3 and RT Duroid 5880 substrates are opted for the design and fabrication of chipless tag.
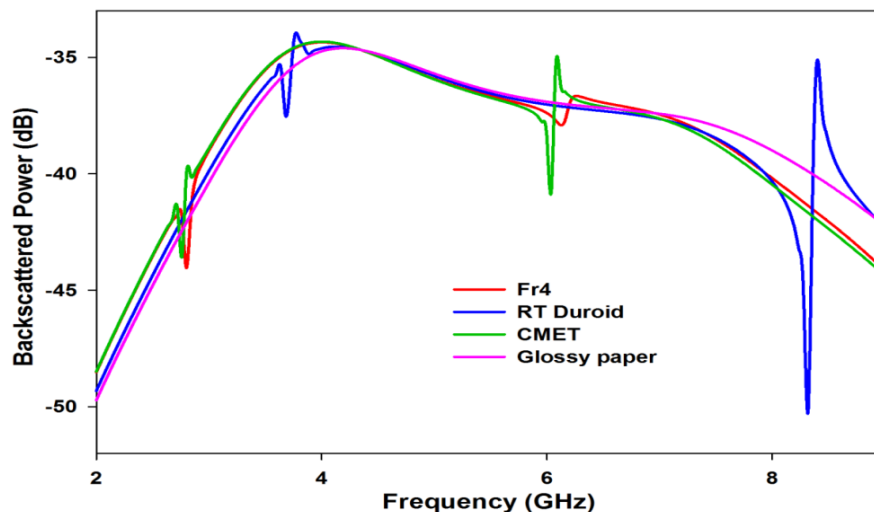
Figure 3.36 Simulated backscattered response of the single SIR tag on four different materials.

3.14. SIR based Chipless RFID Tag for UWB Application

From the above analysis, it is concluded that, SIR have number of advantages compared with other resonators reported as the basic scatterer in the RFID tag application.

❖ Capabilities to control total Electrical Length (θ_t), which can be used to develop compact RFID tag.

❖ Harmonic mode separation, effective utilization of UWB frequency can be achieved.

❖ Independent control over resonant modes, it enables to encode data using harmonic modes.

Most of the reported tags [5]-[17] are not able to use the entire bandwidth of the UWB spectrum ranging from 3.1GHz to 10.6GHz, due to the presence of the harmonic modes at the integral multiples of fundamental modes. Thus usable bandwidth of the tag is limited in between fundamental mode and first harmonic mode of the basic scatterer. In this section, an SIR based chipless RFID tag is designed on the RT Duroid substrate ($\varepsilon_r = 2.2$) for UWB spectrum ranging from 3.1GHz to 10.6GHz. Tag consists of 10 SIRs, which uses the fundamental mode only for encoding the bit information. Fig.3.37 shows the chipless RFID tag using SIRs with an overall dimension of 55x30 mm^2, which is small compared with the size of a standard credit card (85.60 × 53.98 mm^2). Depending on the ascending order in resonant frequency, SIRs are labelled as I, II,.. and X. Resonators in the tags are arranged in an asymmetric way to avoid the mutual coupling effect. Table 3 details the structural dimension, K and α values of each resonator used the design.

SIRs are selected in such way that, first harmonic modes of the resonators are designed outside the UWB (>10.6GHz). Frequency shift coding method [7] is used in this design to enhance the bit encoding capacity of the tag. Therefore, each resonator in the tag is assigned with a frequency band of 750MHz, ie., conditions for SIR-I are, its fundamental mode can be

designed for a frequency band ranging from 3.1GHz to 3.85GHz and its first harmonic frequency should fall above 10.6GHz. The ratio between f_{S1} and f_0 for SIR-I is 3.42 (10.6/3.1), as per Fig.3.20, to design a SIR with above frequency specification, the value of K should be less than 0.25 and the value of α should be in between 0.5 to 0.7. Other SIRs in the RFID tag are also designed in similar way. Table 3 also shows the designed and measured values of resonant frequencies.
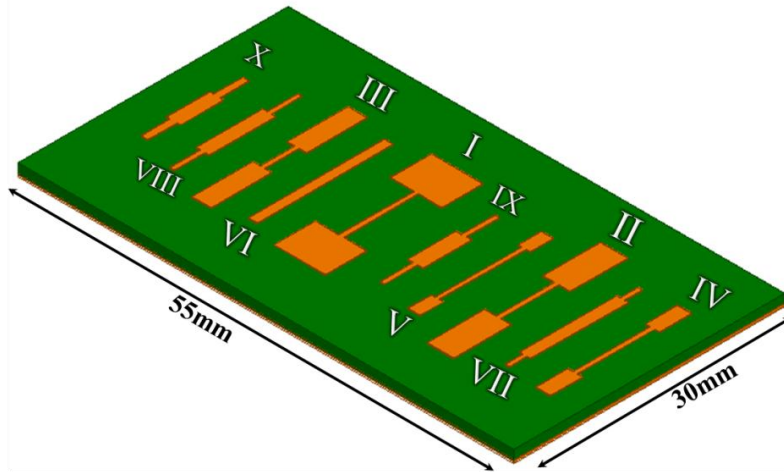
Figure 3.37 Chipless RFID tag for UWB application using 10 SIR.

Table 3: Structural Dimension of SIR Based Chipless RFID Tag for UWB Application
G = 3mm, ε_r = 2.2, h = 1mm

| Design Parameters | | | | | | | | | Measured | |
SIR	K	α	$2L_1$ (mm)	ΔL_2 (mm)	L'_2 (mm)	W_1 (mm)	W_2 (mm)	f_0 (GHz)	f_{S1} (GHz)	f_0 (GHz)
I	0.25	0.6	8.28	1.23	4.60	0.50	5.80	3.3	12.43	3.21
II	0.40	0.7	6.43	0.75	6.42	0.50	3.00	4.0	12.14	3.90
III	0.50	0.8	3.80	0.63	6.76	0.50	2.16	5.1	13.12	5.01
IV	0.60	0.5	8.54	0.55	3.60	0.50	1.60	5.6	13.34	5.52
V	0.65	0.4	9.59	0.52	2.60	0.50	1.35	6.2	13.72	6.16
VI	1.00	--	8.03	0.47	3.53	1.00	1.00	7.0	14.00	7.05
VII	1.50	0.3	10.85	0.41	1.96	1.30	0.50	7.9	15.27	7.88
VIII	1.60	0.5	7.40	0.41	3.39	1.50	0.50	8.6	14.97	8.68
IX	1.75	0.6	5.40	0.41	3.70	1.75	0.50	9.5	15.52	9.61
X	1.40	0.6	4.82	0.45	3.23	1.55	0.75	10.1	17.80	10.20

3.14.1. Method of Encoding - Frequency Shift Coding Technique

Frequency Shift Coding Technique (FSC) [7] is utilized for enhancing the bit coding capacity of the tag. In Absence or Presence Coding method, maximum bit that can represent by an RFID tag is equal to the number of resonators in it, ie. 10 bits for the present tag. Fig.3.38 shows the Frequency Shift Coding technique for chipless tag using N number of resonators. Here each resonator is assigned with specific frequency span (Δf) and each band is divided into different resolution bands (∂f). Hence more number of bits can be encoded by using single resonator. Each division of frequency span can be equal for all resonators or it can be randomly selected depending on the available frequency, which depends on the available frequency spectrum and the number of resonators. Resolution bandwidth is the required frequency band for each resonator to successfully represent its resonant frequency. Resolution bandwidth may vary with frequency due to resonator loses at higher frequencies and excited resonant modes.

The total bit combination expression given in [7] is modified for the calculation of the total bit encoding capacity (T_b) of chipless tag with N resonators as

$$T_b = \log_2\left[\prod_{i=1}^{N}\left(\frac{\Delta f_{0i}}{\partial f_{0i}}\right)\right] \tag{3.14}$$

where Δf_{0i} and ∂f_{0i} are the frequency span and resolution bandwidth allotted for the ith resonator.
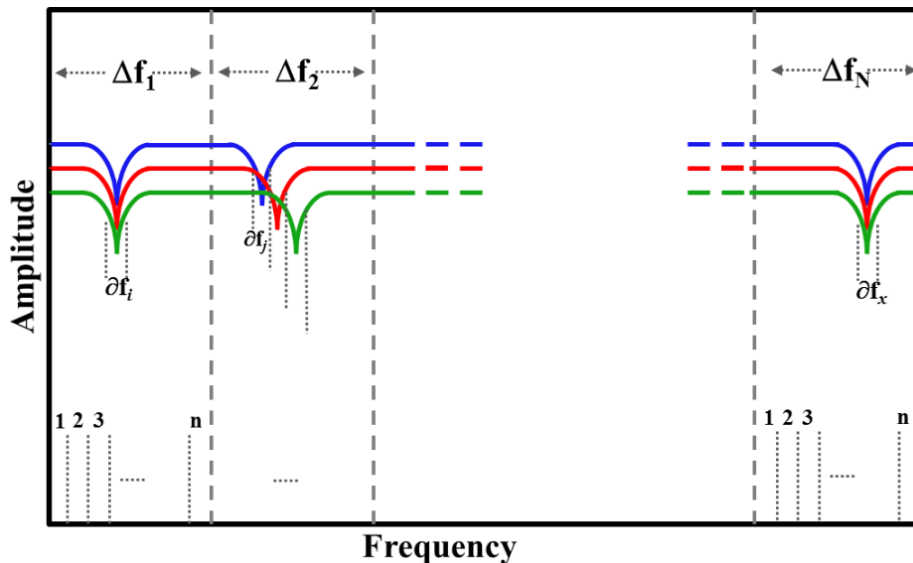
Figure 3.38 Frequency Shift Coding technique for chipless tag using N number of resonators.

3.14.2. Measurement

Measurement is carried out inside the anechoic chamber and calibration explained in earlier section is used for decoding the backscattered signal. Noise level in the anechoic chamber using a medium gain horn antenna as an RFID reader is shown in Fig.3.39, which is measured by subtracting empty room data with data taken at different time interval. Therefore signal consists only the white noise from the surroundings. Backscattered signal measurement from multiscatterer based RFID tag is based on the principles of Radar Cross Section technique with a slight difference, due to the presence of late time response (antenna mode) from the tag. The backscattered signal from the chipless RFID tag should be above this level for the successful extraction of encoded data. Measured backscattered signal strength depends on many factors like transmitting power, reader antenna gain, size of the tag, distance between tag and reader antenna, etc.

Relation between transmitted power, size of the tag and maximum readable distance for an RFID tag is given in [25]. In this analysis, Agilent PNA E8362B Network Analyser with 0dBm (1mW) power is used for the measurement.
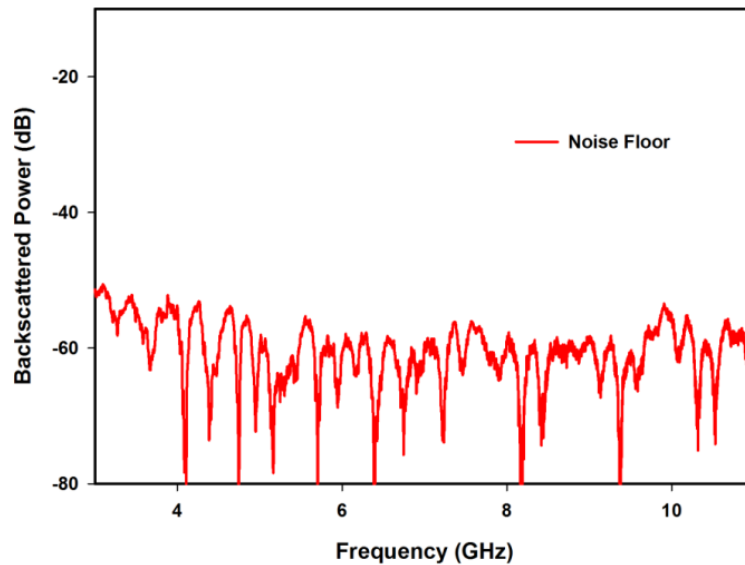
Figure 3.39 Measured noise floor inside the anechoic chamber.

Fig.3.40 shows the measured backscattered signal from the 10 SIR based chipless RFID tag, using single sweep from 3.1GHz to 10.6GHz (without averaging). In this measurement RFID tag is placed at a distance of 50cm from the reader antenna. From the figure it is clear that, backscattered signal is prone to white noise and it can be minimized by applying an averaging. Therefore, all the measurement results presented in this chapter are with an averaging of 16.
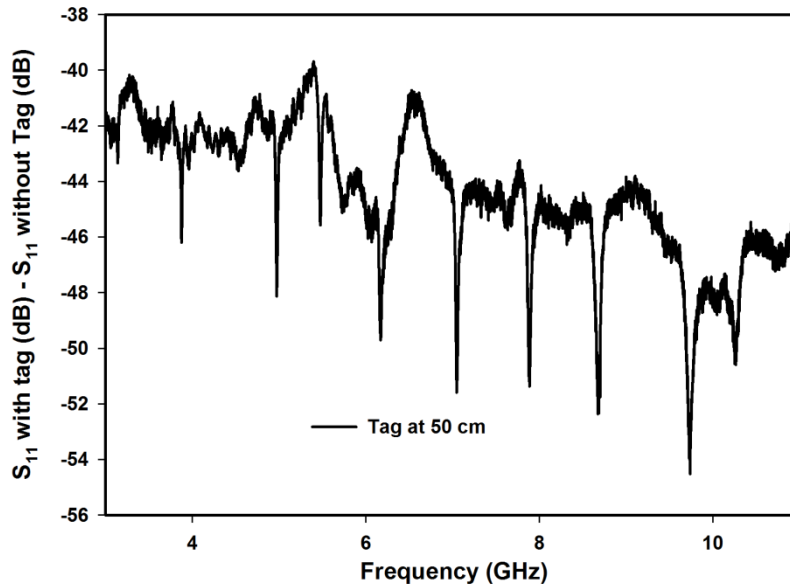
Figure 3.40 Measured backscattered signal from the tag at a distance of 50cm. Inside the anechoic chamber, without averaging $(\theta, \phi) = (0^0, 0^0)$

Fig.3.41 shows the measured backscattered response of the UWB tag with different distances (25cm and 50cm). The Frequency Shift Coding method adopted in this design is also given in the figure. A frequency span (Δf_0) of 750MHz is assigned for each resonator; hence one resonator can represent 25 different frequency points with a resolution bandwidth (∂f_0) of 30MHz. Frequency band of 3.1-3.85GHz is allotted to SIR-I, 3.85-4.6GHz band is allotted to SIR-II,…. and 9.85-10.6GHz is allotted to SIR-X. Thus the total bit encoding capacity of the tag for 10 SIR using equation (3.14) is found to be 46 bits. The calculated Surface Coding Density of the present tag is 2.78bits/cm^2. The bit encoding capacity of the tag can be increased by placing more number of resonators with small frequency span (eg. as per equation (3.14), 15 SIRs with 500MHz frequency span and 30MHz resolution band for each resonator can encode 60 bits of information).

Another tag with different resonant frequency can be easily designed by choosing proper K and α values.
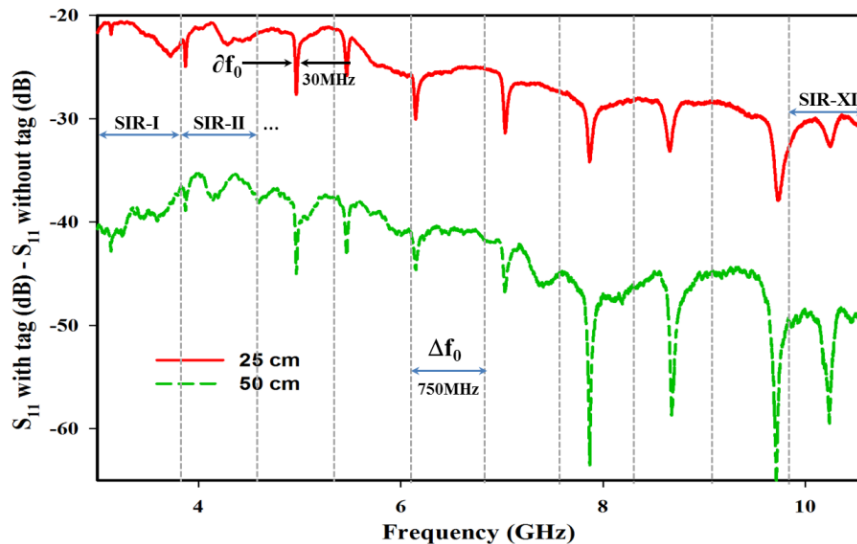
Figure 3.41 Measured back scattered response of the UWB tag with two different distances (25cm and 50cm). Inside anechoic chamber, $(\theta, \phi) = (0^0, 0^0)$ and Avg. = 16.

The post processed amplitude detected signal extracted from Fig.3.41 is shown in Fig.3.42. All the resonant peaks can be identified from the post processed data. As explained in the earlier chapter, backscattered phase will also change with resonant frequencies of the tag and it can be easily identified from the backscattered group delay. Measured backscattered group delay signal from the RFID tag at a distance of 25cm is depicted in Fig.3.43. Measurements are taken inside an anechoic chamber with the reader antenna positioned normal to the tag $(\theta, \phi = 0^0, 0^0)$.
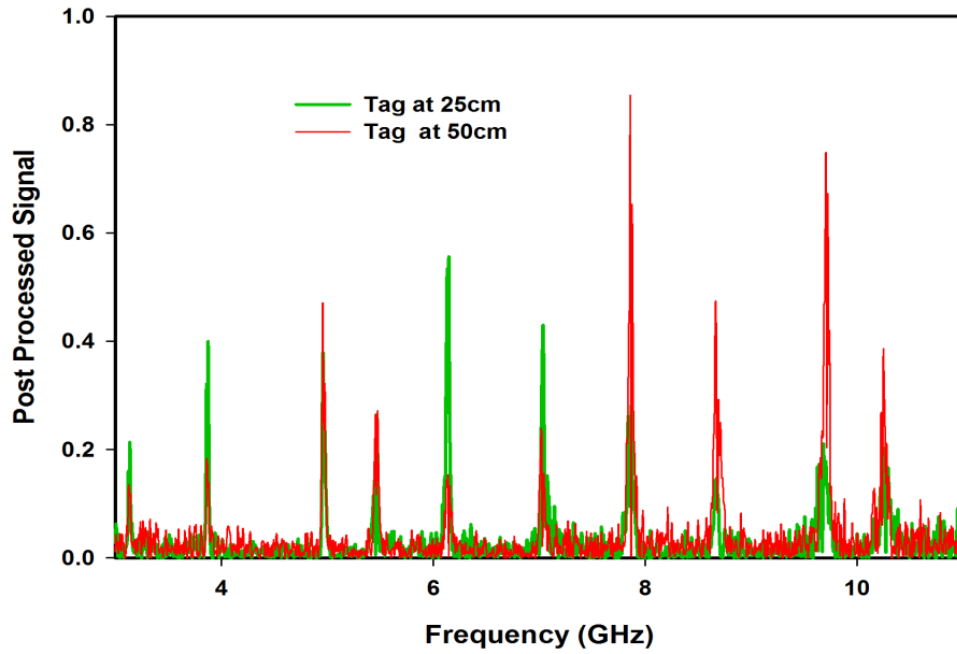
Figure 3.42 Post processed for amplitude detection extracted from Fig.3.41
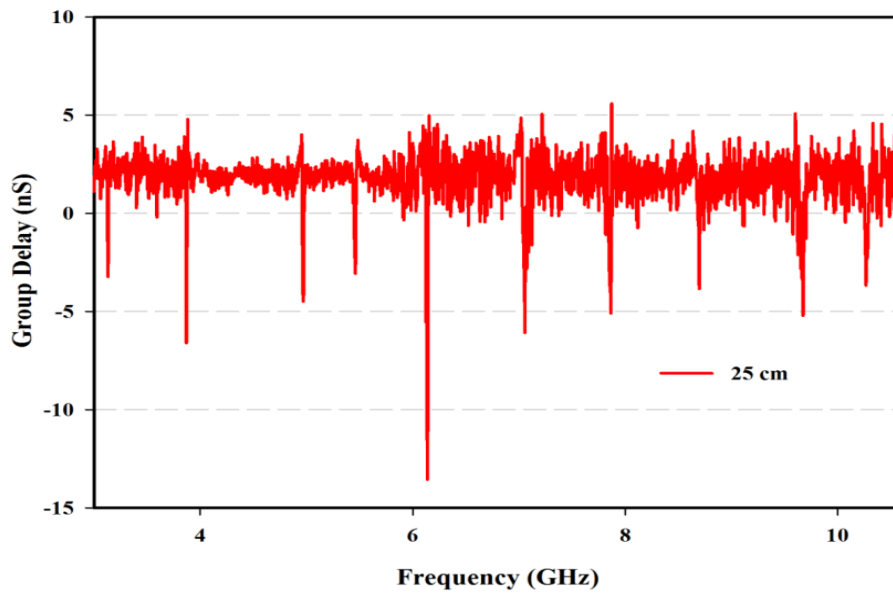
Figure 3.43 Measured back scattered group delay of the UWB tag. Inside anechoic chamber, $(\theta, \phi) = (0^0, 0^0)$ and Avg. = 16.

3.15. SIR Based Chipless RFID Tag using Multiple Mode Encoding Technique

Apart from using fundamental mode of the resonator to encode the information in the tag [5]-[17], this section describes a chipless RFID tag utilizing both fundamental and first harmonic frequency for encoding information. Therefore, single resonator can be used as two separate resonators with reduced tag size. Capability of SIR to independently control the resonant modes can be effectively used for the design of chipless RFID tag.

As per the above knowledge a chipless RFID tag is designed with four SIR using different K and α values for UWB frequency. Multiple mode encoding technique based SIR tag is also utilized for the Frequency Shift Coding technique in such a way that the fundamental mode is tuned for specific frequency band while keeping constant first harmonic mode and vice versa. Different bit combinations are achieved by changing fundamental and first harmonic mode independently. Frequency Shift Coding technique mentioned in the above tag is modified to increase bit encoding capacity. The resonators are designed on an RT Duroid substrate with dielectric constant of 2.2, loss tangent of 0.009 and substrate height of 1mm. Electric field distribution inside the SIR at fundamental and first harmonic frequencies are depicted in Fig.3.44. Half and full wavelength field distributions at fundamental and first harmonic modes are clearly visible from the field pattern.
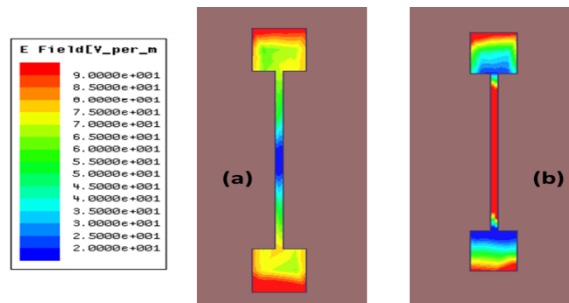
Figure 3.44 Electric Field distribution on SIR at resonant modes. (a) Fundamental mode and
(b) First harmonic mode

Fig.3.45 shows the measurement setup used inside the anechoic chamber. Chipless RFID tag based on 4 SIRs are also shown in Fig.3.45. Detailed dimensions of SIRs and its resonant frequencies are given in Table 4. Resonators are arranged in asymmetric order and they are separated by a distance of 3mm (G) to avoid the mutual coupling between them. As seen in the scattering properties of the SIR, fundamental mode can be detected for an angle of $\phi = 0^0$ to $\pm 60^0$ and $\theta = 0^0$ to $\pm 70^0$. For first harmonic mode, angle of detection is possible for $\phi = 0^0$ to $\pm 60^0$ and $\theta = \pm 10^0$ to $\pm 70^0$, ie, the first harmonic mode will not be able to detect from the broad side direction ($\phi = 0^0$, $\theta = 0^0$) due to the full wavelength current distribution. Simulated 3D far field pattern at fundamental and first harmonic mode from an SIR with X polarised plane wave are shown in Fig.3.46. Second SIR (SIR-II) in this tag is used for far field analysis and its simulated fundamental and first harmonic modes are found to be at 3.88GHz and 7.42GHz, respectively. The measurement setup shown in Fig.3.45 can measure only the fundamental frequency response of the tag. To detect the backscattered signal containing first harmonic mode, either tag or reader antenna has to rotate an angle of 10^0 or more along θ direction as shown in Fig.3.30. The tag is measured at different distances from the horn antenna.
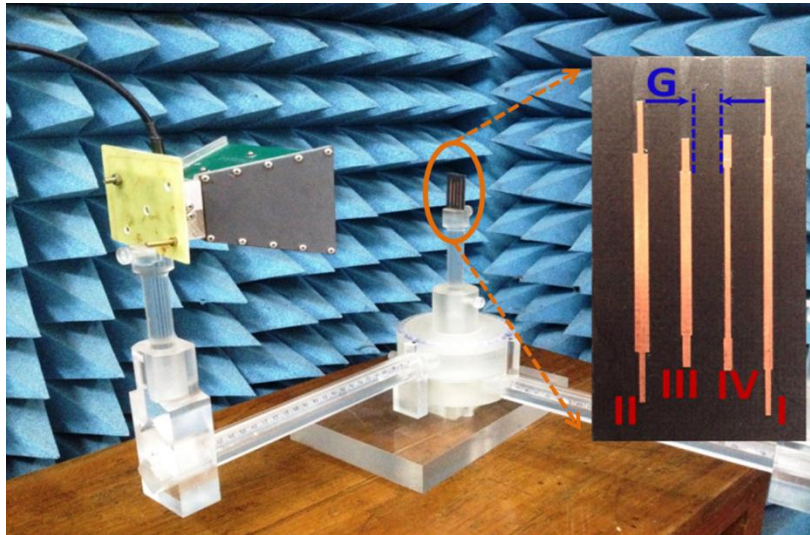
Figure 3.45 Measurement setup inside the anechoic chamber along with fabricated tag. (r,θ,ϕ) = (20cm,0^0,0^0)

Table 4: Structural Dimension of SIR Based Tag. G = 3mm, ε_r = 2.2, h = 1mm

SIR	K	α	$2L_1$ (mm)	L'_2 (mm)	W_1 (mm)	W_2 (mm)	Designed f_0	Designed f_{s1}	Measured f_0	Measured f_{s1}
I	1.2	0.30	24.3	4.84	0.8	0.5	3.4	6.68	3.41	6.68
II	1.5	0.35	20.65	5.26	1.3	0.5	3.9	7.4	3.9	7.44
III	0.85	0.30	17.75	3.32	0.5	0.75	4.3	8.76	4.3	8.75
IV	1.3	0.30	17.05	3.30	1.0	0.5	4.9	9.52	4.8	9.47
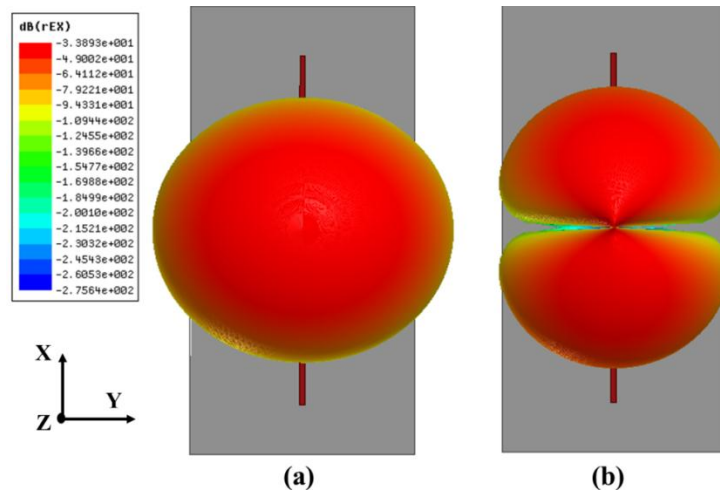
Figure 3.46 3D Far field radiation from SIR at resonance, (a) fundamental frequency (3.88GHz) and (b) first harmonic frequency (7.44GHz).

This chipless RFID tag is designed to operate in a frequency band of 3.1-10GHz. SIR-I shown in Fig.3.45 is designed in such a way that its fundamental frequency can be tuned in between 3.1GHz and 3.6GHz while keeping first harmonic at constant frequency. SIR-I also need to design with its first harmonic frequency vary in between 6GHz and 7GHz while keeping fundamental mode at constant frequency. The ability of the SIR to control its resonant mode independently is already presented in the above section (theoretically, numerically and experimentally). Other SIR's used in this tag are also designed in similar way to operate for other frequency band as shown in the Fig.3.47.

It is clear from Fig.3.47 that, the bandwidth requirement for representation of fundamental (δf_0) and first harmonic mode (δfs_1) are different due to substrate loss in the microstrip structures at high frequencies. It is found to be 30MHz for f_0 mode and 60MHz for f_{S1} mode. Frequency span of 500MHz is allotted for fundamental mode of each SIR and 1GHz frequency span is allotted for the first harmonic mode of same resonator. Bandwidths are allotted randomly within the UWB spectrum ie., 3.1GHz to 5.1GHz band is allotted for the fundamental frequencies of four SIRs. Similarly, 6-10GHz band is allotted to first harmonic frequencies of the same SIRs. Fig.3.47 shows the backscattered signal which is measured inside and outside the anechoic chamber. Even with an averaging of 16 times, outside anechoic chamber measurement at 35cm is more prone to noise. Frequency range from 5.1GHz to 6GHz is avoided in the tag design due to the presence of ISM bands at 5.2GHz and 5.8GHz. Fig.3.48 shows the post processed signal for amplitude detection method, which is calculated from Fig.3.47. Backscattered group delay of the measured tag at 35cm away from the reader antenna is depicted in Fig.3.49.
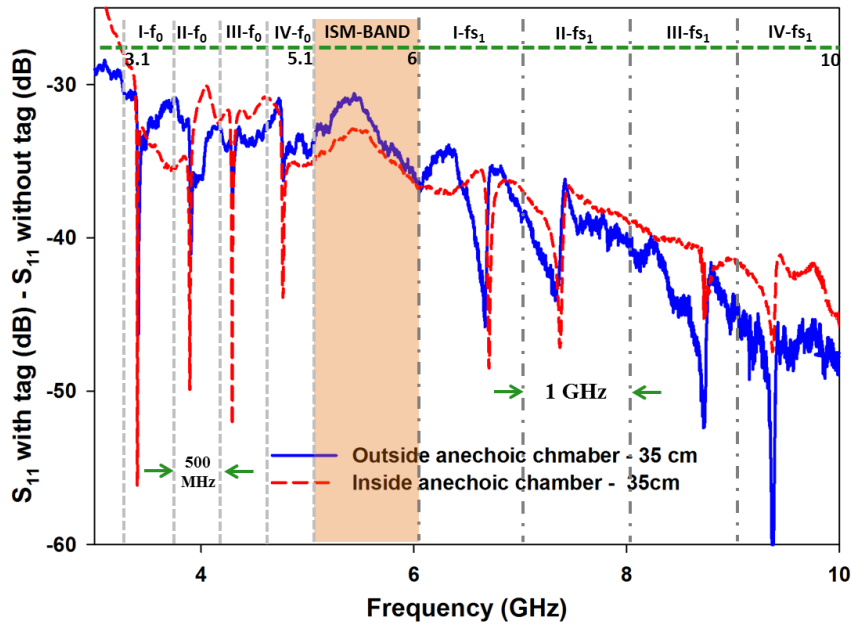
Figure 3.47 Backscattered frequency response of the SIR based RFID tag measured at two different distances. $(\theta, \phi) = (22.5^0, 0^0)$, Avg. = 16.
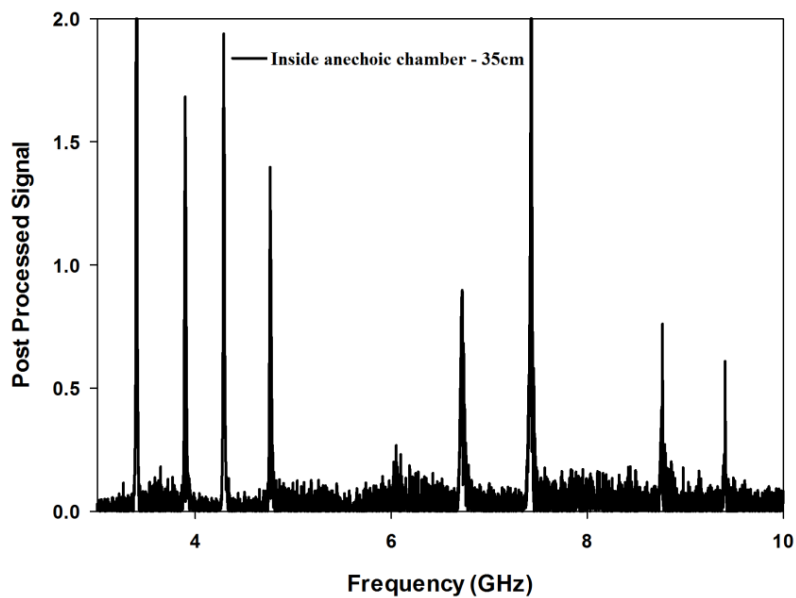
Figure 3.48 Post processed signal extracted from backscattered signal plotted in Fig.3.47.

Cochin University of Science and Technology
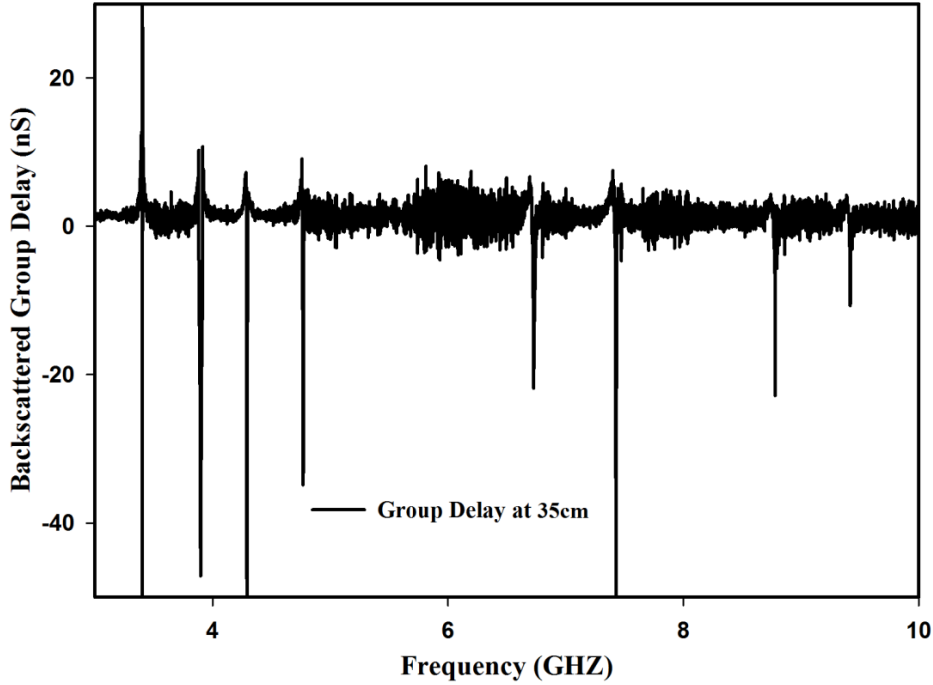
Figure 3.49 Backscattered Group Delay response of the SIR based RFID tag. Anechoic chamber, $(\theta, \phi) = (22.5^0, 0^0)$, Avg. = 16.

For fundamental mode, resolution bandwidth of 30MHz can represent 16 different cases within the 500MHz frequency span. Similarly, for first harmonic mode, resolution bandwidth of 60MHz can represent another 16 different cases within the frequency span of 1GHz band. Therefore single SIR is capable of representing 256 (16x16) different combinations by using two resonant modes. Expression for the calculation of the total bit encoding capacity of the above tag can be modified as,

$$T_b = \log_2 \left[\prod_{i=1}^{N} \left(\frac{\Delta f_{0i}}{\partial f_{0i}} \right) \cdot \left(\frac{\Delta f s_{1i}}{\partial f s_{1i}} \right) \right] \qquad (3.15)$$

where Δf_{0i} and δf_{0i} are the frequency span and resolution bandwidth of the fundamental mode of ith resonator. Similarly, $\Delta f s_{1i}$ and $\delta f s_{1i}$ are the frequency span and resolution bandwidth of the first harmonic mode of ith resonator and N

is the total number of resonator in the tag. As per the equation (3.15) total bit encoding capacity of the tag is found to be 32 bit with and overall tag dimension of 40x20mm^2. The Surface Coding Density of tag is found to be 4 bits/cm^2.

3.16. SIR Based High Data Encoding Tag using Multiple Bit Encoding Technique

The chipless RFID tags explained in the above section hold surface coding density of 4 bits/cm^2. To represent more number of bits in a limited surface area, a new method of encoding data is proposed by using combination of different techniques like, assigning different boundary condition to SIR, utilization of fundamental mode and first harmonic mode, independent control of resonant modes and Frequency Shift Coding technique. In the first section RFID tag is designed by Presence or Absence Coding technique and Frequency Shift Coding is employed in the second method.

3.16.1. Bit Encoding Technique

Bit encoding is performed on a SIR based tag, which is designed and fabricated on C-MET LK-4.3 substrate with K and α are as 0.6 and 0.4, respectively. In this method, boundary condition of the SIR is modified to resonate at different frequencies. A basic $\lambda/2$ SIR is designed and suitable boundary conditions (Open or Short) are applied to remove the undesired mode. Structural parameters of the SIR with different bit configurations are shown in Fig.3.50. From equations (3.8) & (3.9), fundamental and first harmonic mode of the SIR shown in Fig.3.50 (a) is found to be 3.4GHz and 7.68GHz, respectively. Fig.3.50 also shows different boundary conditions of SIR for representing 11, 10 and 01 bit pattern. In bit pattern'10', '1' indicate

the presence of the fundamental mode of the SIR and '0' indicate the absence of its first harmonic mode.

A $\lambda/2$ SIR can represent '11' bit configuration (as seen in Fig.3.50 (a)), ie., it can resonate at both fundamental and first harmonic frequency. Another $\lambda/4$ SIR with short circuited at one end is shown in Fig.3.50 (b). Due to this boundary condition short circuited SIR is resonating only in the fundamental mode and first harmonic frequency is absent in it. Hence it can be used to represent bit '10'. Boundary condition of the above SIR is changed in Fig.3.50 (c). Instead of short circuit, an open circuit is introduced. From the analysis (discuss later), it is clear that, the fundamental mode is absent here and only the first harmonic is present in the frequency band. This configuration can be used to design bit combination '01'. Open end sections in the SIR structures require a correction due to the fringing field at the open end. The extended length ΔL_2 due to the fringing field is incorporated in the calculation of L'$_2$. The length ΔL_2 of the microstrip line (W_2= 1.8mm, ε_r =4.3 and h = 1.6mm) is found to be 0.73mm [23], so the corrected length of a particular resonance is $L'_2 = L - \Delta L_2$, where L is the length of the microstrip line corresponds to electrical length θ_2. The length L_3 in Fig.3.50 (b) can be approximated as $L_3 \cong \frac{L_1}{2} - h$. The height of the substrate is subtracted to compensate the extra length of shorting via. The length L_4 in Fig.3.50 (c) is calculated as $L_4 = \frac{L_1}{2} - \Delta L_1$, where ΔL_1 is the extended length due to open end fringing field. The ΔL_1 for a 0.5mm width microstrip line for the above substrate is found to be 0.63mm.
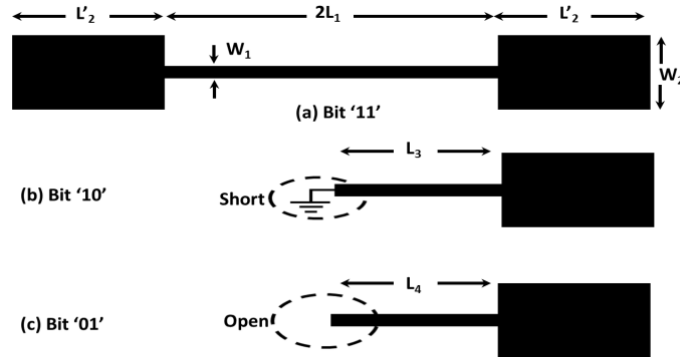
Figure 3.50 SIR for different bit configuration (a) Bit 11 (b) Bit 10 (one end of the SIR is connected to bottom metal plate) and (c) Bit 01, where W_1 = 0.5mm, W_2 = 1.8mm, $2L_1$ = 12.85mm, L'_2 = 3.37mm, L_3 = 4.82mm, L_4 = 5.78mm, ε_r = 4.3, $\tan\delta$ = 0.0018 and h = 1.6mm.

Odd (3.8) and even (3.9) mode equations of the SIR is actually derived from the basic SIR structures or SIR with different boundary conditions, such as $\lambda/4$ SIR with shorted end and $\lambda/4$ SIR open end, respectively [20]. The bit encoding method of this tag can also be explained by analysing the boundary condition of the SIR at resonance. ie., current minimum at the open end and current maximum at the short end. Surface current distributions at fundamental and first harmonic modes of a $\lambda/2$ SIR are shown in Fig.3.51. The simulated resonant frequencies of SIR at f_0 and fs_1 modes are found to be at 3.4GHz and 7.62GHz, respectively. A full SIR structure shown in Fig.3.51 can resonate both at fundamental and first harmonic modes. A $\lambda_0/2$ surface current distribution is obtained for the fundamental mode as shown in Fig.3.51 (a), where λ_0 is the wavelength at fundamental frequency. A full wave variation at λ_{S1}, as shown in Fig.3.51 (b) represents the first harmonic mode, where λ_{S1} is the wavelength at the first harmonic frequency. Therefore, it can be used to represent bit combination '11'. Fig.3.52 shows the simulated backscattered signal from a $\lambda/2$ SIR showing fundamental and first harmonic mode.
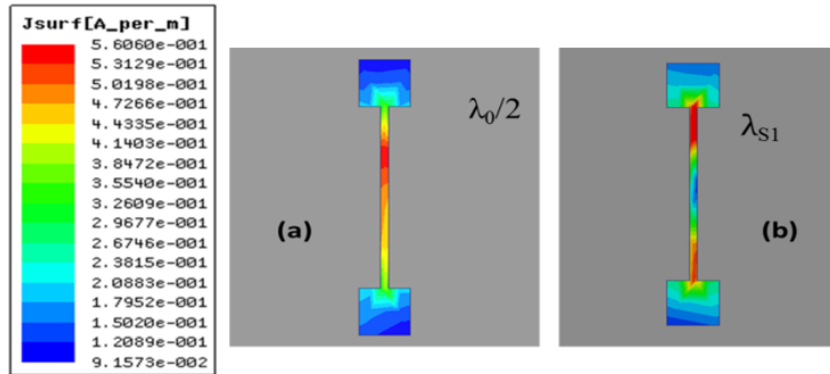
Figure 3.51 Surface current distribution on λ/2 SIR (a) at fundamental mode (3.4 GHz) (b) first harmonics (7.62GHz)
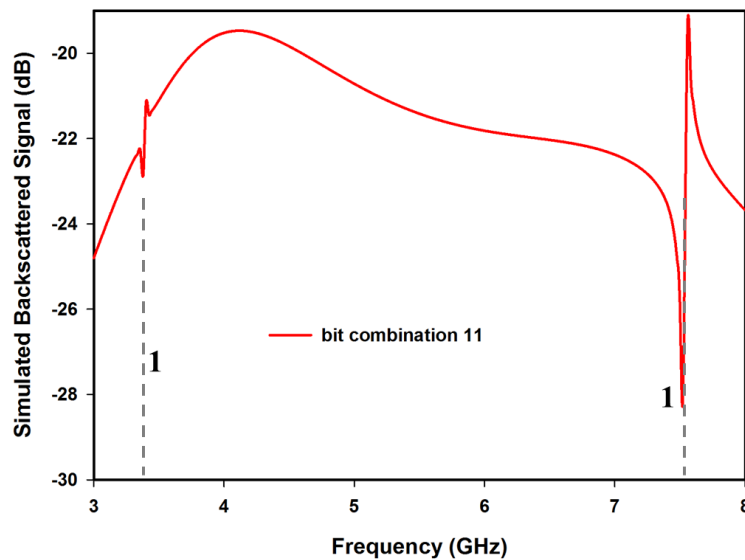
Figure 3.52 Simulated backscattered signal from λ/2 SIR.

Short circuited SIR shown in Fig.3.53 supports quarter wave current distribution with a current maximum at the shorted end. This corresponds to a $\lambda_0/4$ distribution at the fundamental frequency with respect to Fig.3.51 (a). Because of the requirement of current minimum at both ends, shorted SIR cannot resonate at the first harmonic frequency. Only fundamental frequency

exists in the shorted SIR, so it can be used to represent the bit combination '10'. The simulated backscattered response from λ/4 shorted SIR is shown in Fig.3.54 and validates the bit combination '10'.
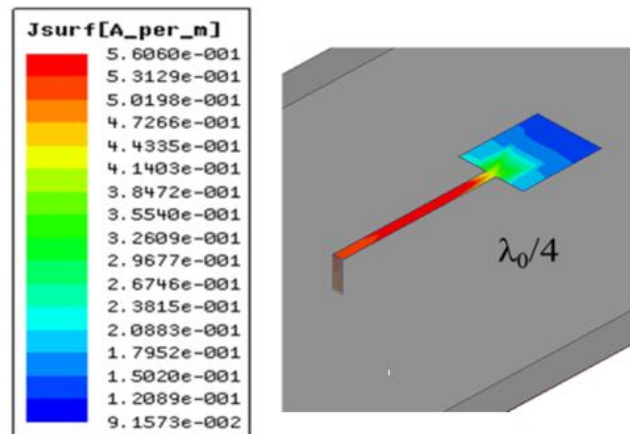
Figure 3.53 Surface current distribution on λ/4 shorted SIR at the fundamental mode (3.4 GHz)
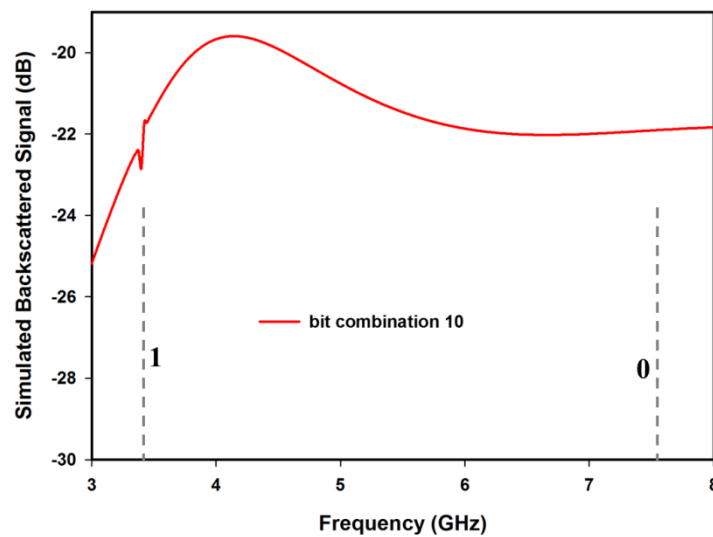
Figure 3.54 Simulated backscattered signal from λ/4 shorted SIR.

Similarly, due to the open end boundary condition, only the first harmonic mode exists in the λ/4 open ended SIR. Fig.3.55 shows the current distribution in a λ/4 open ended SIR at first harmonic frequency (7.62GHz).

This corresponds to a $\lambda_{S1}/2$ distribution at the first harmonic frequency with respect to Fig.3.51 (b). The fundamental mode (3.4GHz) will be suppressed in $\lambda/4$ open ended SIR; due to the requirement of current maximum at the open end. Therefore open ended SIR can be used to represent the bit combination '01'. Simulated backscattered signal from a $\lambda/4$ open ended SIR is shown in Fig.3.56 and it can be used to validate bit combination '01'.
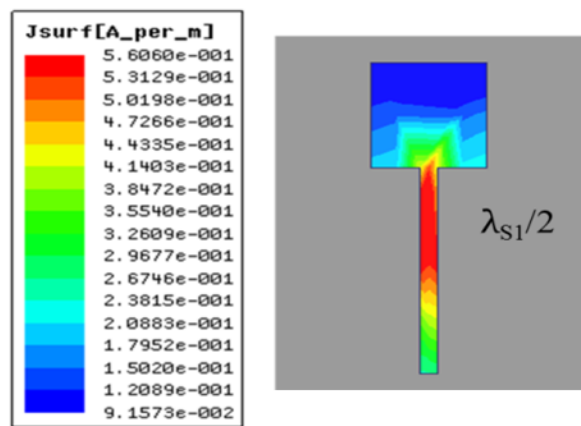
Figure 3.55 Surface current distribution on λ/4 open ended SIR at first harmonic frequency (7.62 GHz)
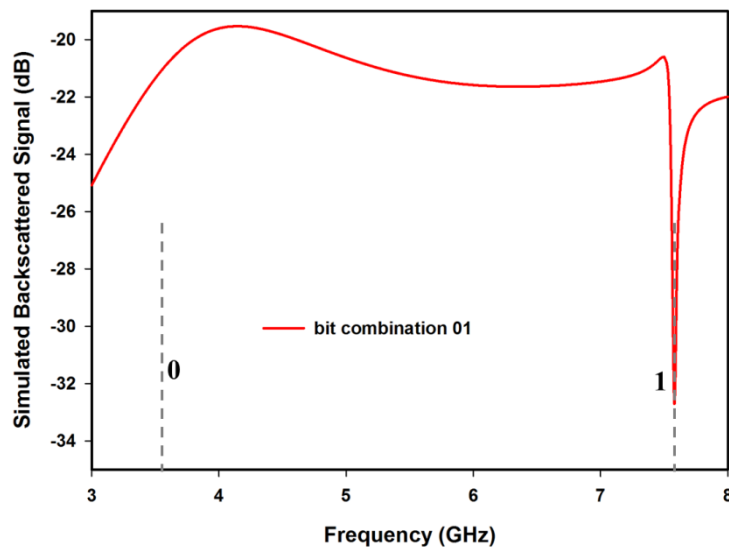
Figure 3.56 Simulated backscattered signal from λ/4 open ended SIR.

The measured and simulated backscattered signal for all combinations of 2 bit RFID tag with single SIR resonator is shown in Fig.3.57. Measured fundamental and first harmonic frequencies are found to be at 3.35 GHz and 7.65 GHz, respectively. The simulated fundamental and first harmonic frequencies are found to be at 3.4 GHz and 7.62 GHz, respectively. Both simulated and measured data are in good agreement with theoretical values.
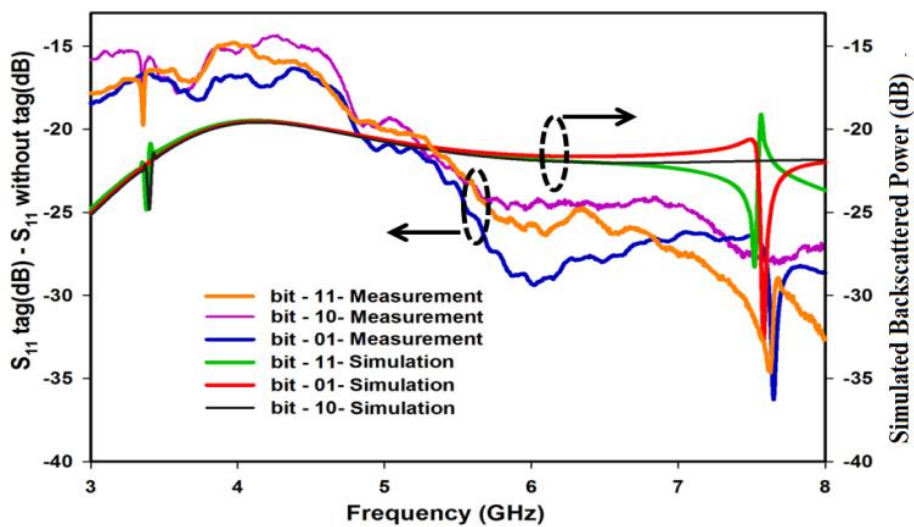
Figure 3.57 Simulated and measured backscattered signal from single SIR with different bit configurations. $(r,\theta,\phi) = (20cm, 22.5^0, 0^0)$ (anechoic chamber)

3.16.2. 8 Bit RFID Tag using Presence or Absence Coding

The experimental results of an SIR based 8 bit RFID tag designed on RT Duroid are discussed in this section. Presence or Absence Coding technique are employed in this tag and it consists of 4 SIRs. SIRs used in the present tag is shown in Fig.3.58 and detailed dimensions are given in Table 5. Fundamental and first harmonic modes of SIRs are effectively used for the design of 8 bit tag. Therefore with 4 SIRs, 8 bits can be encoded using the presence or absence coding, which is only 4 bits for other reported tags.

Different combinations of SIR's as described in Fig.3.50 are used for representing different bit combinations. Resonators in the tag are placed in an asymmetric order to minimise the mutual coupling between them and they are separated by a gap (G) of 3mm.
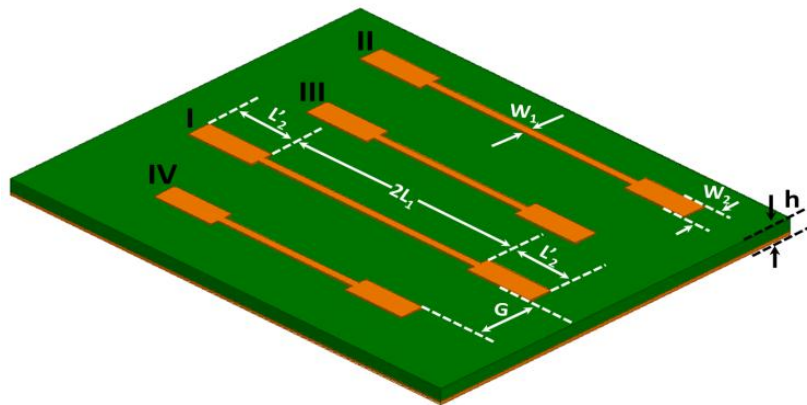
Figure 3.58 8 bit SIR based RFID tag, where W_1 = 0.5mm, W_2 = 1.55mm, G = 3mm, ε_r = 2.2, tanδ = 0.0009 and h = 1mm. ($35 \times 20 \times 1 mm^3$)

Table 5: Structural Dimensions and Resonant Frequencies of SIR Based Tag ε_r = 2.2, tanδ = 0.0009, K = 0.6, α = 0.4 and ΔL_2 = 0.54mm

SIR	L_1 (mm)	L'_2 (mm)	f_0 (GHz)			f_{s1} (GHz)		
			Theory	HFSS	Experi.	Theory	HFSS	Experi.
I	17.01	4.97	3.4	3.4	3.35	7.68	7.6	7.67
II	16.07	4.66	3.6	3.6	3.54	8.13	8.04	8.15
III	15.22	4.39	3.8	3.8	3.75	8.58	8.55	8.62
IV	14.46	4.14	4	3.96	3.95	9.04	8.96	9.02

The measurement setup inside the anechoic chamber is shown in Fig.3.59. With respect to the RFID tag, horn antenna is positioned at (r,θ,ϕ) = (20cm, 22.5^0, 0^0). This arrangement is required to get the first harmonic response from the tag. Measured backscattered signal for three different RFID tags are shown in Fig.3.60 (a). For '1111 1111' bit combination, the first four bits are represented by the fundamental mode of the four SIRs

shown in Fig.3.52 and the last four bits are represented by the first harmonic frequency of the same resonators. All 256 (2^8) bit combinations using four SIRs are possible by either shorting or opening the appropriate resonator. Resonance can also be measured by taking the group delay of the backscattered signal as depicted in Fig.3.60 (b). The group delay response shows better discrimination between different bits than the magnitude. Backscattered group delay below a threshold level of -0.75ns confirms the presence of a bit. Post processing of the measured backscattered magnitude response can be performed for efficient detection of the encoded data. Fig.3.60 (c) shows the post processed amplitude variation of the backscattered signal shown in Fig.3.60 (a). As seen in Fig.3.60 (c), unwanted reflections in the backscattered signals are below the threshold value 0.5 and the signal above this can be considered as the presence of a bit.
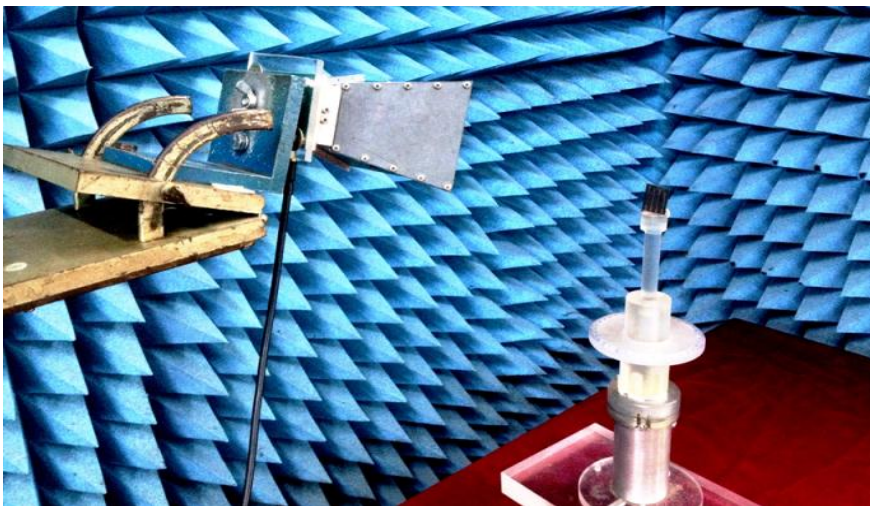
Figure 3.59 Measurement setup inside the anechoic chamber. $(r,\theta,\phi) = (20cm, 22.5^0, 0^0)$
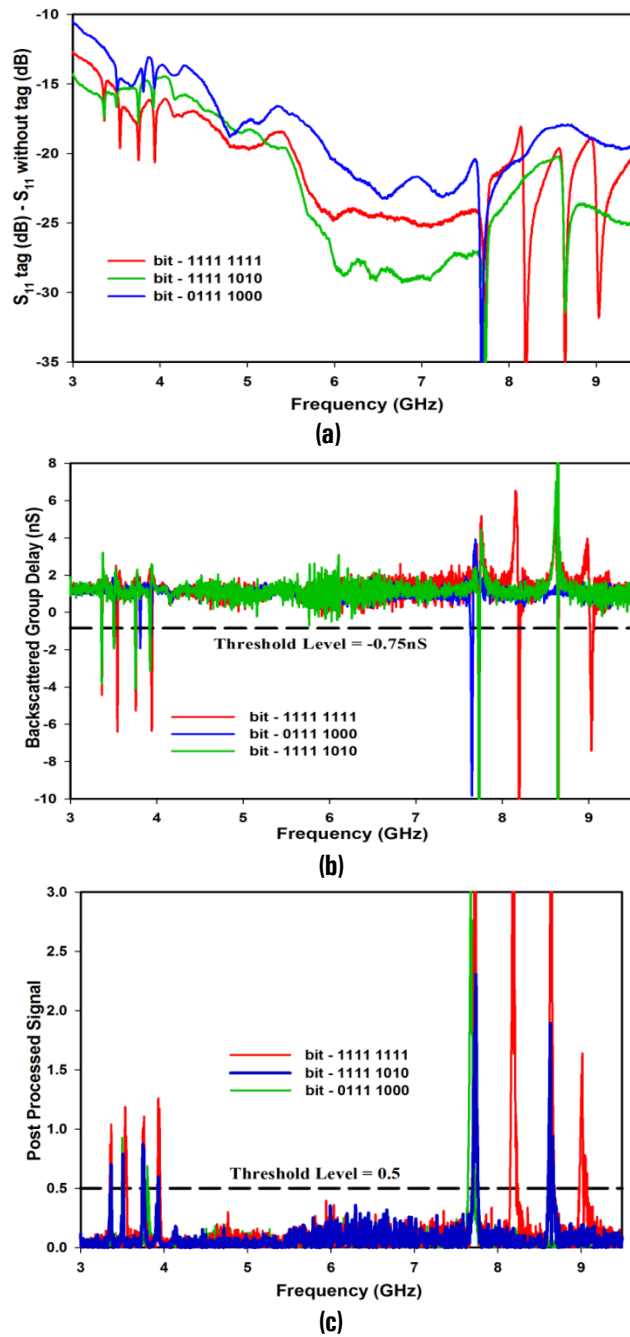
Figure 3.60 Measured tag response of the tag with three different bit combinations, (a) Magnitude of the backscattered signal (b) Backscattered group delay and (c) Post processed response of the signal shown in (a). $(r, \theta, \phi) = (20cm, 22.5^0, 0^0)$, (inside the anechoic chamber) and Avg. = 16.
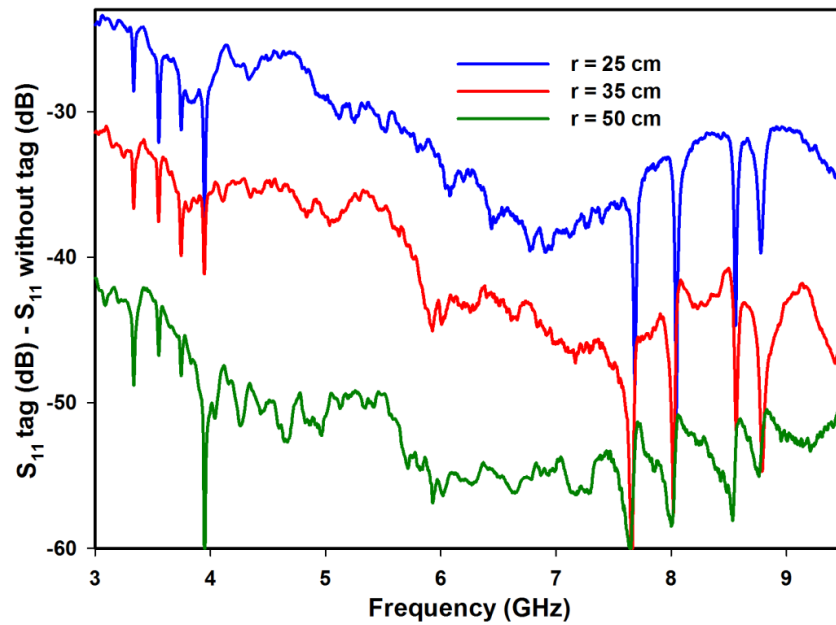
(a)
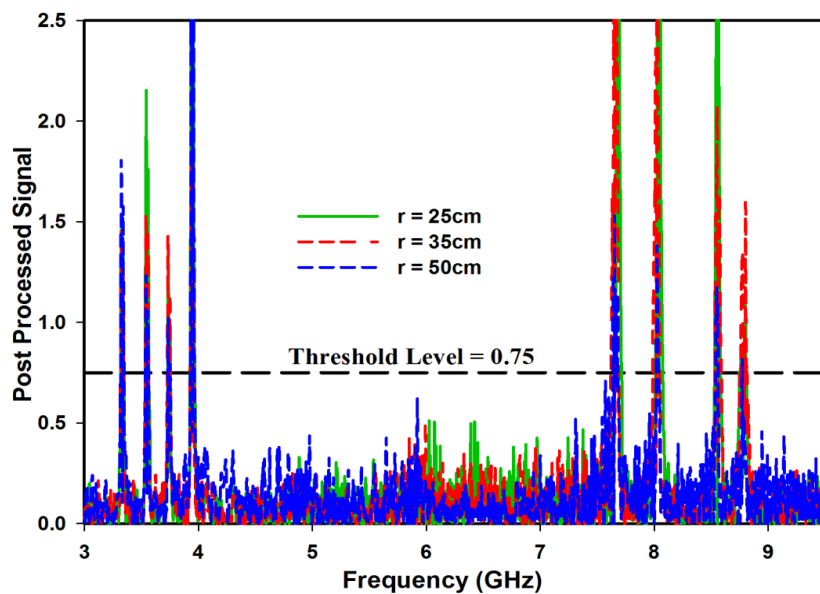
(b)

Figure 3.61 (a) Measured 8 bit tag response representing '1111 1111' for different tag to reader antenna separation, $\theta,\phi = 22.5^0,0^0$(outside the anechoic chamber) and (b) Post processed backscattered signal, Avg. = 32

Backscattered responses of the tag with different distances are shown in Fig.3.61 (a). The measurement is done outside the anechoic chamber at three different distances (25cm, 35cm and 50cm). Averaging of 32 is applied in the backscattered signal to reduce the white noise. Fig.3.61 (b) shows the post processed backscattered signal with different distance plotted in Fig.3.61 (a). Tag responses can be detected up to a distance of 50cm, but reflections from the surroundings contribute to noise. Hence the threshold level is set to 0.75. The overall size of the tag is found to be 30x20mm^2 and the calculated Surface Coding Density of the tag with presence or absence coding technique is found to be 1.06bits/cm^2.

3.16.3. RFID Tag using Frequency Shift Coding Technique

A modified Frequency Shift Coding (FSC) technique is employed on multiple bit encoding technique based RFID tag and it is fabricated on RT Duroid substrate with five SIRs working in the frequency range 3.2GHz to 10.6GHz. FSC technique is employed on different bit combination as shown in Fig.3.60. As shown in the figure, FSC can be employed in four different ways for a single SIR. Apart from controlling the fundamental and first harmonic modes, different boundary conditions are also employed. UWB spectrum is selected randomly for encoding the data. Frequency band ranging from 3.2GHz to 5.7GHz is allotted for the fundamental frequencies of five SIRs with a frequency span (Δf_0) of 500MHz for each resonator. Similarly, 5.7-10.6GHz band is allotted to first harmonic frequencies of the five SIRs with a frequency span (Δfs_1) of 1GHz for each resonator except SIR-V (900MHz). From the measurement, bandwidth resolution (∂f) for detecting

the resonance in the fundamental mode is found to be 30MHz (∂f_0) and for the first harmonic mode is 60MHz (∂fs_1). Within the 500MHz frequency span for f_0 mode, 16 different resolution frequency bands are possible. Similarly, within a 1GHz frequency span for fs_1, another 16 different resolution frequency bands are possible. Therefore, for a λ/2 SIR ('11' combination), both resonances (f_0 and fs_1) can vary, hence 256 (16x16) bit combinations are possible. Similarly, 16 different resolution bands can be achieved for both '01' and '10' combinations. Therefore a single resonator can represent 65536 combinations. Total bit encoding capacity of the tag containing N resonator can be calculated using

$$T_b = \log_2 \left[\prod_{i=1}^{N} \left(\frac{\Delta f_{0i}}{\partial f_{0i}} \right)^2 \left(\frac{\Delta fs_{1i}}{\partial fs_{1i}} \right)^2 \right] \tag{3.16}$$

where i denote the ith SIR. Total bit encoding capacity of the proposed tag is found to be 79 bits with an overall dimension of 40x25mm^2. Surface Coding Density of the tag is now enhanced to 7.9 bits/cm^2.
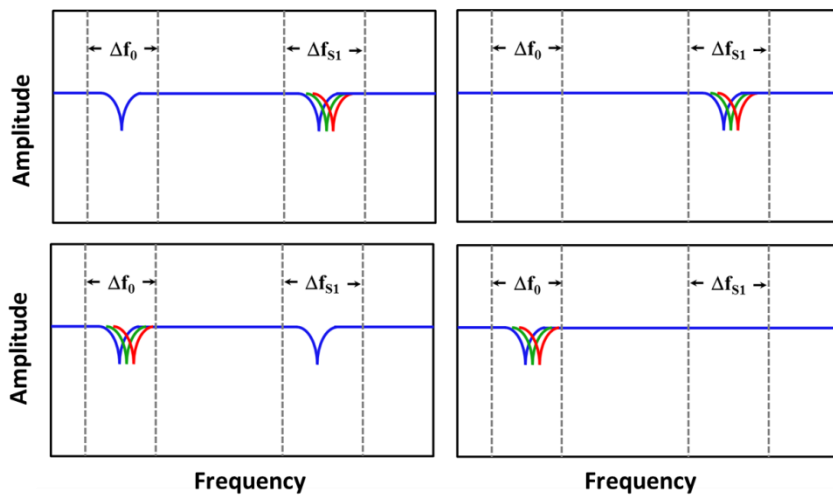
Figure 3.62 Frequency Shift Coding technique for multiple bit encoding based RFID tag.

Fig.3.63 shows the RFID tag containing 5 SIRs and detailed dimensions of the resonators are given in Table 6. To avoid the mutual coupling, each resonator in the tag is separated by 3mm distance. The backscattered response from the tag at a distance of 20cm is shown in Fig.3.64. First five resonances are from the fundamental mode of the SIR and last five are from the first harmonic modes of the same SIR. Fig.3.65 shows required frequency bandwidth or resolution bandwidth for representing f_0 and fs_1 mode. Measured resonant frequencies of the tag are found to be 3.46, 3.85, 4.57, 4.94, 5.54, 6.65, 7.09, 8.37, 9.65 and 10.43 GHz.
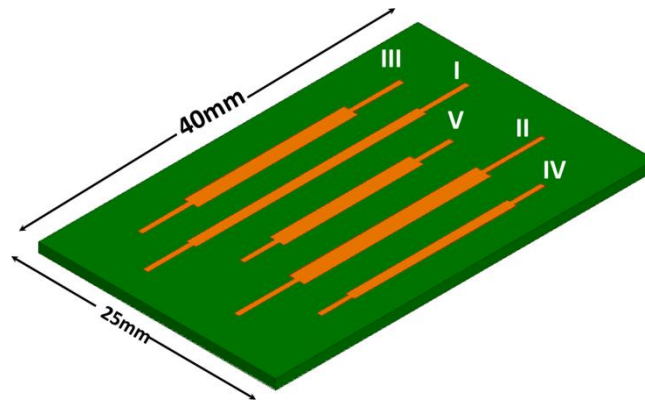
Figure 3.63 Chipless RFID tag consists of 5 SIRs, ε_r = 2.2, tanδ = 0.0009 and substrate height = 1mm.

Table 6: Structural Dimension of SIR Based Tag. G = 3mm, ε_r = 2.2, h = 1mm

SIR	K	α	$2L_1$ (mm)	L'_2 (mm)	W_1 (mm)	W_2 (mm)
I	1.2	0.30	24.3	4.84	1.00	0.5
II	1.7	0.40	19.72	6.34	1.65	0.5
III	1.6	0.40	16.88	5.35	1.50	0.5
IV	1.3	0.30	17.05	3.30	1.00	0.5
V	1.6	0.35	14.75	3.66	1.50	0.5
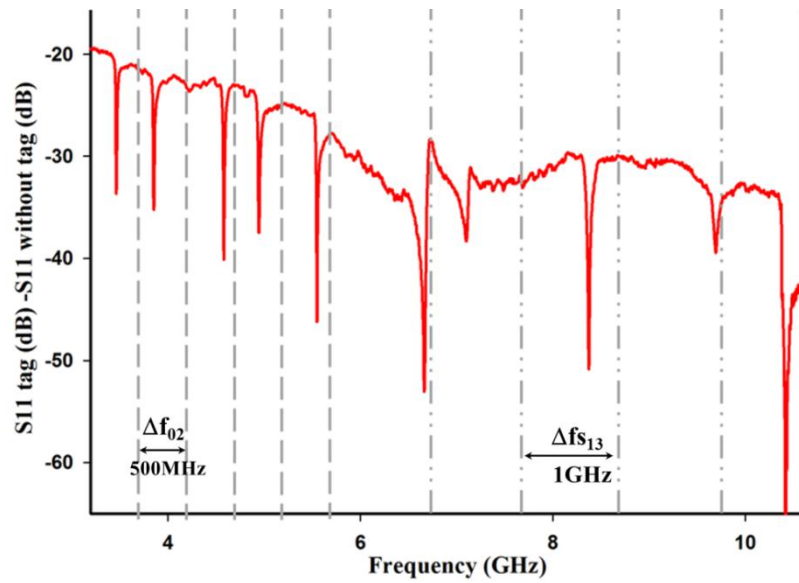
Figure 3.64 Measured backscattered tag response. (r,θ,ϕ) = $(20cm, 22.5^0, 0^0)$, outside anechoic chamber), Avg. = 16.
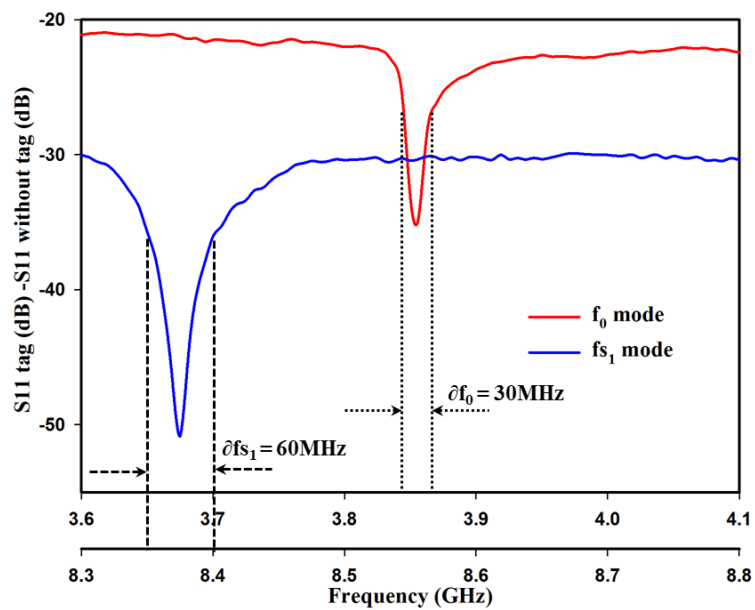
Figure 3.65 Backscattered response showing bandwidth requirement for representing f_0 and fs_1 mode.

Different RFID tag reported in literatures are summarised in Table 7. Most of the reported tags are utilising only two bit combination (0 or 1) using single resonator; here one resonator can represent 4 bit combination (00, 01, 10 & 11). Advantages of SIRs like, independent control of resonant modes, good harmonic separation, electrical length variations, etc. are effectively used in the design of chipless RFID tag.

Table 7: Comparison of Different Chipless RFID Tag

Resonator Type	Encoding Method	Bit States by Single Resonator	Surface Coding Density (bits/cm^2)	Polarisation Independency	Control Over Harmonics
SAW [3]	Y	2	> 1	N	N
Delay Line[28]	N	2	0.17	N	N
Spiral [8]	N	2	0.61	N	N
Open stub [2]	N	2	< 1	N	N
Dual Band [17]	N	3	< 1	N	N
"C" [6]	Y	2	2.86	N	N
Dual Polarised Slot[26]	N	2	> 7	N	N
Ring[14]	Y	2	3.06	Y	N
Depolarised [7]	Y	2	0.66	Y	N
Present tag	**Y**	**4**	**> 7**	**N**	**Y**

3.17. Conclusion

This chapter provides an idea about the multiscatterer based chipless RFID tags and its operation. The evolution of SIR and its properties like total electrical length, the relation between different modes and independent control over resonant mode are explained in detail. Scattering property of the tag with different angular directions is also studied. Measured and simulated

results are in good agreement with theoretical values. The tag is analysed with different substrate properties for selecting best suitable material. A simple calibration method is successfully implemented and validated with different readable distances. Spectral IDs of the RFID tags are successfully decoded from backscattered magnitude or group delay information. A simple post processing method is introduced for the detection of resonances from the backscattered amplitude signal.

Initially a chipless RFID tag utilizing entire bandwidth of UWB (3.1GHz to 10.6GHz) is designed with 10 SIRs. The fundamental mode of the SIR is used for encoding bits in the frequency spectrum. Another RFID tag using multiple resonances encoding method is also proposed, in which RFID tag utilizing both fundamental and first harmonic frequency of SIR. By implementing Frequency Shift Coding Technique on both resonant modes, the Surface Coding Density (SCD) of 4bits/cm^2 is achieved compared earlier tag (2.78bits/cm^2).

SIR based high data encoding tag using multiple bit encoding technique is introduced by applying different boundary conditions to SIR. All four combinations of two bit representations are successfully demonstrated using single SIR. With presence or absence coding technique, proposed tag is capable of representing 2^{2N} number of bit combination using N resonators. Surface Coding Density of 1.06 bits/cm^2 is achieved with the present method. The Bit encoding capacity of the tag is further enhanced by introducing an FSC technique on different bit combinations. Finally an RFID tag with an encoding capacity of 79 bits is proposed. Surface Coding Density of the final tag is found to be more than 7bits/cm^2. Table 8 shows the different properties of chipless RFID tag designed using SIR.

Table 8: Properties of Chipless RFID Tag using SIR

SIR Based RFID	SCD without FSC	SCD with FSC	Readable Range	Detectable Angle (ϕ)	Detectable Angle (θ)
Tag using Fundamental Mode	0.60 bit/cm^2	2.78bit/cm^2	50cm	0^0 to $\pm60^0$	0^0 to $\pm70^0$
Tag using Multiple Resonance Coding Technique	-	4bit/cm^2	50cm	0^0 to $\pm60^0$	$\pm10^0$ to $\pm70^0$
Tag using Multiple Bit Encoding Technique	1.067bit/cm^2	>7bit/cm^2	50cm	0^0 to $\pm60^0$	$\pm10^0$ to $\pm70^0$

3.18. Reference

[1] S. Preradovic and N. Karmakar, "Design of fully printable planar chipless RFID transponder with 35-bit data capacity," in Proc. 39th European Microwave Week, Rome, Italy, Sept. 2009, pp. 13–16.

[2] Nijas C M, Dinesh R, Deepak U, Abdul Rasheed, Mridula S, K. Vasudevan and P. Mohanan, "Chipless RFID Tag using Multiple Microstrip Open Stub Resonators," IEEE Transactions on Antennas and Propagation, Vol. 60, No. 9, pp. 4429-4432, Sep. 2012.

[3] T. Han, W. Wang, H. Wu, and Y. Shui, "Reflection and scattering characteristics of reflectors in SAW tags," IEEE Trans. Ultrason., Ferroelect., Freq. Contr., vol. 55, no. 6, pp. 1387–1390, June 2008.

[4] Md. Shakil Bhuiyan, AKM Azad and Nemai Karmakar, "Dual-band Modified Complementary Split Ring Resonator (MCSRR) Based Multi-resonator Circuit for Chipless RFID Tag" 2013 IEEE Eighth International Conference on Intelligent Sensors, Sensor Networks and Information Processing, Melbourne, VIC, 2-5 April 2013, pp-277 – 281.

[5] I. Jalaly and D. Robertson, "RF barcodes using multiple frequency bands," in IEEE MTT-S Microwave Symp. Dig., Long Beach, CA, Jun. 2005, pp. 139–141.

[6] Arnaud Vena, Etienne Perret and Smail Tedjini, "Chipless RFID Tag Using Hybrid Coding Technique", IEEE Transactions on Microwave Theory and Techniques, Vol. 59, No. 12, December 2011.

[7] Arnaud Vena, Etienne Perret and Smail Tedjini, "A Depolarizing Chipless RFID Tag for Robust Detection and Its FCC Compliant UWB Reading System", IEEE Transactions on Microwave Theory and Techniques, VOL. 61, NO. 8, August 2013.

[8] M.Manteghi, "A space-time-frequency target identification technique for chipless RFID applications," in Proc. IEEE Antennas Propag. Soc. Int. Symp. (APSURSI), 2011, pp. 1–4.

[9] M. Manteghi and Y. Rahmat-Samii, "Frequency notched UWB elliptical dipole tag with multi-bit data scattering properties," in Proc.IEEE Antennas Propag. Soc. Int. Symp., San Diego, CA, USA, 2007, pp. 789–792.

[10] A. Blischak and M. Manteghi, "Pole residue techniques for chipless RFID detection," in Proc. IEEE Antennas Propag. Soc. Int. Symp., 2009, pp. 1–4.

[11] A. Blischak and M. Manteghi, "Pole-residue analysis of a notched UWB elliptical dipole tag," presented at the URSI-USNC National Radio Science Meeting, Boulder, CO, USA, 2009.

[12] A. Vena, E. Perret and S. Tedjini "A Fully Printable Chipless RFID Tag With Detuning Correction Technique," IEEE Microwave and Wireless Components Letters, Vol. 22, No. 4, April 2012.

[13] A. T. Blischak andM.Manteghi, "Embedded singularity chipless RFID tags," IEEE Trans. Antennas Propag., vol. 59, no. 11, pp. 3961–3968, Nov. 2011.

[14] A. Vena, E. Perret and S. Tedjini, "High-Capacity Chipless RFID Tag Insensitive to the Polarization," IEEE Transactions on Antennas and Propagation, Vol. 60, No. 10, October 2012.

[15] M. A. Islam, Y. Yap, N. Karmakar, and A. Azad, "Compact Printable Orientation Independent Chipless RFID Tag", Progress In Electromagnetics Research C, Vol. 33, 55–66, 2012.

[16] F. Costa, S. Genovesi, and A. Monorchio, "A Chipless RFID Based on Multiresonant High-Impedance Surfaces," IEEE Transactions on Microwave Theory and Techniques, Vol. 61, No. 1, January 2013.

[17] Md. Aminul Islam and Nemai Chandra Karmakar "A Novel Compact Printable Dual-Polarized Chipless RFID System", IEEE Transactions on Microwave Theory and Techniques, Vol. 60, No. 7, July 2012.

[18] A. Vena, E. Perret and S. Tedjini, " A Compact Chipless RFID Tag Using Polarisation Diversity for Encoding and Sensing", 2012 IEEE International Conference of RFID, Orlando, Florida, April 3-5, 2012.

[19] A. Vena, E. Perret, and S. Tedjini, "Design rules for chipless RFID tags based on multiple scatterers," *Ann. Telecommun. - Ann. Des Télécommunications*, vol. 68, no. 7–8, pp. 361–374, Feb. 2013.

[20] M. Makimoto and S. Yamashita, "Microwave Resonators and Filters for Wireless Communication, Theory, Design and Application" Springer Series in Advanced Microelectronics, Vol. 4, 2001.

[21] Chi-Feng Chen, Ting-Yi Huang, Chi-Ping Chou, and Ruey-Beei Wu "Microstrip Diplexers Design With Common Resonator Sections for Compact Size But High Isolation," IEEE Transactions On Microwave Theory And Techniques, Vol. 54, No. 5, pp. 1945 – 1952, May, 2006.

[22] Sheng-Yuan Lee, "Optimum Resonant Conditions of Stepped Impedance Resonators," Microwave Conference, 2005 European, 4-6 Oct., 2005.

[23] M. Kirsching, R. H. Jansen, and N. H. L. Koster, "Accurate model for open end effect of microstrip lines," Electronics Letters, Vol. 17, pp. 123-125, Feb. 1981.

[24] P. Kalansuriya, N. C. Karmakar, and E. Viterbo, "On the Detection of Frequency-Spectra-Based Chipless RFID Using UWB Impulsed Interrogation," IEEE Transactions on Microwave Theory and Techniques, Vol. 60, No. 12, pp. 4187–4197, December 2012.

[25] R. Anee and N. C. Karmakar, "Chipless RFID Tag Localization," IEEE Transactions on Microwave Theory and Techniques, Vol. 61, No. 11, November 2013.

[26] Jia-Sheng Hong and M J Lancaster "Microstrip Filters for RF/Microwave Applications" A Wiley-Interscience publication, pp. 112-120, 2001.

[27] David Girbau, Javier Lorenzo, Antonio Lázaro, Carles Ferrater and Ramón Villarino, "Frequency-Coded Chipless RFID Tag Based on Dual-Band Resonators", IEEE Antennas and Wireless Propagation Letters, Vol. 11, 2012.

[28] A. Chamarti and K. Varahramayan, "Transmission delay line- based ID generation circuit for RFID applications," IEEE Micro- wave Wireless Compon. Lett., vol. 16, no. 11, pp. 588–590, Nov. 2006.

.............ﬞ৩২০.............

RFID READER FOR MULTISCATTERER BASED CHIPLESS TAGS

Abstract

The design and development of chipless RFID reader for the multiscatterer based tag is presented in this chapter. The proposed reader is designed to operate for a frequency band of 2.36GHz to 2.54GHz. The evolution of RFID reader system using spectrum analyser and low cost components are discussed in this chapter. Multiscatterer based chipless RFID tags are measured up to a distance of 5cm using proposed reader and the results are validated with Network analyser.

4.1. Introduction to Chipless RFID Reader

The previous chapters described the design and development of multiresonator and multiscatterer based chipless RFID tags. A compact and high data encoded chipless tags is designed by multiscatterer based tag with FSC encoding technique. The attractive features of the tags are low cost, robustness and ease of data encoding. The successful design and testing of the chipless tag demands the design and development of a chipless RFID

reader. This chapter describes the design and development of a single antenna based chipless RFID reader. It can operate in the frequency band from 2.36GHz to 2.54GHzand the reader is designed with different microwave components like VCO (Voltage Controlled Oscillator), LNA (Low Noise Amplifier), Mixer, Splitter, etc.

Various readers for chipped and chipless RFID systems have been reported in the literature. Conventional RFID readers (chipped RFID tags) are operated mostly at LF (125 KHz), HF (13.56 MHz), UHF (915 MHz) and microwave (2.45 GHz) bands. Operation of chipped tags are mostly in industrial, scientific and medical (ISM) bands [1]-[6], which have narrow bandwidths of a few KHz up to 83 MHz (2.45 GHz ISM band) due to free licensing. This type of readers use time domain based demodulation techniques with amplitude shift keying (ASK) and binary phase shift keying (BPSK). Different handshaking algorithms are also used for the data transfer between RFID tag and Reader.

Commercially successful and fully operational chipless RFID system is the Surface Acoustic Wave (SAW) based chipless RFID designed by RFSAW© [7]. SAW tag reader operating at 2.4GHz ISM band [8] is designed to accommodate the unconventional modulating and data encoding properties of the SAW. The company claims that their reader is able to identify up to 1000 tag per sec and other features of reader are given in the Fig.4.1.

READER

Frequency Range	2.4 - 2.483 GHz
RF Power Output	10 mW ERP Max with antenna (0.6 mW at RF output port)
RF Port	RF – single Tx/Rx
Data Ports	RS-485, DB9 connector
Tag Read Speed	1000 per second - data collection
Dimensions	9.1" x 6.6" x 2.1" (23.1 cm x 16.8 cm x 5.3 cm)
Weight	2.5 lbs.
Power Requirements	18-72 volts DC; 6 watts maximum
Temperature	Operating -20° to +50° C

Figure 4.1 Chipless RFID reader designed by RFSAW and its specifications. Courtesy: RFSAW Inc. [7].

All the conventional RFID readers are operating in the ISM bands with low bandwidth. However, chipless RFID tags designed using low dielectric constant materials require wideband operation of several GHz. For most of the frequency domain chipless RFID tags, the processes of characterization of the tag in the frequency domain to extract the data are similar to each other. The RFID reader should be capable of generating and receiving the signals with sufficient bandwidth to cover the operating frequency range of the RFID tag. The key operating principle is the extraction of the amplitude and phase changes in the transmitted and received RF signals, and hence the timing information of the RF signals is not critical.

RF laboratory equipment's such as Network analyser, Digital Oscilloscope, Spectrum analyser, etc. can be used to read chipless RFID tags, although it is not economical to use expensive laboratory equipment in real world applications. To cut down the cost of the tags by using chipless RFID, it is necessary to develop a low cost reader.

The RFID reader designs based on frequency domain chipless tags are reported in [9]-[11] and it can decode the amplitude and phase functions of the chipless tag based on band-stop filters. Coherent detection is achieved with a bi-static frequency-modulated continuous wave (FMCW) radar architecture with two transmitting and receiving antennas. The block diagram of the frequency domain-based reader reported in [11] is shown in Fig.4.2. Three other types of RFID reader models were introduced by the same authors [9]-[11], in which the first two are working in the frequency range of 2-2.5GHz and the third one is working in the UWB band (2-6GHz) with YIG oscillator. The last two readers can decode both amplitude and phase of the backscattered signal, whereas first reader can decode only the amplitude. The reader proposed in [11] is designed to measure the backscattered signal from the multiresonator based tag for a frequency band of 4-8GHz. A VCO (RVC6000) Richardson Electronics is used as microwave source and RFID system requires two antennas at the reader end for transmission and reception of interrogation signal. All the four FMCW based reader circuits reported in the literature are shown in Fig.4.3. Resonance information from the backscattered signal is extracted by subtracting the encoded signal from the chipless RFID tag with a reference tag.
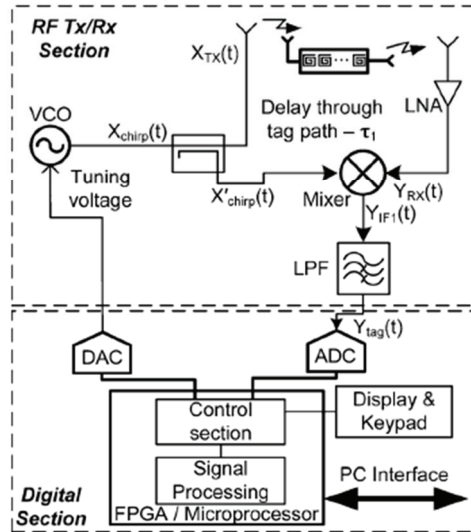
Figure 4.2 Complete block diagram for the chipless RFID reader. Courtesy: R. V. Koswatta et. al. [11].
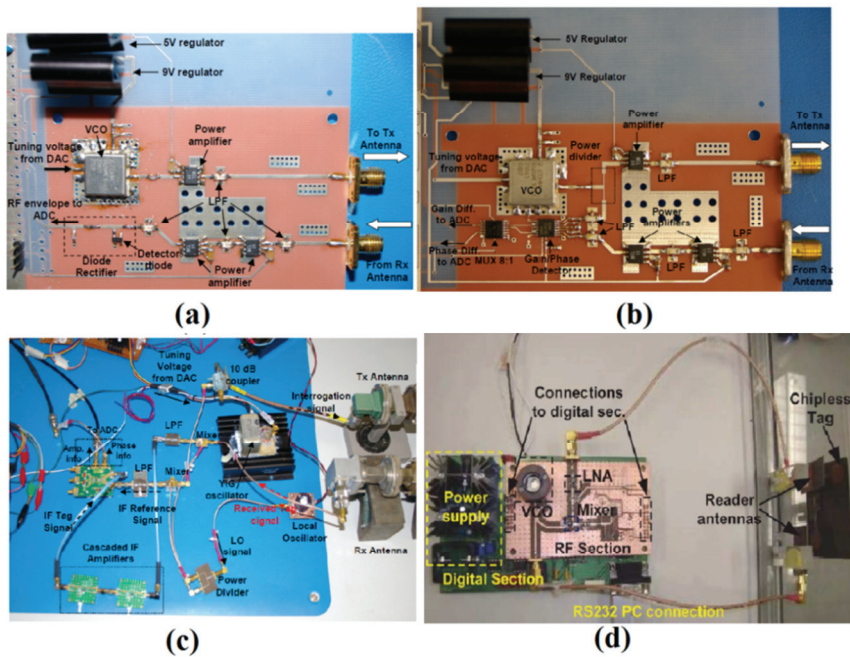
Figure 4.3 Different FMCW chipless RFID reader. (a) Reader with amplitude detection (2-2.5GHz), (b) Reader with amplitude and phase detection (2-2.5GHz), (c) UWB reader with two oscillators (2-6GHz) and (d) UWB reader with single oscillator (4-8GHz)

4.2. Chipless RFID Reader for Multiscatterer Based Tags

In this appendix a chipless RFID reader based on Frequency Modulated Continuous Wave (FMCW) is designed for multiscatterer based tag. The proposed chipless RFID reader is designed for a small frequency band (2.36GHz to 2.54GHz) to demonstrate the feasibility of chipless RFID system. All the components used in the reader are selected from components used in the design of MIT Coffee Can Radar and other lab test equipment. A single bit and two bits multiscatterer based tags is tested with proposed reader system and the results are validated with the Vector Network Analyser. The RFID reader is initially designed with spectrum analyser at the receiver end and later modified to for low cost equipment.

Reader design presented in [9]-[11] consist of two reader antennas, one for the transmitting interrogation signal and the other for the receiving encoded data. The tag presented in the Chapter 3 needs only one antenna for transmission and reception of interrogation signal. Therefore, proposed chipless RFID reader system consist of single antenna. The block diagram of the proposed system with spectrum analyser at the receiver end is shown in Fig.4.4. As shown in the figure, an RFID tag consists of a Uniform Impedance Resonator (UIR) fabricated on an RT Duroid substrate (ε_r = 2.2, tanδ = 0.0009 and substrate height = 1mm). Voltage Controlled Oscillator (VCO, ZX95-2536C+) from mini-circuits is used as the source for RFID reader. Signal generator circuit controls the output of the VCO by generating triangular pulse and applied to tuning voltage pin in the VCO. Low Noise Amplifier (LNA, ZX60-272LN+) is used to amplify the power generated at the VCO. The amplified signal from the LNA is directly connected to the reader antenna (horn antenna) through the main line of the directional

coupler. The backscattered signal from the RFID tag is measured using Anritsu handheld spectrum analyser (10MHz-20GHz) which is connected to the isolation/coupled port of the directional coupler.
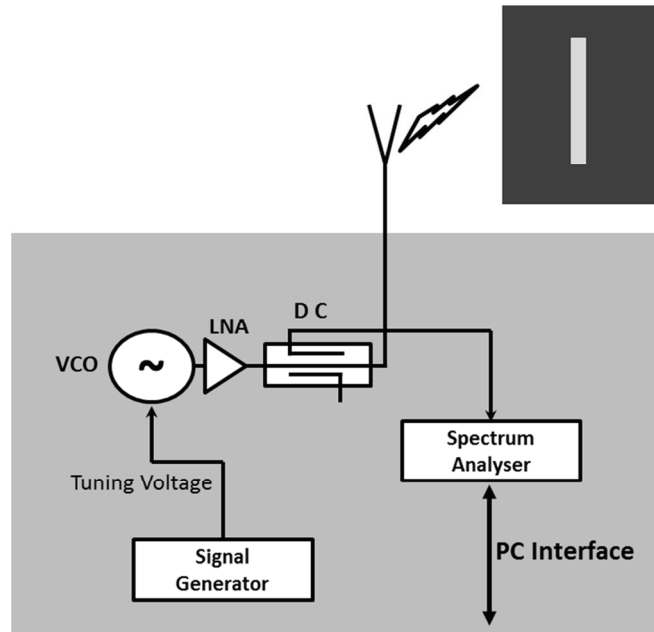
Figure 4.4. Block diagram of an RFID reader with single UIR chipless tag

The working of each block in the diagram shown in Fig.4.4 is detailed in the following section.

4.2.1. Voltage Controlled Oscillator (ZX95-2536C+)

VCO from mini-circuits is used as the source of RFID reader [22] and whose pin diagram is shown in Fig.4.5. It consists of four connections VCC, Ground, Tuning voltage and RF out. The maximum voltage that can be applied to the VCC pin is 5.6V and that to tuning pin is 7.0V. The VCO is able to generate microwave frequency from 2.24GHz to 2.6GHz with a linear voltage variation from 0 to 5V. Frequency and tuning sensitivity of the VCO with tuning voltage is depicted in Fig.4.6. Linear frequency response with

different temperatures is also shown in the figure. The VCO can generate an output power of about 5dBm in the operating band.

Figure 4.5 Voltage Controlled Oscillator from mini-circuits (ZX95-2536C+)
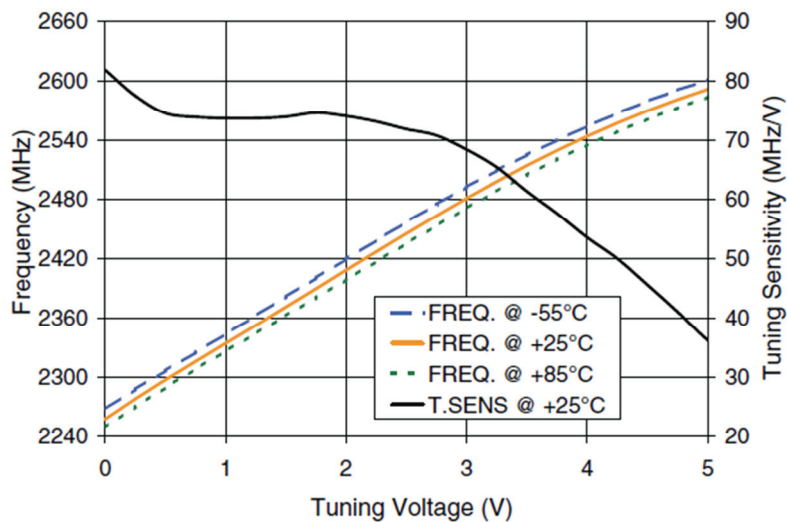
Figure 4.6 Frequency and tuning sensitivity of the VCO with tuning voltage.

4.2.2. Signal Generator

The signal generator is used to control the VCO by generating the synchronising pulse and tuning voltage. XR -2209 IC is used for this purpose. The XR-2209 is a monolithic voltage controlled oscillator (VCO) integrated circuit having excellent frequency stability and a wide tuning range. The circuit provides simultaneous triangular and square wave outputs over a frequency range of 0.01Hz to 1MHz. The block diagram of the IC is given in Fig.4.7, in which block A1 and A2 are the amplifiers. Timing capacitor and

resistor determines the frequencies of the generated triangular and square waves. The square wave output is an "open-collector" type and requires an external pull-up load resistor (nominally 5k) to V+.
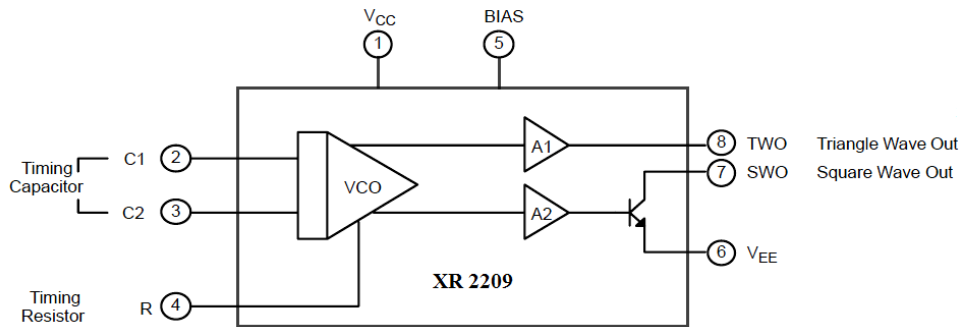
Figure 4.7 XR-2209 Block Diagram

The circuit diagram for triangle and square wave generator using XR2209 is shown in Fig.4.8. The frequency of operation determined by the timing capacitor C and the timing resistor R, is given by 1/RC. The required frequency of 50Hz gives the values of the timing capacitor and resistor as 0.33μF and 62KΩ, respectively. The triangular waveform obtained at pin 8 is centered at about a voltage level V_O and it can be calculated as

$$V_O = V_B + 0.6\ V$$

where V_B is the bias voltage at pin 5. The peak to peak output swing of the triangular wave is approximately equal to $V_{cc}/2$. Ideally, for the generation of waveform by the VCO in ISM band a voltage swing from 2V to 3V is required. The voltage swing obtained from the circuit is from 1.36V to 3.48V at a frequency of oscillation of 50Hz. Hence VCO can generate an output frequency of ~2.36GHz to 2.54GHz. Output waveform from the signal generator circuit is shown in Fig.4.9. During the rising edge of the triangular wave form VCO sweeps its frequency from low to high and while on the

falling edge of the triangular wave VCO sweeps its frequency from high to low.
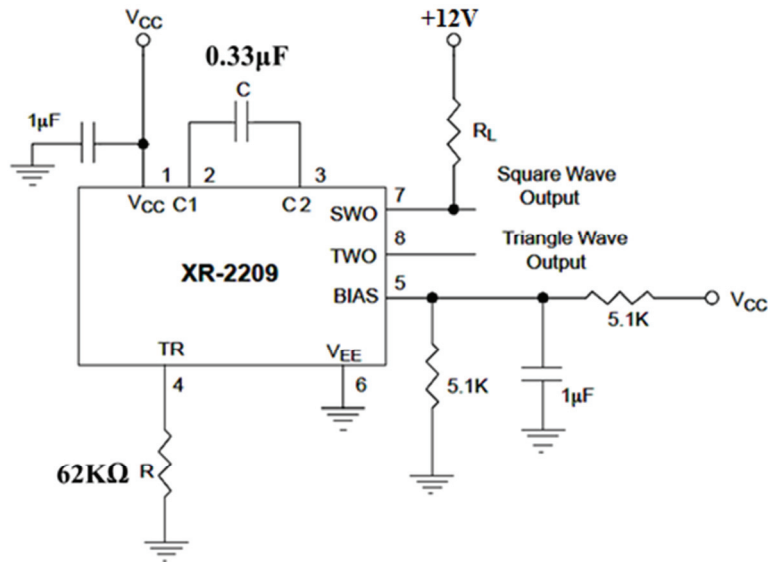
Figure 4.8 Circuit diagram of Signal generator using XR-2209 IC.
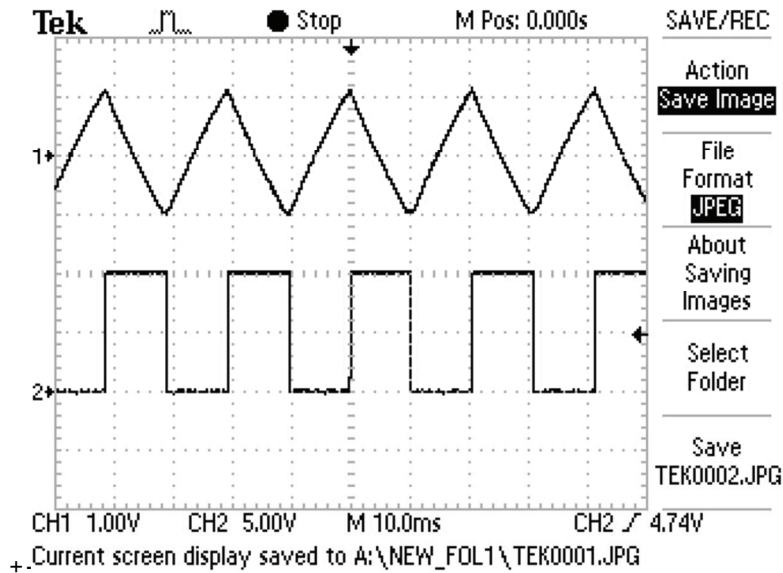
Figure 4.9 Output waveform from the XR-2209 IC based signal generator

4.2.3. Low Noise Amplifier (LNA)

The VCO can generate microwave frequency with ~5dBm of power. But this power may not be sufficient for systems having low sensitivity receiver section. Hence LNA is connected at the RF output port of the VCO. LNA ZX60-272LN+ from mini-circuits [23] is used for this purpose and it can operate in the frequency band 2.3-2.7GHz with maximum power output of 18 to 31dBm. Maximum input power to this LNA can be up to 17dBm. The gain over the operating frequency band is depicted in Fig.4.10 along with the pin diagram of the LNA.
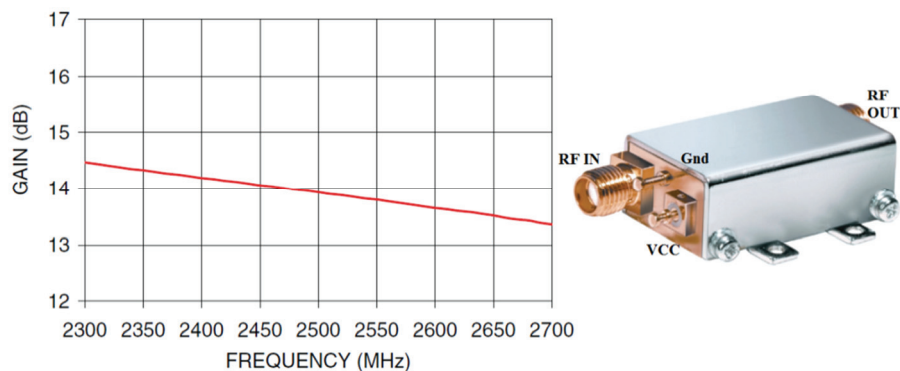
Figure 4.10 Gain of the (LNA ZX60-272LN+) over the operating frequency band

4.2.4. Directional Coupler

A 13.5dB microstrip based directional coupler is used to couple the backscattered signal from the antenna (shown in Fig.4.11) to the receiver section. The main line of the directional coupler is connected between the LNA and the reader antenna. A portion of the backscattered signal from the reader antenna is coupled to the coupling port of the directional coupler. The amount of power coupled to the line depends on the coupling coefficient of

the coupler. Fig.4.12 shows the coupling coefficient and directivity of the coupler over a frequency range of 2-3GHz.
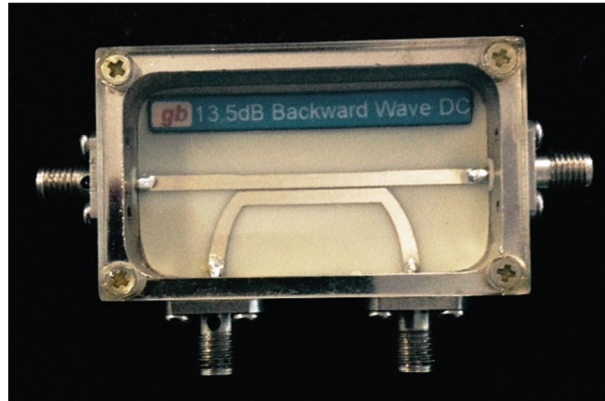
Figure 4.11 13.5dB microstrip based directional coupler
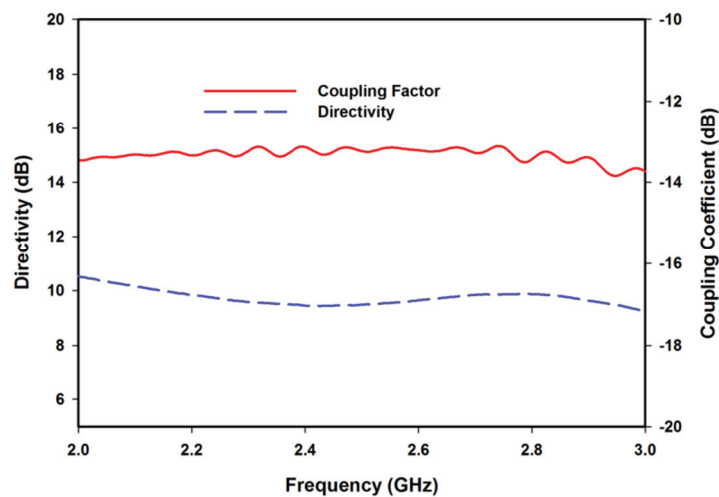
Figure 4.12 Frequency characteristics of directional coupler.

4.2.5. Reader Antenna

A small horn antenna working in the frequency range of 2-12GHz is used as the reader antenna for transmission and reception of the interrogation

signal. This antenna offers a gain of 8dB in the operating frequency range of the reader (refer Chapter 2). Image of the horn antenna is shown in Fig.4.13.
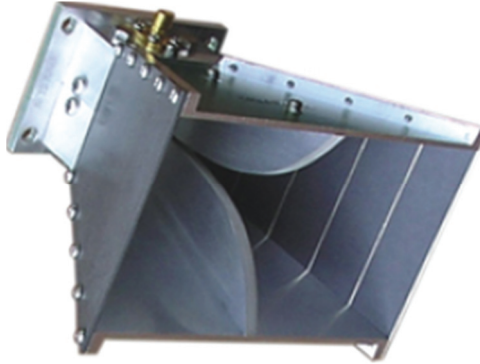
Figure 4.13 Image of the reader antenna (Ridged horn)

4.2.6. Spectrum Analyser

The initial receiver setup to test the backscattered signal from the tag is designed with a spectrum analyser. Anritsu handheld spectrum analyser (Spectrum Master MS2724C) is used, which can operate over a wide frequency range of 10MHz-20GHz (Fig.4.14) and enables the data transfer with personal computer via LAN or USB.

Figure 4.14 Anritsu handheld spectrum analyser (Spectrum Master MS2724C)

4.2.7. Multiscatterer Based Chipless RFID Tag

Owing to the small frequency band of the reader, an RFID tag with single Uniform Impedance Resonator is designed on an RT Duroid substrate with ε_r = 2.2 and tanδ = 0.0009. A half wavelength (λ/2) UIR resonator is designed for a frequency of 2.5GHz and the image of the tag is shown in the reader block diagram (Fig.4.4).

4.3. Mathematical Representation of RFID Reader Signal-1

The mathematical representation of an RFID reader system with two reader antennas is explained in [11] which can be modified for single antenna system. Instantaneous signal (chirp signal) generated by the VCO along with signal generator circuit can be expressed as

$$f(t) = f_0 + Kt \tag{4.1}$$

where K is the chirp rate given by

$$K = \frac{BW}{T_{chirp}} \tag{4.2}$$

and f_0 is the starting frequency, BW is the bandwidth of the transmitted chip and T_{chirp} is the duration of the chirp signal. Output of the chirp generator $X_{chirp}(t)$ can be written as

$$X_{chirp}(t) = A_1 cos\left[2\pi \int_0^t (f_0 + Kt')dt'\right] = A_1 cos\left[2\pi(f_0 t + K\frac{t^2}{2})\right] \tag{4.3}$$

where A_1 is the amplitude of the chirp signal generated at the output port of the LNA which fed into the horn antenna through the directional coupler. Assuming that the reader antenna has a very good impedance matching over the desired frequency band, ie. there is no amplitude and phase distortion, the transmitted signal can be approximated as

$$X_{TX}(t) \approx X_{chirpt}(t) \tag{4.4}$$

The backscattered signal received by the reader antenna energise through the coupled line of the directional coupler and the received signal can be expressed as

$$Y_{RX}(t) = A_{Rx}(f,t).cos[\theta_{RX}(f,t)] \tag{4.5}$$

where $A_{RX}(f,t)$ and $\theta_{RX}(f,t)$ are the total amplitude and phase of the received backscattered signal ($Y_{RX}(f,t)$).

$$A_{Rx}(f,t) = L_{total}A_1A(f') \tag{4.6}$$

$$\theta_{RX}(f,t) = 2\pi f_0(t-\tau) + \pi K(t-\tau)^2 + \phi(f') \tag{4.7}$$

where L_{total} is the sum of all the losses of the received signal due to free space, scattering, coupling coefficient of the directional coupler, etc. The variable τ is the time delay introduced by the tag and wireless propagation. Signal $A(f')$ and $\phi(f')$ are the amplitude and phase variation of the backscattered signal due to the resonance in the chipless RFID tag. f' is the normalized time-varying phase of the transmitted chirped signal, which can be expressed as a function of time as

$$f'(t) = f_0 t + K\frac{t^2}{2} \tag{4.8}$$

By combining equations (4.5), (4.6) and (4.7), the total received signal at the coupled port of the directional coupler can be represented as

$$Y_{RX}(t) = L_{total}A_1A(f').cos[2\pi f_0(t-\tau) + \pi K(t-\tau)^2 + \phi(f')] \tag{4.9}$$

From equation (4.9) it is clear that the amplitude and phase of the backscattered signals are varying with time and is dependent on the chirp signal properties (K and BW), propagation time (τ) (distance between reader antenna and RFID tag) and the resonant properties of the tag.

4.4. Measurement Setup

The VCO and LNA are first tested to verify their operation in the desired frequency band. A general purpose power supply of 12V, 2A is used to power all the circuit elements. A voltage regulator circuit using 7805 IC is used for generating an output volt of 5V. The output power from the VCO and LNA are shown in Fig.4.15. It is measured by connecting the output port of each module to the spectrum analyser. From the figure it is clear that the chirp signal generated by the VCO is in the frequency band ranging from 2.36GHz to 2.54GHz. Power generated by the VCO (chirp signal) over an operating frequency band is about 2-3dBm and the output of the LNA is around 17-18dBm. Amplification of around 15dBm is achieved with LNA and its output is fed to the reader antenna.
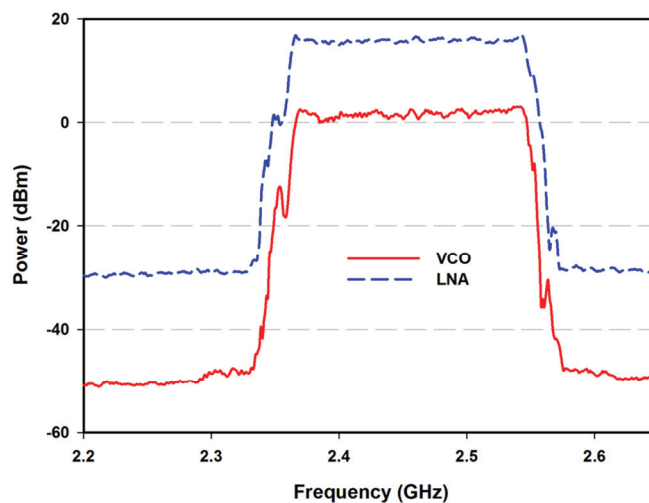
Figure 4.15 Measured power output from VCO and LNA.

Fig.4.16 shows the measurement setup arrangement of the chipless RFID reader. The measurement setup of the reader shown in the block diagram (Fig.4.4) is assembled and tested in a practical environment (outside

the anechoic chamber). One of the coupled lines of the directional coupler is connected to spectrum analyser and other one is terminated with load impedance of 50Ω. Chipless RFID tag consists of a single UIR resonator placed at a distance of 5cm from the reader antenna.
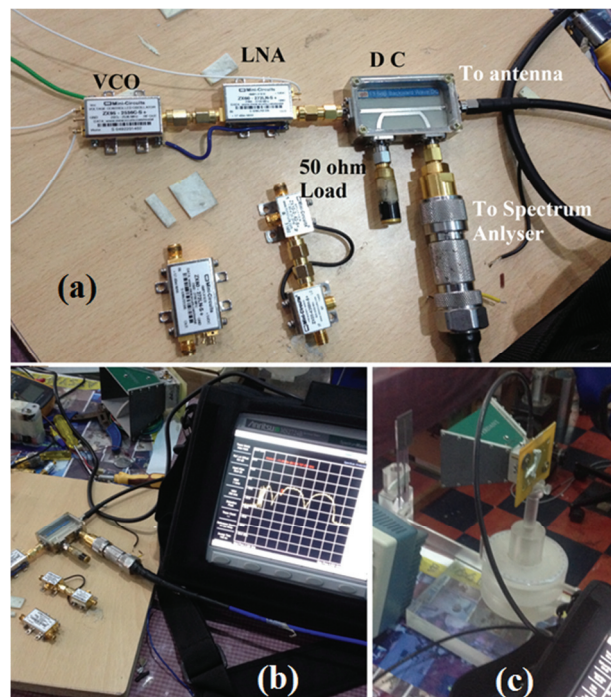
Figure 4.16 Measurement setup with spectrum analyser. (a) Interconnection of RF components, (b) Backscattered signal displayed on spectrum analyser and (c) Single bit chipless tag and reader antenna arrangement (5cm)

Backscattered signal from the tag is measured using spectrum analyser and the response of the tag with and without UIR is depicted in Fig.4.17. Amplitude variation due to the propagation delay and chirp signal explained in the equation (4.9) is clear from the backscattered signal (standing wave like pattern). Both the backscattered signals (with and without resonator) look similar except for the amplitude variation at 2.50GHz. Resonant frequency of the tag is obtained by taking the difference between the two signals (tag with

UIR and without UIR) and the resultant post processed signal is depicted in Fig.4.18. To verify the operation of the RFID reader, resonant frequency of the same tag is measured using network analyser PNA E8362B. The backscattered response from the tag using network analyser is depicted in Fig.4.18. The resonant frequency of the tag is found be the same (2.50 GHz) in both measurements. Thus the proposed system is validated.
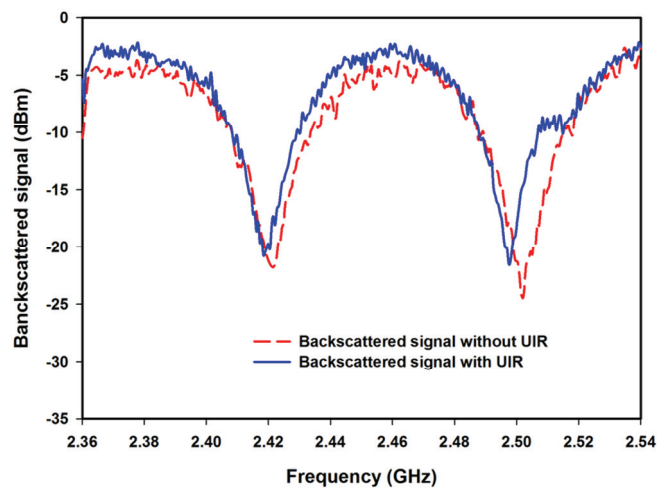
Figure 4.17 Measured backscattered spectrum from the RFID reader, which is measured using spectrum analyser.
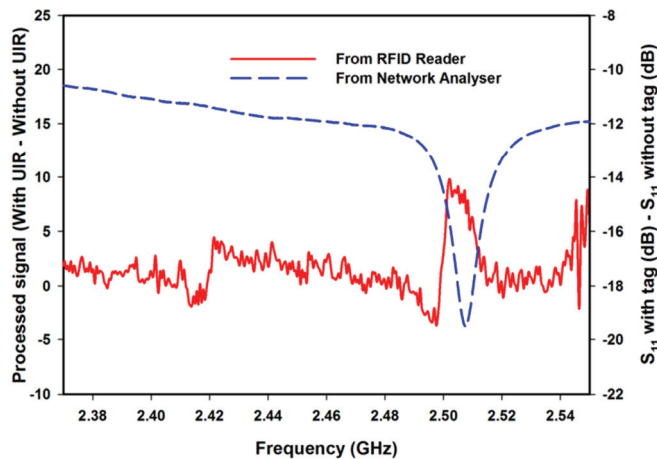
Figure 4.18 Measured tag response of the UIR based Chipless RFID using RFID reader and Network analyser.

4.5. Low Cost Chipless RFID Reader for Multiscatterer Based Tag

The RF sections of the above system consist of VCO, LNA, Directional Coupler and Spectrum analyser. Except for spectrum analyser, the cost of all the items in the reader comes under $100. The cost of the receiver section is at the higher end (spectrum analyser) due to the data analysis in the microwave frequency. Hence another model of RFID reader circuit is designed to create a cost effective system. In this system, the costlier spectrum analyser is replaced with a lower cost Digital Storage Oscilloscope (DSO) having an operating frequency from DC to 40MHz. Block diagram of the proposed RFID reader is shown in Fig.4.19. In this design, some additional RF components are added to the existing RFID reader. Instead of directly sending the amplified chirp signal to the directional coupler, a power splitter is introduced in between two. Half of the amplified chirp signal goes to reader antenna through Directional Coupler (DC) and other half goes to the mixer unit. To amplify the weak backscattered signal from the D C, an additional LNA is connected in between the coupled port of the D C and the mixer. The backscattered signal from the LNA and the transmitted chirp signal from the power splitter are fed into the mixer to generate IF (Intermediate Frequency) signal. A mixer is a three port nonlinear electrical circuit that creates new frequencies from two signals applied to it. When two signals with frequencies f_1 and f_2 are applied to a mixer, it produces two new signals with the sum $(f_1 + f_2)$ and difference $(f_1 - f_2)$ of the original frequencies. Other frequency components may also be produced in a practical frequency mixer. In a practical circuit, when two signals with the same frequencies are fed into a mixer, it generates signals of frequency 0Hz, f_1, $2f_1$, etc. Signal processing in the IF (low frequency) can be used to analyse

backscattered signal from the chipless tag. The IF signal generated by the mixer and the synchronising pulse from the signal generators are fed into the DSO. The DSO which has integrated LPF at the input port, filters all the higher frequency components in the IF signal. Then the filtered analog signal in the DSO is converted into digital signal and sent to personal computer for signal processing. The data communication between the DSO and the PC can be done through the LAN or USB.
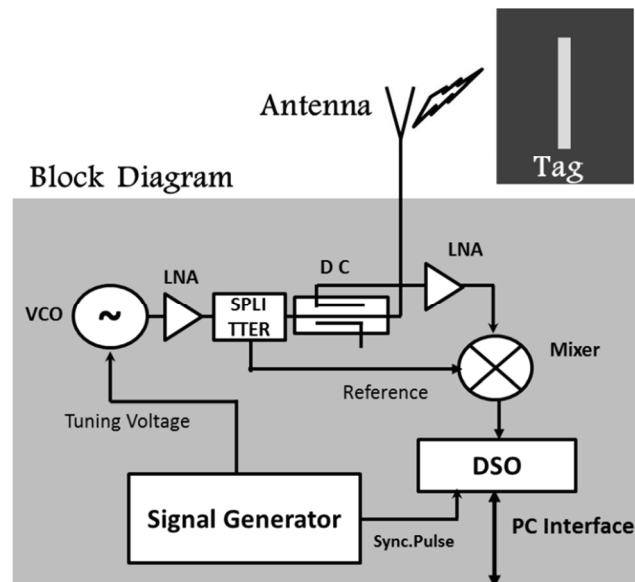
Figure 4.19 Block diagram of chipless RFID reader using DSO

The new RF components used in this design are Power Splitter (ZX10-2-42+) and Mixer (ZX05-43MH+) from mini-circuits. Detailed specifications of these components are described below.

4.5.1. Power Splitter

A 3dB coaxial Power splitter/combiner (ZX10-2-42+) [24] module is used to split the generated chirp signal into two parts, the first half is transmitted through the reader antenna and the second half is used for the

generation of IF signal at the receiver section. The image and schematic block diagram of the splitter is depicted in Fig.4.20. As shown in the figure, power splitter module is a 3 port device. Amplified signal from the LNA is connected to the summing port (S). This circuit splits the signal into two half's and which emerge out from ports 1 & 2. The total loss of the splitter for a frequency band of 1.9GHz to 4.2GHz is depicted in the Fig.4.21. Total power loss of the splitter for reader frequency band is about 3.15 to 3.3dB.
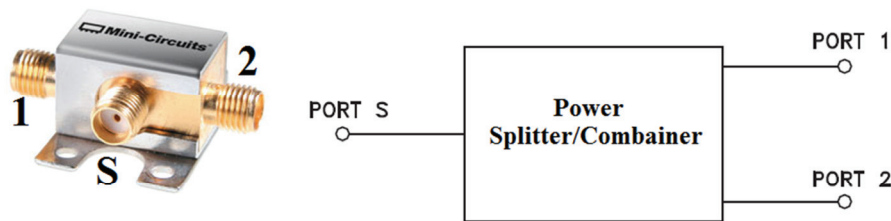
Figure 4.20 Power Splitter/combiner from mini-circuits (ZX10-2-42+) and its schematic diagram
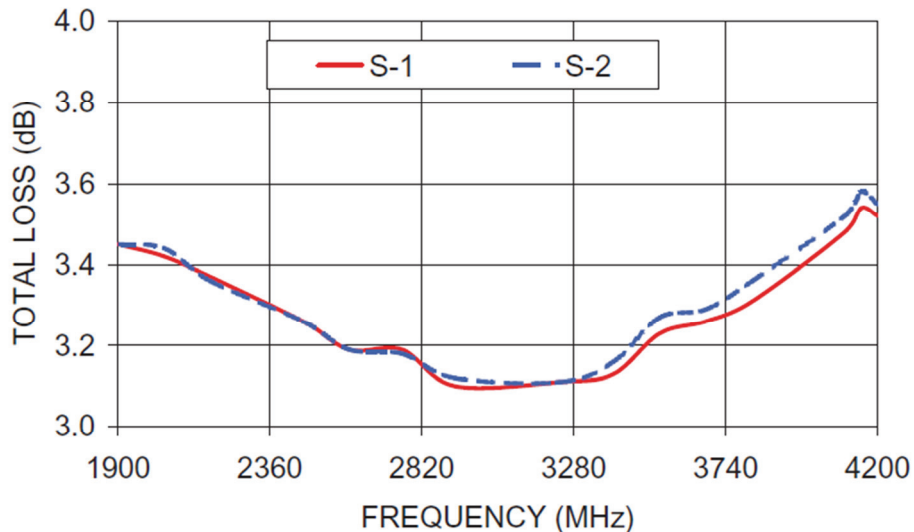
Figure 4.21 Total loss Vs frequency response of the splitter.

The power output from VCO, LNA and Splitter is shown in Fig.4.22. The power from each module is measured using spectrum analyser. While

measuring power from the splitter, the unused port is terminated with 50Ω load to eliminate reflections. It clear from the figure that, the power splitter is able to split the incoming power into two equal portions.
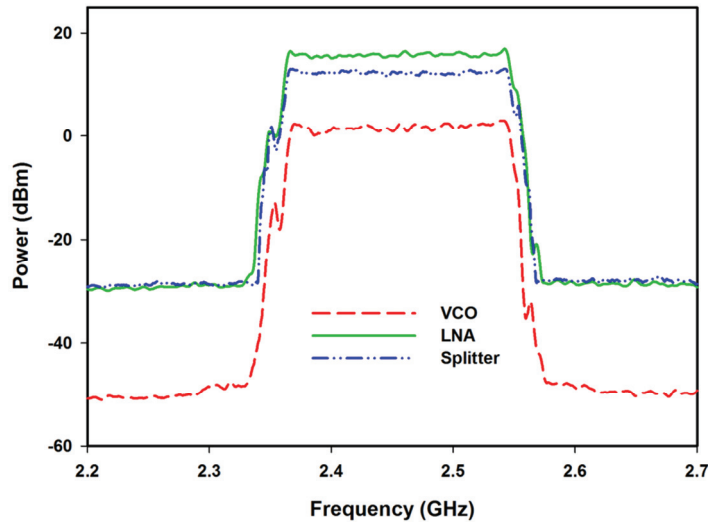
Figure 4.22 Power output spectrum from VCO, LNA and Splitter

4.5.2. Mixer

A mixer is a three port nonlinear electrical circuit that creates new frequencies from two signals applied to it. Image of the mixer (ZX05-43MH+) [25] with its electrical schematic diagram given by the manufacturer is shown in Fig4.23. Power spectrum produced by the mixer when two signals with the same frequencies applied at the input ports (Local Oscillator port and RF port) are shown in Fig.4.24. Two types of measured results using spectrum analyser are depicted in the figure, one with single frequency and the other with transmitted chirp signal. As the operating frequency range of spectrum analyser is10MHz to 20GHz, DC components are not included in the figure. The power spectrum produced by the mixer contains the fundamental and its harmonic frequencies (f1, 2f1,..etc).
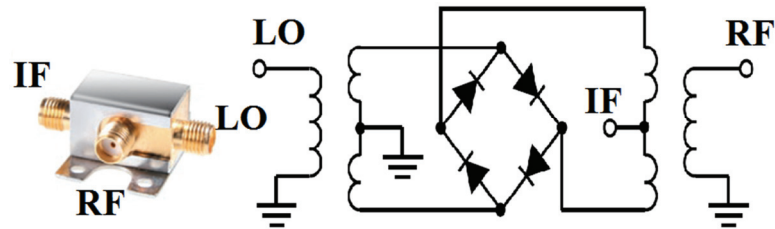
Figure 4.23 Frequency mixer (ZX05-43MH+) and its electrical schematic diagram
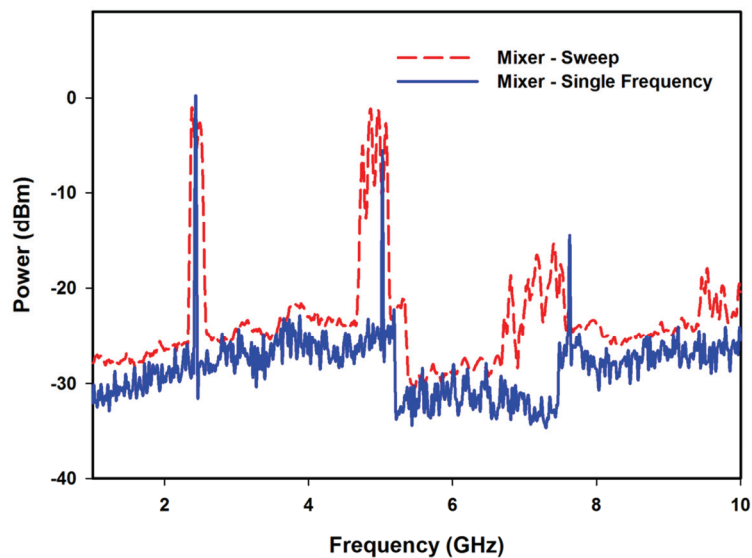
Figure 4.24 Frequency spectrum generated by the mixer when two signals with same frequency applied at its input ports.

4.5.3. Digital Storage Oscilloscope (DSO)

The Digital oscilloscope acts as a Low Pass Filter (LPF) and Analog to Digital Converter (ADC). Low frequency signal in the IF need to be filtered out because it contains a wide range of frequencies as shown in Fig.4.24. An ADC is also required to convert the analog signal to digital signal. The block diagram of the DSO shown in Fig.4.25 contains a preamplifier and an ADC at the input port. Preamplifier section amplifies the input signal and filters out all the high frequency components to avoid the aliasing effect (Nyquist Criteria). Cut off frequency of the filter depends on

the maximum frequency limit of the DSO. The DSO from Tektronix (TDS1001B) with an operating frequency range of DC to 40MHz is used here.
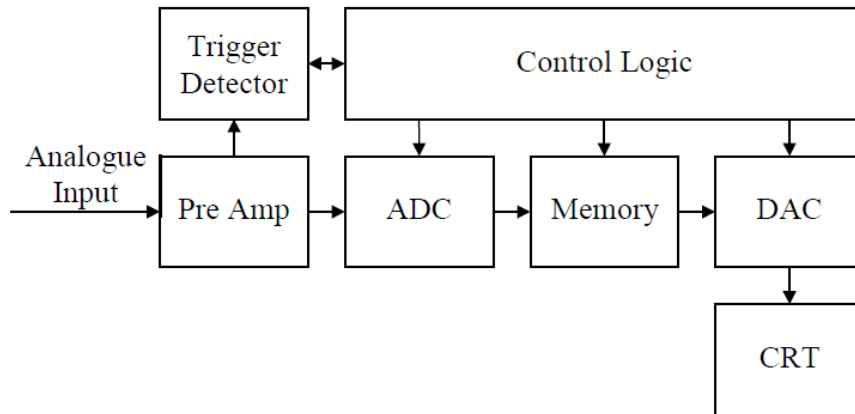
Figure 4.25 Conventional DSO Block Diagram

4.6. Mathematical Representation of RFID Reader Signal -2

The mathematical representation of backscattered signal for RFID system with spectrum analyser can be extended to the proposed system. Equations (4.3) and (4.9) represent the transmitted chirp signal and backscattered signal, respectively at the output of directional coupler. Here a part of the transmitted chirp signal is taken from the power splitter and is fed into Local Oscillator port of the Mixer. The backscattered signal from the directional coupler is amplified and fed to the RF port of the Mixer. These two input signals can be mathematically expressed as

$$X'_{chirp} = K_1 A_1 cos \left[2\pi (f_0 t + K \frac{t^2}{2}) \right] \qquad (4.10)$$

$$Y'_{RX}(t) = L_{total} A_2 A(f') . cos[2\pi f_0 (t - \tau) + \pi K (t - \tau)^2 + \phi(f')] \quad (4.11)$$

where K_1 is coefficient of the power splitter and A_2 is the amplitude gain (due to the LNA) of the backscattered signal. The IF signal generated at the output of the mixer can be expressed as

$$Y'_{IF}(t) = X'_{chirp}.Y'_{RX}(t) \qquad (4.12)$$

Equation (4.12) can be simplified as

$$Y'_{IF}(t) = K_2 A(f')\{\cos(\theta_1 + \theta_2) + \cos(\theta_1 - \theta_2)\} \qquad (4.13)$$

where θ_1, θ_2 and K_2 can be written as

$$\theta_1 = 2\pi\left(f_0 t + K\frac{t^2}{2}\right) \qquad (4.14)$$

$$\theta_2 = 2\pi f_0(t - \tau_1) + 2\pi f_0(t - \tau_2)^2 + \phi(f') \qquad (4.15)$$

$$K_2 = \frac{K_1{}^2 A_1 L_{total}}{2} \qquad (4.16)$$

where K_2 is constant. When signal $Y'_{IF}(t)$ is passed through a LPF, it will filter out all the high frequency components associated with $\cos(\theta_1 + \theta_2)$.

After passing $Y'_{IF}(t)$ through the LPF the output signal $Y_{tag}(t)$ can be approximated as

$$Y_{tag}(t) = K_2 A(f')\cos\left[2\pi \frac{BW}{T_{chirp}}\tau_1 t + 2\pi f_0 \tau_1 + \phi(f')\right] \qquad (4.17)$$

From equation (4.17), it is clear that the frequency of the output signal varies with the parameters: T_{chirp}, τ_1 and BW. Therefore Y_{tag} contains a very low frequency component and it depends more on T_{chirp}, τ_1, and BW. By analysing amplitude $(A(f'))$ or phase $(\phi(f'))$ of the Y_{tag} signal, all the properties of the chipless RFID tag can be decoded.

4.7. Measurement System

The circuit diagram of the chipless RFID reader system for multiscatterer based tag is shown in Fig.4.26. The PCB shown in Fig.4.26 consists of signal generator, power regulator (using 7805) and video amplifier circuits, which is designed for MIT Coffee Can Radar. The system is designed to detect only the amplitude of the backscattered signal. The measurement setup using the proposed system is depicted in Fig.4.27. Two chipless RFID tags with single and two UIRs are tested with proposed reader. All the measurements are carried out inside the laboratory (noisy environment) within a distance of 2cm and 5cm.
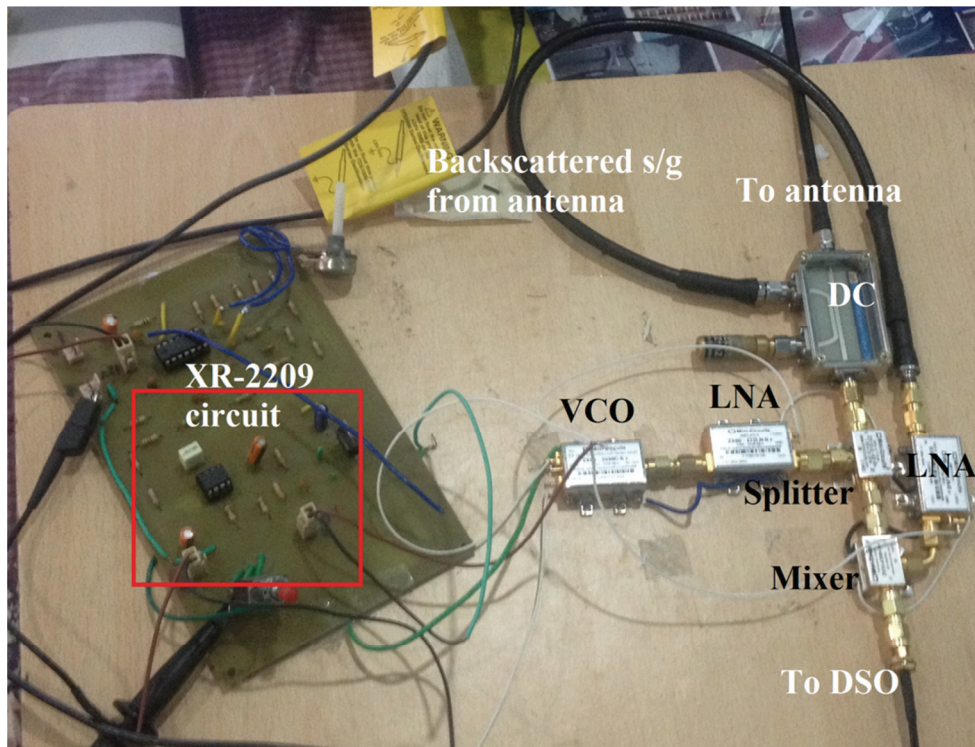
Figure 4.26 Circuit connection of Chipless RFID reader

Figure 4.27 RFID reader measurement setup with an RFID tag placed at 5cm away from the antenna.

All the RF components in the reader work with 5V power supply. The output of the mixer is connected to one channel of the DSO. Synchronising pulse generated by the XR-2209 IC is connected to the second channel in the DSO. Fig.4.28 and 4.29 show the backscattered signal from the RFID tag with and without resonator (UIR), respectively. The figure also shows the synchronising pulse recorded by the DSO. The triangular wave sweeps the VCO from low to high frequency for the high voltage state of the synchronizing pulse and high to low for its low voltage state. This phenomenon can be clearly identified from the Fig.4.28, where backscattered signals are mirror images, when observed from the transition time of synchronising pulse. Here RFID tag is placed 2cm way from the reader antenna and resonant variation in the amplitude of the backscattered is clearly visible in each time period of the synchronising pulse (marked with circles in

Fig.4.28). The sinusoidal variation in the backscattered signal is due to the T_{chirp}, τ_1, and bandwidth of the RFID reader.
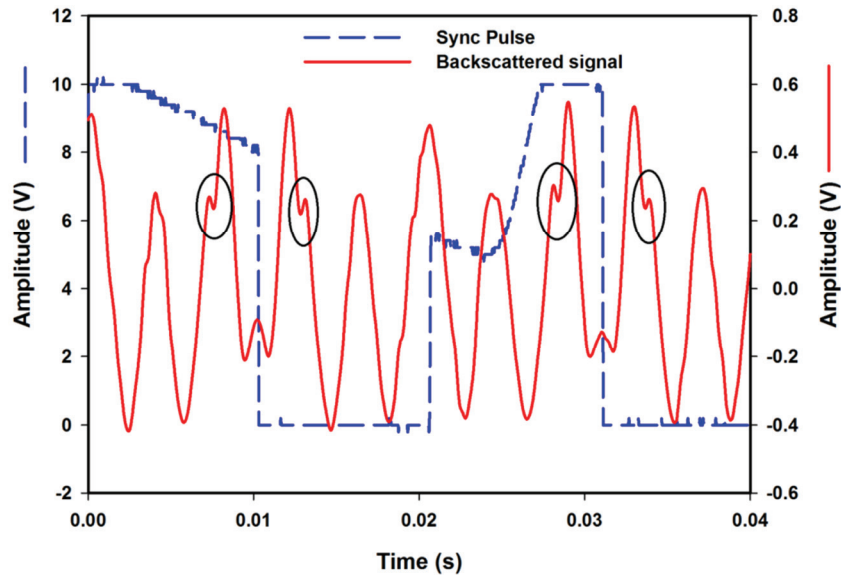
Figure 4.28 Backscattered signal from the RFID tag (with UIR) and synchronising pulse (2cm)

To verify the resonant information from backscattered signal, the same tag is measured without having resonator (UIR) and its response is depicted in Fig.4.29. It is clear that both measured backscattered signals are identical except for the resonant dips. Hence differences between the two backscattered signals (with and without UIR) are taken to identify the amplitude difference in resonant frequency. Fig.4.30 shows the backscattered signal (with and without UIR) from the RFID tags along its frequency axis. The time to frequency conversion of chirp signal can be done by solving equations (4.1) and (4.2). Post processing of the backscattered signal is done by taking the difference of the two signals (backscattered signal with and without tag) and magnitude variation at the resonant frequency is also depicted in Fig.4.30.
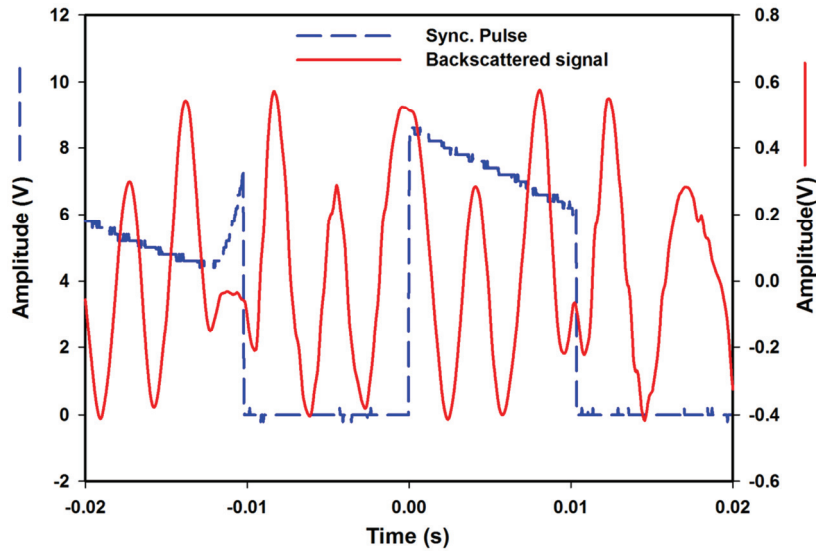
Figure 4.29 Backscattered signal from the RFID tag (without UIR) and synchronising pulse (2cm)
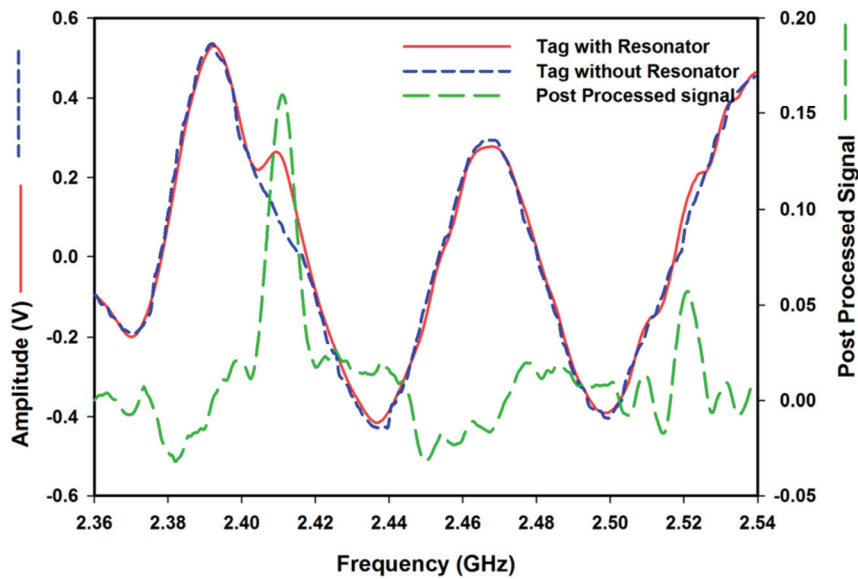
Figure 4.30 Frequency response of the backscattered signal from the tag (with and without UIR) and post processed signal.

To validate the system, backscattered signal from the tag is measured with Vector Network analyser and its result with RFID reader data is compared and is shown in Fig.4.31. In both measurements resonant

frequency of the tag is found to be at 2.41GHz and measurements are in good agreement with each other. Thus the system is validated.
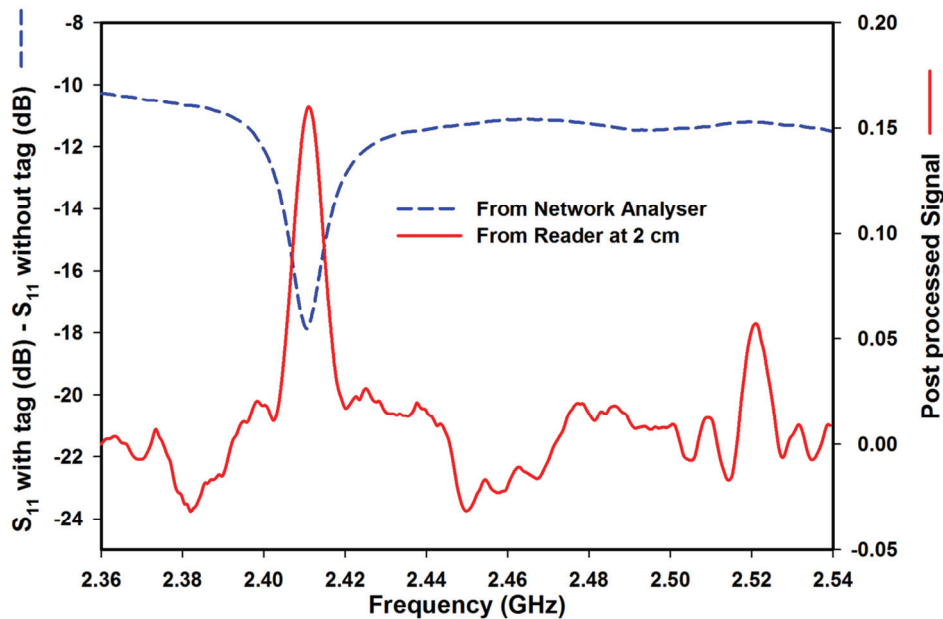
Figure 4.31 Backscattered signal comparison between RFID reader and Network analyser.

The measurement is repeated with 5cm distance between the reader antenna and RFID tag. Synchronising pulse and backscattered signal from the tag having UIR and without UIR are shown in Fig.4.32 and 4.33, respectively. Compared to the previous measurement (with 2cm distance), amplitude and frequency variations of the backscattered sinusoidal signal are different due to the variation in the propagation losses and delay. As shown in the figure, backscattered signals are susceptible to noises. Resonant variations are still able to be identified from the backscattered signal and are marked in Fig.4.32.
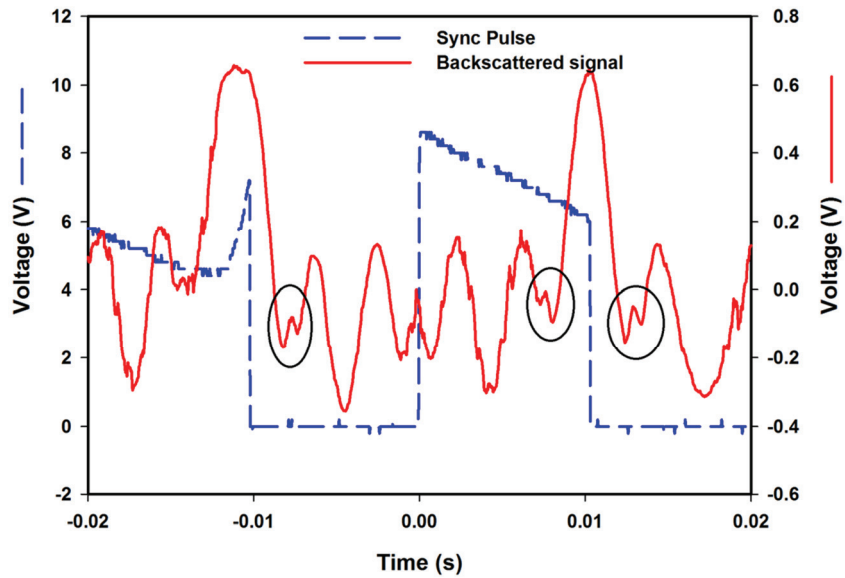
Figure 4.32 Backscattered signal from the RFID tag (with UIR) and synchronising pulse. (5cm)
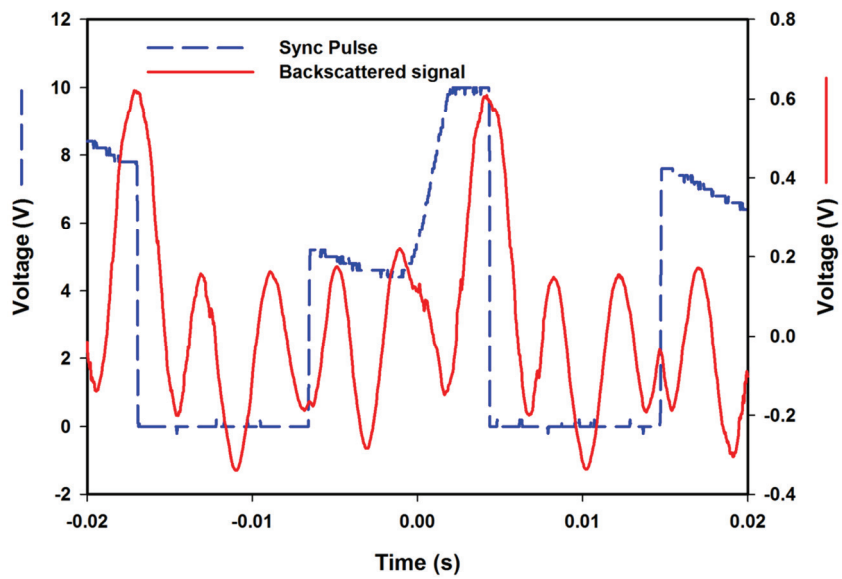
Figure 4.33 Backscattered signal from the RFID tag (without UIR) and synchronising pulse. (5cm)

To extract resonant frequency, difference between the two signals is taken and the resultant signal is plotted against network analyser data.

Frequency response plotted in Fig.4.34 shows the backscattered signal measured using network analyser and RFID reader at different distances.
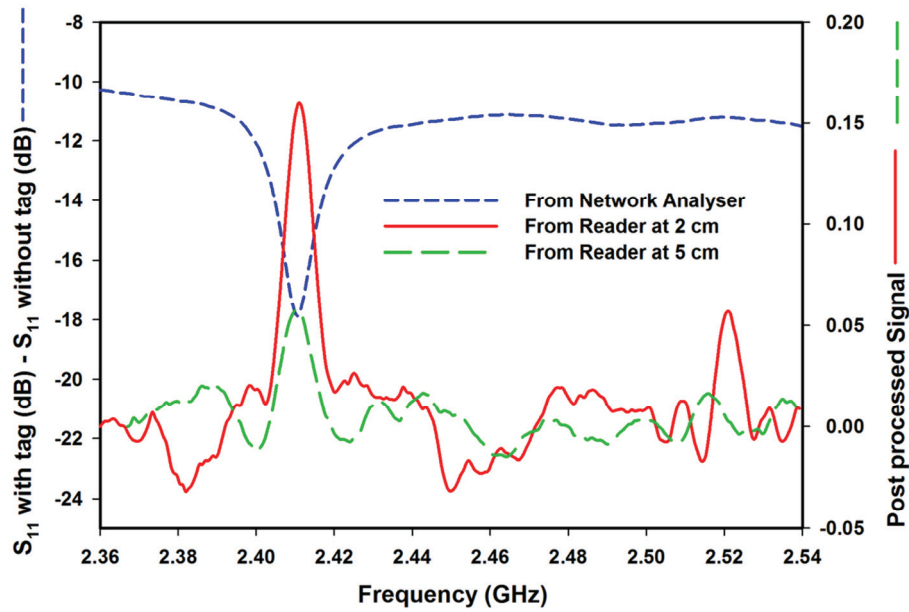
Figure 4.34 Backscattered response of the tag measured using network analyser and RFID reader.

4.7.1. Chipless RFID Tag with Two Uniform Impedance Resonator

All the proceeding measurements were carried on a chipless tag with single UIR. In this section, a new chipless RFID tag is designed on RT Duroid substrate ($\varepsilon r = 2.2$, $\tan\delta = 0.0009$ and $h = 1.6$mm) with two UIR, whose resonant frequencies are selected to be within the reader frequency band. Fig.4.35 shows the fabricated chipless tag. The backscattered signal from the tag is measured using proposed RFID reader at two different distances (2cm and 5cm).

Figure 4.35 Chipless RFID tag using two UIR.

Fig.4.36 shows the synchronising pulse and the backscattered signal from the tag measured at a distance of 2cm. Two resonant frequency variations in the amplitude of the backscattered signal, two in each chirp period are marked for identification. Same resonant variations can be observed in the backscattered signal measured at 5cm distance and is shown in Fig.4.37.
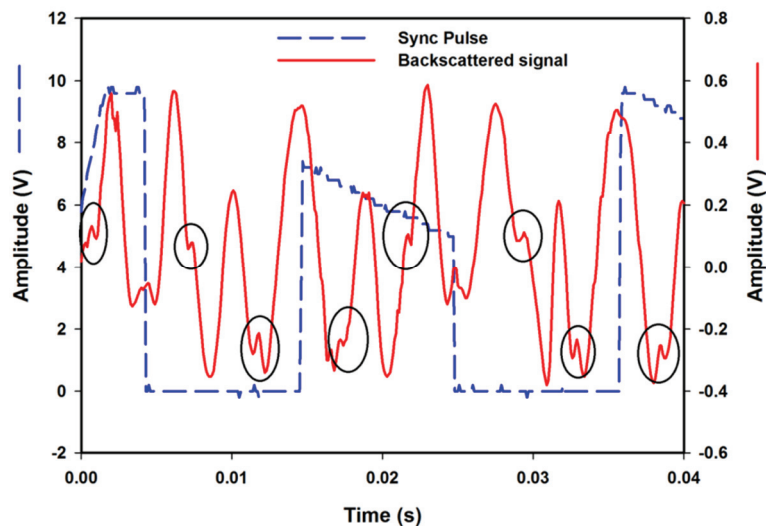
Figure 4.36 Backscattered signal from the RFID tag (with two UIR) and synchronising pulse measured at 2cm.
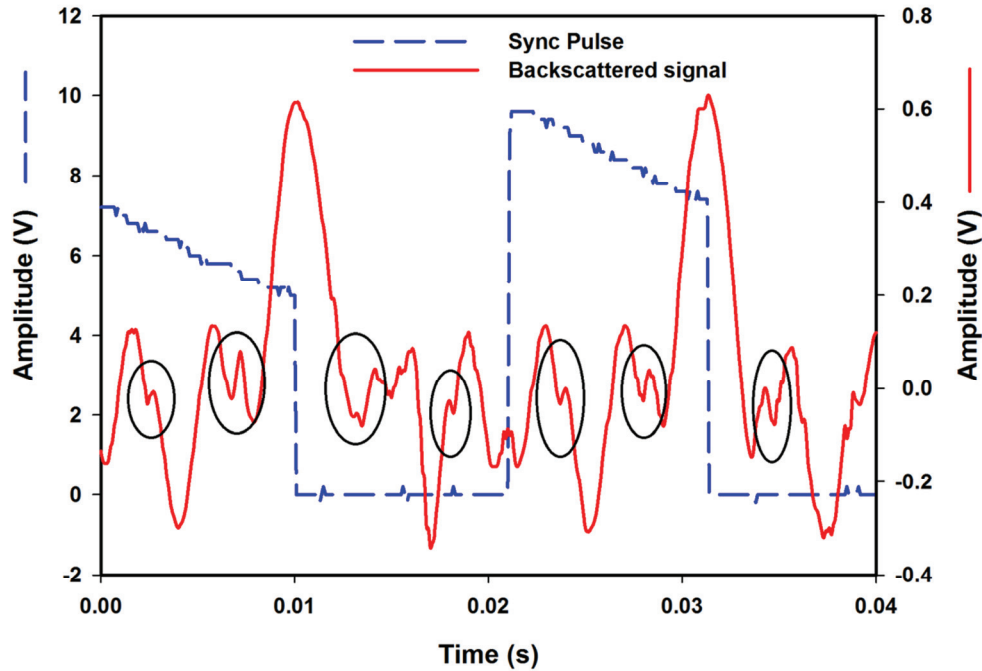
Figure 4.37 Backscattered signal from the RFID tag (with two UIR) and synchronising pulse measured at 5cm.

The backscattered signal from the same RFID tag is measured using network analyser and Fig.4.38 shows its backscattered response plotted against RFID reader data (2cm and 5cm). As shown in Fig.4.38, the results are showing very good agreement with each other. By changing the voltage level of the signal generator, more number of resonances can be represented by the same RFID reader, because tuning voltage is applied only in the range of 1.36V to 3.48V.
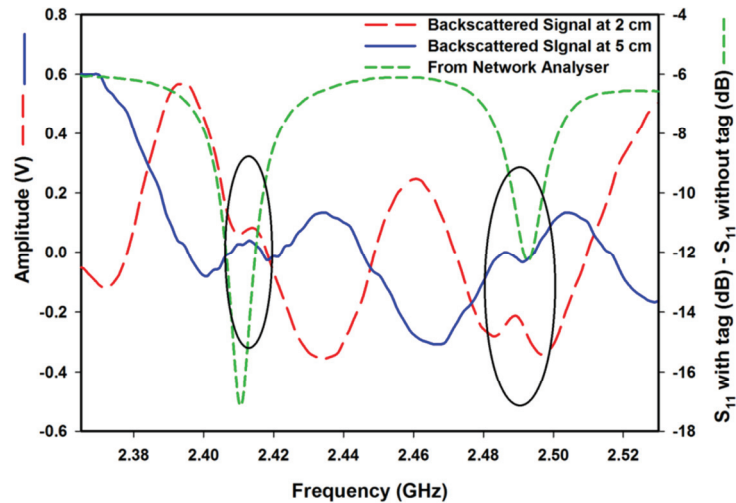
Figure 4.38 Measured backscattered signal using RFID reader and Network analyser.

4.8. Conclusion

In this chapter an RFID reader working in the frequency band of 2.36 GHz to 2.54 GHz is proposed. Chipless RFID reader is initially designed with spectrum analyser at the receiver section. Its working is validated with single resonator based chipless tag. Finally an RFID reader is proposed with low cost RF components and two types of chipless RFID tags (single and two bit) are tested with the proposed system. Validation of the system is done by measuring the tag response using network analyser. All the measurements with RFID reader show very good agreement with analyser data. Backscattered response of the tag is measured successfully up to a distance of 5cm.

4.9. Future Work

Proposed RFID reader is actually derived from MIT Coffee Can RADAR and the detailed working of RADAR is included in the APPENDIX. In place of the DSO, the radar system uses a video amplifier section and personal computer. The video amplifier section having LPF filter with cut off frequency of 15 KHz

is designed and it is used to filter the IF signal from the mixer. The output of the LPF filter and synchronising pulse are converted to digital signals through the ADC inside the audio jack in the computer. This method can also be adopted in the case of RFID reader design because maximum frequencies in the IF signal is in the order of several Hz. Hence the cost of the proposed system can be reduced considerably (DSO-$1200 USD). Table 1 shows the approximate cost of the individual items employed in the proposed reader.

Table 1. Cost of Individual RADAR Components

Item	Qty	Cost
VCO (ZX95-2536C+)	1	$45.00
LNA (ZX60-272LN+)	2	$80.00
Power Splitter (ZX10-2-42+)	1	$35.00
Directional Coupler (13.5dB)	1	$10.00
Mixer (ZX05-43MH+)	1	$46.50
Coaxial Cables		$10.00
Coaxial Connectors	2	$10.00
DSO	1	$1200.00
XR 2209	1	$2.00
Other components		$5.00
Total Cost		**$1443.00**

Proposed RFID reader system requires a reference tag to extract the resonant frequency of the chipless tag. Signal processing technique (Hilbert transform) proposed by R. V. Koswatta et. al. [11] can be implemented to avoid the requirement of reference tag. Another disadvantage of the RFID reader is its low data decoding capacity due to the limited operating bandwidth. This problem can be avoided by replacing low bandwidth VCO with wide band Yig oscillator [10]-[11].

4.10. Reference

[1] WJ Communications Inc, "A compact RFID reader platform for UHF and microwave applications", *Microwave Journal*, vol. 47, no. 5, pp: 42-48, April 2004.

[2] F. Mohd-Yasin, M. K. Khaw, M. B. I. Reaz, "Radio frequency identification: Evolution of reader and antenna circuit design", *Microwave Journal*, vol. 49, no. 5, pp:89-95, May 2007.

[3] M. J. Uddin, A. N. Nordin, M. I. Ibrahimy, M. B. I. Reaz, T. Z. A. Zulkifli, M. A. Hasan, "Design and simulation of RF-CMOS spiral inductors for ISM band RFID reade circuits", *IEEE Workshop on Microelectronics and Electron Devices 2009*, pp: 1-4, April 2009.

[4] G. K. Balachandran, R. E. Barnett, "A high dynamic range ASK demodulator for passive UHF RFID with automatic over-voltage protection and detection threshold adjustment", *IEEE Custom Integrated Circuits Conference CICC 2009*, pp: 383-386, San Jose, USA, Sept. 2009.

[5] G. De Vita, G. Iannaccone, "Ultra low power RF section of a passive microwave RFID transponder in 0.35μm BiCMOS", *IEEE International Symposium on Circuits and Systems ISCAS 2005*, vol. 5, pp: 5075-5078, Kobe, Japan, May 2005.

[6] Mayordomo, R. Berenguer, I. Fernandez, I. Gutierrez, W. Strauss, J. Bernhard, "Simulation and measurement of a long-range passive RFID system focused on reader architecture and backscattering communication", *38th European Microwave Conference EuMC 2008*, pp:1058-1061, Amsterdam, Netherlands, October 2009.

[7] RFSAW Inc, "The global SAW tag – a new technical approach to RFID", internet white paper, 2004. Available: http://www.rfsaw.com/pdfs/SAW%20RFID%20Whitepaper.pdf

[8] RFSAW Inc, "Model 501 SAW RFID Reader System", product data sheet, 2004. Available: http://www.rfsaw.com/pdfs/Data_501_4.pdf

[9] S. Preradovic and N. Karmakar, "Multiresonator based chipless RFID tag and dedicated RFID reader," in IEEE MTT-S Int. Microw. Symp. Dig., Anaheim, CA, 2010, pp. 1520–1523.

[10] S. Preradovic, I. Balbin, N. C. Karmakar, and G. F. Swiegers, "Multiresonator- based chipless RFID system for low-cost item tracking," IEEE Trans. Microw. Theory Tech., vol. 57, no. 5, pp. 1411–1419, May 2009.

[11] R. V. Koswatta and N. C. Karmakar, "A novel reader architecture based on UWB chirp signal interrogation for multiresonator based chipless RFID tag reading," IEEE Trans. Microwave Theory Tech., vol. 60, no. 9, pp. 2925–2933, Sept. 2012.

[12] A. Vena, T. Singh, S. Tedjini, and E. Perret, "Metallic letter identification based on radar approach," in Proc. General Assembly Scientific Symp. 2011 URSI, pp. 1–4.

[13] A. Vena, E. Perret, and S. Tedjini, "Novel compact RFID chipless tag," in Proc. Progress Electromagnetics Research Symp., Marrakesh, Morocco, 2011, pp. 1062–1066.

[14] A. Ramos, A. Lazaro, D. Girbau, and R. Villarino, "Time domain measurement of time-coded UWB chipless RFID tags," Progr. Electromagn. Res., vol. 116, pp. 313–331, July 2011.

[15] A. Vena, E. Perret, and S. Tedjini, "Chipless RFID tag using hybrid coding technique," IEEE Trans. Microwave Theory Tech., vol. 59, no. 12, pp. 3356–3364, 2011.

[16] P. Kalansuriya and N. Karmakar, "UWB-IR based detection for frequency- spectra based chipless RFID," in IEEE MTT-S Int. Microw. Symp. Dig., pp. 1–3,2012.

[17] M. Manteghi, "A novel approach to improve noise reduction in the matrix pencil algorithm for chipless RFID tag detection," in IEEE Int.Antennas Propag. and CNC-USNC Symp./URSI Radio Sci. Meeting., Toronto, ON, Canada, Jul. 11–17, 2010.

[18] Y. Shen, C. L. Law, S. Hu, and J. Xia, "IR-UWB-based chipless RFID system," Ann. Telecommun. -Springer, vol. 68, no. 7–8, pp. 375–383, Jun. 2013.

[19] Smail Tedjini, Nemai Karmakar, Etienne Perret, Arnaud Vena, Randika Koswatta, and Rubayet E-Azim , "Hold the Chip" IEEE microwave magazine, August 2013.

[20] E. Perret, M. Hamdi, G. E. P. Tourtollet, R. Nair, F. Garet, A. Delattre, A. Vena, L. Duvillaret, P. Martinez, S. Tedjini, and Y. Boutant, "THID, the next step of chipless RFID," in Proc. 7th IEEE RFID Conf., Orlando, FL, 2013, pp. 292–299.

[21] Novelda Impulse Radar. [Online]. Available: http://www.novelda.no/

[22] Data sheet of VCO (ZX95-2536C+), Available at: http://www.minicircuits.com/ pdfs/ZX95-2536C+.pdf

[23] Data sheet of LNA (ZX60-272KN+), Available at: www.minicircuits.com/ pdfs/ZX60-272LN+.pdf

[24] Data sheet of Power splitter/combiner (ZX10-2-42+), Available at: http://www.minicircuits.com/pdfs/ZX10-2-42+.pdf.

[25] Data sheet of Frequency Mixer (ZX05-43MH+), Available at: http://www.minicircuits.com/ pdfs/ZX05-43MH+.pdf

.............ॐ.............

Chapter | 5

TIME DOMAIN ANALYSIS OF FREQUENCY SPECTRA BASED CHIPLESS RFID TAGS

Abstract

This chapter proposes a new technique based on UWB Impulse radar (UWB IR) technology using time domain for decoding the backscattered signal of the frequency spectra tag using time domain analysis. The chapter also presents a brief introduction to the already reported literature on UWB IR techniques and its advantages. CST Microwave Studio software is used for the extraction of the structural and the antenna mode from the backscattered signal. Measurement has been conducted using the PNA E8362B network analyser by enabling the time domain option. A simple algorithm is proposed to extract the resonant information from the backscattered signal. Even in the highly noisy environment, analysis on time domain method enables the effective decoding of tag information up to a distance of 80cm.Tag information is also decoded when it is placed on the paper pack and metallic sheets.

5.1. Introduction to UWB IR

Based on the data encoding method, chipless RFID can be divided into two broad categories: Time Domain Reflectometry (TDR) and frequency spectra based chipless RFID. The data encoding capacity of frequency spectra based tags are high as compared with TDR based tag, except the SAW tags. In frequency domain based tag, the cost of RFID reader is high due to the use of expensive wide band application Voltage Controlled Oscillator (VCO). The time domain or TDR based reader employed Ultra Wide Band Impulse Radar (UWB-IR) technology, which uses short duration Gaussian pulse for the interrogation and hence it occupies a broad frequency band. Because of the duality between time and frequency domain, this UWB-IR reader can be used with both categories of tags [1]-[12].

UWB-IR technology is widely investigated for commercial applications since the Federal Communications Commission (FCC) released the legal usage of UWB in the range of 3.1–10.6 GHz. Compared with wide band frequency sweep system, UWB-IR employs a short pulse for transmission. Gaussian or higher order derivatives of the Gaussian pulse can be used as the excitation pules in the UWB IR system. Fig.5.1 (a) shows the different Gaussian pulses used for the UWB systems. It is worth mentioning that the pulse duration of the pulses is of the order of a few picoseconds. The corresponding frequency spectrum of the pulses is shown in Fig.5.1 (b). It is emphasized that Power consumption is much lower compared to the wideband frequency sweep reader because the system is active only during a short period of time. In addition, the UWB-RFID systems have many other advantages like low cost, high data rate, etc.
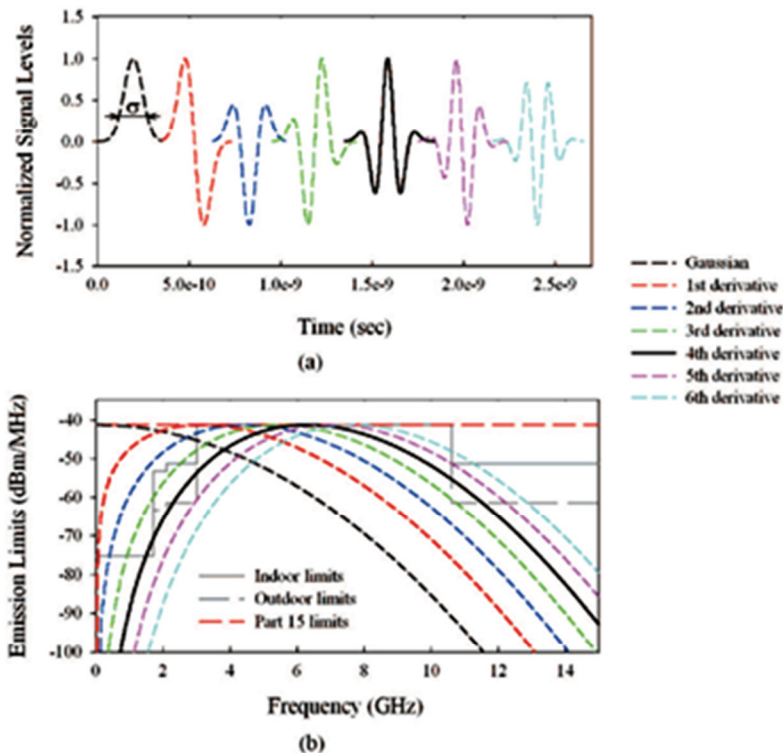
Figure 5.1 Gaussian pulse and its derivatives (a) waveforms in the time domain and (b) their power spectral densities

5.1.1. Introduction to UWB IR Based Time Domain Chipless Tag

UWB IR based time domain chipless tag consist of an UWB antenna and transmission line with different lengths, which may terminate with different loads [1]-[9]. As explained earlier, in time domain based tags are excited with RF pulse; there will be two types of backscattered signals, the structural mode and the antenna mode. The data is encoded by varying the time delay between structural mode and antenna mode. However, a long delay line is required to separate the antenna mode from the structural mode. The basic theory behind the working of time domain UWB RFID is given below [1].

1. Theoretically, the backscattered signal from a UWB antenna consists two parts, i.e., the structural mode and the antenna mode.

2. When the antenna is terminated with a conjugate matched load, i.e., $Z_l = Z^*_c$, then $\Gamma = 0$, which means there will be no antenna mode. (Γ is the reflection coefficient)

3. When the antenna is terminated with the open-circuited ($Z_l = \infty$, then $\Gamma = 1$) and short-circuited ($Z_l = 0$, then $\Gamma = -1$) loads, respectively, the antenna mode reaches its maximum amplitude; and

4. There is a 180^0 phase difference between the open-circuited and short-circuited cases.

Encoding is done by controlling the time interval between the UWB pulses of the structural and antenna modes, it is employing the pulse-position modulation to generate more identification (ID) codes. Antenna feeding line (transmission line) with different length is used for encoding data or the UWB antenna with different terminations can be employed. This is decoded by extracting the detected backscattered signals. Apart from matched-load, open-circuit, and short-circuit cases, other variable loads can also be used to achieve pulse amplitude modulation of the backscattered antenna mode. It means that antenna modes with different amplitude and pulse waveform can be obtained depending on the reflection coefficient (Γ).

Angel Ramos et al. [2] presented a tag which permits to integrate delays up to several nanoseconds enabling the ability to encode a large number of states. In addition, an RFID system based on integrated UWB impulse radar is proposed as a reader, achieving read ranges up to 1.80 meters [2]. Another RFID system uses a commercial low-power Novelda Nanoscale Impulse Radar (NVA6100 IC) as a reader [10]. The transmitter

sends a 1st order Gaussian pulse covering a frequency band of 3.1 – 5.6 GHz which complies with the FCC regulation. Fig.5.2 shows the block diagram of the proposed system consisting of the UWB IR with two UWB reader antennas and an open ended transmission line with the single UWB antenna at the RFID tag end. As shown in the block diagram, the reader antenna will receive three pulses, the direct coupled signal from the transmitter, structural and antenna mode. The transmission line on the tag is kept open to get maximum reflection in the antenna mode. Large delay (about 8ns) is achieved by using the combination of microstrip and coaxial transmission line. Fig.5.3 (a) depicted the fabricated model of time domain based chipless tag and (b) shows the backscattered structural and tag (antenna) mode signal from the tag with different reading distance. Compared with the standard credit card size (8.56 × 5.398cm^2), the proposed tag has a large dimension of 11x10cm^2 and a delay of 8ns is achieved by connecting additional open ended coaxial cable at the end of a microstrip transmission line.
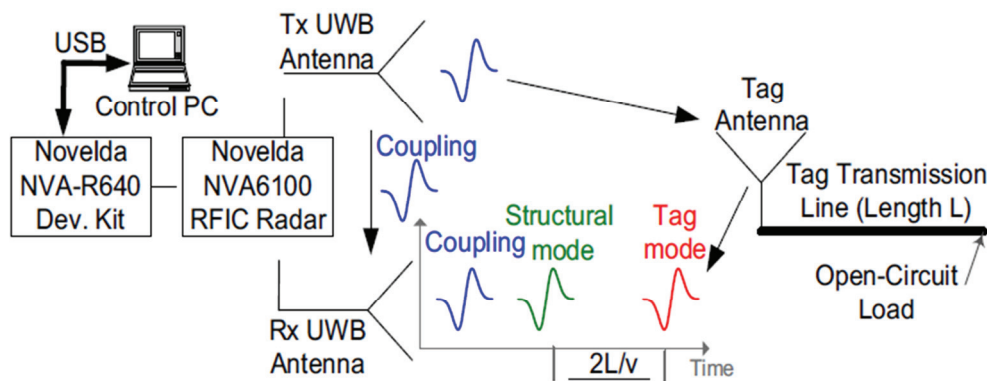
Figure 5.2 Block diagram of IR-UWB RFID system for time coded tag. Courtesy: A. Ramos. et. al. [2].
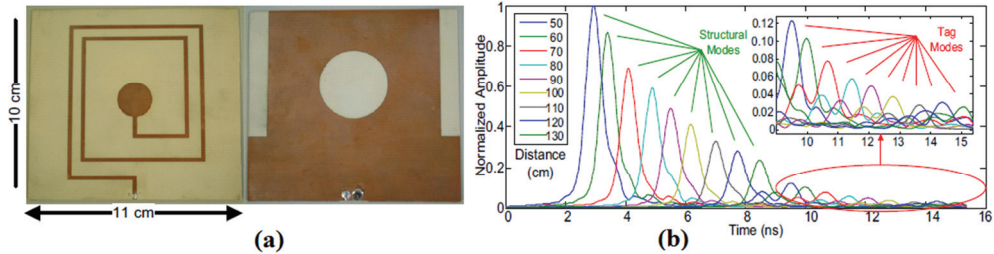
Figure 5.3 (a) RFID tag with UWB antenna and transmission line (top and bottom view), (b) Structural mode and antenna (tag) mode from the tag with different readable distances (cm). Courtesy: A. Ramos. et. al. [2].

Yizhu Shen et. al. presented another time coded chipless RFID system, based on IR-UWB technology [1]. This UWB-RFID system consists of a transmitter, receiver, two tapered slot reader antennas and several chipless tags. The RFID reader is covering the lower UWB frequency from 3GHz to 5GHz and transmitter integrated circuit generates high peak-to-peak amplitude of 6.6 V signals with short pulse duration of 1 ns. Due to the size limitations of the RFID tag, structural mode and antenna modes are combined in the backscattered response. The paper proposed a method to extract structural mode and antenna mode from these backscattered responses by post processing of chipless tags with different termination (load, open and short). Fig.5.4 (a) shows the RFID system with indigenously developed IR-UWB transmitter and receiver (using Digital Storage Oscilloscope) incorporating two tapped antennas. Fig.5.4 (b) shows the RFID tag with different terminations. Type A and B designs are having difference only in the length of CPW section, one with 37.6mm and the other having 41.6mm, respectively. Fig.5.5 (a) depicts the backscattered signal from the tag using UWB-IR pulse centred around 4.1GHz. Fig.5.5 (b) & (c) shows the extracted structural mode and antenna mode signals from the tag.
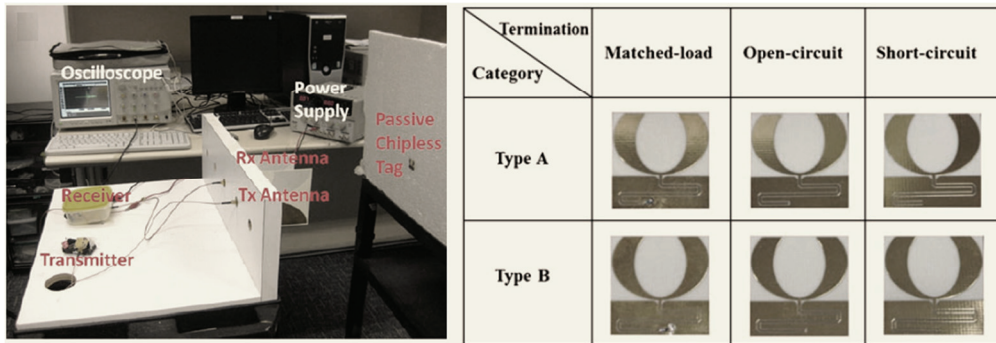
Figure 5.4 (a) Chipless UWB-RFID system prototype, (b) The chipless UWB-RFID tags. Courtesy: Y. Shen et.al. [1].
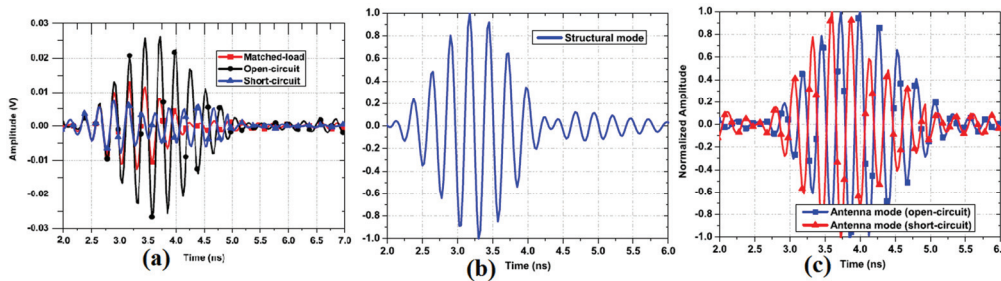
Figure 5.5 (a) Measured boresight backscattered pulses using 4.1 GHz transmitter, (b) Extracted Structural mode from (a), and (c) Extracted Antenna mode from (a). Courtesy: Y. Shen et.al. [1].

This method is useful to detecting the overlapped structural and antenna mode from the backscattered signals and simplifies the passive chipless tag designs. Other time domain based tag requires long transmission line, to generate enough time delay to separate the structural and the antenna mode, to distinguish the two peak positions, in order to use the pulse-position modulation. This creates design complexities and affects the compactness of the tag. Moreover, the signal amplitude of antenna mode is further reduced due to the attenuation offered by the long delay line, and hence the amplitude ratio of structural and antenna mode becomes worse. However, by employing this time-domain measurement method, simple and compact passive tags can be identified and localized, and more ID information can be embedded in the

backscattered signals. The system requires at least three tags with different termination for decoding structural mode and antenna mode. The tag also requires a large CPW (Coplanar Waveguide) transmission lines with different lengths to create small changes in the delay of antenna mode.

In TDR based tags, to separate the structural mode and antenna mode without overlap, it is necessary to add delay lines between discontinuities. The smallest delay depends on the emitted pulse width. Thus, for a pulse width of 1ns, a delay of more than 1ns should be created. To increase the number of time positions, it is necessary to increase the length of delay line or decrease the pulse width. There are some challenges in both cases (delay line and pulse width) [11]:

- The large number of delay line sections affects the compactness of the tag and each discontinuity in the delay line will generate a reflection of the interrogation pulse. Therefore signal amplitude decreases with delay line.

- Decreasing the pulse width is not easy to achieve in practice. The maximum bandwidth used without a license specified by the Federal Communication Commission in USA for UWB communications ranges between 3.1 GHz and 10.6 GHz. This defines a minimum pulse width of a few tens of picoseconds.

5.1.2. Introduction to Time Domain Analysis of Frequency Spectra Based Tag

It is shown in the literature that frequency signature based tags are capable of storing more information than TDR based tags. However, the operation of frequency signature based tags, with longer reading ranges,

requires proper orientation and calibration [12], [18] to remove interference due to clutter and antenna coupling. But TDR based tags do not face these constraints and operate at long ranges [1]-[4]. Time domain analysis is a useful method for extracting information contained in the backscattered interrogation signals. Due to the duality between time and frequency, time domain based reader can be used for decoding information from the frequency signature based tags [17]-[22]. By using time domain techniques on frequency signature based chipless tags, the benefits seen in TDR based chipless tags can be realized.

This chapter is elaborating the decoding methods of spectral information of tag using time domain analysis. Time domain tags fabricated on low permittivity substrate are still very far from reaching the surface coding density of SAW tags (96 bits) [15] or chipless tags with frequency coding techniques [11]–[22]. But there are number of advantages for choosing time domain based decoding method. They are

- Low cost UWB-IR's are commercially available.
- The Reader is active only for a short duration of time, hence low power requirement.
- Great freedom for the positioning of tag and readable up to several meters.
- They do not require the calibration tags or calibration ground planes, that are needed to be placed at the tag location in order to obtain reference measurements.

By using UWB IR based interrogation on frequency signature based chipless RFID tag and analysing its backscattered signal in the time domain, enables to combine the advantages of both types of chipless RFID systems.

Hence a low cost chipless RFID system operating at longer ranges with higher data capacity can be developed and the system is less sensitive to position, orientation, and calibration requirements.

R. Rezaiesarlak et. al. reported this category of tags based on Short-Time Matrix Pencil Method (STMPM) [18]. The bit information is encoded as complex natural resonant frequencies (poles and zeros) of the tag, which consist of a few notches on the elliptical dipole antenna. Fig.5.6 shows the geometry of the elliptical dipole based chipless tag, the backscattered signal from the tag. Sliding window method and STMPM are used to extract the complex resonant frequency from the backscattered signal. Damping factor of the pole and estimated poles along time are depicted in Fig.5.6 (c) and (d), respectively.
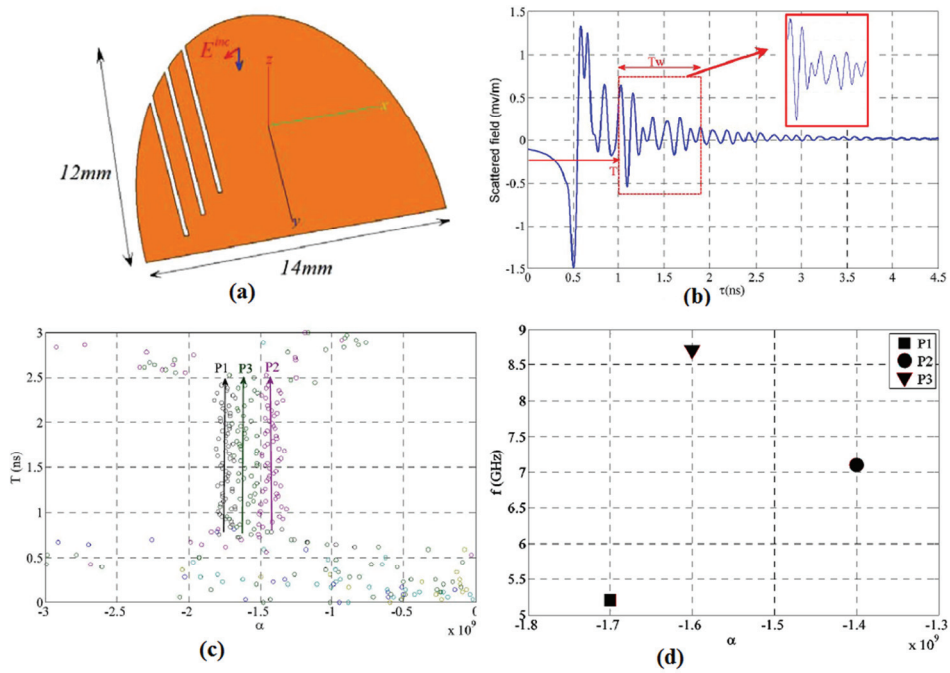
Figure 5.6 (a) Chipless RFID tag using an Elliptical dipole antenna with notches, (b) Simulated scattered signal from the tag, (c) Variation of real part (damping factor) of the poles with backscattered time and (d) Estimated dominant poles in the complex plane. Courtesy: R. Rezaiesarlak et.al. [18].

5.2. Motivation of the Work

The work presented in this chapter is motivated from the work of Prasanna Kalansuriya et. al. [20]. It explains the time domain analysis of backscattered signal from the frequency domain based tags. The resultant system is shown in Fig.5.7 (a). In this design, the 4 bit multiscatterer constitutes a slotted microstrip patch. The structural and antenna mode in the backscattered signal is shown in in Fig.5.7 (b). In this type of tag, antenna mode in the frequency domain is identified as a damped oscillation spread over long time compared to the structural mode. Staring time of the antenna mode is difficult to identify from the backscattered signal and it will begin immediately after the structural mode signal. The advantages of the time domain analysis of backscattered signal is that, the spectral information from any portion of the backscattered signal can be calculated using Fourier Transform.
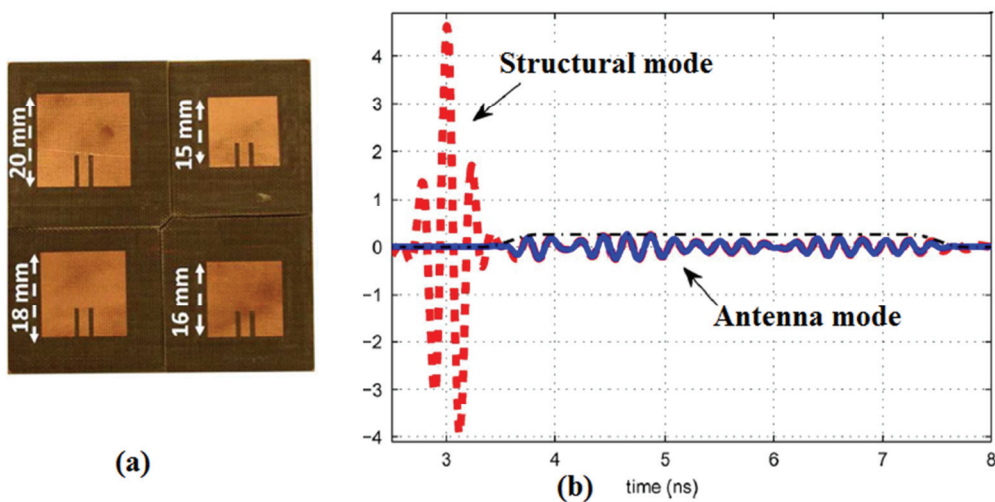
Figure 5.7 (a) Chipless RFID tag based on microstrip patch resonator and (b) backscattered signal from the tag in time domain. Courtesy:P. Kalansuriya et.al. [20].

5.3. UWB Impulse Radar Based Chipless RFID Reader

By exploiting the advantages of time-frequency duality, either frequency or time domain based chipless tags can be read using a UWB IR based system [27]-[31]. THE UWB IR modules available in the markets are in compliance with Federal Communications Commission (FCC) standards [30]. For instance, FCC defines a power spectral density (PSD) of -41.3 dBm for the frequency band of 3.1–10.6 GHz. Instead of using a frequency domain based Continuous Wave signal with extremely low power amplitude (to satisfy FCC standard), an UWB Impulse Radar based approach can be used. In such a case, a very low duty cycle having high power (several watts) and short pulse (having a width lower than 100 ps) can be generated and sent by the reader.

Gaussian pulse or its derivative can be used as the UWB source signal and UWB IR transmitter can be fabricated at a lower cost than FMCW transmitter [32]. The main difficulty is to design the receiver part of the reader. To obtain good accuracy in the reconstruction of the backscattered signal, sampling rate must be twice the highest frequency of the received signal (Nyquist criteria). This sampling rate is achievable with laboratory equipment, such as broadband oscilloscopes having sampling rate as large as 40 GS/s. For a real practical implementation of chipless technology, a compact and dedicated reader is required. A block diagram of the UWB IR based chipless RFID system is shown in Fig.5.8. In addition to the transmitter and receiver antennas, the reader is composed of two blocks: RF and digital sections. The most critical device is the wideband ADC because it requires a very high sampling rate to reconstruct the tag response.
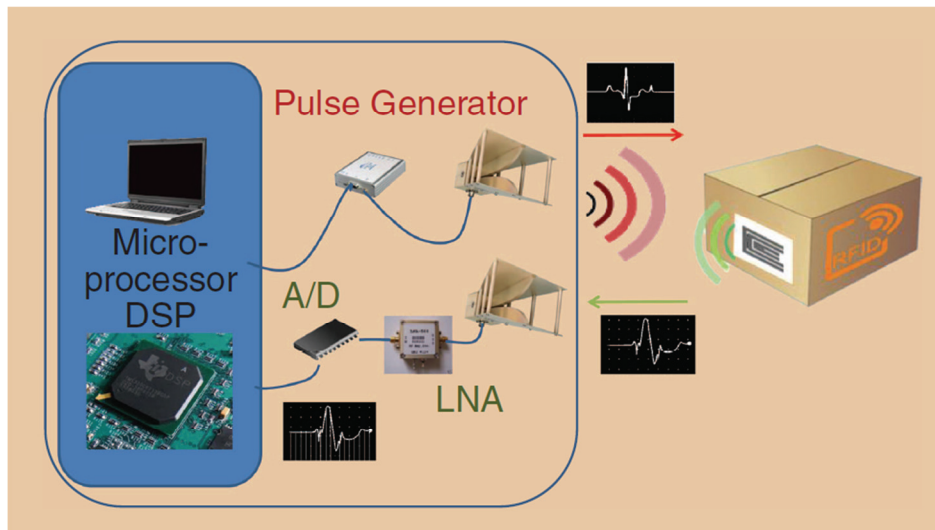
Figure 5.8 Temporal chipless RFID reader based on UWB interrogation signals. Courtesy: Smail Tedjini et. al. [33].

Wideband ADCs are too expensive to realize a chipless reader. Hence the principle of the equivalent- time sampling technique can be used to replace wideband ADC. The chipless tags can be considered as purely stationary devices due to the short time period of the input pulse. With this assumption, it is possible to reconstruct the entire signal from the collection of different backscattered signal. Hence, it is possible to realise a reader based an architecture using equivalent time sampling [34]. In this case, the high sampling rate ADC can be replaced with a moderate (in the order of a few megahertz) one. A delay generator capable of producing short delays (tens of picoseconds) is required for enabling the sampling circuit during the assigned time slots of backscattered signals. Fig.5.9 provides the block diagram of a chipless reader based on equivalent time sampling.
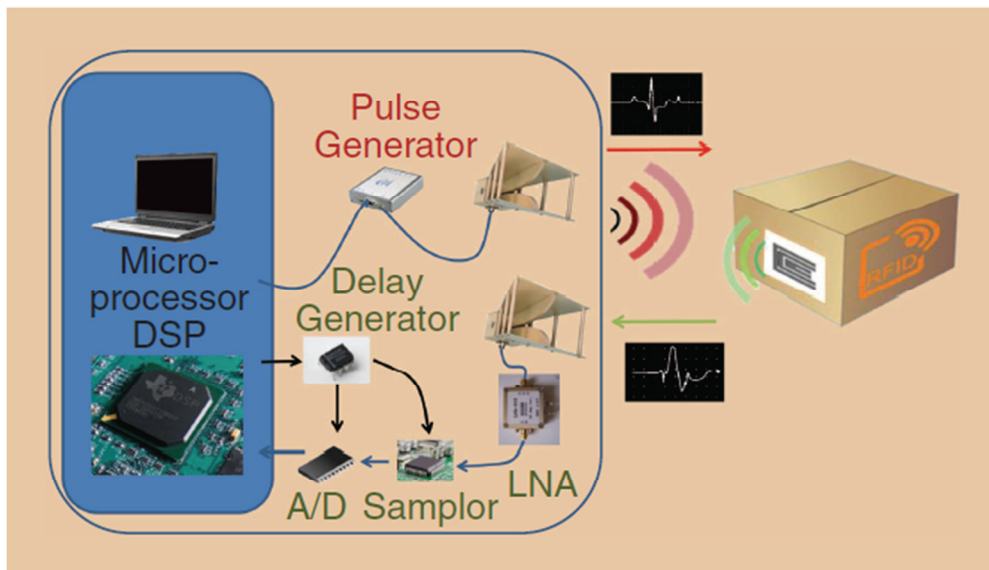
Figure 5.9 Block diagram of a chipless reader based on equivalent time sampling. Courtesy: Smail Tedjini et. al. [33].

Other approaches are also possible by using commercially available UWB IR which is commonly used for localization purposes, particularly through obstacles. These devices can be reused as chipless readers. For example, the Novelda radar has been used to read chipless tags [2],[29]. Like the equivalent-time sampling approach, averaging operations over hundreds of measurements can be used to increase the signal to noise ratio of the radar [10]. The Novelda radar is a complete impulse radar transceiver integrated on a single chip (shown in Fig.5.10). A development kit is also available, allowing the control of the RF front end by a computer, where the localization application can be implemented. Sampling rates of around 35 GS/s are possible, with a bandwidth from 0.85GHz to 9.6GHz. The radar is designed for FCC compliance and relatively low cost, which makes it suitable for chipless applications.

Figure 5.10 Novelda Nanoscale Impulse Radar. Courtesy: Novelda. [10].

5.4. System Model of UWB IR Based Chipless RFID System

The system model presented in [20] is also valid for our design. The RFID reader shown in Fig.5.11 uses a single antenna configuration for transmission and reception of the interrogation signal. The single antenna configuration provides a wider degree of freedom in orienting the tag with respect to the reader. The RFID tag consists of number of SIRs, resonating at distinct frequencies. An UWB pulse x(t) is used for interrogating the chipless RFID tag. In a noise free environment, the total received signal *y(t)* consists of three components
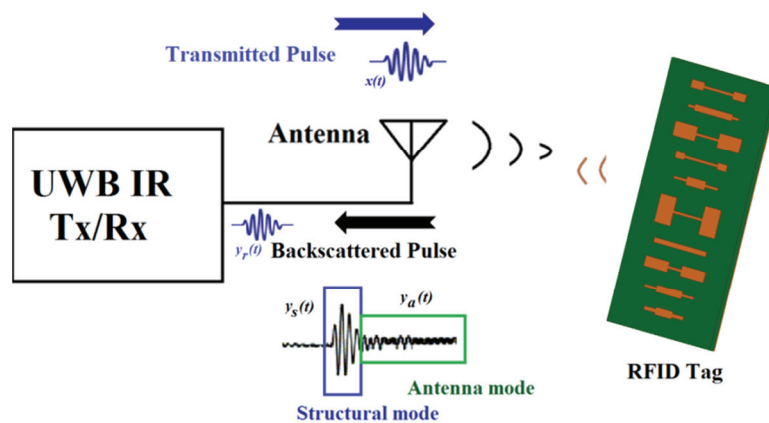
Figure 5.11 Block diagram of UWB IR based chipless RFID system

$$y(t) = y_r(t) + y_s(t) + y_a(t) \tag{5.1}$$

The largest and the first received component $y_r(t)$ is the reflection of the transmit pulse due to the return loss of the antenna. The second component received $y_s(t)$ is the structural mode from the backscatterer. This is followed by the antenna mode from the backscatterer $y_a(t)$, which is the weakest and the last component to be received. Let $S_{11}(f)$ be the return loss of the antenna without chipless tag, which is measured in frequency domain. From the definition of the return loss, the rejected portion of the pulse input into the antenna $(y_r(t))$ can be written as

$$y_r(t) = f^{-1}\{S_{11}(f).X(f)\} \tag{5.2}$$

where $f^{-1}\{.\}$ denotes the inverse Fourier transform. Lower case letters are used to denote time-domain signals and the upper case letters to denote the respective frequency-domain signal. In a practical measurement scenario, backscattered signal S_{11} without tag consist of antenna reflected signal $y_r(t)$, reflection from surrounding objects $(y_o(t))$ and white noise $(y_n(t))$. Therefore backscattered signal without tag $(y_1(t))$ can be expressed as,

$$y_1(t) = y_r(t) + y_O(t) + y_n(t) \tag{5.3}$$

While placing RFID tag in front of the antenna S_{11} is modified, which consist of reflection from the antenna $(y_r(t))$, reflection from the surrounding objects, noise and backscattered signal from the RFID tag $(y_s(t)$ and $y_a(t))$. Equation (5.1) in frequency domain can be written as

$$y(t) = f^{-1}\{S_{11}^{loaded}(f).X(f)\} \tag{5.4}$$

Total received signal $y(t)$ in a practical scenario can be expressed in time domain as

$$y(t) = y_r(t) + y_O(t) + y_n{'}(t) + y_s(t) + y_a(t) \qquad (5.5)$$

where $y_n{'}(t)$ is white noise signal received at another instance of time. By subtracting equation (5.4) from (5.5), the effect of reader antenna and signal from the stationary objects can be eliminated. The calibrated signal $y_C(t)$ can be expressed as

$$y_C(t) = y_s(t) + y_a(t) + y_n{''}(t) \qquad (5.6)$$

where $y_n{''}(t)$ is the white noise signal contributing in the noise floor after the calibration. Same process can be done in the frequency domain by subtracting two S_{11} data represented below.

$$y_C(t) = f^{-1}\{[S_{11}^{loaded}(f) - S_{11}(f)].X(f)\} \qquad (5.7)$$

5.5. UWB IR Based Interrogation using Numerical Methods

Transient analysis of RFID tag is carried out using CST Microwave studio simulation software. A plane wave polarised along X axis used as the interrogation signal. Fig.5.12 shows the simulation setup in the CST microwave studio with an RFID tag having two Stepped Impedance Resonators (SIRs). Electric field probe oriented along the X-direction is used for capturing the scattered field and it is placed at 10cm away from the tag. Simulation is also performed with different distances. The pointing vector 'K' in Fig.5.12 denotes the direction of propagation of the transmitted signal. The resonant frequencies of the SIRs (SIR-I and II) are designed to be 4 GHz and 5GHz, respectively. The design parameters and structural dimensions of the SIRs are given in Table 1.
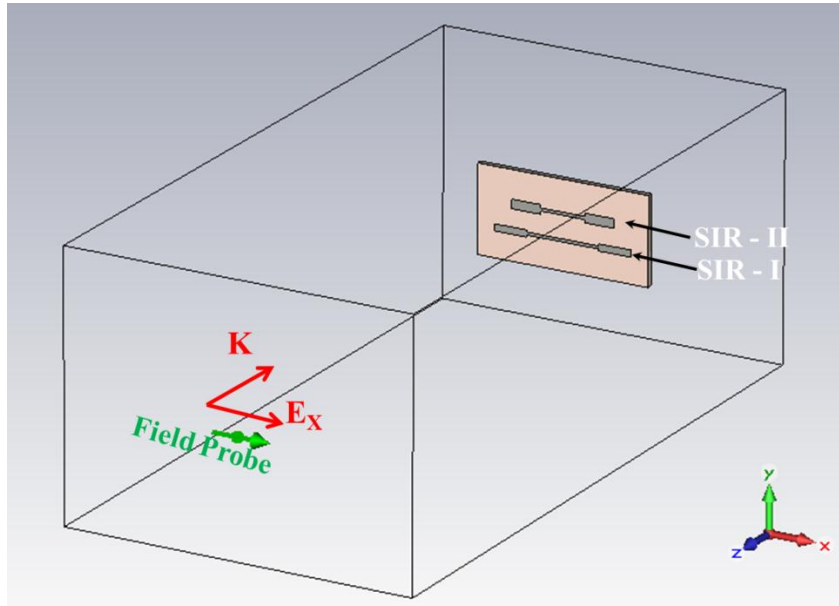
Figure 5.12 Simulation setup used in CST for time domain analysis of frequency spectra based RFID tag with two SIR. The tag is placed at 10 cm away from the Electric (Ex) probe.

Table 1: Structural Dimension of SIR used in Fig.5.12 G = 3mm, ε_r = 2.2, h = 1mm

SIR	K	α	$2L_1$ (mm)	L'_2 (mm)	W_1 (mm)	W_2 (mm)	Designed f_0(GHz)	Simulated f_0(GHz)
I	0.7	0.5	12.65	5.72	0.5	1.17	4	3.92
II	0.6	0.6	7.71	5.09	0.5	1.57	5	4.91

The transmitted UWB pulse x(t) is a modulated Gaussian pulse and can be expressed as

$$x(t) = A_0 \cos(2\pi f_c t) \exp\left(-\frac{(t-\tau)^2}{2\sigma^2}\right) \tag{5.8}$$

where τ (ns) is the time index for the peak value of pulse and σ (ns) is the variance. A_0 and f_C (Hz) are, respe ctively, the amplitude and the frequency of the sinusoidal carrier signal. The excitation pulse along with the normalized frequency spectrum is depicted in Fig.5.13 (a). The time duration of the

transmitted signal is in the order of 1-2 ns. Fig.5.13 (b), shows the normalized frequency spectrum of the UWB pulse. It is seen that the frequency spectrum is centred around 5.5GHz.
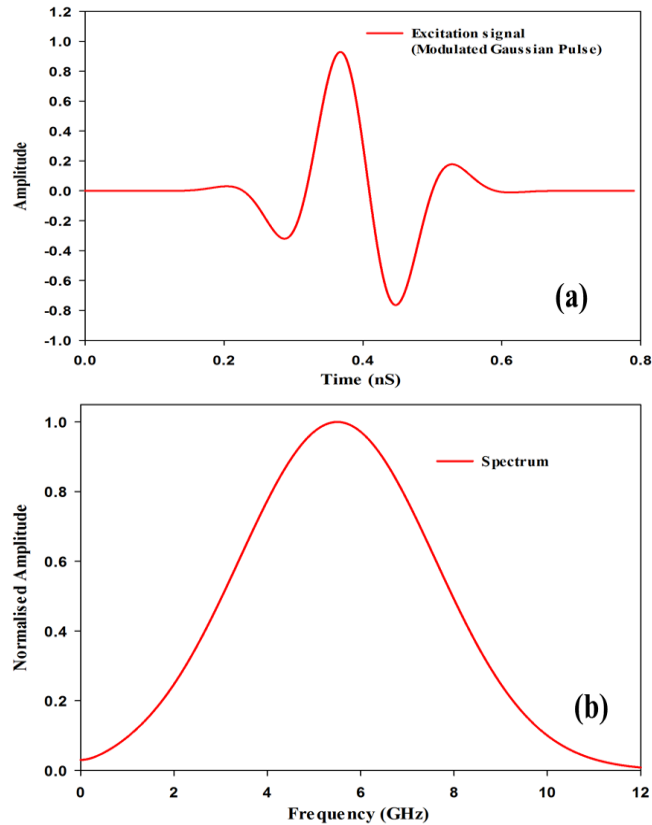
Figure 5.13 (a) Modulated Gaussian excitation pulse and (b) Normalised amplitude spectrum of the excitation pulse

The backscattered signal from the tag consists of structural and antenna mode signals. Structural mode signal is the delayed response of a transmitted pulse due to the distance between tag and reader. The overall time domain response from the tag is expressed as

$$y_C(t) = A_s \cos(2\pi f_c t) \exp\left[-\frac{(t-\tau-\tau_{tag})}{2\sigma^2}\right] + \sum_{n=1}^{N} A_n \exp(a_n + j\omega_n t) + n(t) \quad (5.9)$$

In this expression, the tag's resonance information is represented as the summation of exponentially decaying signals and the number of exponentials depends on the number of resonances present in the tag. A_n is the complex amplitude and $(a_n + j\omega_n t)$ are poles corresponding to the predefined resonant frequencies [18], [20]. τ_{tag} is the delay involved in the tag's backscattering and depends on the distance between the tag and the transceiver.

Fig.5.14 (a) shows the signal picked up by the E field probe along X direction at a distance of 10cm away from the tag. As seen in the Fig.5.12, probe is placed in front of the source, hence transmitted pulse towards the tag will also picked by the probe and it shown in the time domain signal with higher amplitude. Shape and amplitude level of the forward signal is same of that of the transmitted pulse. Second part of the signal is due to the backscattering from the RFID tag. Magnified part of the structural and the antenna mode are depicted in Fig.5.14 (b). Backscattering from the signal is starts with structural mode and it is shown in Fig.5.14 (b). Except the amplitude, shape of the structural mode is also same as that of the input pulse. The information carrying part (Antenna mode) is spread across the large time after the structural mode. The time span of the antenna mode depends on the quality factor of the resonators, ie., time span will be large for high Q structure [18].
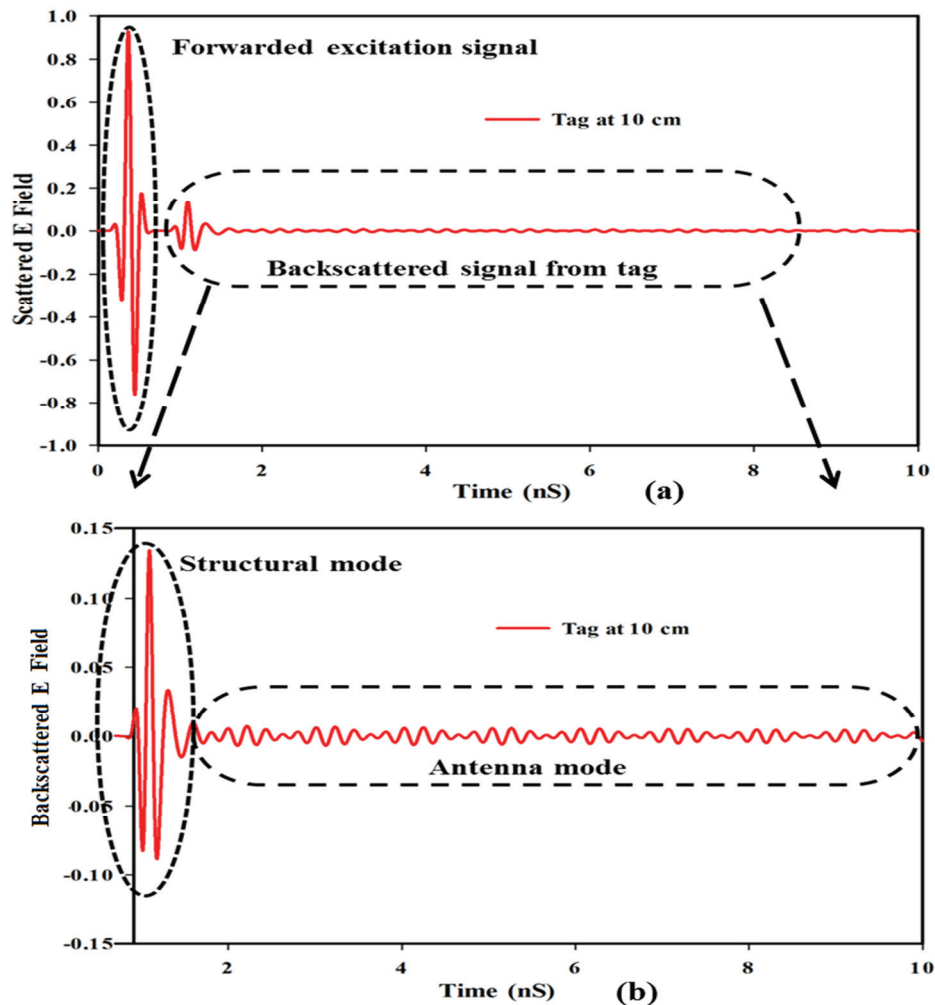
Figure 5.14 Scattered signal from the tag (a) Signal picked by probe (b) backscattered signal from the tag

5.5.1. Frequency Spectra of Structural and Antenna Modes

The frequency spectral response of the time domain signal is separately analysed in this section, by taking the Fourier Transform of the selected portion of the backscattered signal. The first higher amplitude signal is the forward excitation signal from the source and it is picked up by the probe while propagating towards the RFID tag; hence frequency spectrum

will be same as that of the transmitted pulse. Next received signal is the structural mode signal due to the shape and size of metallic structure in the tag. A normalised frequency spectrum of structural mode is shown in Fig.5.15. The structural mode does not contain any information about the resonant characteristics of the tag and its amplitude envelope is same as that of the transmitted pulse. Signal after the structural mode can be referred to as Antenna mode signal and its frequency spectrum is also depicted in Fig.5.15. Spectral content in the antenna mode is extracted by taking the FFT of a backscattered signal ranging from 1.5ns to 10ns. It is clear from the figure that; the information about the resonant property of the tag is stored in the antenna mode and is spread in time. The simulated resonant frequencies of the resonators are found to be at 3.93GHz and 4.92GHz. Amplitude peak levels are different for both the resonances due to the variation in the power spectrum of transmitted pulse [20].
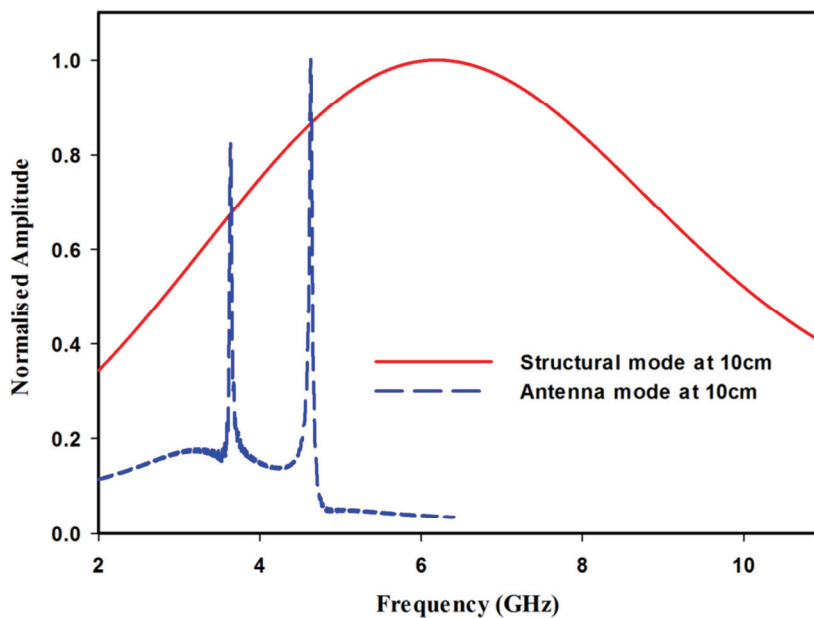
Figure 5.15 Normalised frequency spectrum of structural mode and antenna mode

Fig.5.16 shows the simulated frequency response of the tag using frequency domain method and time domain method. Exact resonant frequency can be identified from both the methods. From the figure it can be concluded that, in simulation, backscattered signal in the frequency domain analysis is the combination of forward excitation signal, structural mode and antenna mode. But in actual measurement, backscattered signal in the frequency domains contains structural mode, antenna mode and noises. Depending on the interference between these signals, resonant can be identified as either dip or peak in the backscattered signal. Time domain analysis enables to extract the information contained part from the backscattered signal and also possible to remove unwanted portions.
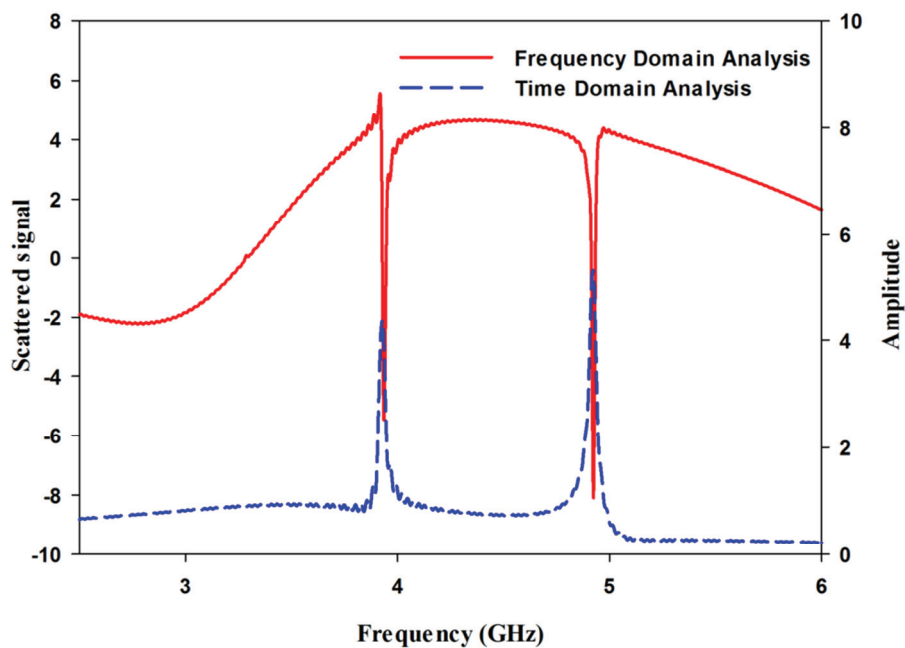
Figure 5.16 Frequency spectral signature of the tag using time and frequency domain methods

5.5.2. RFID Tag Localisation Using Time Domain Method

Simulation is also carried out by placing the tags at different positions from the source. The scattered signal in the time domain is plotted in Fig.5.17 (a). Even though there is no information stored in the structural mode signal, it can be used for tag localisation [23], ie., the position of the RFID tag can be identified by analysing backscattered structural mode. From the figure, it is clear that the structural mode occurring at different time instants depends on the distance between the tag and the source. The time gap between the forwarded excitation signal and the structural mode signal is the round trip time taken by the RF signal. By considering the round trip time, one can easily calculate the distance between the probe and tag (R) by using equation (5.10).

$$R = \frac{c.V_f.t}{2} \tag{5.10}$$

where c is the speed of light, V_f is the velocity factor in the medium (for air V_f = 1) and t is the round trip time. Fig.5.17(a) shows the t_1, t_2 and t_3 are the time taken by the RF signal to travel from E field probe to RFID tag and travel back to E field probe. The tag is simulated with 3 different distances 10cm, 20cm and 50cm, and the corresponding time delays are 0.7397ns, 1.3961ns and 3.418ns, respectively. From the above equation (5.10), one can easily localize the objects. The amplitude of the antenna mode signal at different distances are plotted in Fig.5.17 (b). It can be seen that strength of the antenna mode is also decreasing with respect to the distance between the tag and the probe.

Figure 5.17 (a) time domain signal for RFID tag at different distances (b) Frequency spectrum of the antenna mode at different distances.

5.5.3. Time Vs Frequency Response of the Backscattered Signal

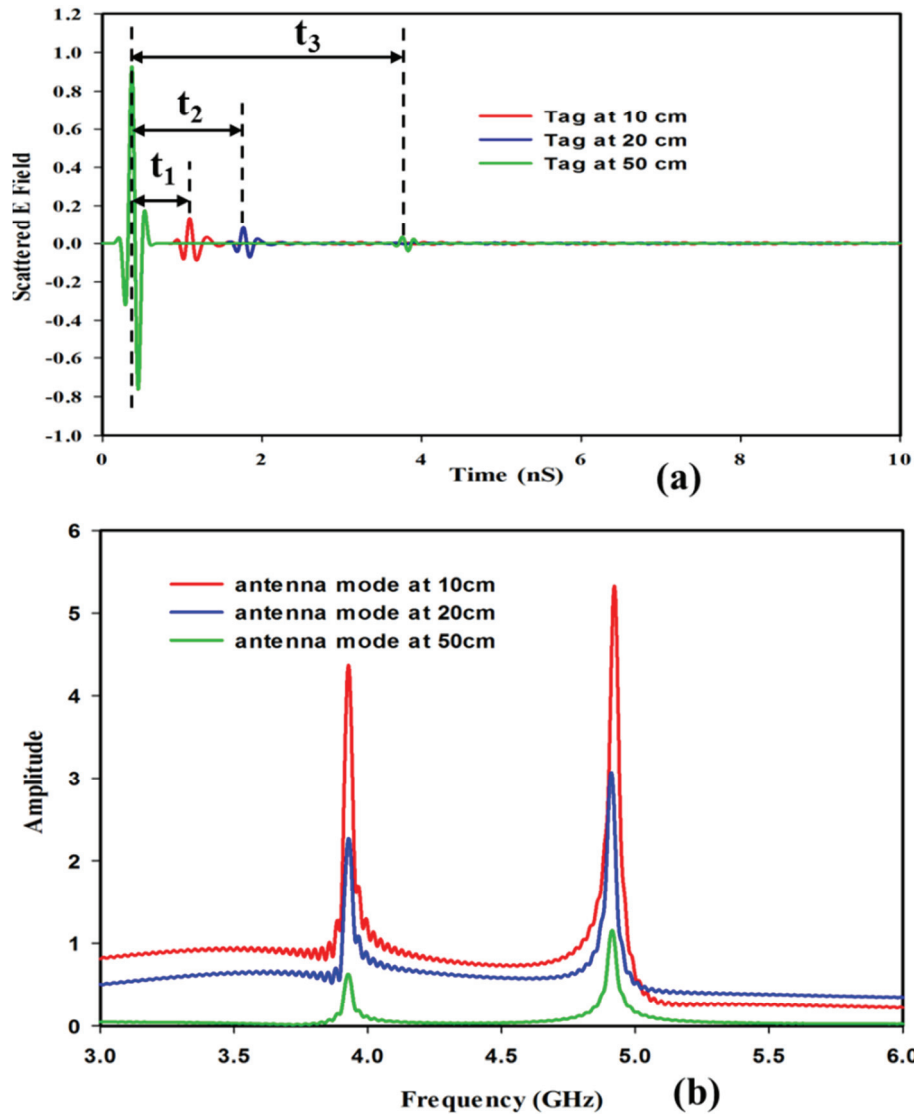Time domain signal analysis is effectively utilised in this chapter for the spectral extraction of frequency domain based RFID tags. The selected portion of time domain signal is separately analysed using the Fast Fourier

Transform (FFT) for getting frequency response. Identification of an exact time instance and duration of the structural and the antenna modes are difficult to identify from the above results. Hence, we have adopted another method for the identification of spectral content in the backscattered signal. The Short Time Pencil Method for chipless RFID detection application [18] introduced by R Rezaiesarlak, Manteghi et al. has demonstrated a different mothed for the detection of early time response (structural mode) and early time response (antenna mode) by calculating complex resonance frequency from the backscattered signal. From the frequency Vs time plot of backscattered signal, authors are able to identify different modes in the backscattered signal.

In this chapter, structural mode and antenna modes are identified by taking the Fourier Transform of the backscattered signal. FFT of the backscattered signal shown in Fig.5.18 (a) is plotted in Fig.5.18 (b). The tag is placed at a distance of 50 cm away from the plane wave source as explained earlier. Two parameters are used to determine the accuracy of spectral contents. One is the Resolution time and second is the Window size. In Fig.5.18 (b) spectral analysis of the backscattered signal is taken every 0.05ns with a time window of 0.01ns. Forwarded transmitted pulse and structural mode exist only for a few nanoseconds and it depends on the width of the transmitted pulse. In order to detect these signals from the backscattered data, resolution time and window size should be less than the time period of the transmitted pulse. Forwarded transmitted pulse and structural mode signals are visible with a Resolution time and Window size of 0.5ns and 0.1ns, respectively (Fig.5.18 (b)).
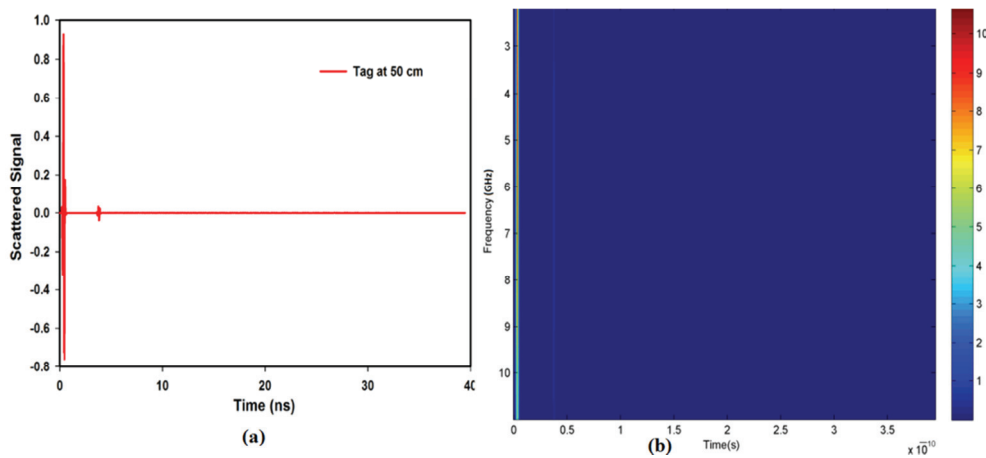
Figure 5.18 (a) Backscattered signal from the tag (CST Simulation) and (b) Spectral content in the backscattered signal when Resolution time = 0.05ns and Window size =0.1ns.

Fig.5.19 shows the backscattered signal after removing forwarded transmitted pulse, ie., remaining signal contains only the structural and antenna mode. Smaller values in the Resolution time and Window size will give an accurate time instance of structural mode signal. To extract the antenna mode, Resolution time needs to be small as possible and Window size needs to be large in time. To identify the antenna mode, which contain spectral components of the RFID tag, the backscattered signal shown in Fig.5.19 is processed with different Window size while keeping Resolution time at 0.05ns. From the figure it is clear that, while increasing the Window size, antenna mode becoming clearer with large spectral amplitude. It is also clear that; antenna mode is starting at a time instance of 3.82ns. Power spectral density variation with time will give the presence (starting and ending) of antenna mode with time. It is seen that the antenna mode is vanishing at exactly 37.5ns. Time duration of antenna mode depends on the power of the incident wave and on the quality factor of the resonator.
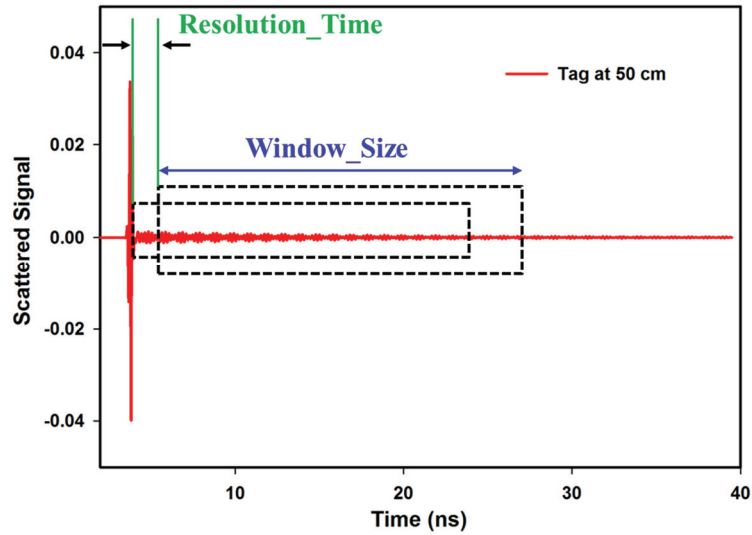
Figure 5.19 Simulated backscattered time domain signal with structural and antenna mode.
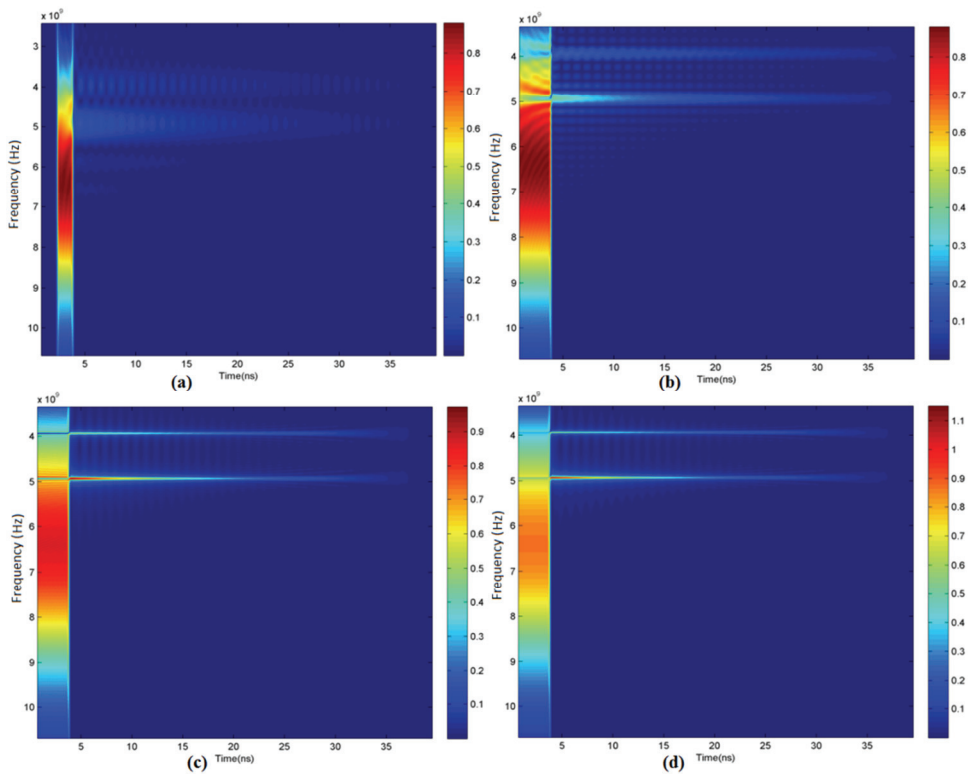
Figure 5.20 2D Power spectral image of antenna mode extracted with different Window size (a) 1.5ns, (b) 5ns, (c) 25ns and (d) 35ns. Resolution time = 0.05ns.

Three Dimensional (3D) power spectral density of the backscattered signal is plotted in Fig.5.21. From the figure, the power spectral variation in the backscattered signal can be easily visualized. The strength of the structural mode signal along the frequency is matching with the transmitted pulse.
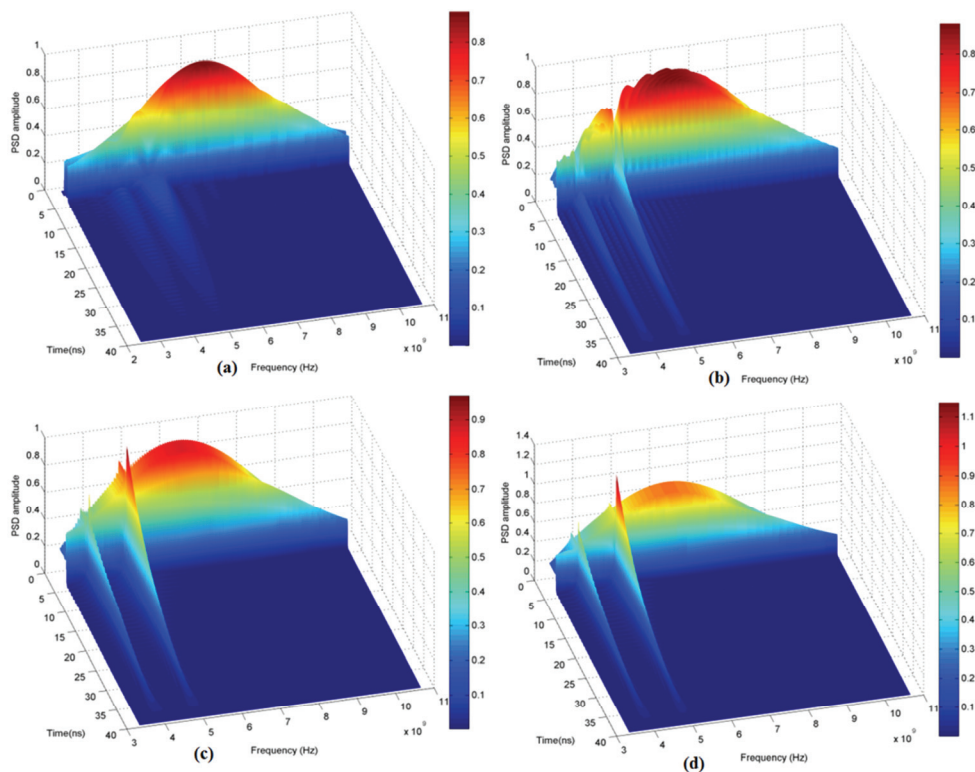
Figure 5.21 3D Power spectral image of antenna mode extracted with different Window size (a) 1.5ns, (b) 5ns, (c) 25ns and (d) 35ns, Resolution time = 0.05ns.

5.6. Time Domain Analysis of SIR Based Tags

Chipless RFID tag consists of 10 SIR, explained in chapter 3 is selected for the time domain analysis. PNA E8362B network analyser with time domain option is used as the UWR IR reader. Rectangular window in the analyser is opted for the measurement, to make sure that the transmitted

power is same for the entire frequency band. The backscattered time domain signal from the RFID tag positioned at 30 cm is shown in Fig.5.22. In this chapter all the measurements were taken outside the anechoic chamber, ie., in a practical environment and also disable the averaging function in the network analyser. Therefore backscattered signal consists of structural mode, antenna mode and white noises. The backscattered signal measured in the frequency domain at 30cm distance is plotted in Fig.5.23. Due to reflections from the surroundings, backscattered signals are more susceptible to noise.
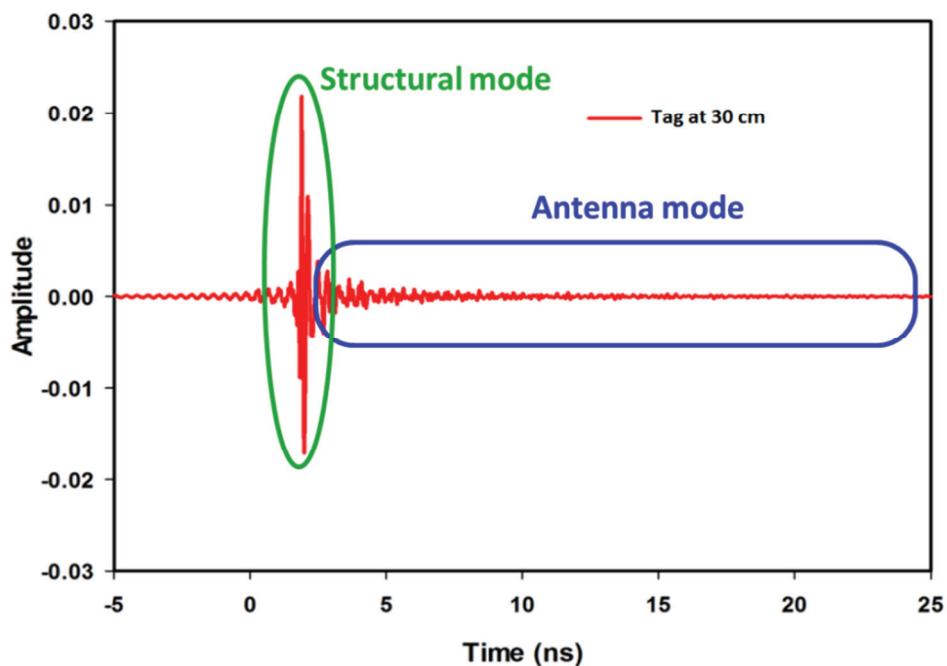
Figure 5. 22 Measured backscattered time domain signal from ten SIR based tag
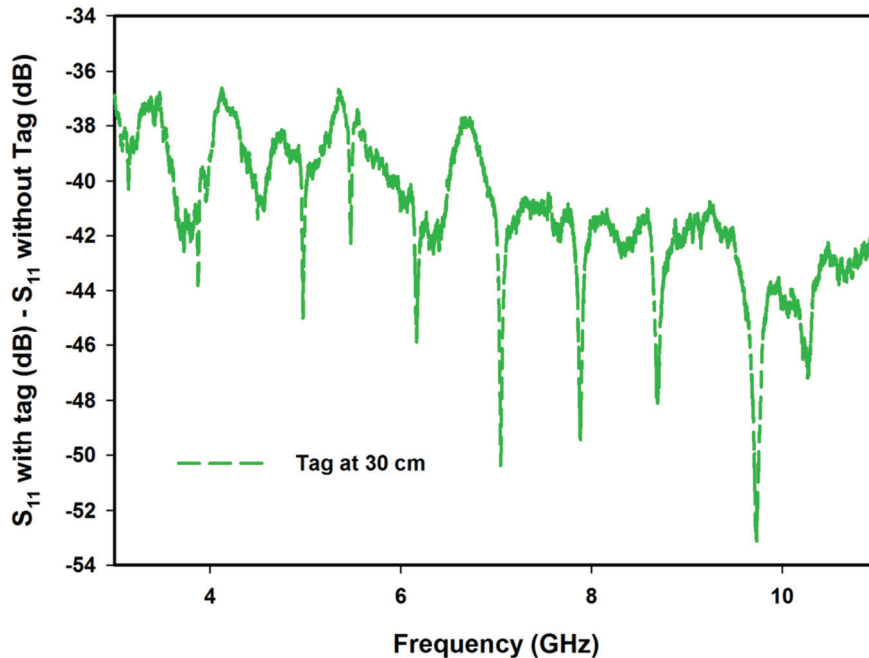
Figure 5.23 Backscattered frequency domain signal from the tag measured outside the chamber with zero averaging

The basic idea in the time domain analysis is to move a time window with a proper time duration (Window size) of the entire signal by small time steps (Resolution time) and apply FFT on each time window. Identifying the structural and antenna mode is the primary goal in this analysis. From the above analysis it is clear that, peak amplitude in the backscattered signal is due to the structural mode and its pulse width is same as that of the transmitted signal. For a known value of transmitted pulse width, it is possible to identify the starting position of antenna mode. By taking the FFT of antenna mode with proper time window, all the frequency components of the tag can be extracted. Fig.5.24 shows the frequency spectrum of the antenna mode at three different tag positions (20cm, 30cm and 50cm). It is interesting to note that each

resonant frequency component can be easily identified from the backscattered signal.
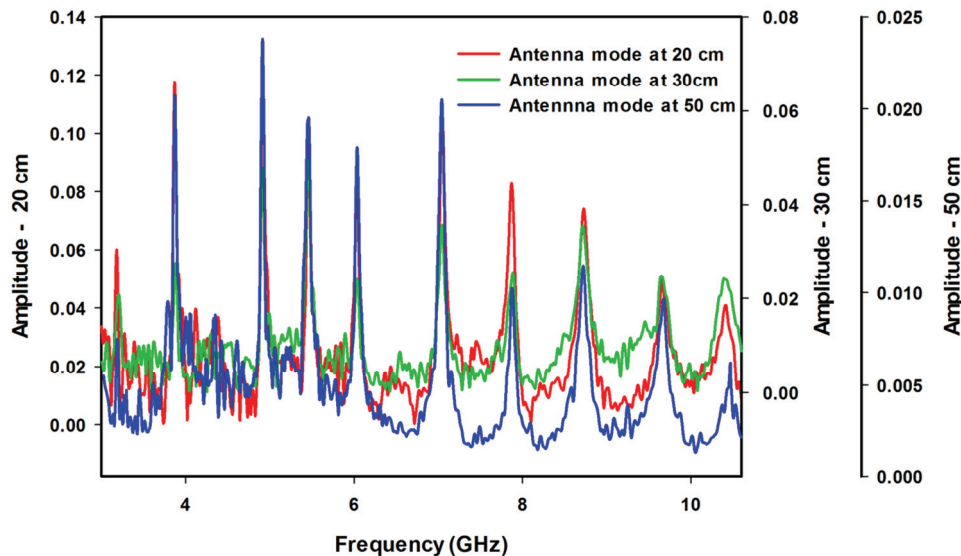
Figure 5.24 Frequency spectrum of antenna modes at different tag positions

Frequency spectral analysis on entire backscattered time domain signal is also conducted. As explained in the above section, exact location of the structural mode is identified by choosing small value of Resolution time with Window size, about 0.05ns and 0.2ns, respectively. Fig.5.25 shows measured 2D power spectral density of the backscattered signal against time. IT is noted that the positon of structural mode is found to be at 1.38ns while placing the tag at 30cm away from the Reader antenna.
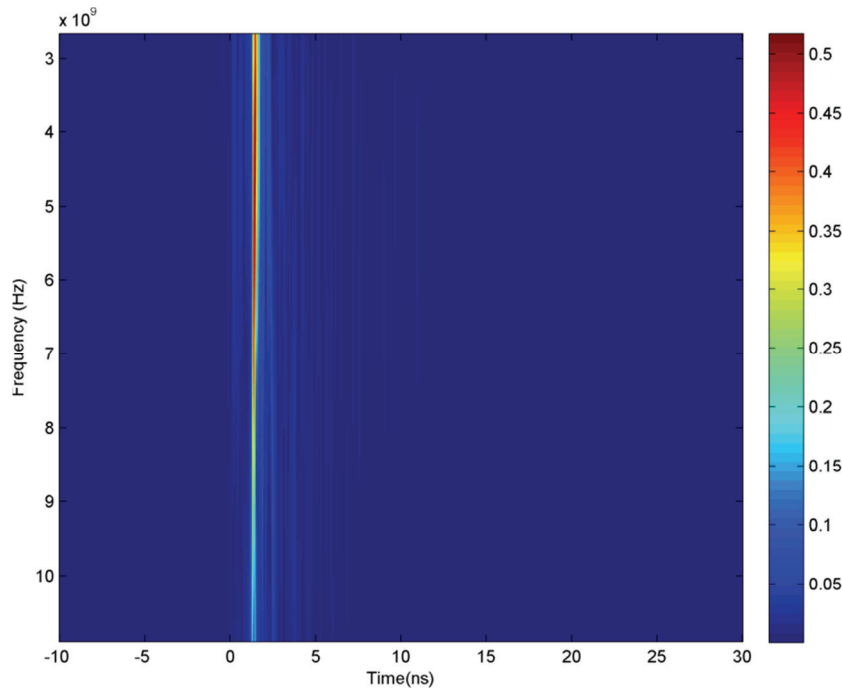
Figure 5.25 Measured 2D Spectral content of backscattered signal when Resolution time = 0.05ns and Window_Size = 0.2ns.

Another study on the effect of Resolution time and Window size are carried out over the measured backscattered signal. Fig.5.26 shows the spectral density of the backscattered signal with different Resolution time. Here it is clear that, reducing the Resolution time is more accurate for the detection of antenna mode and existence of its frequency contents can be identified with a cost of increased processing time. Window sizes in all cases are set to be at 12.5ns.
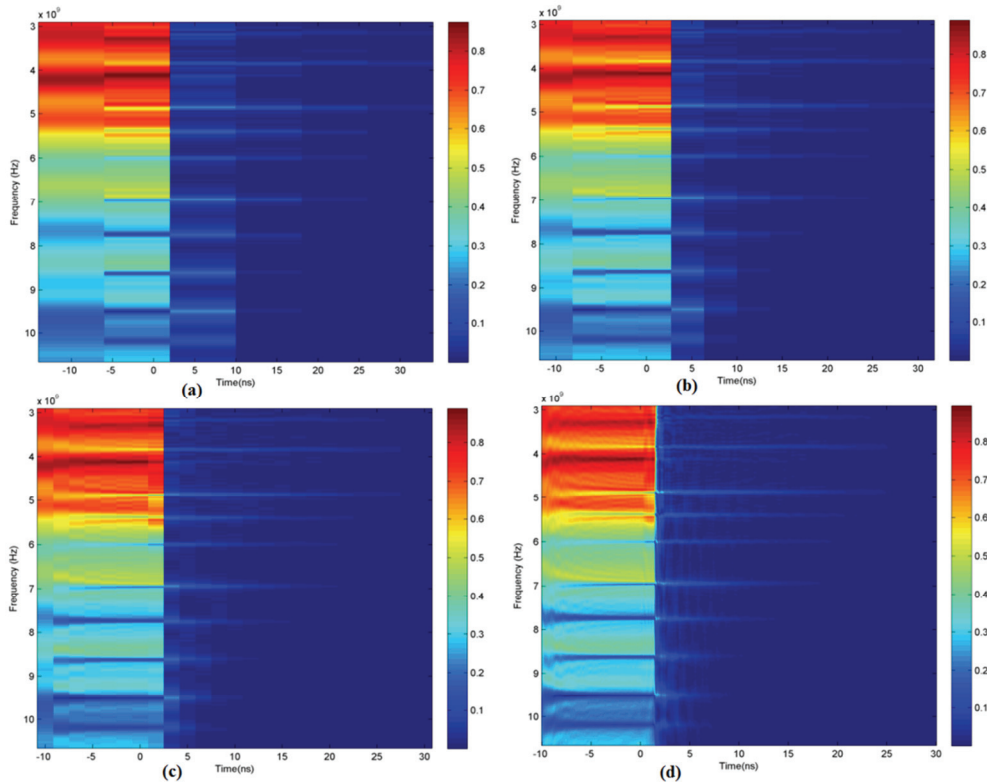
Figure 5.26 Measured 2D Spectral content of the backscattered signal with different Resolution time. (a) 6.3ns (b) 3.15ns (c) 1.5ns and (d) 0.06ns, in all case Window_Size = 12.5ns.

As explained earlier, exact beginning point of the antenna mode can be identified with smaller value of Resolution time and higher value of Window size. Another study on Window size variation is performed and its frequency spectrum along the backscattered time is shown in Fig.5.28. The starting time of the antenna mode is found to be at 1.49ns. From the figure it is clear that, while increasing the Window size, the strength of the frequency components in the antenna mode is increasing and it is converging towards the actual value. All the ten resonant frequencies of the SIRs are clearly visible from the backscattered signal.
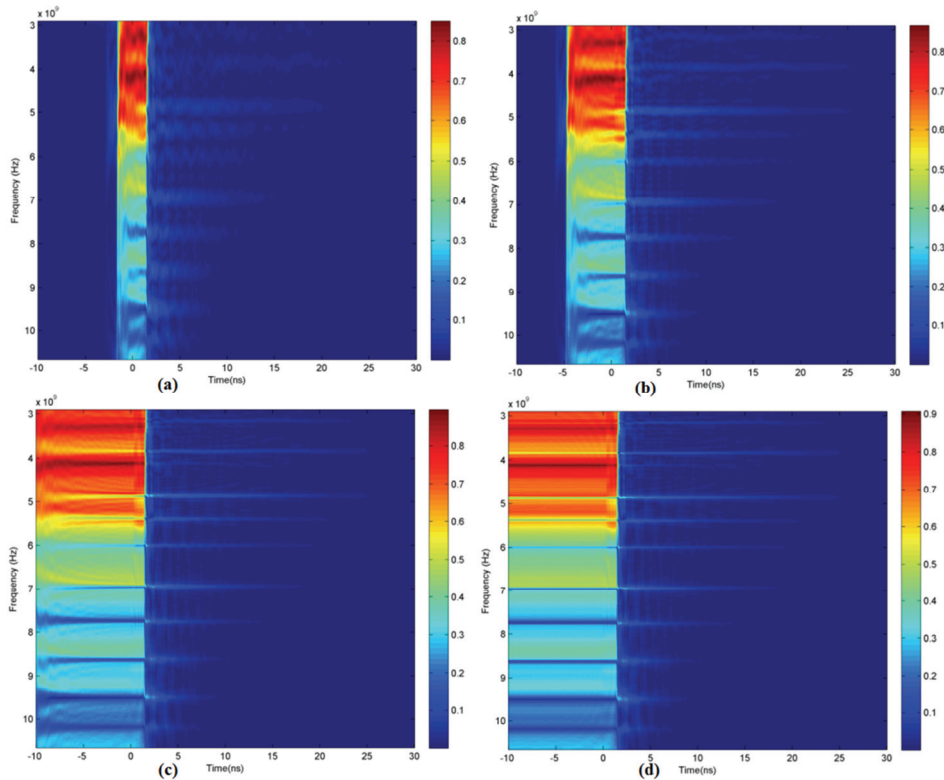
Figure 5.27 Measured 2D Spectral content of the backscattered signal with Window Size. (a) 3ns (b) 6.3ns (c) 12.6ns and (d) 25ns, in all cases Resolution time is set to 0.06ns.

Even though all the resonances can be identified from these analysis, the computational cost is found to be high. To reduce this, another variable called 'Delay' is introduced in the analysis. Delay variable contains a time value corresponding to the peak value of the structural mode. As seen in Fig.5.22 peak amplitude of the backscattered signal is due to the structural mode and it does not contain any frequency component of the RFID tag. The signal appearing before the peak amplitude can be removed from the processing of backscattered signal. It is also clear that, peak amplitude of the structural mode corresponds to centre of the transmitted pulse.

2D and 3D power spectral density of the backscattered signal with different Window size is plotted in Fig.5.28 and Fig.5.29, respectively. Here the 'Delay' variable is loaded with a time instance of the peak amplitude in the time domain signal. The peak amplitude of the backscattered signal is found to be at 1.43ns (Fig.5.22). It is noted that processed signal containing a portion of structural mode signal. Visibility of antenna mode is degraded due to the strength of the structural mode and it is clear from the 3D pattern shown in Fig.5.29.
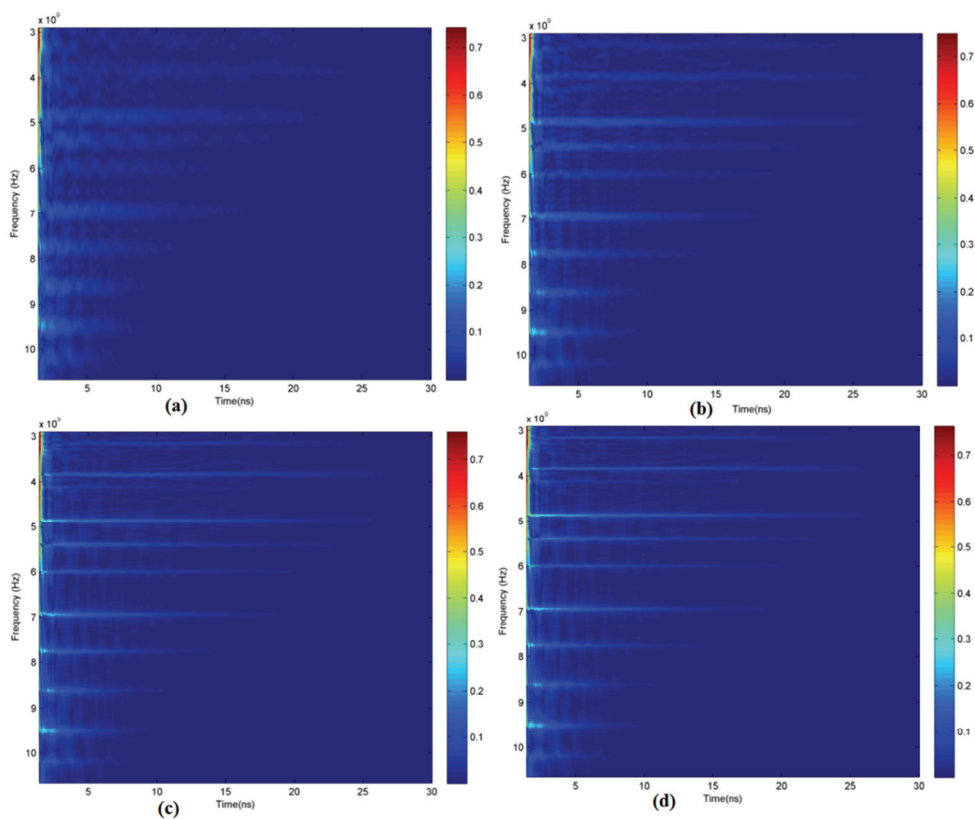
Figure 5.28 Measured 2D spectral density pattern for different Window size a) 3ns (b) 6.3ns (c) 12.6ns and (d) 25ns, In all case Resolution time = 0.06ns, Delay = 1.43ns
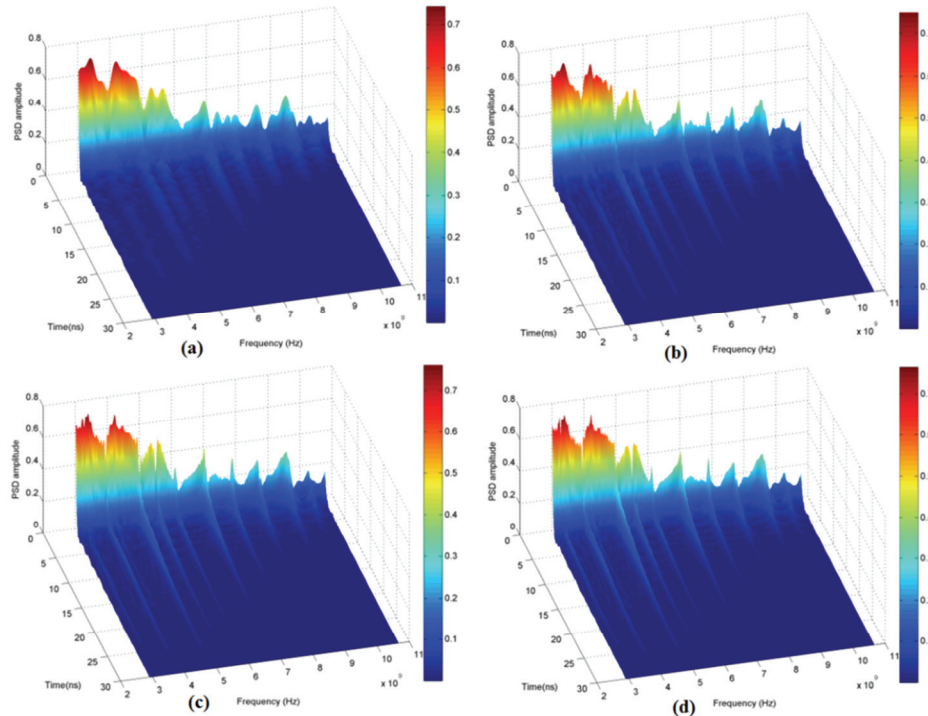
Figure 5.29 Measured 3D spectral density pattern for different Window size a) 3ns (b) 6.3ns (c) 12.6ns and (d) 25ns, In all cases Resolution time = 0.06ns, Delay = 1.43ns

Therefore Delay variable is updated with current time plus half time period of the transmitted pulse and it is set to be at 1.49ns for the above signal. 2D and 3D power spectral density patterns are shown in the Fig.5.30. All the resonant frequencies of the 10 SIR based resonators are very clear from both figures. The low frequency resonators possess higher Quality factor and its spectral signatures are available in large time as compared with higher frequency resonators. At high frequencies the Quality factor of the resonators are degraded due to the microstrip loss at high frequencies.

The new method of spectral extraction simplifies the analysis to a particular time duration in the backscattered signal. Hence the computation resources and processing time can be reduced significantly. The 2D and 3D

power spectral density plots can provide all the information about the resonant frequencies in the RFID tags, such as strength of the antenna mode, Quality factor of each resonance and the time duration in which spectral information exist along the backscattered signal.
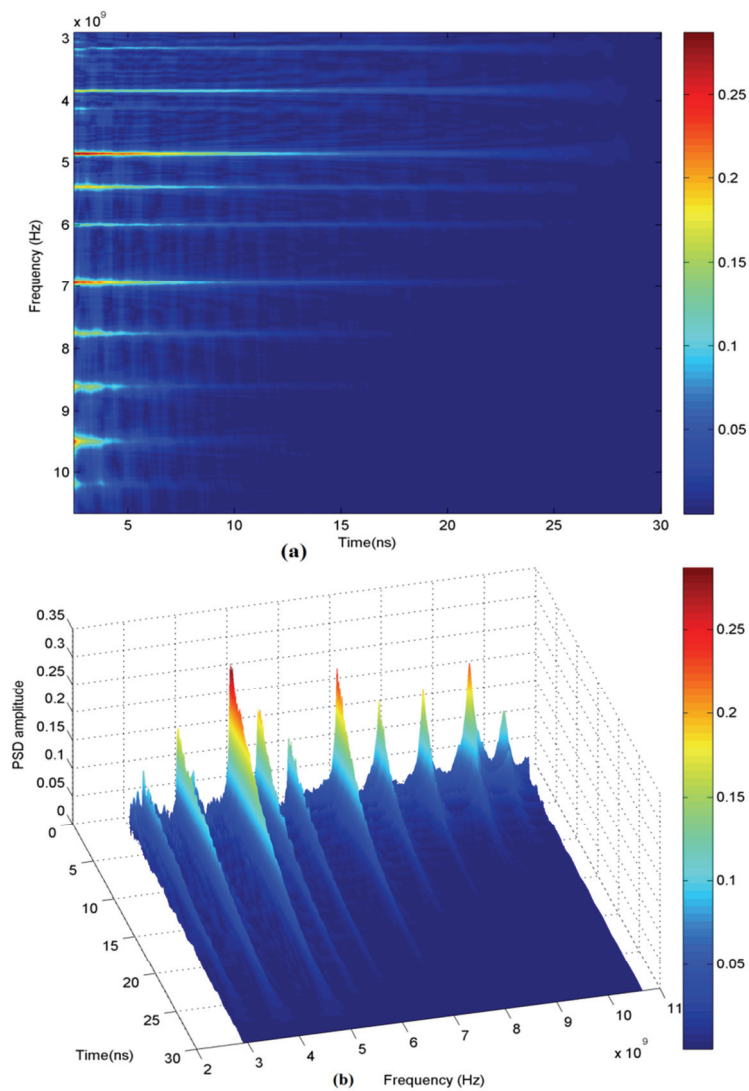
Figure 5.30 Measured 2D (a) and 3D (b) spectral density pattern for different Window size = 25ns, Resolution time = 0.06ns and Delay = 1.49ns

5.7. Algorithm for Extraction of Antenna Mode from the Backscattered Signal

The above method of extraction can be implemented for the analysis of resonant information in all the general multiscatterer based chipless RFID tags, operating in the frequency domain. Different signal processing method on time domain based signal enables the extraction of resonant frequency from the backscattered signal. From the above studies, resonant informations are contained in the antenna mode, which is followed by the structural mode signals. Hence, a small portion of backscattered signals in the time domain is needed for the extraction of resonant frequencies from the RFID tag. The primary goal in this analysis is to identify the antenna mode in the backscattered signal.

The detailed steps for finding the spectral ID from time domain signal can be summarised as,

1. Perform calibration (S_{11} with tag (dB) − S_{11} without tag (dB)) as described in section 5.3.

   Then the backscattered signal contains only the structural mode, antenna mode and noise signal. Reflection from all the stationary and reader antenna can be removed by performing calibration.

2. Signal before the antenna mode does not contain frequency components of the RFID tag. Hence, entire signal before the antenna mode can be removed before FFT analysis. First step is to identify the peak amplitude time in the backscattered signal; it will be in the middle point of the structural mode. Set 'Delay' variable to the peak time and half time period of transmitted pulse.

3. Time value stored in the 'Delay' variable could be the starting point of the antenna mode. Signal before the time stored in the 'Delay' variable can be removed for further analysis in the time domain signal. The resultant backscattered signal contains only the antenna mode and noise.

4. By setting proper 'Delay', 'Resolution time' and 'Window size', all the resonant frequencies in the RFID tag can be extracted. For antenna mode extraction, smaller time (<1ns) in 'Resolution time' variable and large time duration (>5ns) in the 'Window size' variables are preferred.

As seen in the above analysis, the higher frequency resonators having low Quality factor, will decay much faster than low frequency resonators. Therefore, to identify the high frequency resonances in the UWB spectrum, FFT window should start from the beginning of antenna mode.

5.8. Spectral ID from Highly Noisy Signal

The algorithm discussed above can be applied on any backscattered signal from the tags working in noisy environment. Tag to be measured is placed at a distance of 80cm away from the reader antenna outside the chamber with the averaging option disabled. Measurement room consist of different materials like metals, wood, plastic and other signal interference from nearby equipment's, radiation from mobile tower, Wi-Fi, people working around, etc. Backscattered signal from the tag comprise of spectral signature and noise from the surroundings. Fig.5.31 shows the backscattered signal from the ten SIR based tag in frequency domain. It is seen that spectral identification from the dip in the frequency domain fails due to the presence of noises in the backscattered signal. Amplitude variations of consecutive

frequency points are drastic in this case. Hence amplitude detection algorithm proposed in the earlier chapter will not work efficiently. The post processed amplitude detection method proposed in chapter 3 is depicted in Fig.5.32, which is computed from Fig.5.31. It is observed that resonant peaks are immersed in the noise signal and this method will fail if backscattered signal is prone to noise.
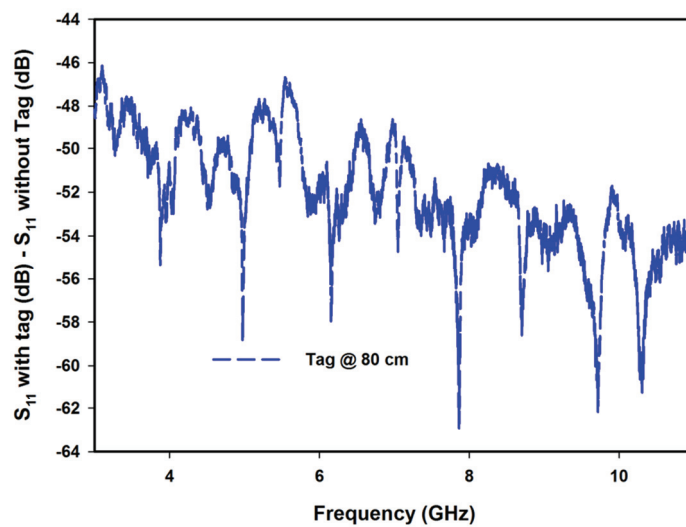
Figure 5.31 Measured Backscattered signal at a distance of 80 cm
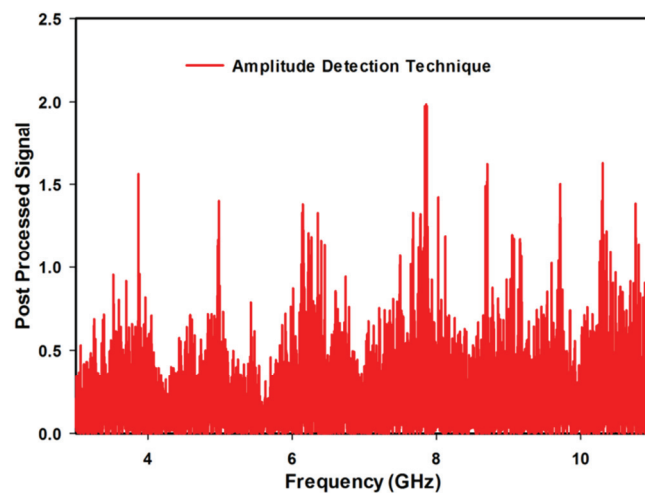
Figure 5.32 Post processed amplitude of the signal plotted in Fig.5.31.

Time domain signal analysis is carried out as per the spectral extraction algorithm mentioned above. The backscattered time domain signal for the tag distance of 80cm is shown in Fig.5.33. The initial step of the algorithm is to find the peak amplitude point in the time domain signal and the removal signals before the first peak amplitude, since it doesn't contain any frequency information of the RFID tag. Post processed time domain signal with the new time axis is depicted in Fig.5.34 and it contains the antenna mode, noise and half portion of the structural mode. The backscattered signal containing the antenna mode and noise as shown in Fig.5.34.
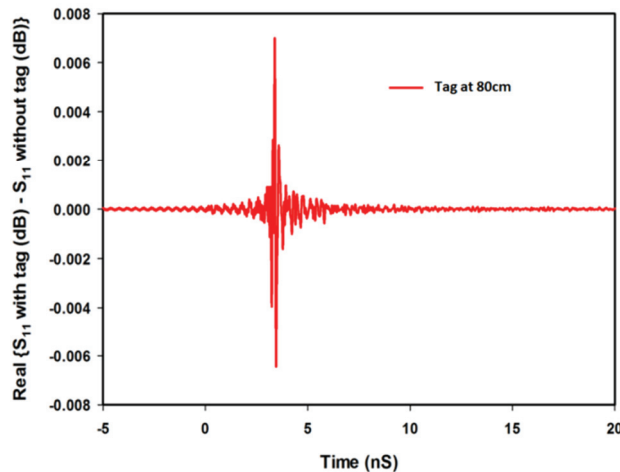
Figure 5.33 Backscattered signal in time domain, when the tag is positioned at 80 cm
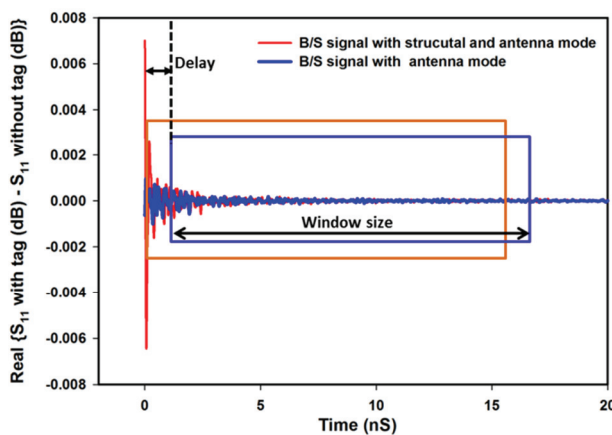
Figure 5.34 Post processed backscattered signal with new time axis.

Extraction of resonant frequencies from the processed signal can be done by taking the FFT of the time windowed signal. The 'Delay' variable contains the time at which the FFT window starts. Fig.5.35 shows the frequency spectra of the RFID tag with different 'Delay' and the analysis is performed on the backscattered signal containing half portion of structural mode. Initially 'Delay' has been varied from 0 ns to 3.75 ns, while keeping 'Window size' at 15 ns. As explained earlier, resonators working in the higher frequency bands are decaying much faster than the lower frequency band resonators. Hence resonant informations of the high frequency microstrip SIRs are predominant for 'Delay' close to structural mode, ranging from 1ns to 2.5ns. Spectral component of the tag with lower resonant frequencies can be extracted even with higher 'Delay', ranging from 2.5ns to 5ns. The interference effect of structural mode and antenna mode (Delay 0ns) is also clear from this figure.
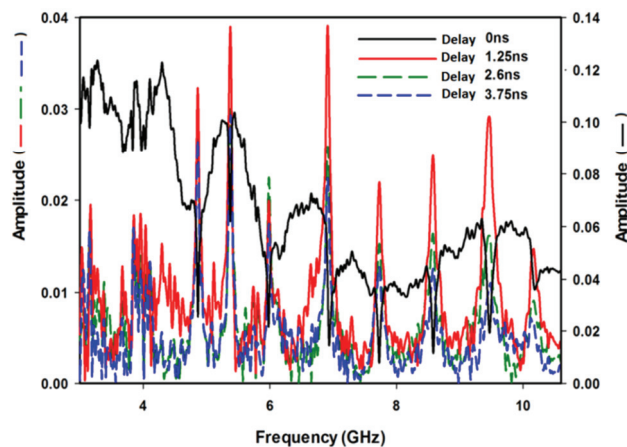
Figure 5.35 Amplitude of the backscattered spectral data with different 'Delay' time. 'Window size' is fixed at 15ns

The Window size is also having a little effect on the tag spectral extraction. Fig.5.36 shows the amplitude of backscattered spectral data with different 'Window size's, while keeping Delay at 2.5ns. It is evident that the amplitude of the antenna mode is increasing with increasing 'Window size'.
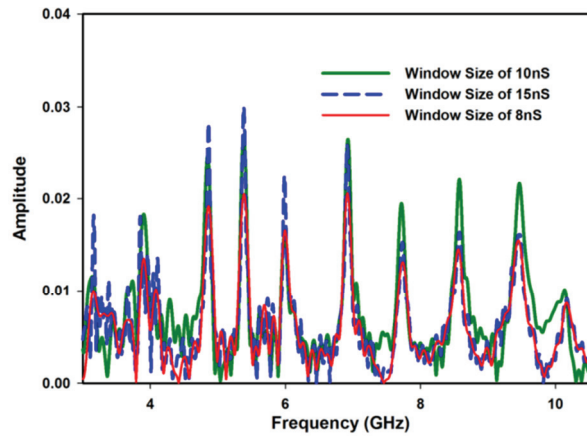
Figure 5.36 Amplitude of the backscattered spectral data for different Window-Size, Delay is fixed at 2.5ns

Fig.5.37 shows the 2D spectral density of post processed backscattered signal. It clearly shows the presence of each resonance along the time axis. High frequency resonances are decaying much faster than the low frequency resonators. Plotting 2D and 3D pattern requires a large computational time due to requirement of multiple FFT computations and it also depends on the values of 'Resolution time' and 'Window size'.
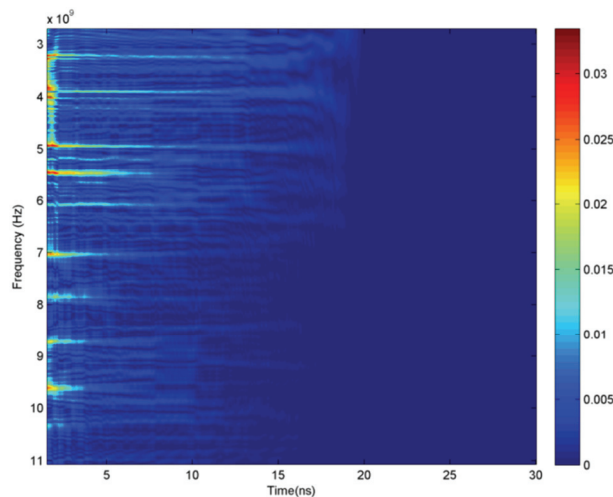
Figure 5.37 2D Spectral density of post processed backscattered signal with resolution time of 0.06ns and window size of 15ns.

5.9. Averaging in Time Domain– Spectral ID Extraction from Moving Objects

UWB-IR transmitter can send an UWB pulse within a short period of time (1-2 ns). Therefore, the total time required for getting the backscattered signal from the tag of the order of 4-20 ns. This time is negligible for the case, where the tag is moving on the conveyor belt or vehicle. In practical systems, noise generated by nearby objects and the white noise plays an important role in the read performance of the tag. Noise in the backscattered signal can be minimised by applying coherent averaging in time domain data. In the case of a Network Analyser, single sweep from 3.1-10.6 GHz with 6401 frequency points requires about 90ms of time. Hence, to demonstrate averaging, measurements have been performed for various tag positions. In Fig.5.38 the backscattered signal measured while placing tag at 10cm, 20cm and 50cm away from the antenna.

The above algorithm can be applied in this analysis. From Fig.5.38, it is clear that, the spectral content stored in the antenna mode is same for all the backscattered signals, but there are slight variations due to the presence of noise. Hence the entire time domain signals at different distances are post processed by removing unwanted portions by setting 'Delay' variable at the middle of the structural mode. Performing averaging on the time domain signal with its new time axis, can reduce the noise in the backscattered signal. It also enhances the Signal to Noise Ratio. Fig.5.39 shows the averaged time domain signal starting from the middle point of its structural mode.
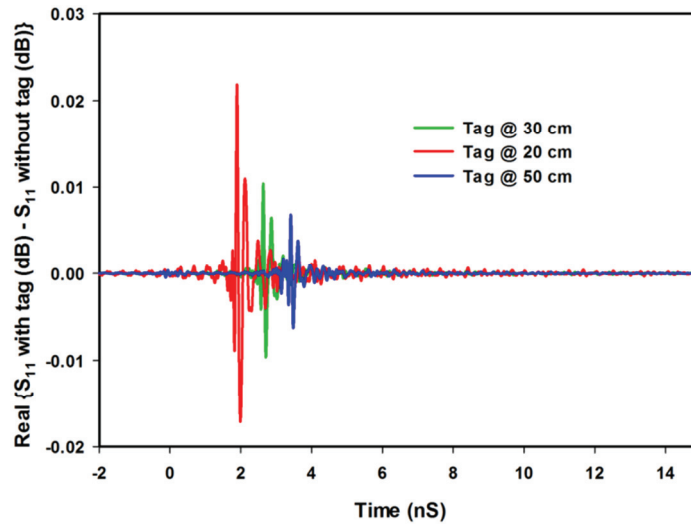
Figure 5.38 Backscattered signal from the RFID tag at different distances
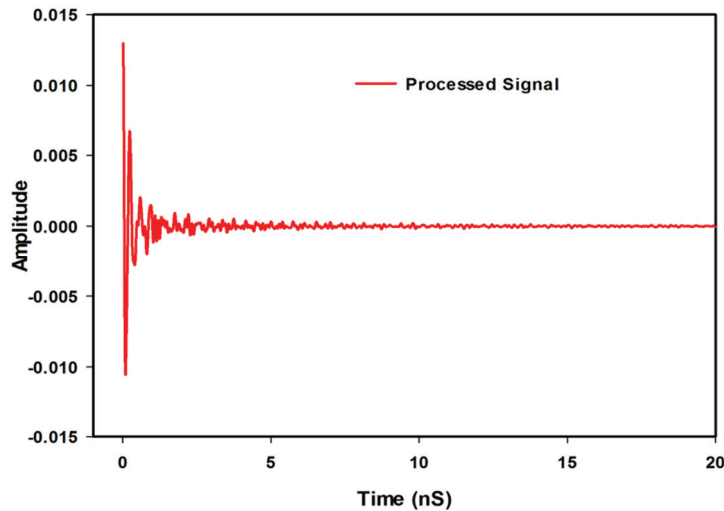
Figure 5.39 Averaged backscattered signal after post processing

Fig.5.40 shows the extracted spectral signature of the RFID tag, which is calculated by taking the average of the three backscattered signals measured at three different distances. All the resonant frequencies can be easily identified from the amplitude itself. The window properties selected as, Window Delay = 2nS and Window Size = 10nS. The 2D spectral density of the averaged antenna

mode along the time axis is plotted in Fig.5.41. All the resonances are clearly visible in the graph and low noise levels are observed in the spectrum.
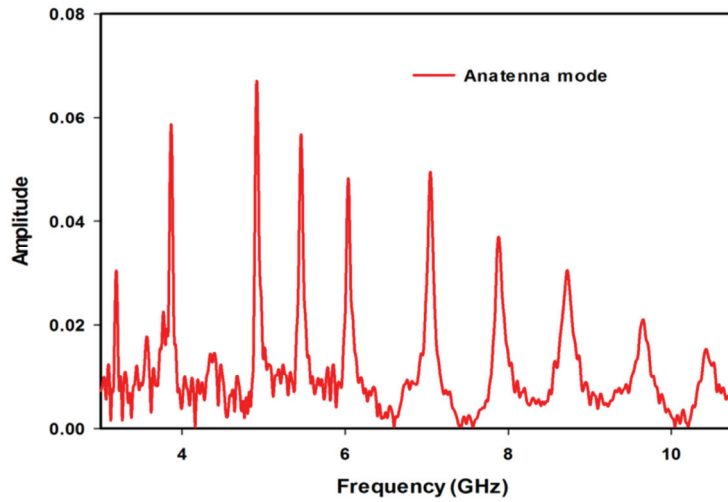
Figure 5.40 Frequency spectrum of the antenna mode extracted from the post processed signal shown in Fig. 5.39
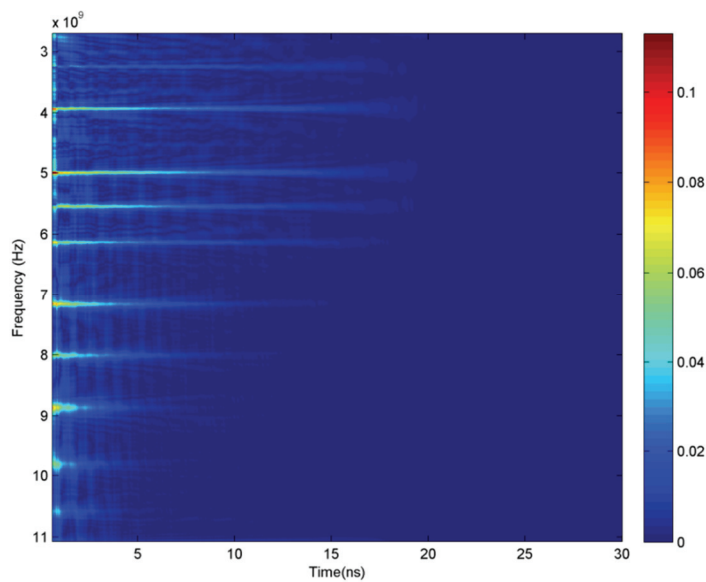
Figure 5.41 2D spectral density of averaged signal plotted in Fig.5.40, Resolution time = 0.06ns and Wind size = 15ns.

5.10. Measurements in Practical Scenario

There are wide varieties of applications of RFID tags are reported, such as asset tracking, automatic bill collection, security purpose, sensing, etc. All these applications are being conducted in real time measurements with a high dynamic range. To analyse backscattered signal in a practical scenario, the RFID tag is placed on different materials or items like paper pack and metallic sheet. All the measurements are carried out in the lab, which contain different types of materials (metal, wood, plastic) and interference from surrounding wireless systems (Wi-Fi, Mobile Tower, etc.).

5.10.1. RFID Tag on Paper Pack

Here, the RFID tag is placed on a paper pack bundle and the backscattered signal is analysed for different distances. Measurement setup inside the laboratory is depicted in Fig.5.42. Frequency domain responses of the backscattered signal at different distances are plotted in Fig.5.43 and it shows good discrimination between different bits. Time domain analysis of backscattered signal is also performed at different distances and the frequency response of the extracted antenna modes from the above signals are plotted in Fig.5.44.

Figure 5.42 Measurement setup while placing RFID tag on a paper pack
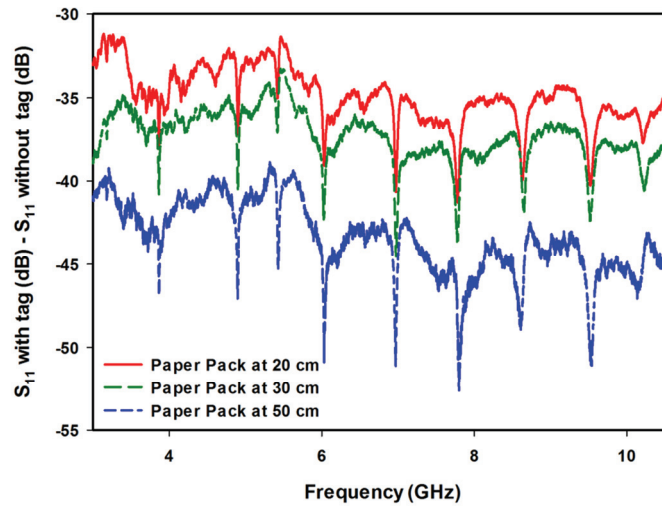
Figure 5.43 Frequency domain response of the backscattered signal from the RFID tag, while placing it on a paper pack.
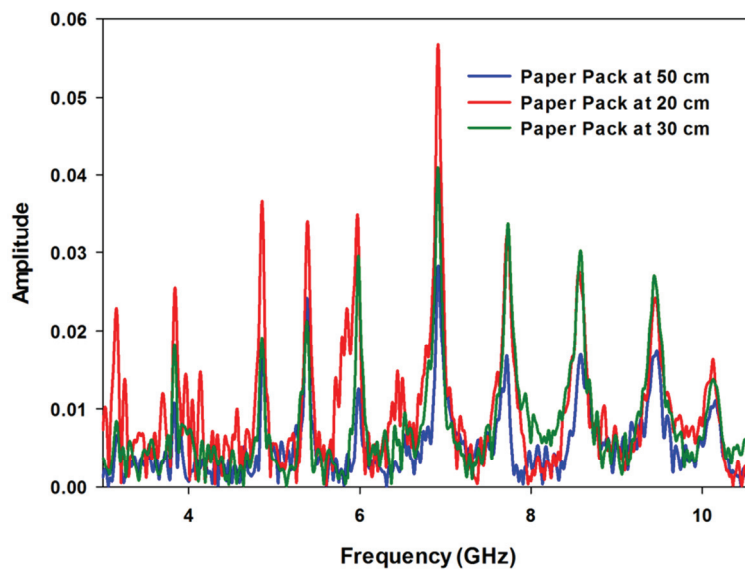
Figure 5.44 Antenna mode signal from the tag at different distances.

As explained earlier, averaging of RFID tag with different distances is carried out and 2D spectral density of the same is plotted in Fig.5.45. From the figure it is again proved that the same method can be used for the spectral extraction of moving tag even it is placed on paper pack.
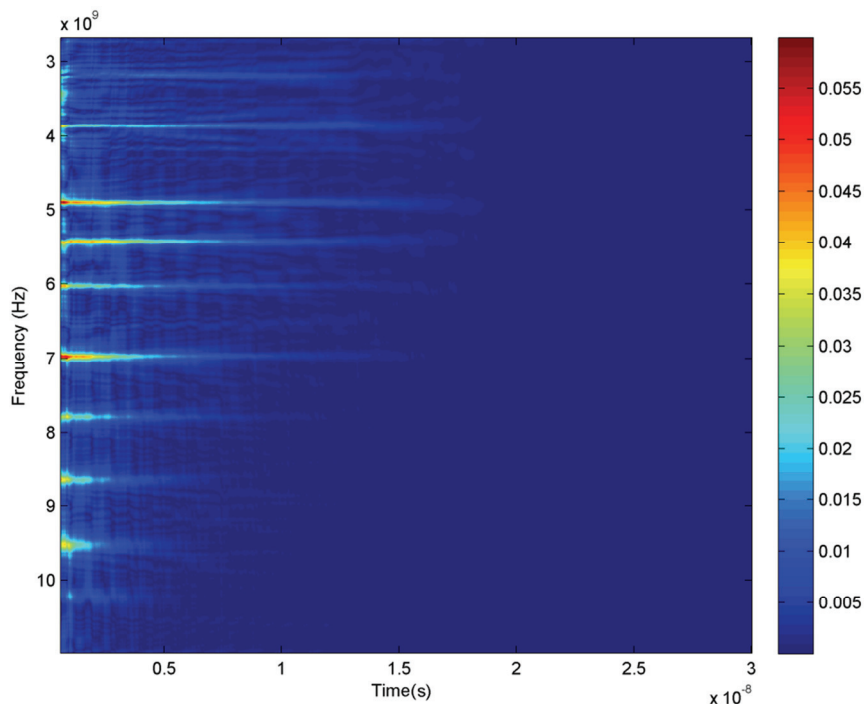
Figure 5.45 2D spectral density of the averaged signal when the tag is placed at different distances (20cm, 30cm and 50cm). Resolution time = 0.06ns and Window size = 15ns.

5.10.2. RFID Tag on a Metallic Sheet

The main advantages with RFID tag using the microstrip structure is that, it can be used for item tagging in many practical applications. For a uniplanar structure (resonator without ground plane), the resonant frequency of the tag will vary significantly with surrounding materials, especially due to the presence of metals and high dielectric constant materials. Due to the presence of the metal at the backplane of the microstrip structure, the resonant frequencies of the resonators are nearly independent of the material in which it is tagged. While using RFID tag on metallic containers, it will reflect the entire incident wave with higher amplitude than the structural mode signal from the RFID tag. Hence, extraction of structural mode and antenna mode will become

very difficult from the backscattered signal. Here RFID tag is placed on a metallic sheet of dimension 50cmx30cm as shown in Fig.5.46. The backscattered timed domain signals from metal sheet and paper pack is shown in Fig.5.47. From the figure it clear that, backscattered amplitude in the structural mode is very high with metal sheet compared with that of paper pack backing.
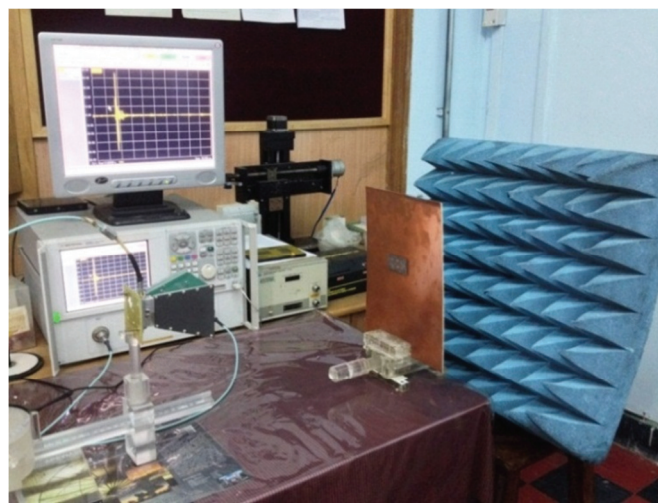
Figure 5.46 Measurement setup with metallic sheet
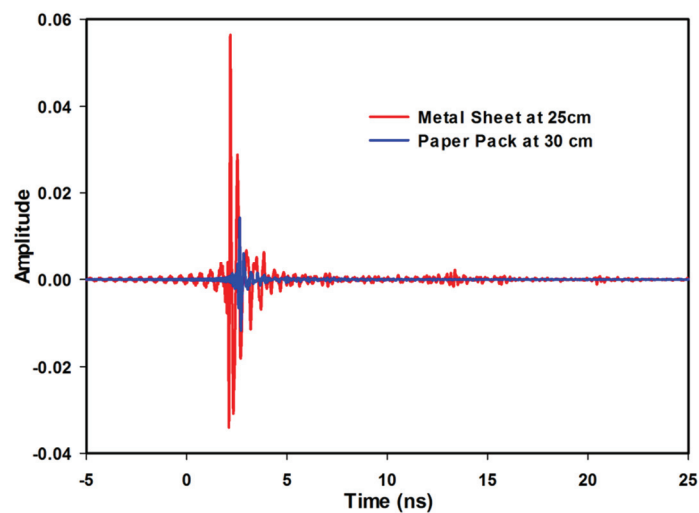
Figure 5.47 Backscattered signal in time domain from metallic sheet and paper pack

Here, two types of calibration method are adopted, one is the free space and the other is that with metal plate. In free space calibration, empty room measurement is taken in free space. For metal plate calibration, empty room data are taken with the proximity of metallic sheet. The frequency domain responses with the above calibrations are shown in Fig.5.48. Identification of resonance in both cases is difficult in the frequency domain. Therefore, time domain analyses are carried out on both the backscattered signals (calibrated signal with metal plate and free space). Using the above mentioned algorithm, resonant peaks are well identified from both calibration methods. It is very difficult to identify the presence of resonance for a distance greater than 25cm due to the degradation of antenna mode. Fig.5.49 shows the antenna mode signal with two different calibration methods. The 2D spectral density of the backscattered signal with free space calibration is shown in Fig.5.50.
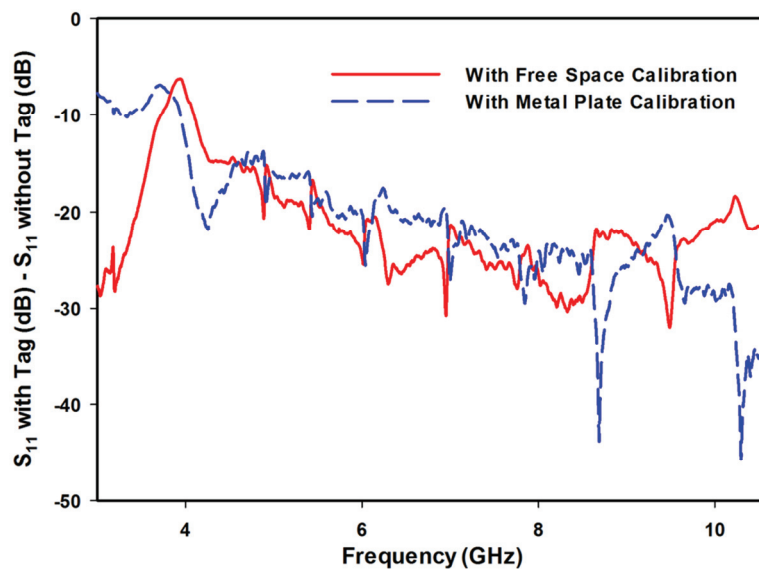
Figure 5.48 Backscattered frequency domain response with different calibration method.
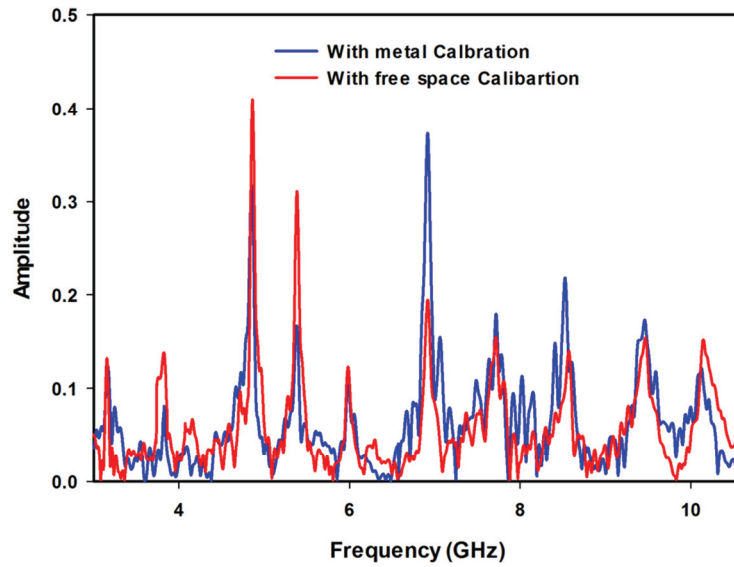
Figure 5.49 Backscattered antenna mode response with different calibration technique (distance between antenna and tag is 25cm).
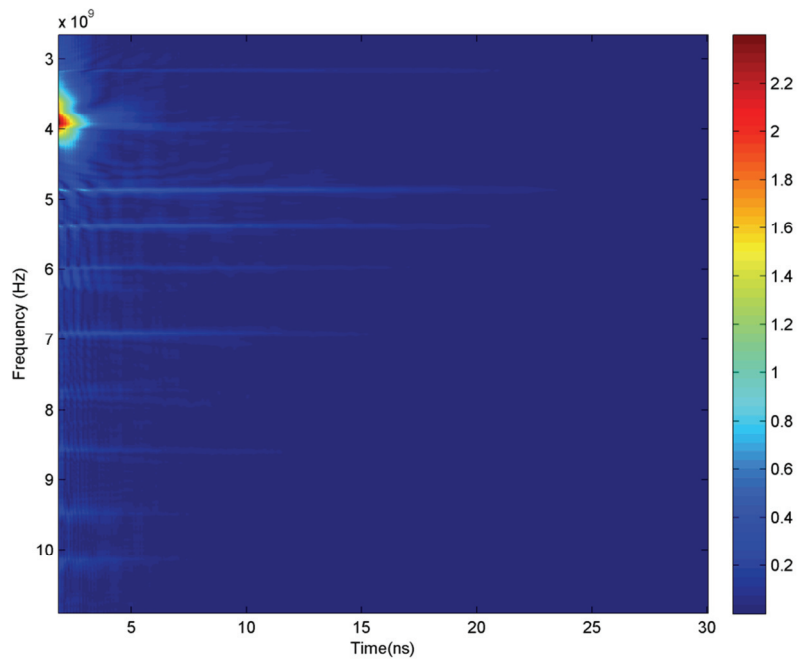
Figure 5.50 2D spectral density of backscattered signal when the tag is placed at a distance of 25 cm. (Free space calibration, Resolution time = 0.06ns and Window size = 15ns)

5.11. Conclusion

This chapter proposed the detailed time domain analysis of frequency spectra based tags using UWB IR technology. Simulation analysis using CST Microwave studio is presented with a demonstration of structural and antenna mode extraction. UIW IR based time domain measurements are carried out using the PNA 8362B network analyser. An algorithm for finding antenna mode from the backscattered signal is proposed and is validated with the measured data. Time domain analyses have been successfully carried out on backscattered signal measured in highly noisy environments. Coherent integration on the time domain signal is performed for decoding the information from a moving target. Spectral extractions of RFID tag from different practical scenarios like RFID tag on paper pack and with metallic plate backing are also demonstrated. The backscattered signal from the RFID tag is decoded successfully for a distance of 80cm.

5.12. Reference

[1]   Y. Shen, C. L. Law, S. Hu, and J. Xia, "IR-UWB-based chipless RFID system," *Ann. Telecommun. - Ann. Des Télécommunications*, vol. 68, no. 7–8, pp. 375–383, Jun. 2013.

[2]   A. Ramos, D. Girbau, A. Lazaro, and S. Rima, "IR-UWB Radar System and Tag Design for Time- coded Chipless RFID," 6th European Conference on Antennas and Propagation (EUCAP), pp. 2491–2494, 2011.

[3]   A. Ramos, D. Girbau, A. Lazaro, and D. Kit, "Influence of materials in time-coded chipless RFID tags characterized using a low-cost

UWB reader," Proceedings of the 42nd European Microwave Conference, pp. 526–529, 2012.

[4] A. Ramos, A. Lazaro, D. Girbau, and R. Villarino, "Time-Domain Measurement of Time Coded UWB Chipless RFID Tags", Progress In Electromagnetics Research, Vol. 116, pp. 313-331, 2011.

[5] S. Hu, S. Member, Y. Zhou, C. L. Law and Wenbin Dou, "Study of a Uniplanar Monopole Antenna for Passive Chipless UWB-RFID Localization System," IEEE Transactions on Antennas and Propagation, Vol. 58, No. 2, pp. 271–278, February 2010.

[6] Davide Dardari, Raffaele D'Errico, Christophe Roblin, Alain Sibille, and Moe Z. Win "Ultrawide Bandwidth RFID : The Next Generation ?", Contributed Paper, Proceedings of the IEEE, Vol. 98, No. 9, September 2010.

[7] A. Lazaro, A. Ramos, D. Girbau, and R. Villarino, "A Novel UWB RFID Tag Using Active Frequency Selective Surface," IEEE Transactions on Antennas and Propagation, Vol. 61, No. 3, pp. 1155–1165, March 2013.

[8] B. Shao, Q. Chen, Y. Amin, R. Liu, and L.-R. Zheng, "Chipless RFID tags fabricated by fully printing of metallic inks," Springer, Ann. Des Télé communications, vol. 68, no. 7–8, pp. 401–413, Jun. 2013.

[9] Z. Zou, B. Shao, S. Member, Q. Zhou, C. Zhai, J. Mao, M. Baghaei-nejad, Q. Chen, and L. Zheng, "Design and Demonstration of Passive UWB RFIDs: Chipless versus Chip Solutions," IEEE 2012 International Conference on RFID -Technologies and Applications (RFID - TA), pp. 6–11, 2012.

[10] Novelda Impulse Radar. [Online]. Available: http://www.novelda.no/

[11] A. Vena, E. Perret, and S. Tedjini, "Design rules for chipless RFID tags based on multiple scatterers," Ann. Telecommun. - Ann. Des Télécommunications, vol. 68, no. 7–8, pp. 361–374, Feb. 2013.

[12] S. Preradovic and N. Karmakar, "Design of fully printable planar chipless RFID transponder with 35-bit data capacity," in Proc. 39th European Microwave Week, Rome, Italy, Sept. 2009, pp. 13–16.

[13] Nijas C M, Dinesh R, Deepak U, Abdul Rasheed, Mridula S, K. Vasudevan and P. Mohanan, "Chipless RFID Tag using Multiple Microstrip Open Stub Resonators," IEEE Transactions on Antennas and Propagation, Vol. 60, No. 9, pp. 4429-4432, Sep. 2012.

[14] David Girbau, Javier Lorenzo, Antonio Lázaro, Carles Ferrater and Ramón Villarino, "Frequency-Coded Chipless RFID Tag Based on Dual-Band Resonators", IEEE Antennas and Wireless Propagation Letters, Vol. 11, 2012.

[15] RFSAW Inc, "The global SAW tag – a new technical approach to RFID", internet white paper, 2004. Available: http://www.rfsaw .com /pdfs/ SAW%20RFID%20Whitepaper.pdf

[16] I. Jalaly and D. Robertson, "RF barcodes using multiple frequency bands," in IEEE MTT-S Microwave Symp. Dig., Long Beach, CA, Jun. 2005, pp. 139–141.

[17] P. Kalansuriya and N. Karmakar, "Time domain analysis of a backscattering frequency signature based chipless RFID tag," pp. 183–186, 2011.

[18] R. Rezaiesarlak, S. Member, M. Manteghi, and S. Member, "Short-Time Matrix Pencil Method for Chipless RFID Detection Applications," IEEE Transactions On Antennas And Propagation, Vol. 61, No. 5, pp. 2801–2806, May 2013, 2013.

[19] M. Manteghi, "A novel approach to improve noise reduction in the matrix pencil algorithm for chipless RFID tag detection," in *IEEE Int.Antennas Propag. and CNC-USNC Symp./URSI Radio Sci. Meeting.*, Toronto, ON, Canada, Jul. 11–17, 2010.

[20] P. Kalansuriya, S. Member, N. C. Karmakar, S. Member, and E. Viterbo, "On the Detection of Frequency-Spectra-Based Chipless RFID Using UWB Impulsed Interrogation," IEEE Transactions on Microwave Theory and Techniques, Vol. 60, No. 12, pp. 4187–4197,December 2012.

[21] P. Kalansuriya and N. Karmakar, "UWB-IR based detection for frequency- spectra based chipless RFID," in *IEEE MTT-S Int. Microw. Symp. Dig.*, 2012, pp. 1–3.

[22] M. I. Skolink, *Radar Handbook*, 3rd ed. New York, NY, USA: Mc-Graw-Hill, 2008.

[23] R. Anee and N. C. Karmakar, "Chipless RFID Tag Localization," IEEE Transactions on Microwave Theory and Techniques, Vol. 61, No. 11, November 2013.

[24] Y. Shen, C. and L. Law, "A Low-Cost UWB-RFID System Utilizing Compact Circularly Polarized Chipless Tags," IEEE Antennas and Wireless Propagation Letters, Vol. 11, pp. 1382–1385, 2012.

[25] Arnaud Vena, Etienne Perret, and Smail Tedjni, "A Depolarizing Chipless RFID Tag for Robust Detection and Its FCC Compliant," IEEE Transactions on Microwave Theory and Techniques, Vol. 61, No. 8, pp. 2982–2994, August 2013.

[26] R. A. Ross, "Radar cross section of rectangular flat plates as a function of aspect angle," *IEEE Trans. Antennas Propag.*, vol. AP-14, no. 3, pp. 329–335, May 1966

[27] A. Vena, T. Singh, S. Tedjini, and E. Perret, "Metallic letter identification based on radar approach," in Proc. General Assembly Scientific Symp. 2011 URSI, pp. 1–4.

[28] A. Vena, E. Perret, and S. Tedjini, "Novel compact RFID chipless tag," in Proc. Progress Electromagnetics Research Symp., Marrakesh, Morocco, 2011, pp. 1062–1066.

[29] A. Ramos, A. Lazaro, D. Girbau, and R. Villarino, "Time domain measurement of time-coded UWB chipless RFID tags," Progr. Electromagn. Res., vol. 116, pp. 313–331, July 2011.

[30] A. Vena, E. Perret, and S. Tedjini, "Chipless RFID tag using hybrid coding technique," IEEE Trans. Microwave Theory Tech., vol. 59, no. 12, pp. 3356–3364, 2011.

[31] P. Kalansuriya and N. Karmakar, "UWB-IR based detection for frequency- spectra based chipless RFID," in IEEE MTT-S Int. Microw. Symp. Dig., pp. 1–3, 2012.

[32] Y. Shen, C. L. Law, S. Hu, and J. Xia, "IR-UWB-based chipless RFID system," Ann. Telecommun. -Springer, vol. 68, no. 7–8, pp. 375–383, Jun. 2013.

[33] Smail Tedjini, Nemai Karmakar, Etienne Perret, Arnaud Vena, Randika Koswatta, and Rubayet E-Azim , "Hold the Chip" IEEE microwave magazine, August 2013.

[34] E. Perret, M. Hamdi, G. E. P. Tourtollet, R. Nair, F. Garet, A. Delattre, A. Vena, L. Duvillaret, P. Martinez, S. Tedjini, and Y. Boutant, "THID, the next step of chipless RFID," in Proc. 7th IEEE RFID Conf., Orlando, FL, 2013, pp. 292–299.

............ೞ಼ೞ.............

CONCLUSION AND FUTURE PERSPECTIVE

Abstract

This chapter highlights the accomplishments and achievements of the research work carried out on Chipless RFID. A summary of the results and the directions for future study are discussed.

The main objective of this research is to develop a compact chipless RFID tag with high data encoding capacity. From the literature, it is concluded that, reasonably good data encoding capacity on a substrate with low dielectric constant can be achieved by employing frequency spectra based chipless RFID tag. Multiresonator and multiscatterer based chipless RFID tags are designed and developed during the research. While the chipless RFID technology is still under development, a low cost RFID tag having a data encoding capacity of 79 bits has been developed. A chipless RFID reader for multiscatterer based tag working in a frequency band of 2.36GHz to 2.54GHz is designed for demonstrating the feasibility of RFID system. Most of the measurements reported in the journals carried out in a controlled environment (Anechoic Chamber) with complicated calibration procedure. For a practical system, a new approach based on UWB Impulse Radar (UWB IR) technology is employed and the decoding methods from

noisy backscattered signal are successfully demonstrated. The thesis also proposes a simple calibration procedure, which is able to decode the backscattered signal up to a distance of 80cm with 1mW output power.

Findings in the research works detailed in this thesis are summarized in the following sections.

6.1. Multiresonator Based Chipless RFID Tag using Microstrip Open Stub Resonator

An 8 bit multiresonator based chipless RFID tag using multiple open stub resonators is proposed in chapter 2. The quarter wavelength resonance of the open stub resonator makes the proposed tag more compact than the other tags reported based on this principle. Equivalent circuit model analysis and different parametric studies are conducted on the open stub resonator. The tag enables the encoding of data in magnitude as well as in group delay. Without having any additional calibration technique, the proposed system is able to decode the tag information up to a distance of 40cm. The method introduced in this chapter can be effectively implemented on other low cost substrate materials, which in turn reduce the overall cost. The problems associated with this type of tags like variation in the radiation pattern of the tag antennas at frequencies, proper orientation requirement with tag and reader, mutual coupling effects between the resonators and low surface coding density due to space requirement of two UWB antennas, made to think for new encoding methods.

6.2. Multiscatterer Based Tags using Stepped Impedance Resonator (SIR)

Chapter 3 provides an idea about the multiscatterer based chipless RFID tags and its operation. Compared with multiresonator based tag,

multiscatterer based tags show good data encoding capacity, surface coding density and readability. The evolution of SIR and its properties like total electrical length, harmonic separation between different modes and independent control over resonant mode are explained. Scattering property of the tag at different angular directions is also studied. The multiscatterer based tag requires a low loss substrate to encode more number of resonances in a limited bandwidth. The reported tags are not able to utilize full UWB spectrum (3.1-10.6GHz) due to the presence of the harmonic modes at the integral multiple frequencies of the fundamental mode. Because of the harmonic separation capability of SIR, chipless tag with an effective utilization of entire UWB is designed and developed. Independent control of resonant modes (fundamental and first harmonic) is demonstrated with theoretical, numerical and measured results.

Three types of UWB chipless tag using different modes of SIR are proposed. In the first design, fundamental mode of the SIR is used for encoding bits in the frequency spectrum. In the second design, an RFID tag using multiple resonance encoding method is also proposed, in which data is encoded both in fundamental and first harmonic frequency of the SIR. By implementing Frequency Shift Coding Technique (FSC) on both resonant modes, the Surface Coding Density (SCD) of 4bits/cm^2 is achieved compared with the first design (2.78bits/cm^2).

In the third design, an SIR based high data encoding tag using multiple bit encoding technique is introduced, in which different boundary conditions are applied to SIR. All four combinations of two bit representations using fundamental and first harmonic modes of the SIR are successfully demonstrated. With presence or absence coding technique,

proposed tag is capable of representing 2^{2N} number of bit combinations using N resonators. The Surface Coding Density of 1.06 bits/cm^2 is achieved with the coding method. The bit encoding capacity of the tag is further enhanced by introducing FSC technique on different bit combinations. Finally, an RFID tag with an encoding capacity of 79 bits is proposed with an SCD more than 7bits/cm^2. A simple calibration method is successfully implemented and validated with different readable distances. The spectral IDs of the RFID tags are successfully decoded from the backscattered magnitude and group delay signal. Due to the full wave current pattern on SIR at first harmonic mode, there is a null in the backscattered field along the broadside direction. Therefore, second and third types of RFID tags in the above design require a reading angle between $\pm 10^0$ to $\pm 70^0$ along θ direction. The measured and simulated results are in close agreement with theoretical values. A simple post processing method is introduced for the detection of resonance from the backscattered amplitude signal.

6.3. RFID Reader for Multiscatterer Based Chipless RFID Tag

A Chipless RFID reader for multiscatterer based tag is designed for a frequency band of 2.36 GHz to 2.54 GHz. The RF components used in the MIT Coffee Can radar are effectively utilised for the design of an FMCW based chipless RFID reader. Single antenna based RFID reader is initially designed with spectrum analyser at the receiver section and the working of a single resonator based chipless tag is validated. Finally, a low cost RFID reader is proposed and the backscattered signal from chipless RFID tags (single and two bits) are analysed. The validation of the system is done by measuring the tag response using a network analyser and all the measurements with proposed RFID reader shows very good agreement with

analyser data. The backscattered response of the tag is measured successfully up to a distance of 5cm.

6.4. Time Domain Analysis of a Frequency Spectra Based Chipless RFID Tag

Chapter 5 discussed about the time domain analysis of frequency spectra based tags using UWB IR technology. Simulation analysis using CST Microwave studio is presented with a demonstration of structural and antenna mode extraction from the backscattered time domain signal. The UWB IR based time domain measurements are carried out using the PNA E8362B network analyser. An algorithm for finding antenna mode from the backscattered signal is proposed and validated with measured data. The time domain analyses are successfully carried out for backscattered signal which is measured in a highly noisy environment. Coherent integration over time domain signal is performed for decoding the information from a moving target. The spectral extractions of RFID tag from different practical scenarios like RFID tag on paper pack and metallic plates are demonstrated. The backscattered signal from the RFID tag is decoded successfully for a distance of 80cm.

6.5. Future Work

The multiscatterer chipless tag shows more attractive characteristics than multiresonator chipless tag based on frequency spectra technique. As shown in the scattering property of the SIR, proposed tag excites only with single polarisation along the length of the resonator. The polarisation independent RFID system can be attained in two ways. The first method is to arrange the two SIRs with same dimension in orthogonal directions as shown

in Fig.6.1. Therefore, any one of the resonator will excite with incident random polarized RF signal (horizontal or vertical). Another method is to use two orthogonal polarised linear antennas at the reader end and use separate interrogation signals as shown in Fig.6.2. In this case, the modification is required only on the reader side. A circularly polarised antenna working in the UWB band can also be used at the reader end to achieve polarisation independent property.
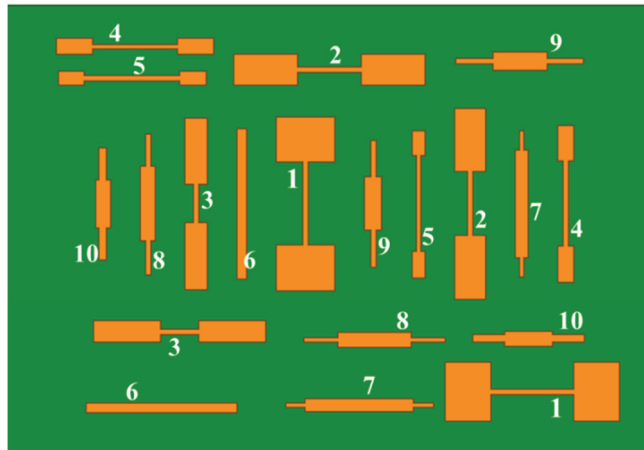
Figure 6.1 Polarisation independent tag
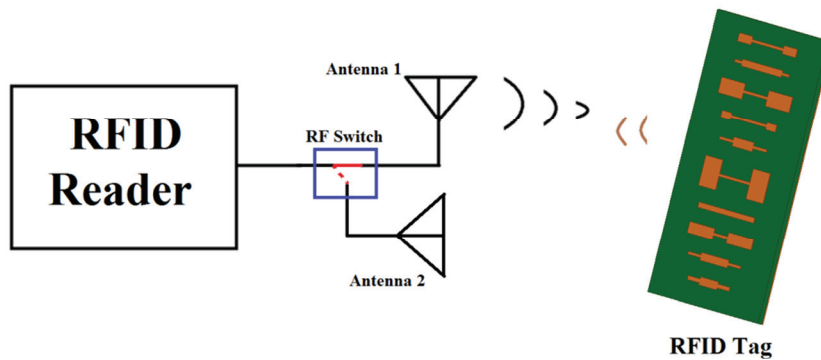
Figure 6.2 Polarisation independent reader architecture

UWB Impulse Radar (UWB IR) based reader is going to be the promising solution to chipless RFID system, due to its low cost, low power

and availability in the market. UWB IR based tag also enables the post processing of backscattered signal, hence the signal below noise level can be extracted using advanced signal processing methods.

.............❀.............

<div align="right">

Appendix
2.4GHz ISM BAND DOPPLER RADAR

</div>

<div align="center">

Abstract

</div>

This appendix describes the design, development and testing of 2.4GHz (ISM band) Doppler or Continuous Wave RADAR, which is used to measure the speed of the target. The basic idea is taken from the MIT Coffee Can Radar and the system is designed using various RF components like VCO, LNA, Splitter, Mixer and antennas. Instead of using Coffee Can as antenna, microstrip patch antennas operating at 2.4GHz are employed here. A personal computer is used for estimating the doppler frequency shift. Real time measurements are taken on the public road inside the university campus and the results are discussed.

A.1. Introduction

The radar is a target detection system that uses RF signals to determine the range, altitude, direction and speed of the target. It can be used to detect the targets like aircraft, ships, spacecraft, guided missiles, motor

vehicles, weather formations, terrain, etc. The radar antenna transmits pulses of radio waves or continuous microwaves and detects the reflected energy from any object in its path. Reflected signal can be picked up by the same antenna or separate receiver antenna which can be placed near to transmitting antenna or at a different location (bistatic). Pulsed Radar was the first technology developed during World War II, following which different types of radar technologies have been developed for different applications. Some of the common radar technologies are

1. Pulsed Radar [1]

2. Continuous Wave Radar [2]

3. Frequency Modulated Continuous wave Radar [3]

4. Frequency-Modulated Interrupted Continuous Wave Radar (FMiCW Radar) [4]

5. Bistatic Radar [5]

6. Side Looking Airborne Radar (SLAR) [6]

High tech radar systems with digital signal processing are capable of extracting target information containing high noise levels. The modern Radar technology has many applications like [7] the following

A.1.1. Civilian Applications

- Airport surveillance

- Marine Navigation

- Weather RADAR (Storm avoidance, wind shear warning, weather mapping)

- Altimetry (Aircraft or spacecraft)

- Aircraft Landing

- Burglar Alarms

- Speed measurements (Police RADAR)

- Mapping

- Security (Hidden weapon detection)

A.1.2. Military Applications

- Air and Marine navigation

- Detection and tracking of Aircraft, Missiles, Spacecraft, etc.

- Missile Guidance

- Fire control for missile and artillery

- Weapon fuses (Guided weapon systems require a proximity fuse to trigger the explosive Warhead)

- Ground Penetrating Radar

A.1.3. Scientific Applications

- Astronomy

- Mapping and Imaging

- Precision distance measurement

- Remote sensing of natural resources

Different applications in the radar use different frequency spectrums which depend on the range resolution and size of the target. Presence of water and other atmospheric conditions causes considerable attenuation to some frequencies. Different frequency bands used in the radar technology and their applications are listed in Table. 1.

Table 1: Radar Bands, Frequencies, Wavelengths and their Applications

Band	Frequency	Wavelength	Application
HF	3 to 30 MHz	10 m to 100 m	Coastal radar systems, over-the-horizon (OTH) radars; 'high frequency'
P	30 to 300 MHz	1m to 10 m	'P' for 'previous', applied retrospectively to early radar systems
UHF	300 to 1000 MHz	0.3 m to 1 m	Very long range (e.g. ballistic missile early warning), ground penetrating, foliage penetrating; 'ultrahigh frequency'
L	1 to 2 GHz	15 cm to 30 cm	Long-range air traffic control and surveillance; 'L' for 'long'
S	2 to 4 GHz	7.5 cm to 15 cm	Terminal air traffic control, long-range weather, marine radar; 'S' for 'short'
C	4 to 8 GHz	3.75 cm to 7.5 cm	Satellite transponders; a compromise (hence 'C') between X and S bands; weather radar
X	8 to 12 GHz	2.5 cm to 3.75 cm	Missile guidance, marine radar, weather, medium-resolution mapping and ground surveillance; in the USA the narrow range 10.525 GHz ± 25 MHz is used for airport radar. Named X band because the frequency was kept secret during World War 2.
Ku	12 to 18 GHz	1.67 cm to 2.5 cm	High-resolution mapping, satellite altimetry; frequency just under K band (hence 'u')
K	18 to 27 GHz	1.11cm to 1.67 cm	K band is used by meteorologists for detecting clouds and by police for detecting speeding motorists. K band radar guns operate at 24.150 ± 0.100 GHz. Automotive radar uses 24 . 26 GHz.
Ka	27 to 40 GHz	0.75 cm to 1.11 cm	Mapping, short range, airport surveillance; frequency just above K band (hence 'a'); photo radar, used to trigger cameras that take pictures of license plates of cars running red lights, operates at 34.300 ± 0.100 GHz
mm	40 to 300 GHz	1 mm to 7.5 mm	Millimeter band, subdivided as below. The letter designators appear to be random, and the frequency ranges dependent on waveguide size. Multiple letters are assigned to these bands by different groups.
Q	40 to 60 GHz	5 mm to 7.5 mm	Used for military communications
V	50 to 75 GHz	4 mm to 6 mm	Very strongly absorbed by the atmosphere
W	75 to 110 GHz	2.7 mm to 4 mm	76 GHz LRR and 79 GHz SRR automotive radar, high-resolution meteorological observation and imaging

A.2. RADAR Range Equation

The radar range equation expresses the factors affecting the radar performance, which gives radar characteristics in terms of received power. Radar technologies are used to find the target properties like range, speed, direction, etc. Signal strength at the receiver section in the radar is usually of the order of nano watts compared to the transmitted power of several Watts. The reflected power in the radar system depends on many factors like free space path losses, radar cross section of the target (σ_{target}), fading and other environmental parameters. The general radar system is described in Fig.A.1, which transmits a pulse of energy through the transmit antenna of gain G_t. Depending on the wavelength (λ) of the transmitted signal and distance between the transmitter and receiver (R), the amplitude of the signal is reduced due to the free space propagation loss. At the target a part of this power is reflected back towards the radar. The ratio of the backscattered power to the incident power is the Radar Cross Section (RCS) (σ_{target}) of the target. The signal is then received by the receiver antenna with gain G_r and detected by the receiver. The power level P_r is the power received in the radar receiver [1]-[3].

$$P_r = \frac{P_t.G_t G_r.\sigma_{target}.\lambda^2}{(4\pi)^3.R^4} \qquad\qquad (A.1)$$

where P_t is the transmitted power from the radar transmitter. Block diagram with power at each section in the radar system is described in Fig.A.2.
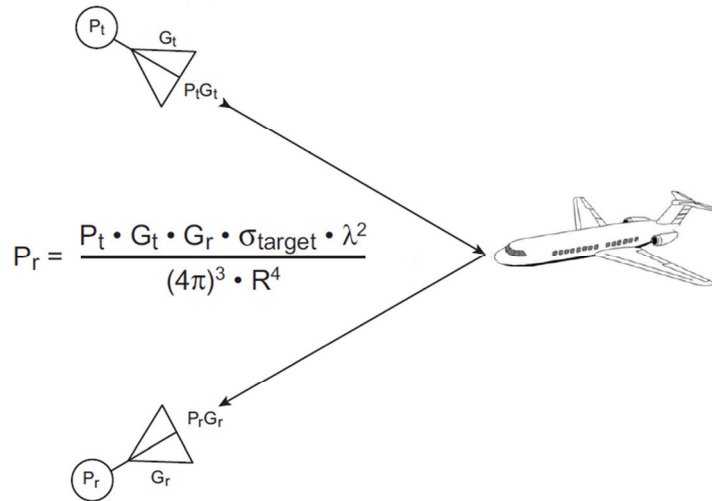
Figure A.1 Typical diagram showing bistatic radar having separate transmitter and receiver, Courtesy: Martin I. Grace. et al. [7].
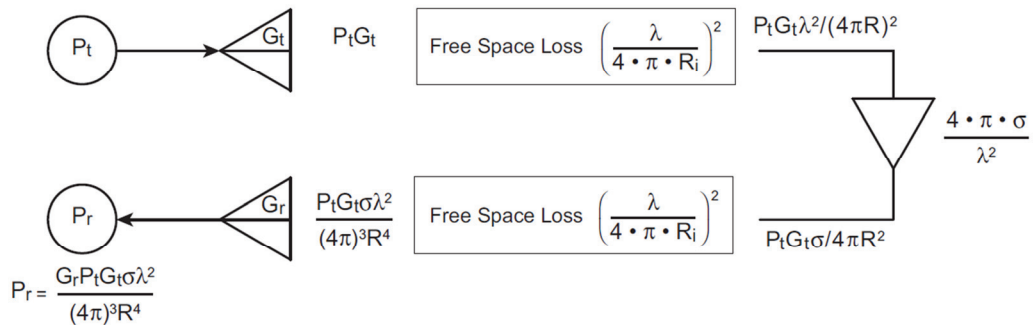
Figure A.2 Physical Block diagram of the RCS measurement. Courtesy: Martin I. Grace. et. al. [7].

A.3. Radar Cross Section (RCS)

RCS or echo area (σ or σ_{target}) of a target is defined as the area intercepting that amount of power, which when scattered isotopically, produces at the receiver a density equal to that scattered by the actual target [8]. In equation form

$$\lim_{R \to \alpha} \left[\frac{\sigma W_i}{4\pi R^2} \right] = W_s \tag{A.2}$$

or

$$\sigma = \lim_{R \to \alpha} \left[4\pi R^2 \frac{W_s}{W_i} \right] \tag{A.3}$$

where

W_i = incident power density (W/m^2)

W_s = scattered power density (W/m^2)

A.4. Range

The distance between the target and radar can be calculated by finding total round trip time taken by the RF signal to travel between the radar and the target. In the case of Pulsed Radar, consider a pulse of energy being sent at a given instant in time. It travels towards the target at a speed of light ('c' meters/sec). After hitting the target it gets reflected back at the same speed. After T_R seconds, radar receiver receives the reflected signal, then the distance or range R (in meter) to the target is given by

$$R = \frac{cT_R}{2} \tag{A.4}$$

In the case of FMCW radar, the transmitter sends a band of frequency which is controlled by a sweep generator. Therefore receiver section also receives the same frequency band after a short time delay of Δt (as shown in Fig.A.3), which represents the range between radar and target. Therefore distance R for continuous type radar can be calculated as

$$R = \frac{c.\Delta f}{4 \times \Delta F \times f_m} \tag{A.5}$$

where Δf is the instantaneous difference in frequency (Hz) of the transmitter at the times the signal is transmitted and received, ΔF is the RF modulation bandwidth (Hz) and f_m is the RF modulation rate.
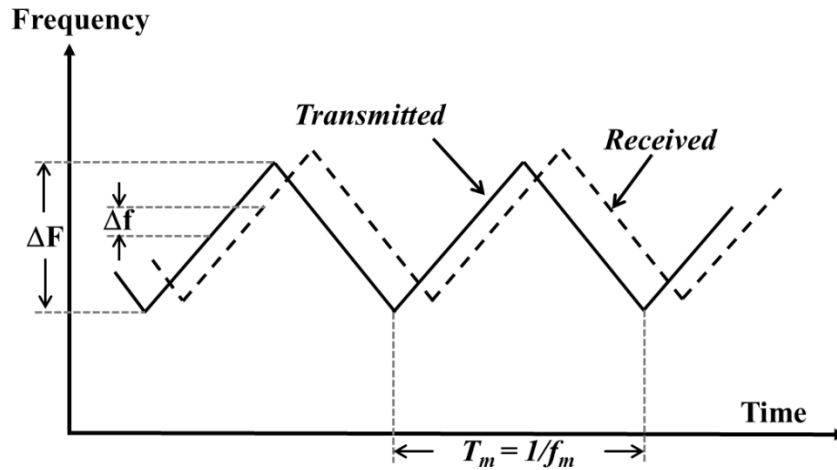
Figure A.3 FMCW radar waveform pattern

A.5. Doppler Frequency

The doppler frequency is used to calculate the relative speed and direction of the target. The radar transmitter generates an RF pulse or continuous frequency f_0 and radiated by the antenna. Receiver antenna will pick up the reflected signal from the target. If the target is moving with a relative velocity V_r with respect to the radar, the received signal frequency will be shifted from the transmitted signal frequency f_0 by an amount $\pm f_d$. The plus sign indicates target is moving towards the radar and the minus sign indicates the target is moving away from the radar. The shifted frequency f_d is called doppler frequency and it can be calculated as

$$f_d = \frac{2V_r}{\lambda} = \frac{2V_r f_0}{c} \tag{A.6}$$

where λ is the wavelength of the transmitting frequency. Fig.A.4 shows the relation between doppler frequency shift and target speed. A radar system with measurement capability of 15 kHz can detect a target speed of 60m/s (216km/hr).
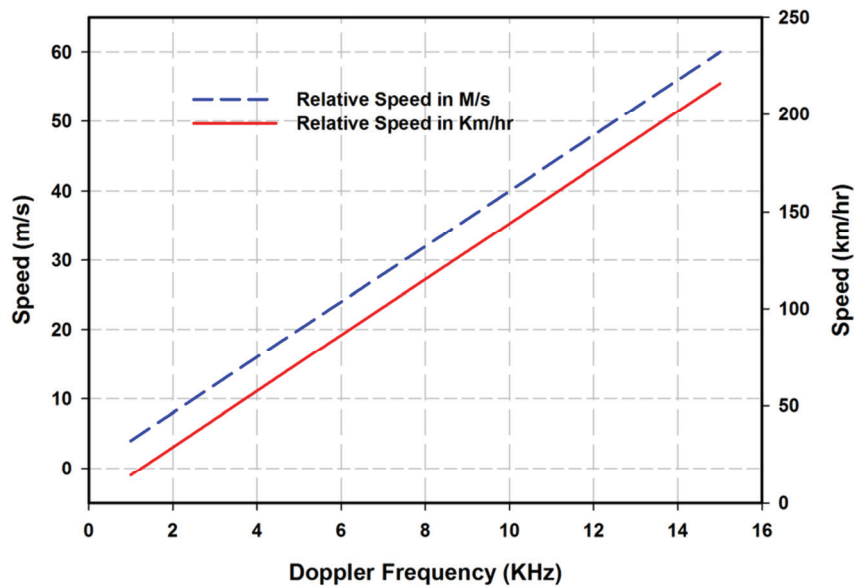
Figure A.4 Relation between Doppler Frequency and target speed.

A.6. Doppler or Continuous Wave (CW) Radar

Doppler or CW Radar is used to measure the relative speed of the target or vehicle based on the Doppler frequency shift and it cannot determine the distance or range of the target. The CW radar system may consist of single or two separate antennas for the transmission or reception of RF signal. In single antenna system duplexer is needed to isolate the reflected signal from the high power transmitted signal. Radar continuously transmits a single frequency with constant amplitude. The reflected signal has either exactly the same frequency for stationary target, or shifted by the amount of doppler frequency (f_d) due to the relative movement of the target. Fig.A.5

shows the transmitted and received frequency spectrum of doppler radar with different target conditions. From Fig.A.5 it is very easy to understand the doppler frequency variation for the target when it's stationary, approaching and receding.
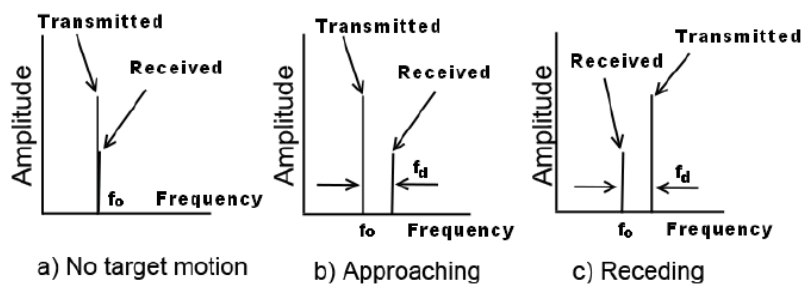
Figure A.5 Transmitted and received signal frequency of CW Radar

The CW radar devices are dedicated for processing doppler frequency shift in the reflected signal. Radar using two separate antennas is proposed in this chapter and block diagram of the radar is shown in Fig.A.6. A 2.4GHz signal generated by the RF source is amplified by the LNA, which is connected at the output of the attenuator. The attenuator is used to protect the LNA from the high input signal. A power splitter section is used in the transmitter section to couple a portion of transmitting energy to the receiver section through one o output port and the other port is connected to the transmitter antenna. Transmitted signal 'E$_t$' from the radar can be expressed as

$$E_t = E_0 cos\omega_0 t \tag{A.7}$$

where E$_0$ and ω_0 are the amplitude and the angular frequency of the transmitted signal. Depending on the speed of the moving target, frequency and phase of the reflected signal will vary and it can be expressed as

$$E_r = K_1 E_0 cos[(\omega_0 \pm \omega_d)t + \phi] \tag{A.8}$$

where,

K_1 = constant calculated from the radar equation representing the reduction in power of the reflected signal

ω_d = doppler angular frequency shift

ϕ = a constant phase shift, which depends upon the range of initial detection (i.e., the distance between the radar and the target)

The receiver antenna picks up this weak reflected signal and it is fed to the LNA for amplification. The output of the LNA is connected to the mixer unit. Transmitted and received signals are combined at the mixer and it generates an IF (Intermediate Frequency) signal which consists of the sum and difference of the input signals. Therefore, the low IF signal at the output of the mixer is fed into the Video amplifier section. Video Amplifier section consists of an amplifier and active LPF filter with cutoff frequency of 15kHz. A video amplifier section amplifies and removes all the high frequency components at mixer output. The output of the video amplifier section is connected to the computer for further processing. A 16 bit ADC (Analog to Digital Converter) inside the mic jack of the computer with a sampling rate of 44.1kHz is used for digitizing the analog signal. Another purpose of the computer is to extract the doppler frequency and to estimate the speed of the target.
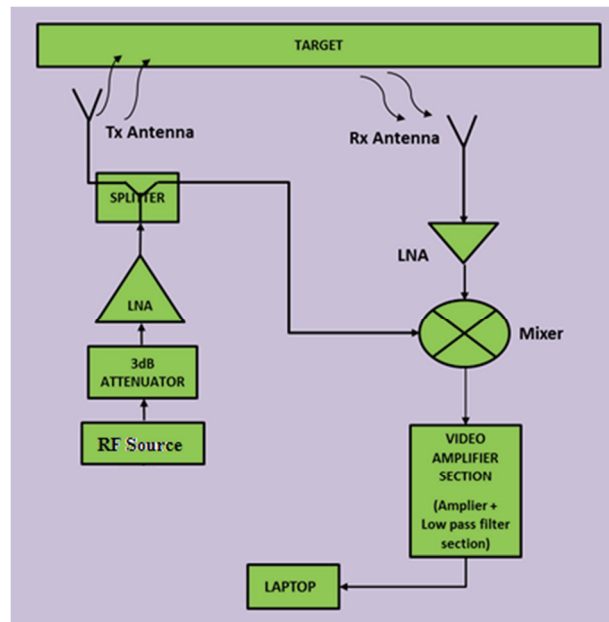
Figure A.6 Block diagram of Continuous Wave Radar

Most of the components inside the circuits have been explained in the earlier chapter. New additional components in the circuits such as 2.4GHz microstrip rectangular patch antenna and video amplifier are detailed in the following sections.

A.6.1. 2.4 GHz Microstrip Patch Antenna

Radar system requires two antennas working at 2.4GHz ISM band. The characteristics required for the antennas are, good isolation between transmitter and receiver antenna, directive radiation pattern, and good impedance match. A rectangular microstrip patch antenna with coaxial feed [8] is designed and fabricated in an FR4 substrate with dielectric constant 4.3, loss tangent 0.02 and substrate height 1.6mm. Fig.A.7 shows the rectangular microstrip patch antenna geometry with detailed dimensions. The antenna is simulated with the Ansys HFSS software and its simulated reflection

coefficient is shown in Fig.A.8. The antenna shows very good impedance match for the desired 2.4GHz frequency. Isolation between the two antennas can be improved by placing them about 40-50cm apart. As shown in the 3D radiation pattern (Fig.A.9), maximum radiated power is towards the broadside direction of the antenna.
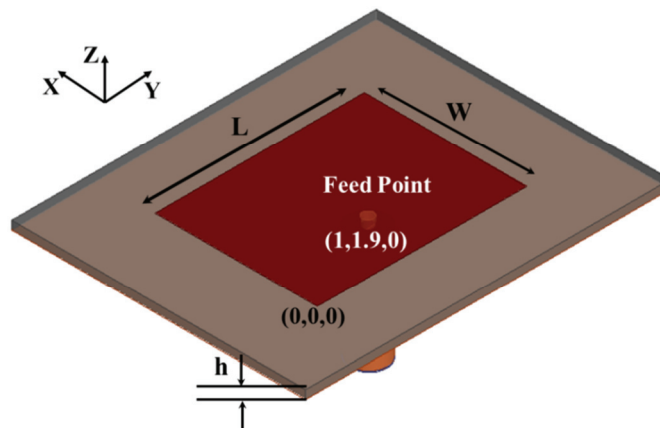
Figure A.7 Geometry of the rectangular patch antenna with coaxial feeding, where ε_r = 4.3, $\tan\delta$ = 0.02, L = 3.84, W = 2.98 and h = 0.16 (all dimensions are in cm)
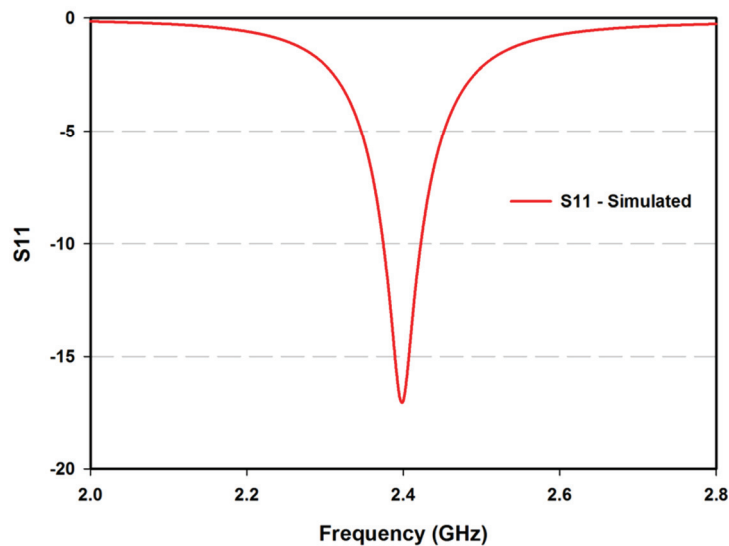
Figure A.8 Simulated frequency response of the patch antenna
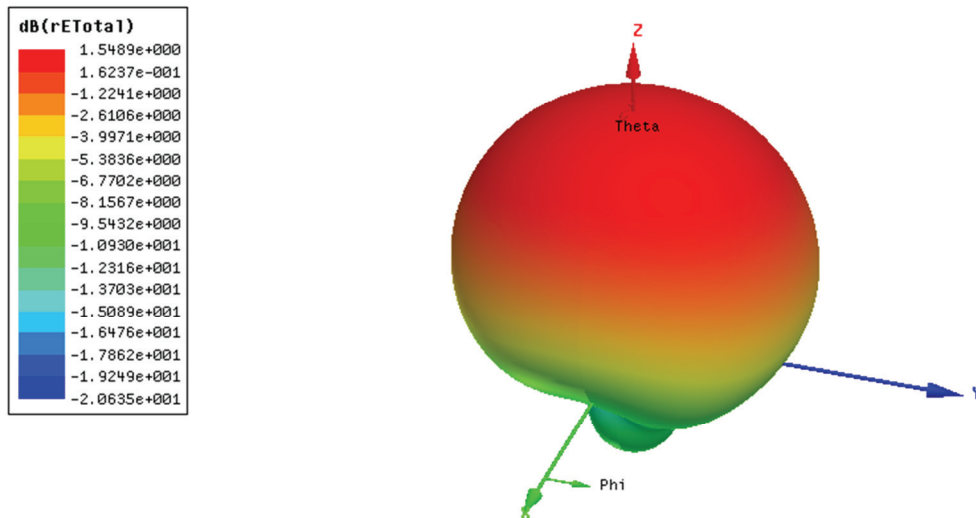
Figure A.9 Simulated 3D radiation plot of the patch antenna at 2.4GHz

A.6.2. Video Amplifier Section

A large reflector in front of the antenna can generate a voltage of 50mV at the mixer output and this is insufficient for the ADC inside the computer. Thus an amplifier section is required to boost the backscattered signal. The signal from the mixer (IF) comprises of many frequency components, hence an antialiasing filter is also required before doing analog to digital conversion. Therefore video amplifier section proposed in the MIT Coffee Can Radar, comprises of three opamps, an amplifier and an LPF designed using LM 324 IC [10]. The first stage of the amplifier has a gain of about 50 and it can be varied using a 10K potentiometer in the feedback path. The second and the third stages are low pass filters (based on Sallen-Key architecture) [11] with cutoff frequency of the filter at 15 kHz. Circuit diagram designed is for video amplifier using ORCAD Capture software and its circuit model is shown in Fig.A.10.
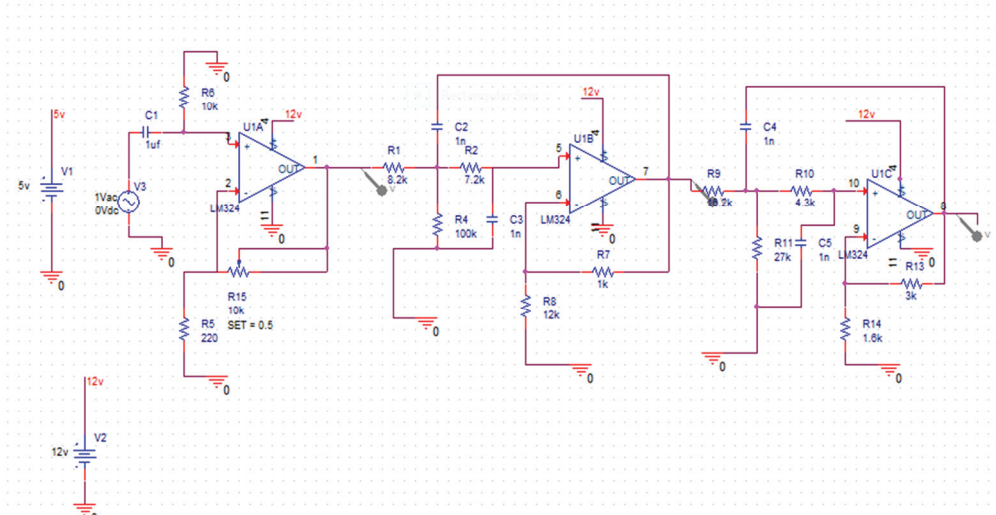
Figure A.10 Circuit diagram of video amplifier section designed using ORCAD Capture software.

The low frequency circuits consist of video amplifier section, power supply section and sweep generator (using XR 2209 IC) designed on a printer circuit board using Eagle PCB design software. PCB layout and fabricated circuit with electronic components are shown in Fig.A.11. The power regulator section shown in Fig.A.11 (b) is designed using 5V regulating IC (7805) for powering all the RF components and XR 2209 signal generator section. The sweep generator circuit is designed for the development of chipless RFID reader and FMCW radar. The circuit board is powered by 12V DC and it is used for powering video amplifier section and also used as in input voltage for 7805 regulating IC.
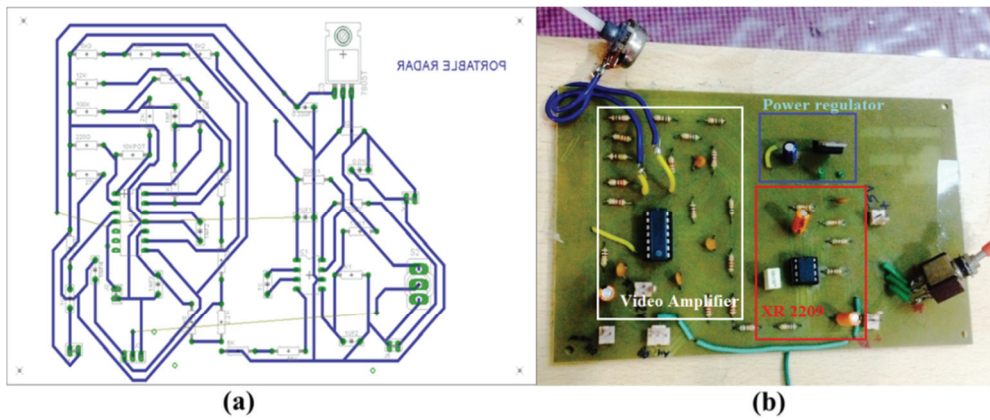
Figure A.11 (a) PCB layout design (b) fabricated circuit

A.7. Result and Measurement

All the components and circuits are interconnected as per the block diagram given in Fig.A.6. A voltage controlled oscillator (ZX95-2536C+) from mini-circuit is used as the single frequency RF source with an output frequency of 2.4GHz by setting 1.8V at the V-tune pin. Fig.A.12 shows the full system assembly consists of two microstrip patch antennas, RF components, PCB circuit, battery pack and laptop computer. Field test of the Doppler radar was carried out along the University campus road and photograph taken during the measurement is shown in the Fig.A.13. During the measurement, reflected signal is stored as 'wav' file and latter processed in Matlab software.
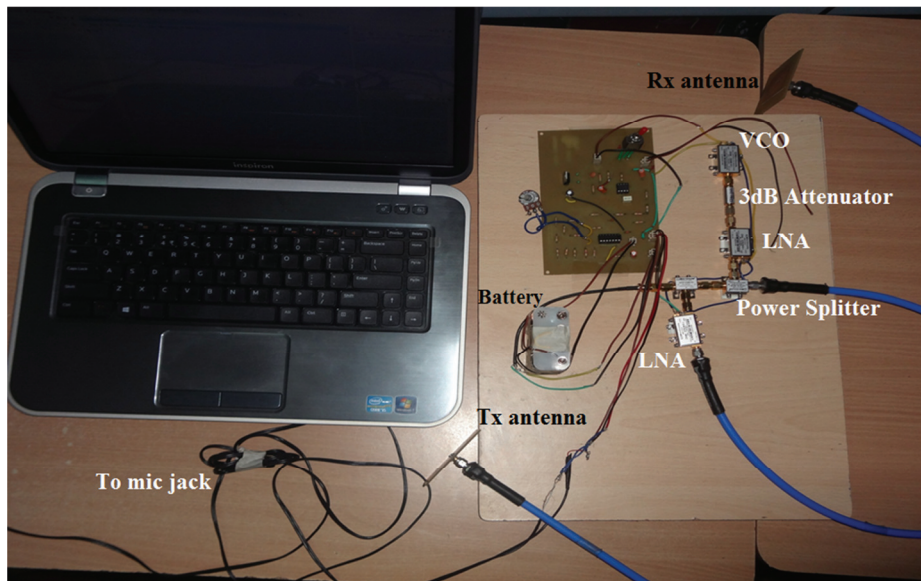
Figure A.12 2.4GHz ISM band CW radar based on MIT Coffee Can Radar

Figure A.13 Filed measurement of CW radar in public road

Measured doppler signal using CW radar is depicted in Fig.A.14 and the speed of vehicles calculated are plotted in Fig.A.15. Total measurement is taken for a time of 25 seconds and during that time four vehicles were passed through the road. The speed of each vehicle can be understood from the measured data. It is 29 km/hr (8m/s) for first 3 vehicles and about 36km/hr (10m/s) for last one. The strength of the doppler signal is dependent on the size of the target and it is clear from the Fig.A.14. It is also noted that when the target is leaving the radiation zone of the radar antenna, doppler frequency is reduced drastically and hence corresponding variation in speed occurs. Fig.A.15 shows the measured vehicle speed at different instants and confirms that almost all of the vehicles passing through the University campus are travelling below 40Km/hr speed.
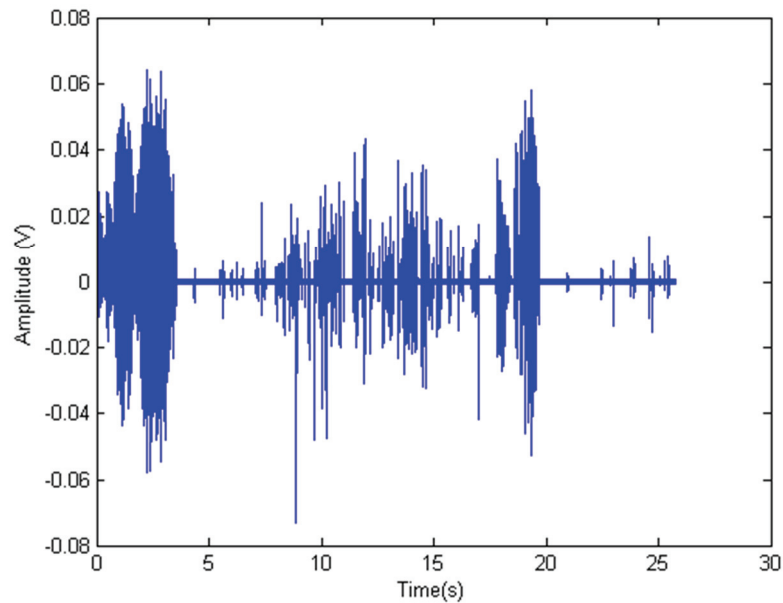
Figure A.14 Measured doppler signal
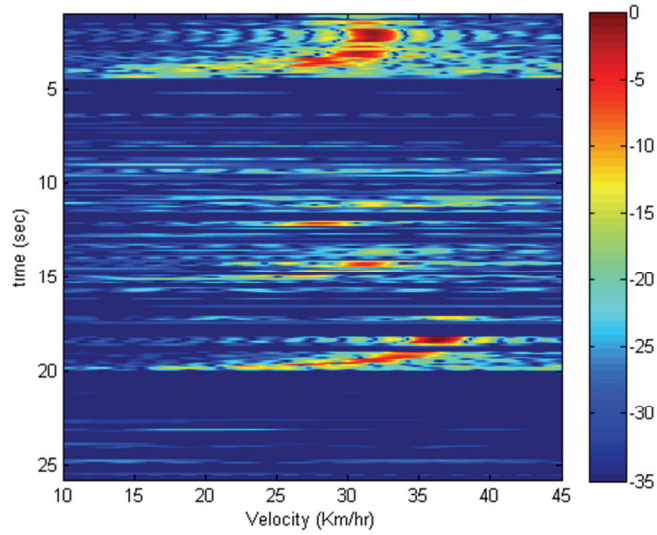
Figure A.15 Measured speed of the vehicles using Doppler Radar
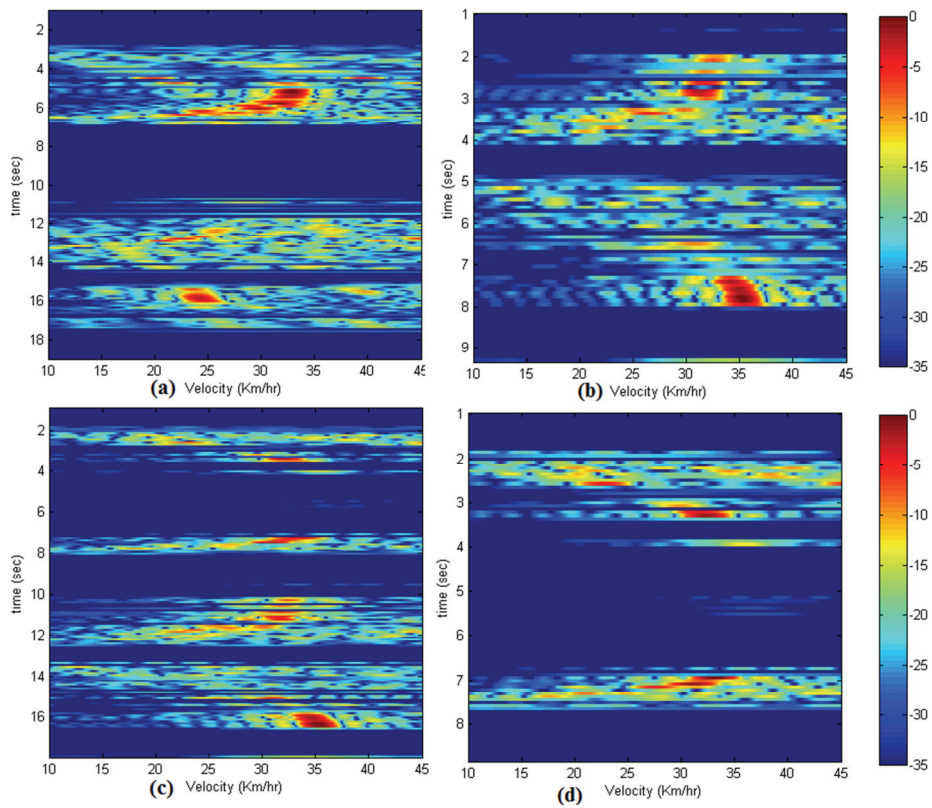
Figure A.16 Measured speed of the vehicles using Doppler Radar

A.8. Conclusion

This Appendix briefly describes different radars, applications, radar characteristics like radar range equation, range calculation, doppler, etc. The design and development of a Doppler Radar working at 2.4GHz ISM band is described. Two microstrip patch antennas are designed and fabricated for the transmission and reception of the radar signal. The real time measurements are taken along the University campus road and its calculated speeds are presented.

A.9. Future Works

The PCB and RF circuit designed for the proposed radar can be extended for the development of FMCW (Frequency Modulated Continuous Wave) Radar and SAR (Synthetic Aperture Radar). The FMCW radar can be used for the estimation of both speed and range of the target. Instead of using a constant frequency in the doppler radar, a band of frequencies is used in FMCW radar for the estimation of target range and speed. Wide band frequency can be produced by the combination of VCO and sweep generator circuit (XR2209 IC). The FMCW radar setup can be extended to SAR with an additional moving platform.

A.10. Reference

[1] Marcum, J., "A statistical theory of target detection by pulsed radar", IRE Transactions on Information Theory, pp. 59 – 267, April 1960.

[2] Boyer Wesley D, "Continuous wave radar", US patent no. US 3155972 A, Nov 3, 1964.

[3] A.J. Hymans and J. Lait, "Analysis of a frequency-modulated continuous-wave ranging system", Proceedings of the IEE - Part B:

Electronic and Communication Engineering, Volume 107, Issue 34, p. 365 – 372, July 1960.

[4] Brooker, G.M., Birch, D. and Solms, J., "W-band airborne interrupted frequency modulated CW imaging radar", IEEE Transactions on Aerospace and Electronic Systems, Volume:41 , Issue: 3, pp. 955 – 972, July 2005.

[5] Nicholas J. Willis, "Bistatic Radar, Second Edition" December 31, 2005.

[6] Ming Li, Guisheng Liao and Liang Zhang, "An approach to suppress short-range clutter for non-side looking airborne radar", Journal of Electronics (China), Volume 28, Issue 1, pp 64-70, January 2011.

[7] Martin I. Grace, Measurement of Radar Cross Section Using the "VNA Master" Handheld VNA, Application Note by Anritsu.

[8] C. A. Balanis, Advanced Engineering Electromagnetics, John Wiley and Sons, New York, 1989.

[9] G. T. Ruck, D. E. Barrick, W. D. Stuart, and C. K. Krichbaum, Radar Cross Section Handbook, Vols. 1, 2, Plenum Press, New York, 1970.

[10] Gregory L. Charvat, "Small and Short-Range Radar Systems", CRC Press, 09-Jan-2015.

[11] Saraga, W., "Sensitivity of 2nd-order Sallen-key-type active RC filters", Electronics Letters Vol. 3 , Issue. 10, pp.442 – 444, October 1967.

[12] Charvat, G.L.; Fenn, A.J.; Perry, B.T., "The MIT IAP radar course: Build a small radar system capable of sensing range, Doppler, and synthetic aperture (SAR) imaging," Radar Conference (RADAR), 2012 IEEE , vol., no., pp.0138,0144, 7-11 May 2012

.............ଓଃ୫ଠ.............

LIST OF PUBLICATIONS

International Journals

1. **Nijas, C.M**., Deepak, U., Vinesh, P.V., Sujith, R., Mridula, S., Vasudevan, K., Mohanan, P., "Low-Cost Multiple-Bit Encoded Chipless RFID Tag Using Stepped Impedance Resonator," IEEE Transactions on Antennas and Propagation, vol.62, no.9, pp.4762,4770, Sept. 2014

2. **Nijas, C.M.,** Dinesh, R., Deepak, U., Rasheed, A., Mridula, S., Vasudevan, K., Mohanan, P., "Chipless RFID Tag Using Multiple Microstrip Open Stub Resonators," IEEE Transactions on Antennas and Propagation, vol.60, no.9, pp.4429,4432, Sept. 2012.

3. Deepak, U., Roshna, T.K., **Nijas, C.M.,** Vasudevan, K., Mohanan, P., "A Dual Band SIR Coupled Dipole Antenna for 2.4/5.2/5.8 GHz Applications," Antennas and Propagation, IEEE Transactions on , vol.PP, no.99, pp.1,1 2015.

4. P. V. Vinesh, **C. M. Nijas**, R. Anitha, R. Vivek, C. K. Aanandan, P. Mohanan, and K. Vasudevan, "A Compact Capacitive Coupled Dual Band Planar Inverted F Antenna", Progress in Electromagnetic Research, Vol. 52, 93-99, 2014.

5. S. Mathew, R. Anitha, T. K. Roshna, **C. M. Nijas**, C. K. Aanandan, P. Mohanan, and K. Vasudevan, "A Fan-Shaped Circularly Polarized Patch Antenna For UMTS Band", Progress In Electromagnetics Research C, Vol. 52, 101-107, 2014.

6. Sumi M, Dinesh R, **Nijas C M**, S. Mridula and P. Mohanan, "Frequency coded Chipless RFID Tag using Spurline Resonators" Radio Engineering, pp.203-208; vol. 23, April 2014.

7. M. Nair Sreejith, V. A. Shameena, **C M Nijas**, and P. Mohanan "Novel ChiplessRf Identification Technology for On-Touch Data Transfer Applications" Microwave and Optical Technology Letters, Vol. 54, No. 10, pp. 2325–2327, October 2012.

8. S. Jacob, A. O. Lindo, **C. M. Nijas**, C. K. Aanandan, and P. Mohanan, "Analysis of CPW-fed UWB antenna for wimax and WLAN band rejection," Progress In Electromagnetics Research C, Vol. 52, 83-92, 2014.

9. Anila P V, Indhu K K, **Nijas C M**, Sujith R, Mridula S, and P Mohanan "A Planar Compact Metamaterial- Inspired Broadband Antenna" Microwave and Optical Technology Letters, Vol. 56, No. 3,pp. 610–613, March 2014.

10. Deepak, U., Roshna, T.K., **Nijas, C.M**., Mohanan, P., "Compact CPW fed electrically small antenna for WLAN application," Electronics Letters, vol.50, no.2, pp.62,64, January 16 2014.

11. Laila D, R Sujith, **Nijas C M**, P Mohanan "CSRR based Microstrip Antenna for compact wireless applications" Microwave and Optical Technology Letters, Volume 55, Issue 4, pages 814–816, April 2013.

12. Sreejith M. Nair, Shameena V.A, **Nijas C.M**, C.K. Aanandan, K. Vasudevan, P. Mohanan "Compact Slotline Fed Enhanced Gain Dipole Antenna for 5.2 GHz/5.8-GHz Applications" International Jrnl of RF and Microwave Computer-Aided Engineering Journal, Vol. 23, Issue 1, pp. 40–46, January 2013

13. Laila D, Sujith R, **Nijas C M**, Sarin V P and P Mohanan "Compact modified printed monopole antenna for enhanced gain performance" International Journal of Applied Information Systems, Volume 1, Number 3, February 2012.

14. Sreejith M. Nair, V. A. Shameena, **C. M. Nijas**, C. K. Aanandan,K. Vasudevan, P. Mohanan, "Slot Line Fed Dual-Band Dipole Antenna for 2.4/5.2 GHz WLAN Applications" International Journal of RF and Microwave Computer-Aided Engineering, Vol. 22, No. 5, September 2012.

15. Laila.D, Sujith R, **Nijas C.M**, C. K Aanandan, K Vasudevan and P. Mohanan "Modified CPW fed monopole antenna with suitable radiation pattern for mobile handset", Mikrotalasnarevija, Microwave Review Journal, Vol. 17, pp. 8-12, September 2011.

16. Laila. D, Sujith.R, Shameena V. A, Deepak.U, **Nijas. C. M** and P. Mohanan "CPW fed antenna for moble handset with metal wire mesh", International Journal of Computer Applications (IJCA), No.1, 2011.

Conferences:

1. **Nijas C M,** Sajitha V R, Vivek R, Binu Paul, Mridula S and Mohanan P, "Spectral Extraction of Chipless RFID Tag using Time Domain Analysis", Accepted in 2015 IEEE International Symposium on Antennas and Propagation and North American Radio Science Meeting.19-25 July, 2015, BC, Canada.

2. **Nijas C M**, Deepak U, Sujith R and P. Mohanan "Multi Resonance Based Chipless RFID Tag with High Data Encoding Capacity" General Assembly and Scientific Symposium of the International Union of Radio Science, August 16-23, 2014, Beijing, China.

3. **Nijas C M**, SreekalaSuseela, Deepak U, Parveen Wahid and P. Mohanan "Low Cost Chipless Tag with Multi-bit Encoding Technique" 2013 IEEE MTT-S International Microwave and RF Conference (IMaRC), December 14-16, 2013, New Delhi, India.

4. **C. M. Nijas**, P. V. Vinesh, V. R. Sajitha, P. V. Anila and P. Mohanan "Optimisation of Quarter Wave Microstrip Open Stub Resonators for Chipless RFID Applications" IEEE International Symposium on Antennas and Propagation and USNC-URSI National Radio Science Meeting, July 7-12, 2013, Orlando, Florida, USA.

5. V.R. Sajitha, **C.M. Nijas**, T. K. Roshna and P. Mohanan, "Chipless RFID Tag Based on Stepped Impedance Resonators", International Symposium on Antennas and Propgation (APSYM), December 17-19, 2014, Kerala, India.

6. Laila .D, Riny Thomas, **Nijas C M** and P. Mohanan, "Compact Polarization Independent Chipless RFID Tag" International Symposium on Antennas and Propgation (APSYM), December 17-19, 2014, Kerala, India.

7. Sumi M, **Nijas C M**, Dinesh R, Mridula S and Mohanan P "Compact chipless RFID tag using coplanar multiresonators" National Technological Congress 2014 (NATCON 2014),February 20-21, Kerala, India.

8. Sumi M, **Nijas C M**, Dinesh R, S. Mridula "Chipless RFID tag based on Spurline resonators" National APSYM 2012, 17-19, Cochin, Kerala.

9. Shari Mohan, P.R. Harikrishnan, V.R. Sajitha, **C. M. Nijas** and P. Mohanan "Chipless RFID Tag with SMD Inductors" International

Conference on Information Science 2014 (ICIS'14), July 4-5, 2014 at Cochin, Kerala, India.

10. U. Deepak, T. K. Roshna, **C. M. Nijas**, R. Dinesh, P. Mohanan ,"Compact CPW Fed ZOR Antenna for WLAN Application,APS/URSI - 2013 IEEE International Symposium on Antennas and propagation, July 7-13 2013, Orlando, Florida, USA.

11. Laila.D, Sujith.R, Shameena V.A, Deepak.U, **Nijas. C. M** and P.Mohanan, "CPWfedantennafor moble handsetwith metal wiremesh" ICVCI-2011,St.Gits, Kottayam, India.

12. Laila D, Sujith R, **Nijas,C M**, Shameena V.A, Dinesh R, P Mohanan "A Metamaterial antenna with reduced radiation hazards towards human head" PIERS 2012, Kuala Lumpur.

13. Dinesh R, Laila D, V P Sarin, **Nijas C M**, Shameena V A, P Mohanan "Asymmetric coplanar strip seemilliptical dual band antenna" PIERS 2012, Kuala Lumpur.

14. Sujith.R, Laila.D, **Nijas.C.M,** Deepak. U, R.Dinesh and P.Mohanan, "CPW Feeding techniques to excite slot on an Open Ended coplanar waveguide transmission line" PIERS 2012 Kuala Lumpur.

Nijas C M
Senior Research Fellow
Department of Electronics
Cochin University of Science and Technology
Kerala, India
Mobile: +91 9846236042,
E-mail: nijasmhmmd@gmail.com.

EXPERIENCE

- **6 years of** research experience in Microwave Antennas, Antenna Arrays, Chipless RFID, Electromagnetics and Dielectric measurements.

- **International Publications – 16;**

- Proficiency in Design and Development of various types of **Antennas, Antenna Arrays and Chipless RFID tags.**

- Proficiency in **Microwave Material Characterization**.

HONORS, AWARDS & ACHIEVEMENTS

1. Awarded **Junior Research Fellowship (JRF)** in 2010 and qualified **National Eligibility Test (NET)** for lectureship by University Grants Commission (**UGC**), Government of India

2. **University Second Rank Holder** in MSc. Electronics from Cochin University of Science and Technology, Cochin, India.

3. **Third Position** in test conducted by Science and Engineering Research Board (SERB), Govt. of India, on Fundamentals of Radars for Atmospheric Research (FORFAR).

AREAS OF INTEREST

Microwave Antennas, Active Antenna Arrays, Reconfigurable antennas, Implantable and Wearable antennas, Microwave Sensors, Biological effects of Microwaves, Chipless RFID, Filters, Microwave material characterization   etc.

TECHNICAL SKILLS

1. Experienced in using **HP 8510C** Vector Network Analyzer, **PNA E8362B** Network Analyzer, **R&S ZVB20** Network Analyzer, Spectrum Analyzer, **Microtech PM5** RF probe station, Anechoic chamber, Power Amplifiers, Power Meters, etc.

2. Experience in Antenna and RF/Microwave circuit design tools like **Ansoft HFSS, CST MWS, Agilent ADS, etc.**

3. Developed **MIT Coffee Can Radar** at 2.4GHz.

4. Developed a **Chipless RFID reader** working in the frequency band of 2.36GHz to 2.54GHz.

5. Involved in the design and simulation analysis of **619 element Yagi Array for 207MHz ST RADAR**.

6. Involved in the design and development of **Glucose Sensor** design using Microwave technology.

7. Involved in the designing of various **ultra compact wide band uniplanar antennas** for multiband applications highly suitable for wireless gadget.

8. Involved in the design of **radiation hazardless antenna** suitable for mobile handset.

9. Experience in the **Microwave Material Characterisation** measurement using **the Cavity Perturbation Method.**

10. Hands-on experience in **building of antenna prototypes** using photolithography and CNC Machine, and antenna experimental work.

11. Experienced in working both industry and Government projects (Dieplexer, Wireless Power Transfer, Dielectric Measurements, etc.).

SCHOLARLY WORK AND SERVICES

1. Active participant and Member in the Organizing Committee of International Biennial Symposium on **Antennas and Propagation Symposium (APSYM)**, from 2008 to 2014.

2. Active Member in the Organizing Committee of Biennial **International Symposium on Ocean Electronics (SYMPOL)** from 2009-2013.

3. Participated in **Fundamentals of Radars for Atmospheric Research** (FORFAR), course conducted by Science and Engineering Research Board (SERB), Govt. of India

4. Actively engaged in organizing various events and workshops.

5. Attended various National and International conferences and presented research papers.

WORK PROFILE

2011- Present:-

- **PhD,** "**Design and Development of Compact Chipless RFID Tags with High Data Encoding Capacity**", at Centre for Research in Electromagnetics and Antennas (CREMA), Cochin University of Science and Technology, India.

  Design and development of compact UWB chipless RIFD tag for low cost application. Chipless RFID system consist of different microwave components like different resonators, compact UWB antennas and high gain antennas. Frequency and Time domain analysis of backscattered signals are carried out for decoding resonant information from the RFID tag. An RFID reader working in the ISM Band (2.4GHz) is developed and verified its working with 2 bits chipless RFID tag.

2010-2011:-

- **Project Fellow, Design and Development of S Band Dielectric Diplexer for Space Application,** it is a collaborative project with **Cochin University of Science and Technology (CUSAT), Cochin, India** and **Vikram Sarabhai Space Centre (VSSC), Indian Space Research Organisation (ISRO)**, **Thiruvananthapuram, India.**

   To replace existing S Band Diplexer with compact Diplexer using high dielectric resonators ($\varepsilon_r = 82$) for space application. A six cavity Diplexer is designed with magnetic coupling and the final product meets all the specifications given by the funding agency (ISRO). Compared to existing Diplexer, size reduction more than 50% is achieved.

2009-2010:-

- **Intern, Wireless Power Transfer Project in Global Research Center at General Electricals (GE), Bangalore, India.**

   The project is for achieving Wireless Power Transfer for contactless charging in motor vehicles, rotating system and underwater equipment. Power level targeted is in the order of 10Watts to few Kilo Watts and distance requirement is about 1 to 10cm. Different resonators and antennas are designed and developed to obtain an efficiency of 80% at 200MHz.

QUALIFICATION

Course	Year of Passing	University	Institution	Class
Ph.D	Pursuing	Cochin University of Science and Technology (CUSAT, Cochin, Kerala, India	Department of Electronics, CUSAT, Kerala, India	--
M.Sc. Electronics	2007-2009	Cochin University of Science and Technology (CUSAT), Cochin, Kerala, India	Department of Electronics, CUSAT, Kerala, India	First class with Distinction CGPA **8.63** (2nd Rank)

PERSONAL

Date of birth	:	7th May 1987
Sex	:	Male
Languages Known	:	English, Hindi, Malayalam and Tamil
Nationality	:	Indian
Marital status	:	Unmarried
Passport Number	:	G-9828231
Father's Name	:	Mohammed Kunju V M
Mother's Name	:	Naseema A A
Permanent Address		Chakkanattu House
		Vaduthala Jetty P O,
		Arookutty, Alappuzha
		Kerala, India 688535